TOWARDS THE RATIONAL DEVELOPMENT OF ORGANIC SUPER ELECTRON DONORS FOR TRANSITION METAL-FREE BIARYL COUPLING

by

GREG ANDERSON

A thesis submitted to the Department of Pure and Applied Chemistry, University of Strathclyde, in part fulfilment of the regulations for the degree of Doctor of Philosophy in Chemistry.

DECLARATION OF OWNERSHIP

This thesis is the result of the author's original research. It has been composed by the author and has not been previously submitted for examination which has led to the award of a degree.

The copyright of this thesis belongs to the author under the terms of the United Kingdom Copyright Acts as qualified by University of Strathclyde Regulation 3.50. Due acknowledgement must always be made of the use of any material contained in, or derived from, this thesis.

Signed: Date: 28/09/2016

"One, remember to look up at the stars and not down at your feet. Two, never give up work. Work gives you meaning and purpose and life is empty without it. Three, if you are lucky enough to find love, remember it is there and don't throw it away."

– Stephen Hawking

Acknowledgements

First and foremost, I wish to offer my sincerest thanks to Dr Tell Tuttle and Professor John Murphy for granting me the opportunity to complete my postgraduate studies under their supervision. I am forever grateful for the invaluable support and guidance I have received over these challenging and educational years.

I would like to also extend my gratitude to Dr Stefan Senger and Dr Colin Edge, who supported me during my time with GSK's computational department, and facilitated my integration into the team.

I could not have made it to this stage without the unconditional support of my family, who have stood by me through everything my PhD has thrown at me; words cannot express the extent of my gratitude.

To all past and present members of both the Murphy group and TuttleLab, thank you for the many helpful discussions and enjoyable outings over the years. Notable thanks go to the post-doctoral researchers Dr Shengze Zhou, Dr Eswararao Doni, Dr Bhaskar Mondal and Dr Graeme Coulthard, all of whom have been integral throughout my studies.

Robin Bond, my closest friend of almost twenty years; you have always been there to support me when I've needed you most. Our nights out and various adventures over the years have undoubtedly kept me above water, thank you.

Dr's Daniel Cannon and Ivan Ramos Sasselli, you have both been with me from the start, and we've all made it through to the other side. Thank you for a memorable time, and I wish you both the very best in your future endeavours.

Dr Jonathan Taylor, it seems that you beat me to the finish line; congratulations. Thank you for showing me the ropes during my time in Stevenage, and most importantly for the pints we've shared.

Max Adler, you're one of the few non-chemists who has been a huge part of my time at the University of Strathclyde. It's been a pleasure sharing so many enjoyable memories with you (even the innumerate bore-draws on FIFA), and I hope that we will share many more in the future.

Finally, I'd like to thank members of technical staff at the University: Craig Irving (NMR), Patricia Keating (Mass Spectrometry), Richard Martin and Karina Kubiak (ARCHIE-WeSt), who have all assisted with various aspects of my research.

Abbreviations

Å	-	Angstrom(s)
AA	-	Atomic absorption
APCI	-	Atmospheric pressure chemical ionisation
BHAS	-	Base-promoted homolytic aromatic substitution
Bn	-	Benzyl
Boc	-	*Tert*-butyloxycarbonyl
^{n}Bu	-	Normal butyl
^{s}Bu	-	Secondary butyl
^{t}Bu	-	Tertiary butyl
^{o}C	-	Degrees Celsius
CPCM	-	Conductor-like polarisable continuum model
Cy	-	Cyclohexyl
dba	-	Dibenzylideneacetone
DBU	-	1,8-diazabicyclo[5.4.0]undec-7-ene
DCM	-	Dichloromethane
DFT	-	Density functional theory
DKP	-	2,5-diketopiperazine
DMEDA	-	*N,N'*-dimethylethylenediamine

DMF	-	*N,N*-dimethylformamide
DMSO	-	Dimethyl sulfoxide
EDA	-	Ethylenediamine
ee	-	Enantiomeric excess
EPR	-	Electron paramagnetic resonance
eq.	-	Equivalents
Eqn.	-	Equation
ESI	-	Electrospray ionisation
Et	-	Ethyl
Et_2O	-	Diethyl ether
g	-	Gram(s)
GC	-	Gas chromatography
Glu	-	Glutamic acid
h	-	Hour(s)
H_2O	-	Water
His	-	Histidine
HOMO	-	Highest occupied molecular orbital
HRMS	-	High-resolution mass spectrometry
Hz	-	Hertz
ICP	-	Inductively coupled plasma
J	-	Coupling constant

K	-	Kelvin
kcal mol^{-1}	-	Kilocalorie(s) per mole
KHMDS	-	Potassium hexamethyldisilazane
lit.	-	Literature value
LOD	-	Limit of detection
LRMS	-	Low-resolution mass spectrometry
LUMO	-	Lowest unoccupied molecular orbital
Lys	-	Lysine
m	-	Metre(s)
M.Pt.	-	Melting point
Me	-	Methyl
MeCN	-	Acetonitrile
MeOH	-	Methanol
mg	-	Milligram(s)
MHz	-	Megahertz
min	-	Minute(s)
mL	-	Millilitre(s)
mm	-	Millimetre(s)
mmol	-	Millimole(s)
mol%	-	Mole percentage
MS	-	Mass spectrometry

Ms	-	Mesylate
MW	-	Microwave
µm	-	Micrometre(s)
N	-	Molar
NHC	-	*N*-heterocyclic carbene
nm	-	Nanometre(s)
NMM	-	*N*-methylmorpholine
NMR	-	Nuclear magnetic resonance
NSI	-	Nanospray ionisation
OAc	-	Acetoxy
PCI+	-	Positive chemical ionisation
PES	-	Potential energy surface
Ph	-	Phenyl
ppb	-	Parts per billion
ppm	-	Parts per million
^{i}Pr	-	Isopropyl
r.t.	-	Room temperature
SED(s)	-	Super electron donor(s)
Ser	-	Serine
TBAB	-	Tetrabutylammonium bromide
TEMPO	-	2,2,6,6,-tetramethylpiperidine-1-oxyl

tert	-	Tertiary
TFA	-	Trifluoroacetic acid
THF	-	Tetrahydrofuran
TLC	-	Thin layer chromatography
TMP	-	2,2,6,6-tetramethylpiperidide
TMS	-	Trimethylsilyl
Trp	-	Tryptophan
TS	-	Transition state
Tyr	-	Tyrosine
UV	-	Ultraviolet
W	-	Watt(s)

Publications

1. *Predicting the Reducing Power of Organic Super Electron Donors*

   G. M Anderson, I. Cameron, J. A. Murphy and T. Tuttle, *RSC Adv.*, 2016, **6**, 11335-11343. DOI: 10.1039/C5RA26483A

   As first author of this paper, I was responsible for performing all theoretical calculations along with manuscript preparation and submission. The work carried out in this article is discussed in Chapter 7 of the thesis.

2. *Identifying the Role of Amino Acids, Alcohols and 1,2-Diamines as Mediators in Coupling of Haloarenes to Arenes*

   S. Zhou, E. Doni, **G. M. Anderson**, R. G. Kane, S. W. MacDougall, V. M. Ironmonger, T. Tuttle and J. A. Murphy, *J. Am. Chem. Soc.*, 2014, **136**, 17818-17826. DOI: 10.1021/ja5101036

   As co-author on this article, my inputs included initial experimental studies, which were subsequently repeated to give consistent data sets, and performing the associated theoretical calculations. Contributions to this work, and related investigations are discussed in Chapter 6 of the thesis.

3. *Organic Super-Electron-Donors: Initiators in Transition Metal-Free Haloarene-Arene Coupling*

   S. Zhou, **G. M. Anderson**, B. Mondal, E. Doni, V. Ironmonger, M. Kranz, T. Tuttle and J. A. Murphy, *Chem. Sci.*, 2014, **5**, 476-482. DOI: 10.1039/C3SC52315B

   As second author on this paper, my involvement was primarily the computational investigation of the biaryl coupling chemistry along with some preliminary experimental investigations, discussed in Chapter 5 of the thesis.

Table of Contents

1 Abstract

Within both the industrial and academic laboratory, the coupling of two aryl moieties is a process of significant synthetic use. To achieve such transformations typically requires the use of expensive transition metal catalysts that cannot always be recovered from the reaction mixtures. Consequently, the investigation of biaryl coupling reactions without the requirement for any such catalysts has been of key interest amongst chemists.

Throughout the literature, a variety of simple organic molecules have been incorrectly termed as "ligands" or "catalysts" with respect to their role in transition metal-free biaryl coupling reactions. We have discovered that these molecules in fact undergo reaction with a strong base to form an organic electron donor *in situ*, capable of reducing aryl iodides to their respective radical anions. This reduction can then initiate a cyclic radical reaction mechanism, furnishing the desired biaryl product.

A number of key structures, identified through experimental studies, have helped to guide the early theoretical investigations. These allowed the feasibility of the formation of organic electron donors *in situ*, based on their free energy profiles, to be investigated. The mechanistic understanding gained from these calculations was then applied to rationalise the reactivity of other molecules shown to effectively promote this chemistry. To fully understand the reactivity in this chemistry, the computational application of Marcus Theory was called upon to predict the relative reducing ability of the proposed donor species.

Shortcomings of the present protocol for the computational application of Marcus Theory prompted the development of a novel reaction model utilising electron transfer complexes. These complexes more accurately capture the internal reorganisation energy associated with the electron transfer reaction, affording calculated reaction energetics in stronger agreement with experiment. The foundations for the predictive application of this model to identify novel electron donors have been laid. Synthetic routes towards novel electron donor precursors have been identified for future work on this research.

2

Introduction

2.1 Motivation of the Thesis

Within the recent literature, there has been a surge in interest in the area of transition metal-free coupling reactions, operating in both reductive and oxidative manners. In particular, there has been an increase in the number of publications focussing on the reductive chemistry following the work by Itami[1] and co-workers in 2008, described in Chapter 3. This work suggested that a radical mechanism was responsible for the observed transformation, and subsequent research by other groups reiterated this observation. Although there is widespread agreement that the base-promoted homolytic aromatic substitution (BHAS) mechanism[2] was active in these reactions, there has been a lack of clarity surrounding the initiation of this reaction cycle.

The work discussed herein aims to provide a clear explanation of how the reported organic additives, in the presence of potassium *tert*-butoxide, are capable of initiating the BHAS cycle. This will involve a predominantly computational approach, which will be both guided and supported by experimental investigations. This research will focus on three primary objectives. The first of these is to develop an understanding of the nature of the active species in these reactions. Secondly, methods by which the effectiveness of the active species to initiate the BHAS mechanism will be investigated. Bringing together the learning outcomes of these two objectives, our final aim with this work is to be able to use computational methods to design new organic additives that might be capable of promoting this chemistry under milder reaction conditions.

2.2 Layout of the Thesis

The thesis begins with a discussion of the relevant literature in Chapter 3, which includes the mechanistic details, scope and limitations of palladium-catalysed cross coupling chemistry. This is followed by an overview of the use of aryne chemistry in synthesising biaryl motifs. A thorough discussion of reductive transition metal-free biaryl coupling chemistry, encompassing the range of organic compounds known to promote this chemistry, will comprise the majority of the review, along with

discussions of the use of theoretical and experimental approaches in tandem in order to provide mechanistic understanding.

The theoretical nature of this research requires a description of the methodology used which, in this case, was density functional theory (DFT). Chapter 4 of the thesis begins with a discussion of the fundamentals of quantum chemistry, after which the underlying theories of DFT will be introduced. The main applications of DFT within this work are transition state theory and Marcus theory, both of which will be described in this chapter. Specific DFT methods used throughout this research, such as the choice of functionals and basis sets, choice of solvation model and any additional details, will be outlined within the relevant chapters.

The main results from this research will be divided into four chapters. Chapter 5 will investigate the nature of the active species involved in some of the seminal publications within the field of transition metal-free coupling. Extending on the outcomes of this research, Chapter 6 will apply our mechanistic understanding to elucidating the active species formed from simple organic molecules as demonstrated in subsequent publications within this field. Chapter 7 comprises an investigation into the theoretical modelling of electron transfer reactions, and proposes a novel and more accurate method to that widely accepted within the literature. Drawing on the previous three chapters, Chapter 8 will investigate the possibility of designing new organic compounds that can effectively promote transition metal-free coupling reactions.

Chapter 9 will draw conclusions from the research discussed in the thesis, and outline ideas that could be investigated to further this work. Finally, Chapter 10 will outline the details of the experimental work discussed throughout Chapters 5 and 6, including procedures, instrumentation used and compound characterisation.

3

Literature Review

3.1 Palladium-Catalysed Cross Coupling Reactions

The first examples of a palladium-catalysed cross-coupling reaction were published by Mizoroki[3] and Heck[4] in the early 1970's (Scheme 3.1a and b respectively). Their research demonstrated the ability to form a carbon-carbon bond using an aryl halide and either an aromatic or aliphatic alkene as the reaction feedstocks. Both research groups demonstrated that, under similar reaction conditions, iodobenzene **3.1** and styrene **3.2** could be coupled to afford *trans*-stilbene **3.3** as the major product. Mizoroki *et al.* demonstrated that 1,1-diphenylethylene **3.4** was produced as a side-product, resulting from coupling at the sterically hindered position on the alkene. Common features highlighted in both reactions include the requirement for only substoichiometric quantities of palladium catalyst, elevated temperature and the presence of a mild base.
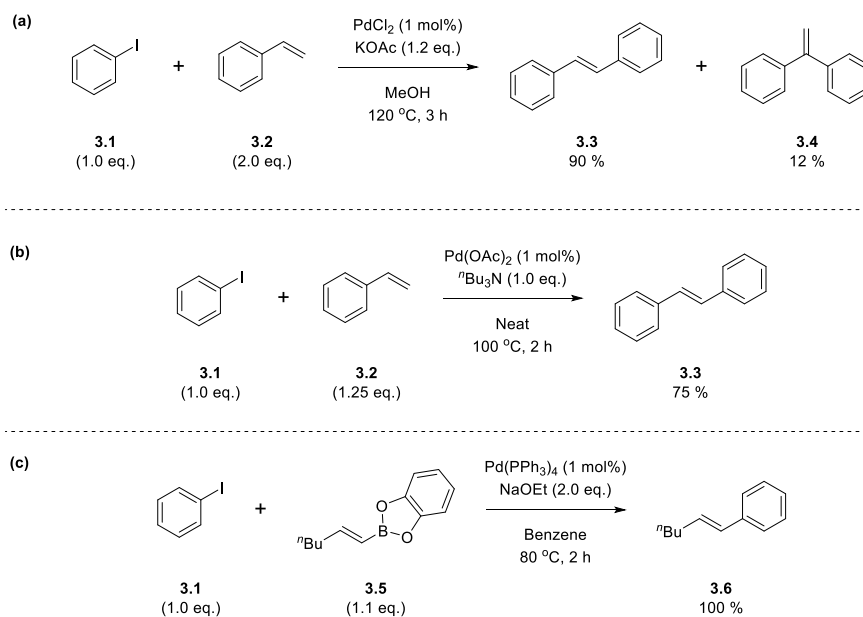
Scheme 3.1: Palladium-catalysed cross coupling chemistry published by (a) Mizoroki,[3] (b) Heck[4] and (c) Suzuki.[5]

A number of years later, a new set of reaction conditions was published by Suzuki *et al.,* who demonstrated the ability to cross couple alkenylboranes with aryl halides.[5] Using tetrakis(triphenylphosphine)palladium as the catalyst, they were able to couple iodobenzene **3.1** with *(E)*-hex-1-eny^{-1},3,2-benzodioxaborole **3.5**, affording hex-1-enylbenzene **3.6** in quantitative yield (Scheme 3.1c).

Stemming from this work, a vast amount of research has focussed on developing this chemistry further and has given chemists the ability to induce, for example, chemo- and enantioselectivity through careful selection of reaction conditions. For example, Fu and co-workers demonstrated in 2000 that the choice of catalyst could determine if cross-coupling occurred selectively at the halide or triflate position.[6] This is best illustrated in the cross-coupling of 4-chlorophenyltriflate **3.7** with 2-methylphenylboronic acid **3.8**, where the reaction conditions can be tailored to afford either the coupled triflate **3.9** or the corresponding chloride **3.10** (Scheme 3.2a). More recently, Takeda *et al.* have shown that the enantioselective arylation of 2-arylaziridines such as **3.11** can be achieved using a palladium *N*-heterocyclic carbene (Pd/NHC) catalyst.[7] Using the [SIPr-Pd(cinnamyl)Cl] catalyst, they were able to selectively form the desired product **3.13** in good-to-excellent yield as a single isomer, as determined by chiral chromatography (Scheme 3.2b). It is evident that palladium chemistry has come a long way from its humble origins almost 50 years ago, and its importance in modern synthesis is most notably highlighted by the awarding of the Nobel Prize in chemistry to Suzuki, Heck and Negishi back in 2010.[8]
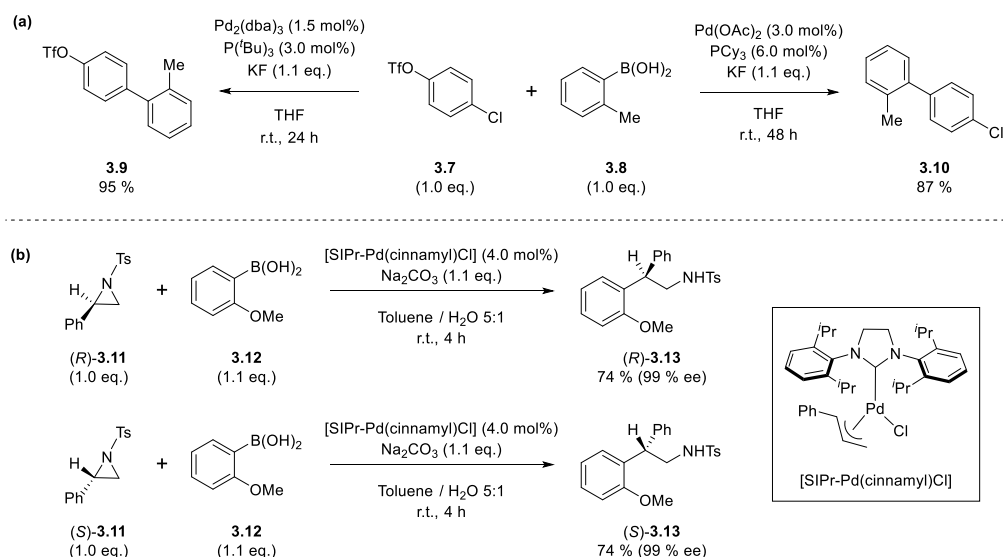
Scheme 3.2: (a) Chemoselective cross-coupling demonstrated by Fu *et al.*;[6] (b) enantioselective arylation of 2-arylaziridines performed by Takeda *et al.*[7]

The earliest suggestion that such cross-coupling reactions might be achieved without the requirement for a transition metal catalyst came in 2003 from the work by Leadbeater and Marco.[9] Their initial work[10] focussed on the microwave-assisted

ligand-free Suzuki cross-coupling of aryl halides with boronic acids in water as solvent. Using 4-bromotoluene **3.14** and phenylboronic acid **3.15**, optimal reaction conditions for the synthesis of 4-methylbiphenyl **3.16** were determined as shown in Scheme 3.3. It was found that the addition of 0.5 equivalents of tetrabutylammonium bromide (TBAB) to the reaction mixture led to an improved yield of 87 % for the coupled product (versus 40 % without). Increasing from 0.5 to 1.0 equivalent afforded the desired product in 96 % yield.
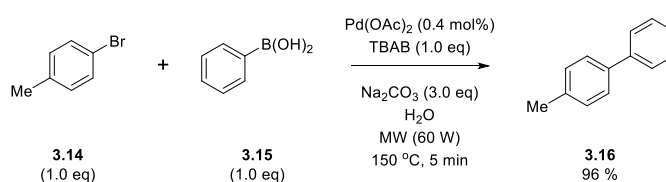
Scheme 3.3: Ligand-free Suzuki cross coupling reaction investigated by Leadbeater and Marco.[10]

Building on their initial work, they sought to better understand the role of the TBAB additive in these reactions.[9] It was suggested that the additive had two roles; to act as a phase-transfer catalyst, increasing the solubility of organic species in the aqueous medium, and to promote the formation of the corresponding boronate species, thus preventing hydrodeboronation. Interestingly they observed that, even in the absence of palladium catalyst, the reaction still furnished the desired coupling product in quantitative yield. In this instance, 4-bromoacetophenone **3.17** was the aryl halide chosen for the optimisation of the reaction conditions (Scheme 3.4). Measures were taken to ensure this reactivity was not an artefact of contamination. These included the use of new equipment and reagents, and analysis of the crude product mixture for palladium and other metals by inductively-coupled plasma atomic absorption (IPC-AA). No palladium could be detected above the instruments limit of detection (LOD) of 0.1 ppm, nor could any other metals be detected above the LOD of 0.5-1.0 ppm.
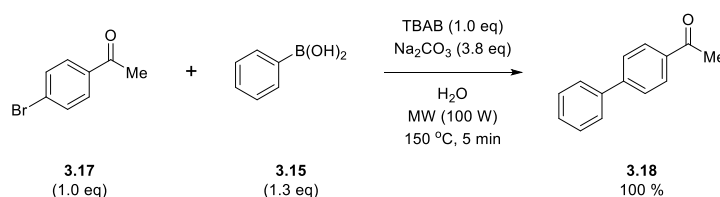
Scheme 3.4: Palladium-free cross coupling of aryl bromides under microwave irradiation.[9]

Despite the evidence in support of these transformations operating in the absence of a palladium catalyst, and following subsequent work[11] where the substrate scope and limitations were probed, it was ultimately discovered that ultra-low palladium contamination of the sodium carbonate was responsible for the observed reactivity.[12] Leadbeater *et al.* showed by inductively-coupled plasma mass spectrometry (ICP-MS) that the 'ultrapure' sodium carbonate contained between 20-50 ppb of palladium at reaction concentration, which they note could be sufficient to catalyse the reaction based on previous work by de Vries.[13, 14] As proof of concept, experiments were run using potassium carbonate as the base both in the presence and absence of palladium acetate at an approximate concentration of 50 ppb. Potassium carbonate was shown to contain a palladium concentration of only 0.09 ppb at reaction concentration, and was shown to be ineffective in their previous study.[11] The spiked reaction afforded the coupled product in 75 % yield, while the reaction without additional palladium gave less than 5 % of the desired product. Although this work didn't ultimately lead to a palladium-free protocol for cross-coupling reactions, it did demonstrate the possibility to synthesise biaryls with extremely low catalyst loading, with palladium nitrate representing the ideal palladium source due to improved water- solubility.

3.2 Benzyne-Mediated Cross Coupling Reactions

The utilization of aryne intermediates has emerged as a convenient synthetic route which sidesteps the use of palladium catalysts, allowing for transition metal-free synthesis of biaryl motifs.[15-17] Generation of these highly reactive intermediates has held precedent within the scientific literature since the 1960's, following research conducted by Cadogan and Hibbert.[18] They observed that *ortho-tert*-butyl-*N*-nitrosacetanilide **3.19**, following rearrangement to the corresponding diazoacetate **3.20**, could decompose to generate the aryne intermediate *ortho-tert*-butylbenzyne **3.22**. This intermediate could then react with the acetic acid formed, affording a mixture of *ortho-* and *meta-tert*-butylbenzene acetates **3.23** and **3.24** respectively (Scheme 3.5).
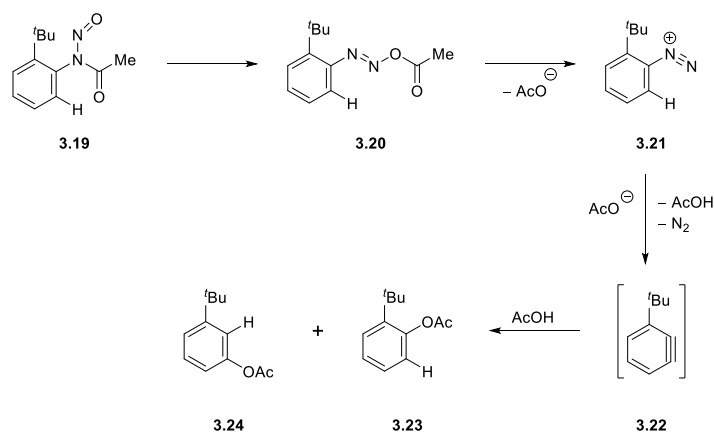
Scheme 3.5: Mechanism for the generation of benzyne via the Cadogan method.[18]

At around the same time, Cram and Day demonstrated that 4-bromo-[2.2]paracyclophane **3.25**, upon reaction with a strong base such as potassium *tert*-butoxide, could generate aryne intermediate **3.26** by deprotonation followed by elimination of a bromide anion.[19] Reaction of this intermediate with the solvent (DMSO) or the *tert*-butoxide anion then afforded the observed products **3.27**, **3.28** and **3.29** (Scheme 3.6).
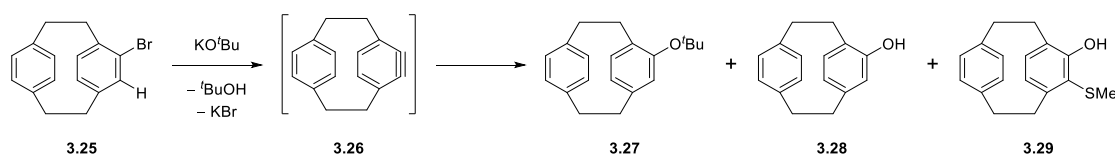
Scheme 3.6: Base-induced generation of aryne intermediate **3.26** and products resulting from attack by nucleophiles present in the reaction mixture as demonstrated by Cram.[19]

Looking at recent applications of this chemistry within the literature, the application of *ortho*-(trimethylsilyl)phenyl triflates such as **3.33** as precursors to reactive aryne intermediates predominates.[20-30] This methodology was first developed by Kobayashi *et al.* in 1983,[31] who synthesised *ortho*-(trimethylsilyl)phenyl triflate **3.33** from 2-chlorophenol **3.30** over four steps (Scheme 3.7a). Since then, Bronner and Garg have developed a three-step route to the same precursor from phenol **3.34** (Scheme 3.7b).[32]

(a)

(b)
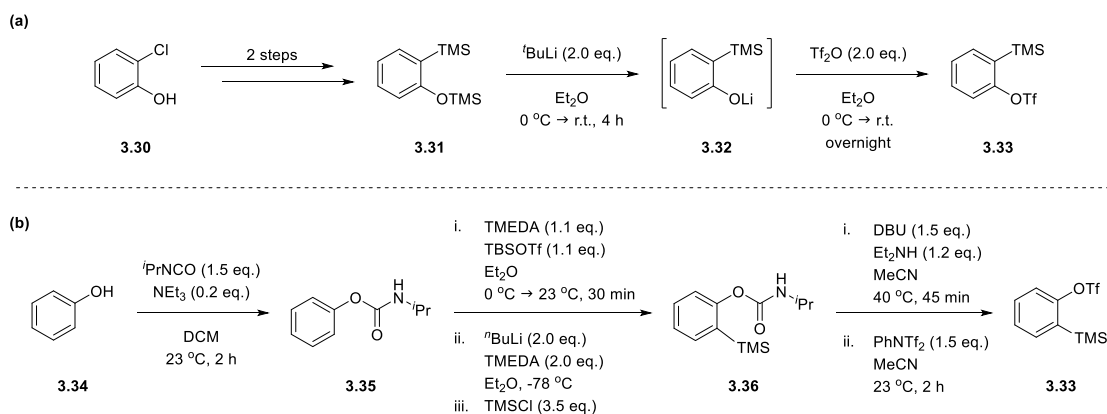
Scheme 3.7: Synthetic routes to *ortho*-(trimethylsilyl)phenyl triflates developed by (a) Kobayashi *et al.*[31] and (b) Bronner and Garg.[32]

Using *ortho*-(trimethylsilyl)phenyl triflates as aryne precursors avoids the requirement for a strong base; only a source of fluoride is required to generate the aryne via a 1,2-elimination reaction. It is worth mentioning that although the Kobayashi method is the most commonly encountered means of *in situ* aryne generation, examples do exist in recent literature of the application of the Cram and Day method.[15-17, 33, 34] Bajracharya and Daugulis demonstrated in 2008 that the intramolecular coupling of phenols with aryl halides could be achieved using substrates such as **3.37** in the presence of potassium *tert*-butoxide (Scheme 3.8a).[15] Similar work from the same research group demonstrated the ability to generate arynes from aryl chlorides and even aryl fluorides when using lithium 2,2,6,6-tetramethylpiperidide (LiTMP) as the base.[16, 17] These substrates were then coupled to activated arenes such as benzothiophene **3.40** and 2-naphthylamine **3.43** (Scheme 3.8b).
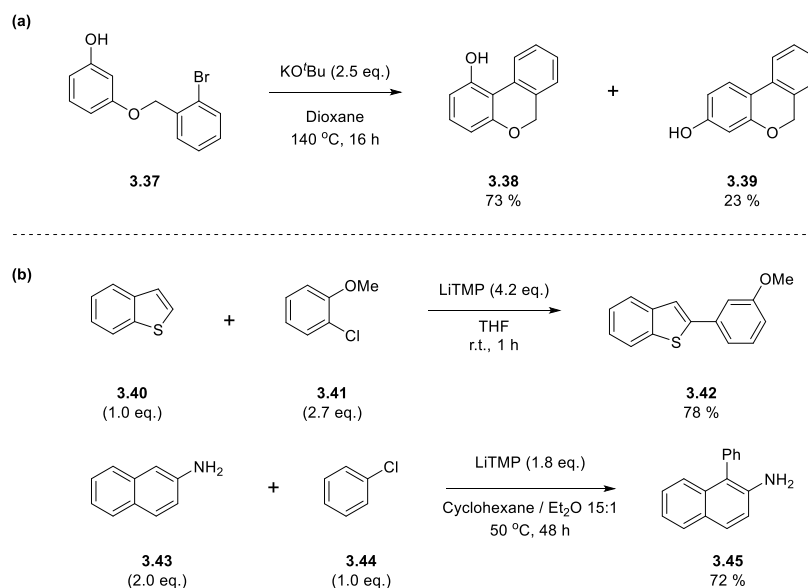
Scheme 3.8: Applications of (a) intramolecular and (b) intermolecular aryne chemistry to synthesise biaryl motifs demonstrated by Daugulis *et al.* using the Cram methodology.[15-17]

In addition to these transformations, this chemistry has been used in order to construct a number of more complex polyaryl moieties. Representative examples include the synthesis of aporphine alkaloids (**3.48**) via [4 + 2] cycloadditions by Raminelli *et al.*, (Scheme 3.9a)[30] and the synthesis of 9-aryldihydrophenanthrenes (**3.50**) via Diels-Alder reactions by Biju *et al.* (Scheme 3.9b).[24]
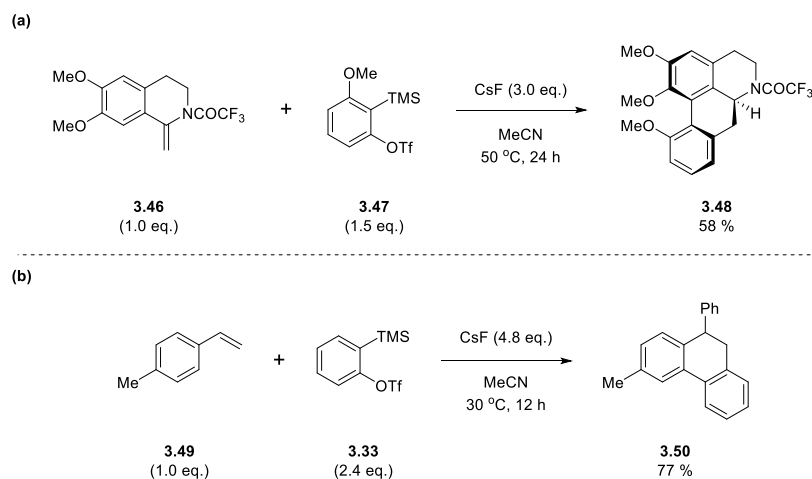
Scheme 3.9: Application of aryne intermediates in cycloaddition reactions for the synthesis of (a) aporphine alkaloids[30] and (b) 9-aryldihydrophenanthrenes.[24]

Though it has been demonstrated that this chemistry can be used for the formation of C—C bonds, more common in this field of chemistry is the coupling of arynes with a nucleophilic heteroatom. This reactivity can give rise to a diverse range of products

including *O*-arylated ethers and esters,[35] *N*-arylated amines and sulfonamides,[36] *N*-aryl sulfoximines[28] and aryl sulfones[27] (Figure 3.1).
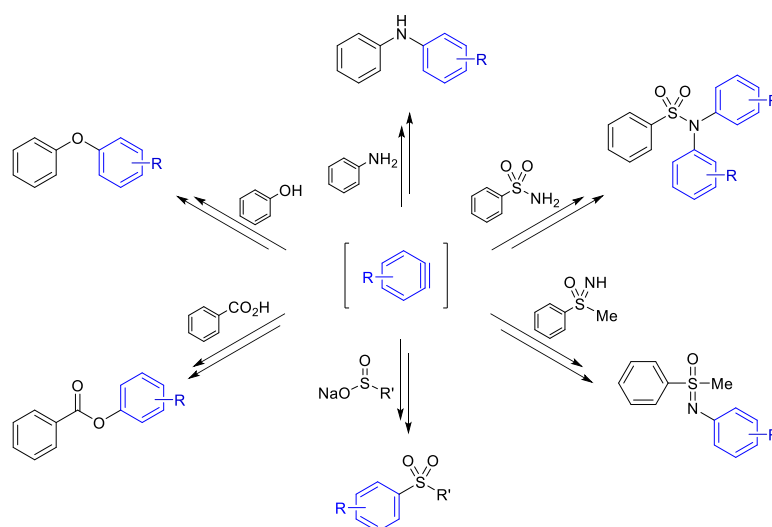
Figure 3.1: Common applications of aryne chemistry to form carbon-heteroatom bonds.[27, 28, 35, 36]

Despite the potential to synthesise biaryls under transition metal-free conditions via reactive aryne intermediates, another means of performing this chemistry emerged in 2008[1] which demonstrated an alternative route to these synthetically useful targets.

3.3 Transition Metal-Free Coupling Reactions Initiated by Organic Additives in the Presence of Base

In 2008, the research group of Itami was investigating the microwave-assisted coupling of iodoarenes with heterocyclic compounds in the presence of iridium catalysts.[1] During their study, they discovered that a number of structurally distinct catalysts were capable of affording the coupled product **3.52**, as a mixture of regioisomers, in similar yields. Intrigued by this, they performed a test reaction in the absence of iridium catalyst and were surprised to observe that the reaction proceeded to a comparable yield of 39 % (Scheme 3.10).
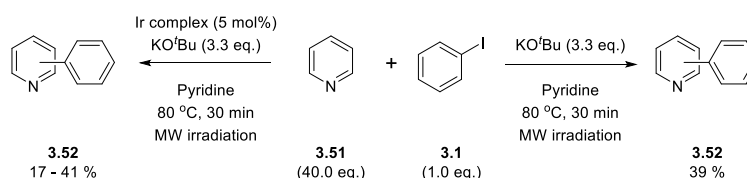
Scheme 3.10: Microwave-assisted arylation of heteroarenes as demonstrated by Itami *et al.*[1]

To probe this unusual reactivity, the group sought to optimise the reaction conditions in a bid to improve the overall yield of the reaction. To eliminate the formation of regioisomers, they chose pyrazine as their heterocyclic substrate for this series of reactions. The coupling of pyrazine **3.53** with iodobenzene **3.1** was observed to proceed in almost quantitative yield under microwave irradiation. In addition to this, excellent reactivity could be achieved using solely thermal reaction conditions for the same transformation, albeit a longer reaction time of 13 hours was required (Scheme 3.11). Substituting iodobenzene for bromobenzene led to a decreased yield of 54 %, while chloro- and fluorobenzene afforded phenylpyrazine **3.54** in less than 1 %.
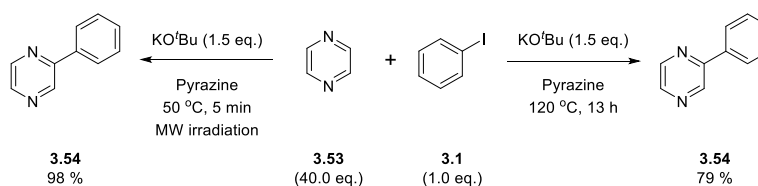
Scheme 3.11: Arylation of pyrazine under both microwave irradiation and thermal heating.[1]

With regards to the mechanism of this transformation, Itami suggested that the underlying pathway must be radical-based; his proposal was that either a homolytic aromatic substitution[37] or an $S_{RN}1$ reaction[38] was active under these conditions. Seeking experimental support for a radical-mediated mechanism, they added a number of known radical scavengers to their reaction mixtures. It was noted that the yield decreased from 98 % in the absence of scavenger to less than 1 % in the presence of galvinoxyl, 2,2,6,6-tetramethylpiperidine-1-oxyl (TEMPO) and acrylonitrile.

Within two years of this initial finding, three independent research groups published work detailing the ability of certain additives to promote the same reactivity observed by Itami.[39-41] Looking firstly at the work of Hayashi[39] and Shi,[40] both groups investigated the ability of 1,10-phenanthroline **3.57** and a number of related derivatives, in the presence of *tert*-butoxide salts (either potassium or sodium), to

promote the coupling of haloarenes with benzene. Hayashi *et al.* observed that using sodium *tert*-butoxide afforded the coupled product **3.16** in greater yield; however it should be noted that a comparable yield was obtained using potassium *tert*-butoxide (67 % versus 72 %).[39] This difference in yield was attributed to competition between the radical pathway and a benzyne mechanism, which led to the generation of *meta*- and *para*-(*tert*-butoxy)toluene as side products. Within this work, it was demonstrated that the additives 1,10-phenanthroline **3.57** and 4,7-diphenyl-1,10-phenanthroline **3.60** afforded the greatest yield of the desired product (72 % and 82 % respectively). Looking at the remaining derivatives tested, we see that 1,7-phenanthroline **3.58** and 4,7-phenanthroline **3.59** were both extremely ineffective at promoting this chemistry. Slightly improved, but nevertheless poor reactivity was observed for 2,9-diphenyl-1,10-phenanthroline **3.61** and 4,7-dimethyl-1,10-phenanthroline **3.62**.
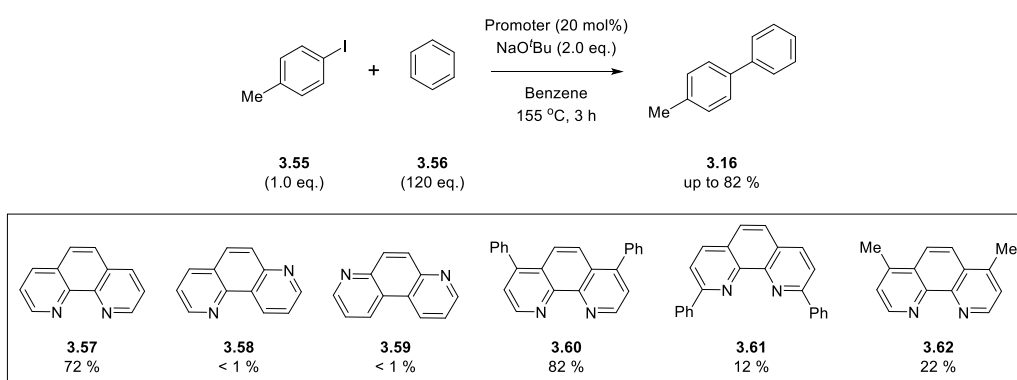
Scheme 3.12: Transition metal-free biaryl coupling reaction promoted by various phenanthroline derivatives performed by Hayashi *et al.*[39]

At around the same time, research probing the efficiency of a similar set of phenanthroline derivatives emerged from Shi and co-workers, who looked at 6-nitro-1,10-phenanthroline **3.65** and 2,9-dimethyl-1,10-phenanthroline **3.66** in addition to phenanthrolines **3.57** and **3.60**.[40] In this instance, the base utilised was potassium *tert*-butoxide and the haloarene used was 4-bromoanisole **3.63** (Scheme 3.13). As was observed by Hayashi *et al.*, phenanthrolines **3.57** and **3.60** produced the greatest reactivity (87 % and 92 % respectively). Interestingly, using 2,9-dimethyl-1,10-phenanthroline **3.66** as the additive led to the coupled product **3.64** being formed in 59 % yield, despite the equivalent diphenyl derivative **3.61** previously being a poor

promoter of this chemistry. The nitro-substituted derivative **3.65** was the least effective of the species tested, with no coupling observed when using this additive.
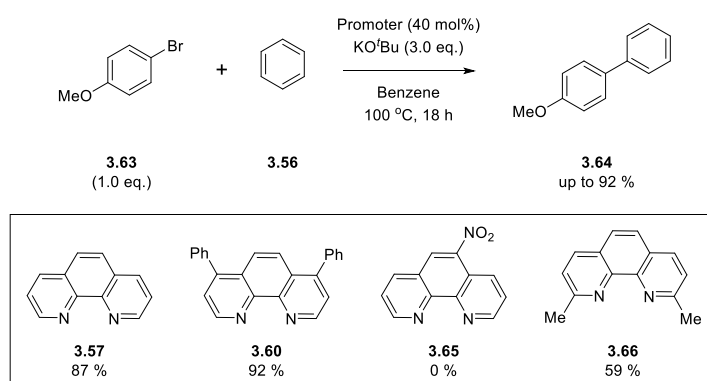
Scheme 3.13: Transition metal-free biaryl coupling reaction promoted by various phenanthroline derivatives performed by Shi *et al.*[40]

Within these first two pieces of work, reference is made to the work of Lei *et al.*, who used *N,N'*-dimethylethylenediamine (DMEDA) **3.67** and some structurally-related compounds to effect similar coupling reactions (Scheme 3.14).[41] In his work, Lei used 4-iodotoluene **3.55** as his substrate, and was capable of producing the coupled product **3.16** at a temperature of only 80 $^{\circ}$C, which is lower than those used by Hayashi and Shi (155 $^{\circ}$C and 100 $^{\circ}$C respectively). The importance of the potassium cations in this transformation was demonstrated through the addition of 18-crown-6 to the reaction mixture, which produced a significantly decreased yield of 15 %. Additionally, a benzyne-mediated pathway under these reaction conditions was ruled out due to the absence of regioisomers when using substituted haloarenes such as **3.55**. In agreement with prior studies, Lei concluded that a radical mechanism must be responsible for the observed reactivity on the grounds of reactivity being shut down by addition of radical scavengers.
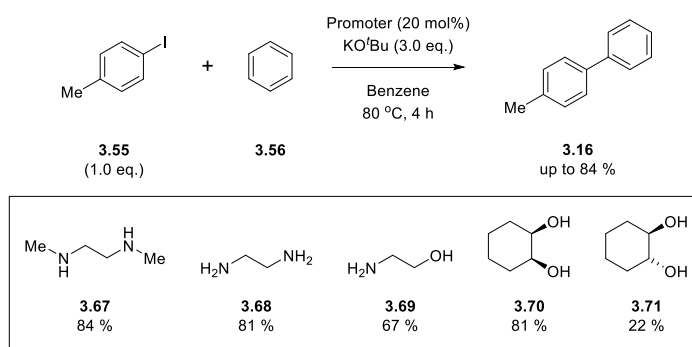
Scheme 3.14: Simple diamines, diols and aminoalcohols capable of promoting transition metal-free coupling reactions.[41]

Regarding a potential mechanism for these reactions, two tentative proposals came from the works of Hayashi and Shi (Scheme 3.15).[39, 40] Firstly, the proposal of Hayashi *et al.* involves **3.72**, the chelate complex of sodium *tert*-butoxide with 1,10-phenanthroline (or any other bidentate additive such as DMEDA), acting as an electron donor to reduce the haloarene **3.73** (Scheme 3.15a). The alternative proposal of Shi *et al.* is that a benzene C—H bond is activated through interaction with 1,10-phenanthroline and potassium *tert*-butoxide prior to reaction (Scheme 3.15b).
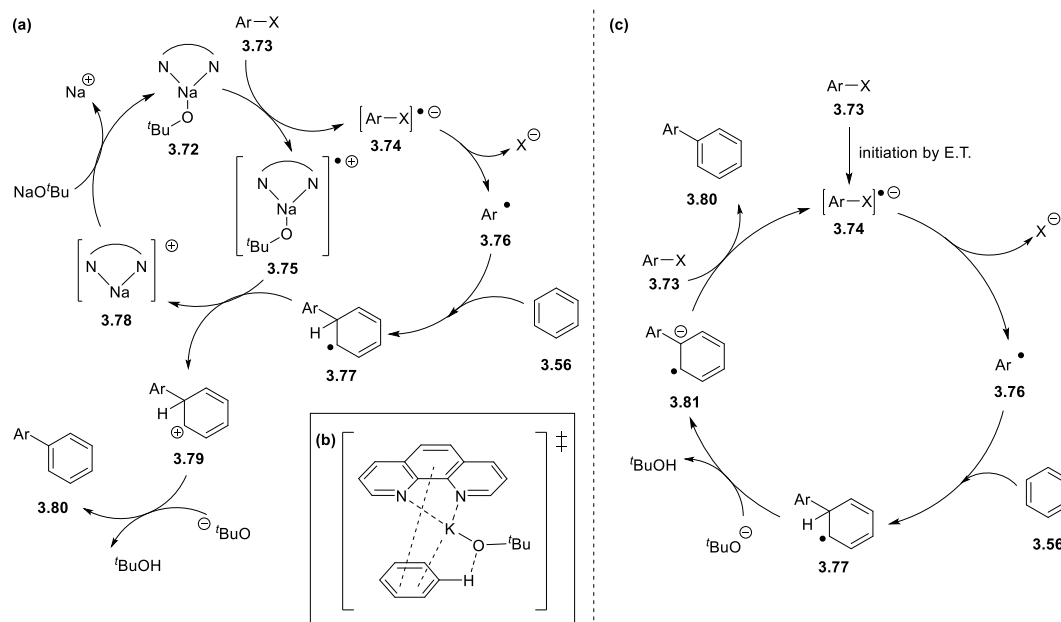
Scheme 3.15: (a) Mechanism proposed by Hayashi *et al.* to explain observed reactivity;[39] (b) benzene C—H bond activation model proposed by Shi *et al.*;[40] (c) BHAS mechanism proposed by Studer and Curran to be active in these transformations.[2]

In light of these publications, an essay from Curran and Studer provided an insightful perspective on the transformations described therein.[2] Based on the evidence

available from these early works [H/D isotope effects; effect of radical inhibitors; intramolecular cyclisations], they agreed with previous hypotheses that the reactions did indeed proceed via a radical pathway. One disagreement they held, however, was in relation to the mechanism proposed by Hayashi *et al.* (Scheme 3.15a),[39] which is not representative of a radical chain reaction. Two steps within this proposal were deemed to be problematic, the first of which is the reduction of **3.75** by **3.77**. This is due to the low probability of these two species reacting as a result of their respective low concentration. The second problem in this proposal is the reduction of **3.73** by **3.72**, which is expected to be a highly endothermic process. A counter-proposal for the mechanism active in these reactions, termed the base-promoted homolytic aromatic substitution (BHAS), proceeds following a clear initiation step and is a cyclic pathway, thus meeting the requirements of a radical chain process (Scheme 3.15c).

In the years that followed, publications from a number of independent research groups demonstrated the ability of a number of simple organic molecules to effectively promote these transition metal-free coupling reactions (Scheme 3.16). [42-50] These range from small organic molecules such as amino acids (**3.87**, **3.88**),[47] diamines (**3.89**, **3.90**)[48, 49] and diols (**3.86**)[46] to heterocyclic derivatives (**3.82**, **3.84**),[42, 44] alkaloids (**3.83**),[43] carbene precursor salts (**3.85**)[45] and porphyrin derivatives (**3.91**-**3.94**),[50] all of which have been shown to afford biaryl coupling in good-to-excellent yield.
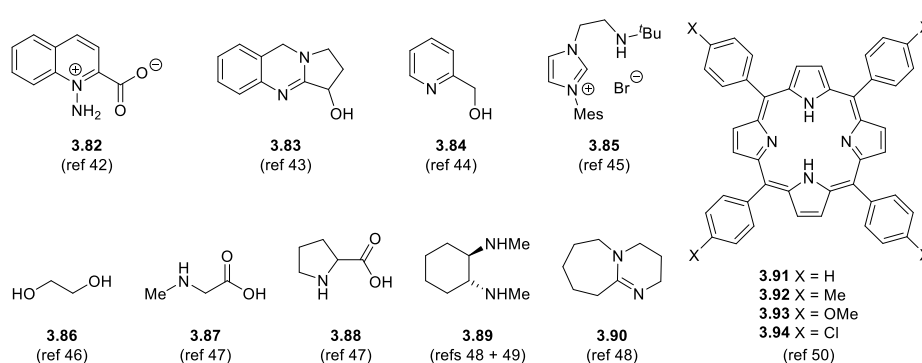
Scheme 3.16: A selection of organic additives currently known to promote transition metal-free coupling reactions under various reaction conditions.[42-50]

The work of Kwong *et al.*[46] showed that vicinal diols such as **3.86** and **3.70** work most effectively in promoting the intramolecular coupling of aryl chloride **3.95**, furnishing the desired product **3.96** in quantitative yield (Scheme 3.17). Interestingly, nitrogen-

containing compounds such as 1,10-phenanthroline **3.57**, DMEDA **3.67** and *trans*-cyclohexane-1,2-diamine **3.97** were significantly less effective under the reaction conditions employed, with yields no greater than 10 % obtained using these additives. For the linear diols, it was noted that extending the carbon chain length was detrimental to the efficiency of the coupling, with yields of 48 and 34 % obtained from propane-1,3-diol **3.98** and butane-1,4-diol **3.99** respectively (Scheme 3.17). In this work, the superior reactivity of diols **3.70** and **3.86** is credited to the potential of their corresponding anions to coordinate a potassium counter ion, although it would be expected that anions of diamines **3.67** and **3.97** would be equally able to fulfil this same role.
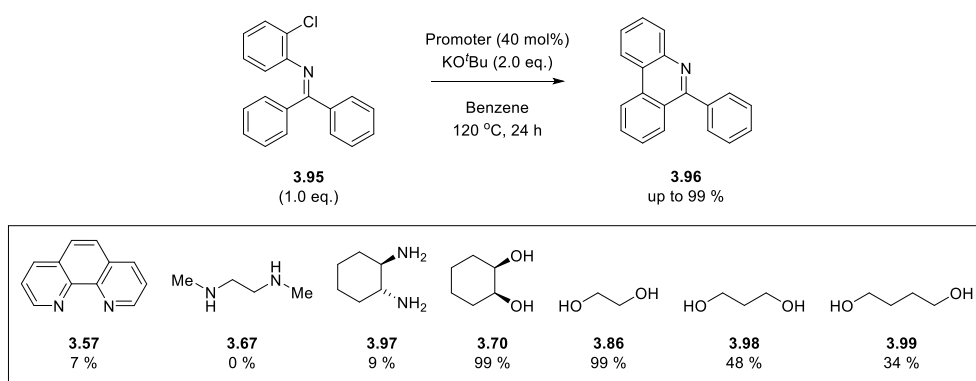
Scheme 3.17: Efficiency of various organic additives to promote the synthesis of phenanthridines by an intramolecular transition metal-free cross-coupling reaction.[46]

A number of amino acids were shown to be capable of promoting biaryl coupling reactions by the research group of Tanimori.[47] The most effective of these were sarcosine **3.87** and proline **3.88**, which afforded 4-methoxybiphenyl **3.64** in 80 % and 87 % yield respectively (Scheme 3.18). Moderate reactivity was also observed for pipecolic acid **3.101**, 2-phenylglycine **3.103** and leucine **3.104** (Scheme 3.18). Interestingly, the addition of a hydroxyl group to the 4-position of proline (**3.102**) led to a lower yield, and similarly the addition of a second methyl group to sarcosine (**3.106**) also furnished a lower yield of coupled product. Curiously, two interesting results from this research failed to be sufficiently explained. The first of these was the blank reaction, run in the absence of an amino acid additive with potassium *tert*-butoxide as the base, which produced 4-methoxybiphenyl **3.64** in 35 % yield. This result hints towards the existence of a less efficient competing reaction pathway,

which operates in the absence of an effective additive such as sarcosine **3.87**. The second result of interest here is the use of valine **3.105** as an additive which, despite its structural similarity to leucine **3.104**, affords the coupled product in only 6 % yield. Of the additives tested under the optimised reaction conditions, only valine **3.105** failed to produce greater reactivity than the blank reaction.
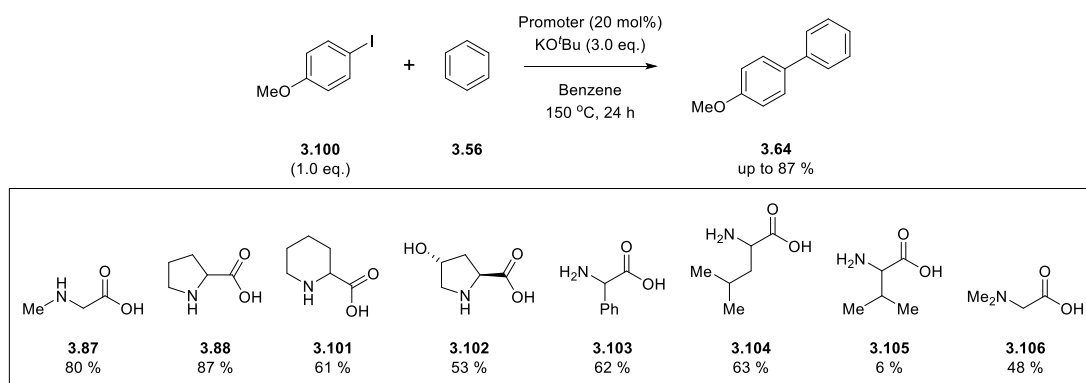
Scheme 3.18: Efficiency of various amino acids to promote transition metal-free cross-coupling reactions.[47]

The application of heterocyclic derivatives to effect these transformations was the focus of work performed by Jiang,[42] Kumar,[43] Kwong[44] and Chen.[45] The earliest of these looked at a number of substrates designed specifically to promote these transition metal-free coupling reactions.[42] The abilities of a number of zwitterionic compounds (**3.82**, **3.107**-**3.110**) to promote this chemistry were compared with proline **3.88**, which gave a reasonably good yield of 67 % under the conditions employed (Scheme 3.19). Of the additives tested, **3.82** produced the greatest yield, while **3.107** was least effective. The use of a low reaction temperature eliminates the possibility of a competing benzyne-mediated pathway, highlighted by the reaction run in the absence of additive yielding no coupled product. With this in mind, each of these five compounds must therefore be capable of initiating the radical pathways, despite showing different levels of efficiency at doing so.
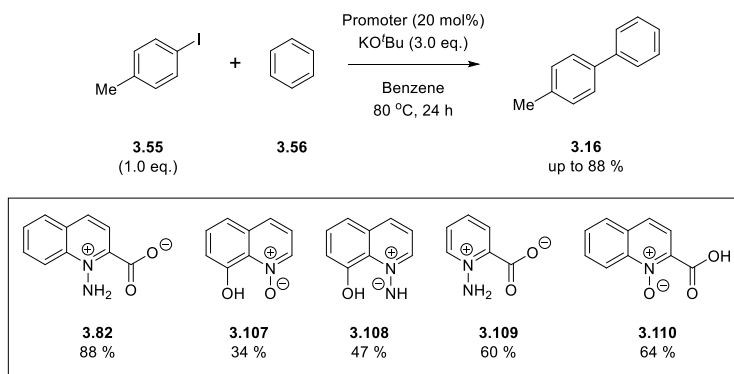
Scheme 3.19: Zwitterionic compounds and their relative abilities to promote transition metal-free coupling reactions.[42]

Chen and Ong demonstrated the ability of the *N*-heterocyclic carbene (NHC) **3.111** and its corresponding precursor salt **3.85** to effect the same coupling reaction in respective yields of 78 % and 74 % (Scheme 3.20).[45] In their study, they also showed the inability of weaker bases such as sodium *tert*-butoxide and potassium carbonate to produce coupling efficiency on par with that observed when using potassium *tert*-butoxide. The use of more sterically hindered NHC's such as **3.112** and **3.113** was also found to be detrimental to this chemistry (Scheme 3.20).
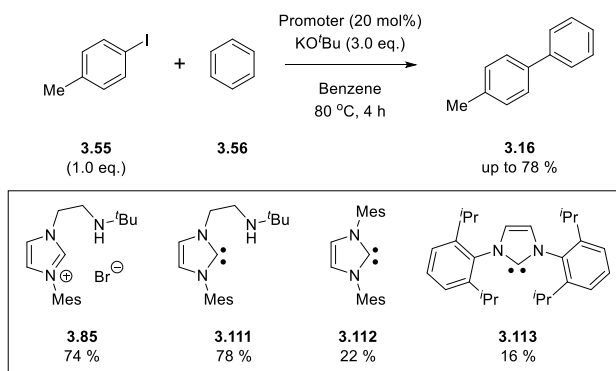
Scheme 3.20: Relative abilities of a number of NHC's and their precursor salts to promote transition metal-free biaryl coupling reactions.[45]

Vasicine **3.83**, a quinazoline alkaloid isolated from the plant *Adhatoda vasica*, is another substrate capable of promoting the coupling of iodoarenes with arenes.[43] Kumar *et al.* have recently shown that this compound and the structurally-related vasicinone **3.114** are both able to initiate radical coupling reactions in the presence of potassium *tert*-butoxide at elevated temperatures (Scheme 3.21). In addition to these two species, a variety of other natural compounds **3.115**-**3.118** were tested for

reactivity under the same reaction conditions; however the best of these four compounds produced the coupled product in only 32 % yield (Scheme 3.21).
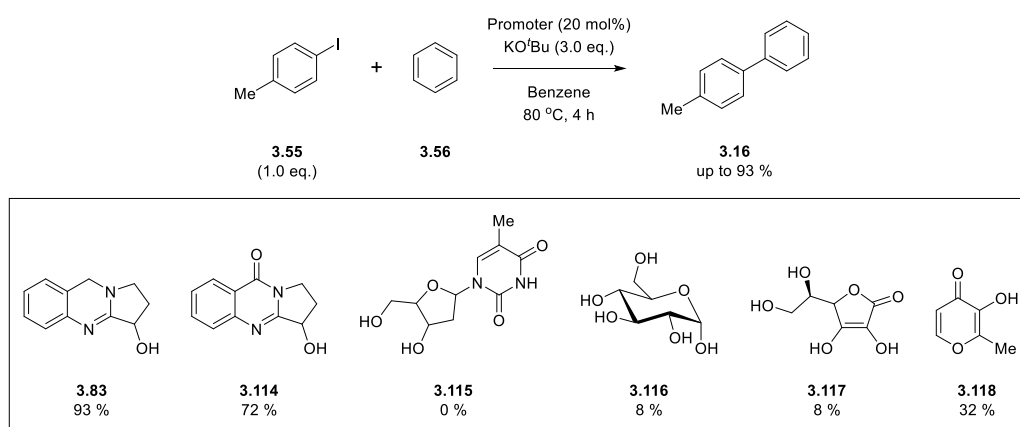
Scheme 3.21: The relative abilities of a number of natural compounds to promote transition metal-free biaryl coupling reactions.[43]

Some larger organic molecules have also been used as promoters of this chemistry. Ng *et al.* have used functionalised porphyrins to effect the coupling of aryl iodides and, to a lesser extent, aryl bromides with benzene.[50] These reactions were performed at a significantly high temperature, and required a large excess of base (potassium hydroxide) and *tert*-butanol, however there was no requirement for an inert atmosphere. Porphyrins **3.91**-**3.94** all produced similar yields, indicating that the different substitutions have minimal effect on the reactivity (Scheme 3.22). It is also worth noting that by testing all four porphyrins over different reaction times (10 – 15 hours), comparability might be limited.

Porphyrin	X	Reaction Time (h)	Yield (%)
3.91	H	14	78
3.92	Me	10	75
3.93	OMe	15	75
3.94	Cl	14	76
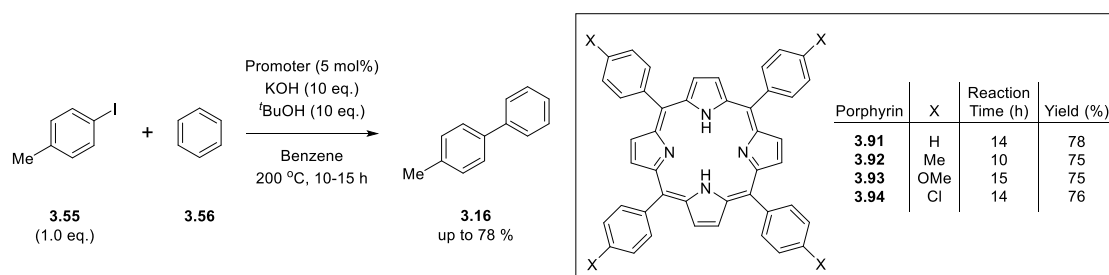
Scheme 3.22: Porphyrin derivatives as promoters of transition metal-free biaryl coupling reactions.[50]

When potassium *tert*-butoxide was used instead of potassium hydroxide, a yield of only 17 % of the coupling product was obtained, with 33 % and 31 % yields obtained for *meta*- and *para*-(*tert*-butoxy)toluene respectively. Based on the reaction

conditions, it would be expected that lowering the reaction temperature when using potassium *tert*-butoxide as the base would lead to a greater yield of the desired coupling product; however such an investigation was not performed in this particular study.

The transition metal-free cross coupling of aryl bromides has been demonstrated in the presence of a number of organic additives already, and another such additive shown to efficiently promote this coupling reaction is 2-pyridyl carbinol **3.84**, as Kwong *et al.* have recently demonstrated (Scheme 3.23).[44] In addition to **3.84**, structurally-related compounds **3.119** and **3.120** were also tested under identical reaction conditions. However neither was capable of producing the desired reactivity (Scheme 3.23). They found that the desired coupling reaction could be performed in excellent yield using only 10 mol% of **3.84** rather than 40 mol%. Also, other bases such as sodium *tert*-butoxide and potassium carbonate were found to be ineffective. Further to their standard reaction conditions, it was also demonstrated that by using a greater amount of additive and extending the reaction time from 24 to 72 hours, moderate yields could be obtained when performing the reaction at room temperature.
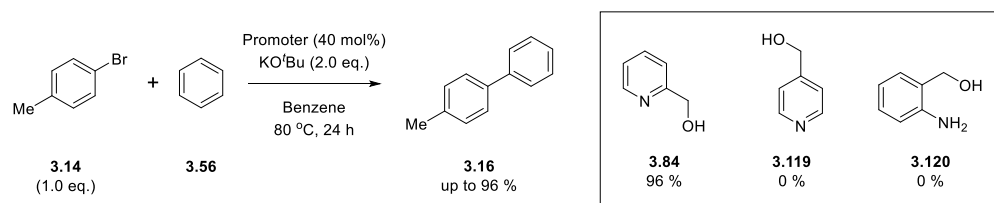
Scheme 3.23: Comparison of the relative abilities of pyridyl carbinols and related compounds to promote transition metal-free biaryl coupling reactions.[44]

Returning to the additive-free reactions published in the seminal work of Itami, the group of Charette developed and applied similar conditions to promote the intramolecular biaryl coupling of derivatives such as **3.121**.[51] Their initial experiments used an iron(II) catalyst in the presence of a diamine ligand and strong base in benzene as solvent, which afforded only moderate yields of the desired product **3.122** along with small amounts of the reduced starting material **3.123** (Scheme 3.24a). Switching the solvent to pyridine produced a significant increase in reactivity, which didn't drop in the absence of the iron catalyst. Furthermore, carrying out the reaction in the

absence of both the iron catalyst and a diamine furnished the desired product in a reasonable yield of 50 % along with an increased quantity of **3.123** (Scheme 3.24b).
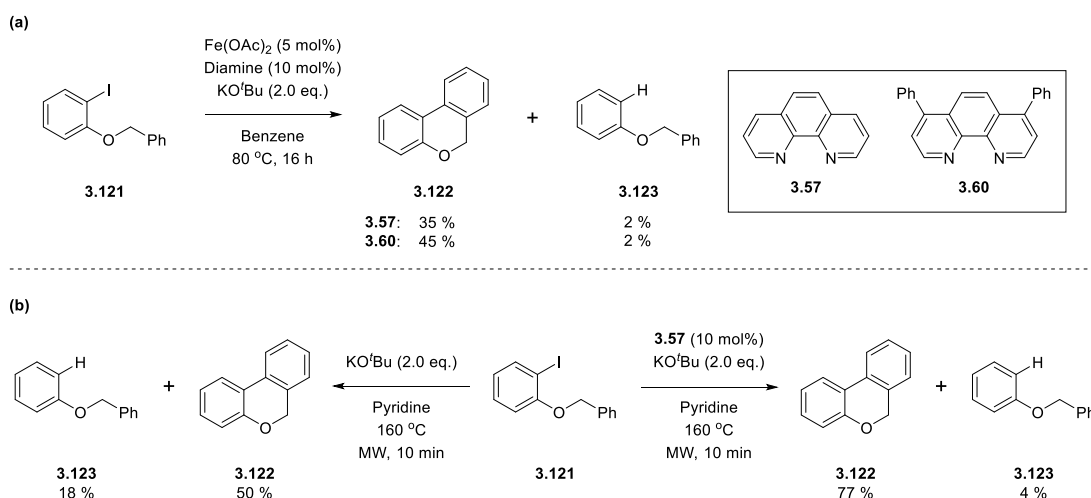
Scheme 3.24: (a) Intramolecular biaryl coupling reaction investigated by Charette *et al.* illustrated using the test substrate **3.121**; (b) comparison of reactivities in pyridine in the presence and absence of a diamine ligand, using **3.57** as an example.[51]

Expanding on their test substrate, it was found that substrates incorporating a substituted nitrogen in the tether rather than an oxygen, or indeed an entirely carbon-based tether, were also compatible with the microwave-assisted conditions. Similarly, a selection of aryl bromides could be coupled in yields greater than 70 %. An interesting observation from this study was the formation of regioisomers when using a substituted benzyl moiety such as **3.124** (Scheme 3.25a). When substrates of this type were reacted, there was significant preference for the formation of isomer **3.125** relative to **3.126**. When substrate **3.127** was used, however, this selectivity diminished and in fact showed a slight preference for the opposite regioisomer **3.129**. Based on these observations, a mechanism was proposed involving the formation of the spirocyclohexadienyl radical intermediate **3.131** (Scheme 3.25b). From this intermediate, two pathways were identified as possible routes towards the regioisomers. The first of these involves a ring expansion of **3.131**, affording the intermediate **3.132** which, upon rearomatisation, would then produce the observed major product **3.125**. This pathway involves the attack of a saturated carbon by the radical in a 6-endo-Tet reaction, which is disfavoured in accordance with Baldwin's rules.[52] In support of this proposal, Charette cites the work of Nanni.[53] However, the

ring expansion discussed in their research results from the attack of the radical centre onto a C—C double bond, a favourable 6-endo-Trig reaction, and therefore does not sufficiently support this pathway. An alternative mechanism must therefore be responsible for the formation of **3.125**. The second pathway involves the formation of the fused cyclic radical **3.133** which, following a neophyl rearrangement and subsequent rearomatisation, affords the observed minor product **3.126**.
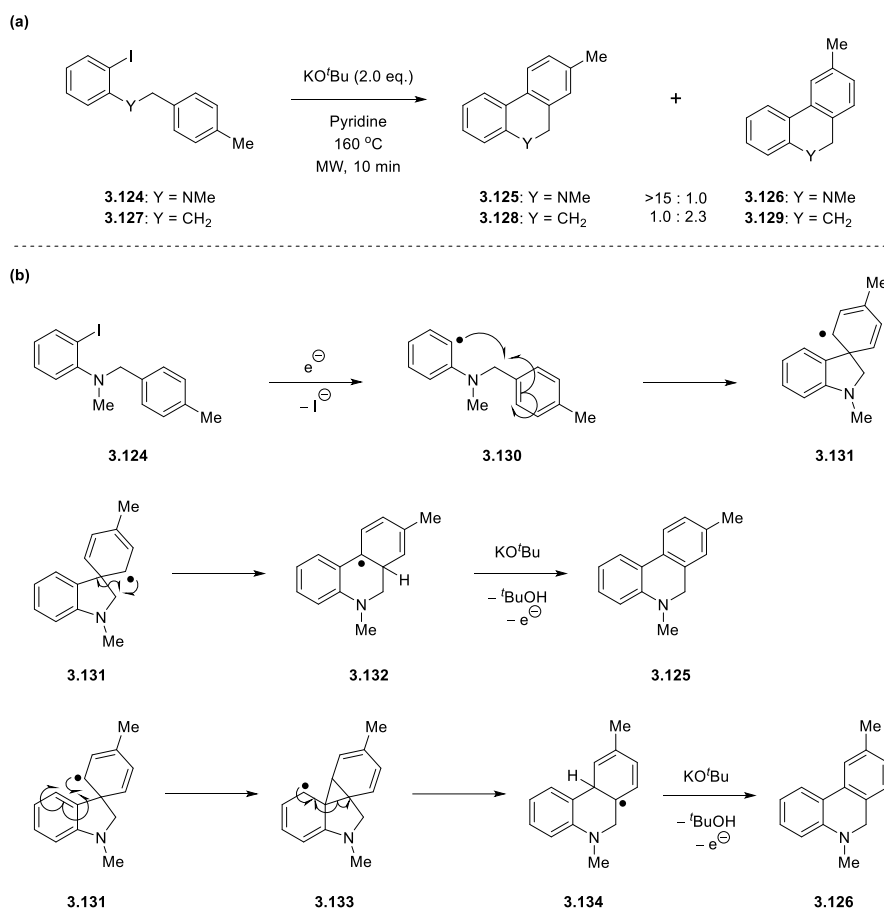
Scheme 3.25: (a) Opposing regioselectivity observed by Charette *et al.* when reacting substrates **3.124** and **3.127**; (b) mechanisms proposed to rationalise the observed regioselectivity.[51]

A number of recent articles from various different research groups have detailed the observation of useful chemical reactivity from similarly additive-free reaction conditions in solvents other than pyridine. For example, publications from two independent research groups have emerged where the combination of *N,N*-dimethylformamide (DMF) and potassium *tert*-butoxide has given rise to coupling chemistry.[54-56] Within these articles, two different modes of activity are proposed for this same combination of reagents. The articles from the group of Ming Yan[54, 55]

propose that the carbamoyl anion **3.136** is formed by deprotonation of DMF **3.135**, and that this donates an electron to a second equivalent of DMF. The resulting carbamoyl radical **3.138** is proposed to be responsible for the observed reactivity through a number of hydrogen atom abstractions (Scheme 3.26).
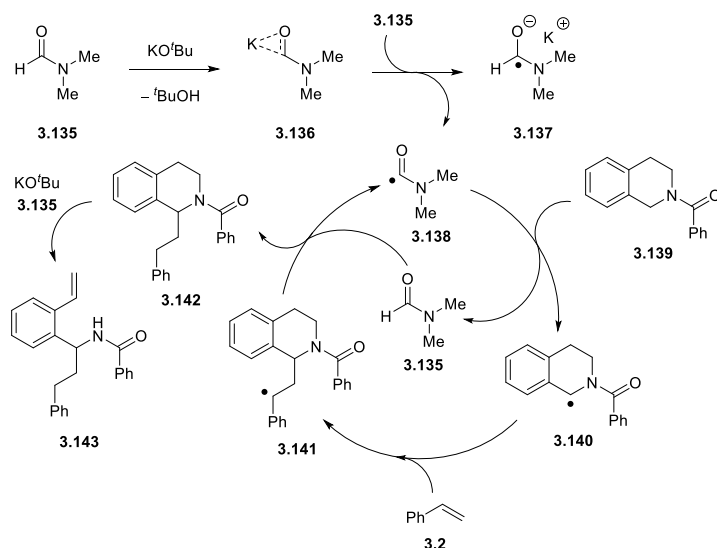
Scheme 3.26: Proposed mechanism by which DMF promotes the addition of amides to arylalkenes as demonstrated by Yan *et al.*[55]

The work of Taillefer[56] proposes a similar starting point, with the formation of the carbamoyl anion **3.144** as a stabilised complex with the potassium cation and *tert*-butanol. This species then donates an electron to the iodobenzene **3.1**. The phenyl radical **3.145** forms following dissociation of the corresponding radical anion and initiates an $S_{RN}1$ reaction mechanism to form the coupled product **3.149** (Scheme 3.27).
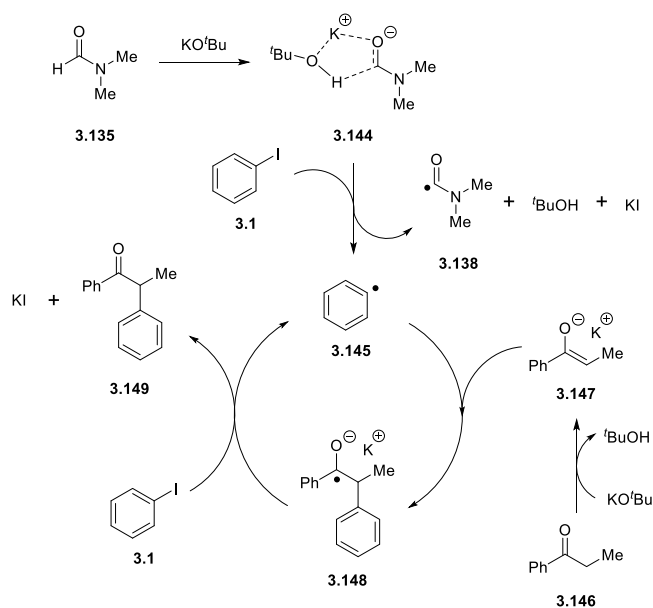
Scheme 3.27: Mechanism proposed by Taillefer *et al.* to explain the arylation of aryl ketones via an $S_{RN}1$ reaction.[56]

Throughout the literature related to this chemistry, the term "organocatalysis" arises on numerous occasions. However, it has been demonstrated that the additives themselves are not catalysing these coupling reactions. Instead, evidence suggests that the additives promote these coupling reactions by initiating a BHAS or an $S_{RN}1$ reaction mechanism following an electron transfer. Recently, Studer and Curran proposed an alternative way of looking at these reactions, whereby the electron itself can be considered to behave as a catalyst.[57] To illustrate this, both the BHAS and $S_{RN}1$ reaction cycles can be redrawn as per Scheme 3.28 to incorporate the electron more explicitly. The mechanistic viewpoint shown isn't restricted to these two examples, but can be extended to look at other reactions such as radical Heck-type arylations,[58] cross-dehydrogenative coupling reactions[59] and the alkoxycarbonylation of aryl halides.[60]
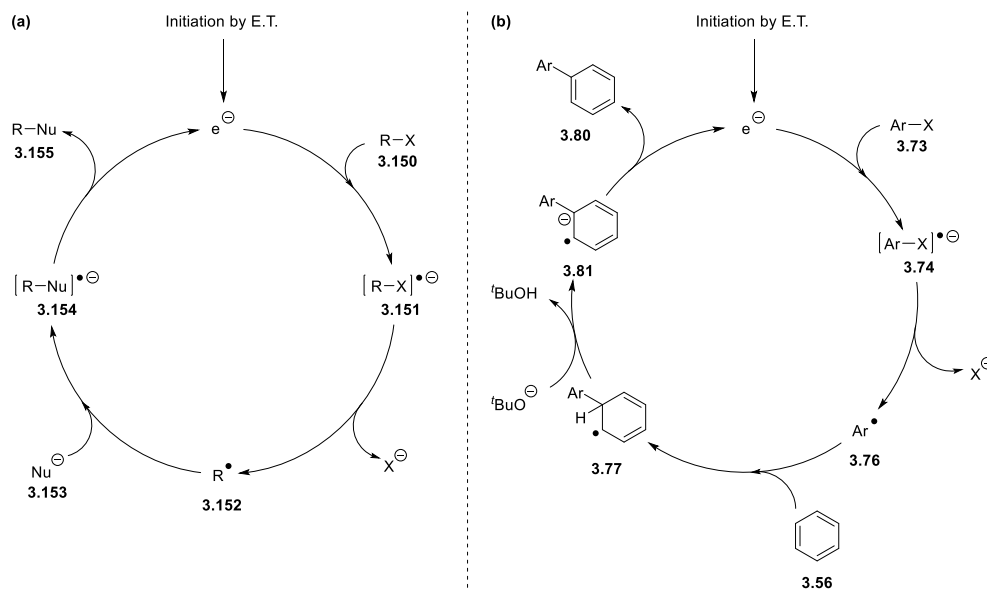
Scheme 3.28: Representations of (a) the $S_{RN}1$ mechanism and (b) the BHAS mechanism where the electron can be portrayed to behave as a catalyst.[57]

An alternative chemistry that requires less harsh reaction conditions is photoredox catalysis.[61] This chemistry has previously been used in order to perform C—C bond formations via reductive pathways, using aryl, alkyl and alkenyl iodides[62] and arenediazonium salts[63] as precursors. Similar to the coupling chemistry already discussed, there is an interest in performing this type of chemistry in the absence of transition metal-based catalysts.

3.4 Transition Metal-Free Coupling Reactions Initiated by Organic Photoredox Chemistry

Since 2010, a number of research groups have focussed on the optimisation of chemical transformations mediated through the use of organic photocatalysts in place of traditional transition metal photocatalysts.[64-73] The commonly encountered organic species are organic dyes such as eosin Y **3.156**,[64] perylenes **3.157**[68] and the 9-mesityl-10-methylacridinium ion **3.158** (Scheme 3.29).[69]
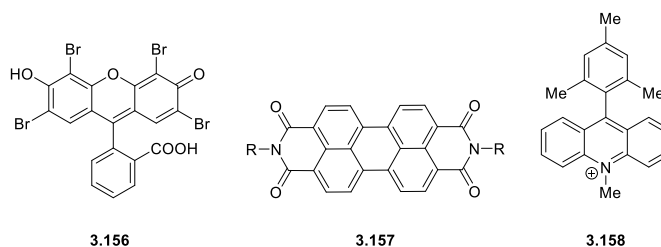
Scheme 3.29: Chemical structures of commonly encountered organic photoredox catalysts.[64, 68, 69]

The earliest demonstration of an organic dye being used to mediate the formation of a C—C bond came in 2010, when the group of König photocatalytically α-alkylated aliphatic aldehydes using eosin Y **3.156** under 530 nm LED irradiation (Scheme 3.30).[64] In addition to achieving good-to-excellent yields, by using the imidazolidinone organocatalyst **3.161** developed by Macmillan *et al.*[74] they were also able to perform the reaction with enantioselectivities of 76 % or greater.
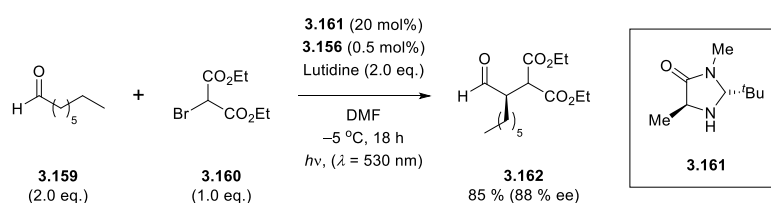
Scheme 3.30: Enantioselective α-alkylation of aliphatic aldehydes by eosin Y photocatalysis.[64]

The König group proceeded to use this same organic photocatalyst to perform the α-amino functionalisation of tetrahydroisoquinolines such as **3.163**, where C—C and C—P bonds could be constructed (Scheme 3.31a).[65] As before, the reactions proceed in excellent yield under mild conditions, and represent alternative pathways to reactions previously requiring transition metal photocatalysts.[74] Based on observations in this work, and on the mechanism of related transition-metal mediated processes, they proposed a potential mechanism for these reactions (Scheme 3.31b). The photoexcited eosin Y **3.156*** can accept an electron from the tetrahydroisoquinoline **3.163** to generate the corresponding dye radical anion **3.168** and the tetrahydroisoquinoline radical cation **3.169**. This species is then oxidised by one of two possible pathways; through hydrogen atom abstraction by an unspecified oxidant, or loss of a proton followed by the loss of an electron, affording the reactive iminium intermediate **3.170**. Subsequent reaction of this with a nucleophile then yields the final product **3.171**.
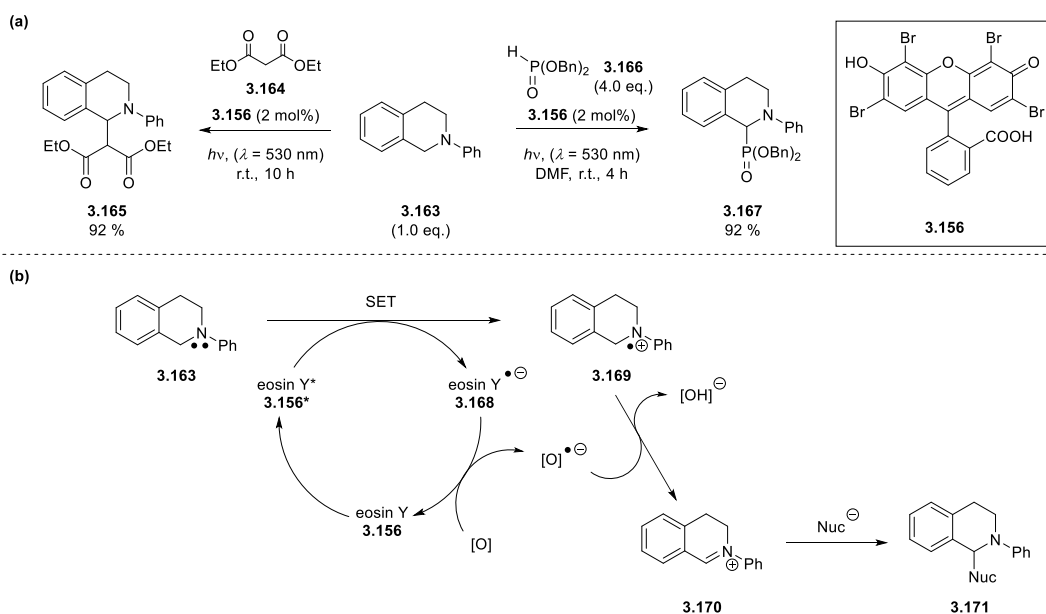
Scheme 3.31: (a) Formation of C—C and C—P bonds by organic photocatalysis using eosin Y **3.156**; (b) the proposed mechanism by which these reactions proceed.[65]

Moving away from oxidative pathways, the same organic dye has also been shown to effect reductive coupling reactions under photoirradiation when arenediazonium salts are used as substrates.[66, 67] This chemistry has been used to arylate furans, *N*-protected pyrroles and thiophenes (Scheme 3.32a),[67] as well as for the synthesis of benzothiophenes via a radical annulation reaction.[66] Whereas the photoexcited dye in previous work was behaving as an electron acceptor, here it donates an electron to the arenediazonium salt **3.175**. This dissociates to the corresponding radical **3.177** which can then attack the heteroarene at the 2-position. The radical intermediate **3.178** can now transfer an electron either to the dye radical cation **3.176**, or to another equivalent of **3.175**, with the latter of these options giving a radical propagation. The resulting cation **3.179** is subsequently deprotonated to yield the final product **3.180** (Scheme 3.32b).
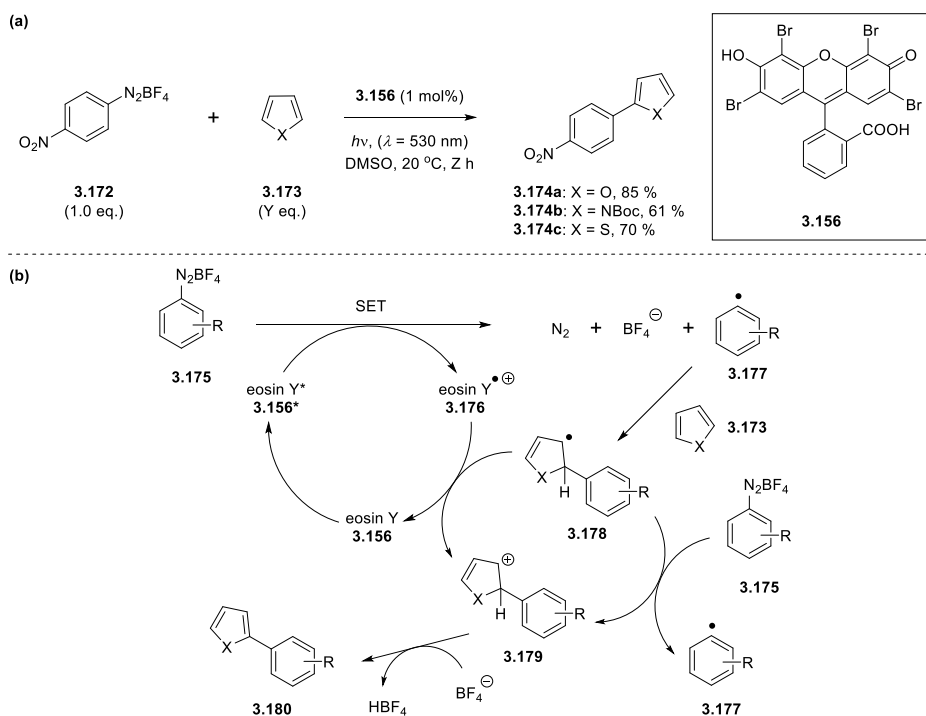
Scheme 3.32: (a) Photoarylation of heteroarenes with arenediazonium salts [Reaction conditions; X = O, Y = 10.0 eq., Z = 2 h; X = NBoc, Y = 2.0 eq., Z = 14 h; X = S, Y = 5.0 eq., Z = 4 h]; (b) proposed mechanism for this process.[67]

A more recent development from the group of König used a different organic dye, perylene-based species *N,N*-bis(2,6-diisopropylphenyl)perylene-3,4,9,10-bis(dicarboximide) (PDI) **3.184** rather than eosin Y.[68] In this work, the PDI dye is photoexcited, with the excited-state species then receiving an electron from a sacrificial amine (for example, triethylamine) to give a stable radical anion. This radical anion can subsequently be photoexcited to give a powerful reducing agent, capable of reducing a selection of electron-deficient aryl halides, including aryl chlorides. The aryl radicals formed following dissociation of the aryl halide radical anions can then be coupled with a variety of pyrrole derivatives in good-to-excellent yield (Scheme 3.33a). The double excitation discussed, and the radical process initiated following electron transfer from the photoexcited radical anion is illustrated in Scheme 3.33b.
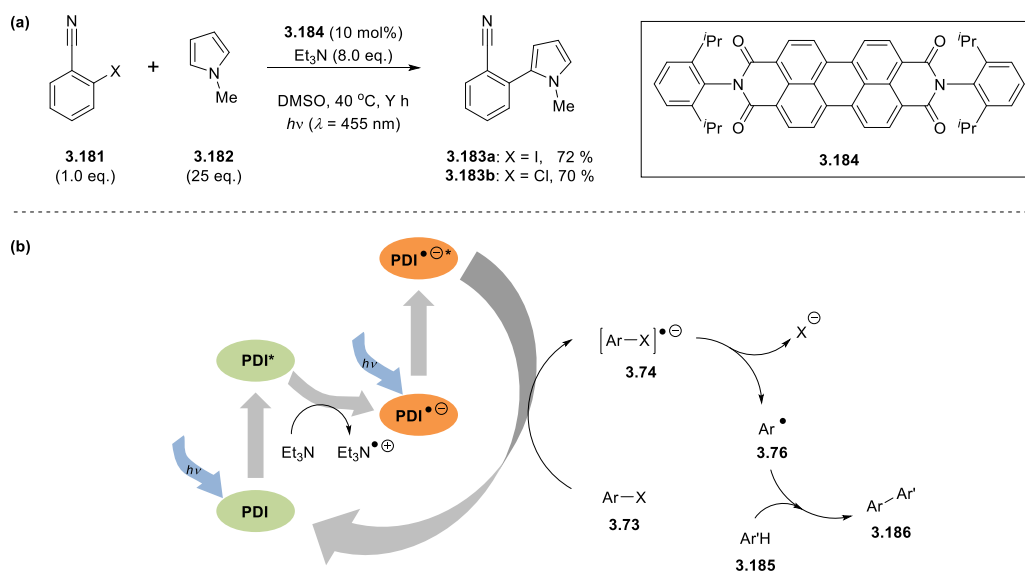
Scheme 3.33: (a) Biaryl coupling of aryl halides with *N*-methyl pyrrole promoted by photoexcited PDI **3.184**; (b) proposed mechanism for PDI-catalysed biaryl coupling reaction [Reaction conditions: X = Cl, Y = 12 h; X = I, Y = 22 h].[68]

In 2004, Fukuzumi *et al.* designed the 9-mesityl-10-methylacridinium ion **3.158** as an artificial photosynthetic reaction centre (Scheme 3.34).[69] This species is capable of forming a photoexcited electron transfer state with a significantly long lifetime, making it an ideal candidate for organic photocatalytic transformations. Research groups have since used this reagent to perform a variety of transformations, such as the oxygenation of anthracene[70] and *para*-xylene,[71] the intramolecular anti-Markovnikov hydroetherification of alkenols[75] and the trifluoromethylation of alkenes,[72] all of which have recently been collated in an excellent review by Fukuzumi and Ohkubo.[73]
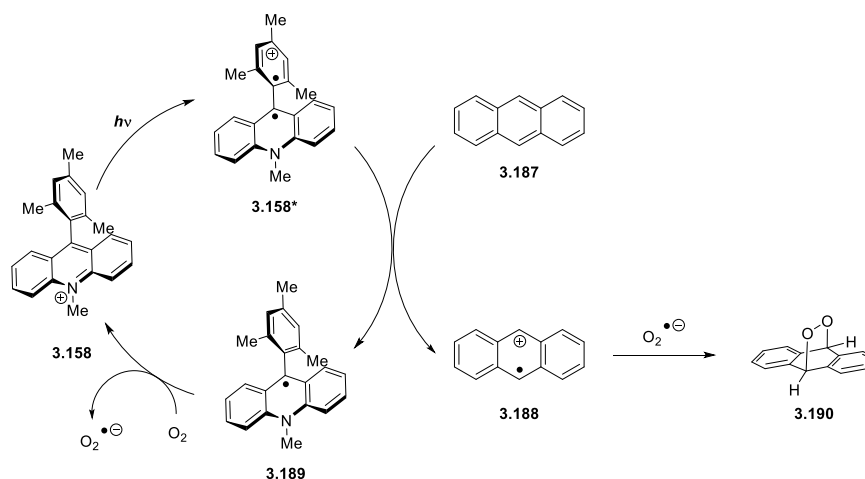
Scheme 3.34: Reaction mechanism for the oxygenation of anthracene catalysed by the 9-mesityl-10-methylacridinium ion photocatalyst **3.158**.[70]

The mechanism for these transformations is summarised in Scheme 3.34, using the oxygenation of anthracene as an example.[70] Photoexcitation of **3.158** produces the highly-oxidising triplet species **3.158*** which receives an electron from anthracene **3.187** to form **3.189** and the corresponding substrate radical cation **3.188**. These transformations are performed in the presence of oxygen, which then receives an electron from **3.189** to form its corresponding radical anion and regenerate **3.158**. This radical anion can then react with the radical cation **3.188** to yield the product **3.190**.

3.5 The Role of Combined Theoretical and Experimental Studies to Enhance Mechanistic Understanding

The continuing evolution of computational hardware, along with both the availability and improvement of chemical modelling software, has allowed for computational and experimental chemistry to co-exist in a synergic manner. Indeed, within our own research group we have previously used such combined approaches to predict, rationalise and support chemical outcomes for a diverse range of chemistries.[76-78] Within the wider literature there are a number of insightful articles outlining how combined approaches towards chemical problems can be beneficial to, for example, drug discovery,[79-81] the development of new (organo)catalysts[82-87] and mechanistic understanding.[87-91] Based on the nature of the research discussed later in Chapters 5-8,

this chapter will focus on combined approaches to understanding reaction mechanisms and selectivities.

In a recent article from Córdova *et al.*, density functional theory (DFT) was used to try to understand the experimental observations from their organocatalytic synthesis of chiral phosphines such as **3.196** (Scheme 3.35a).[92] Under their optimal conditions, it was demonstrated that the desired product could be obtained with % ee values exceeding 76 % when amines **3.193** or **3.194** were employed as the organocatalyst. For their DFT studies, calculations were performed at the B3LYP/6-311+G(2d,2p) // B3LYP/6-31G(d,p) level of theory. They began with a conformational investigation of the iminium intermediate, which showed a 2.0 kcal mol^{-1} energetic preference for the *trans*-conformation **3.197** relative to the *cis*-equivalent **3.198** Scheme 3.35b). For their transition state search, a total of nine possible transition states for the stereochemistry-inducing phosphination step were investigated, demonstrating the energetic disfavour (2.1 – 5.6 kcal mol^{-1}) for attack from the shielded face of intermediates **3.197** and **3.198** relative to the unshielded face (Scheme 3.35c).
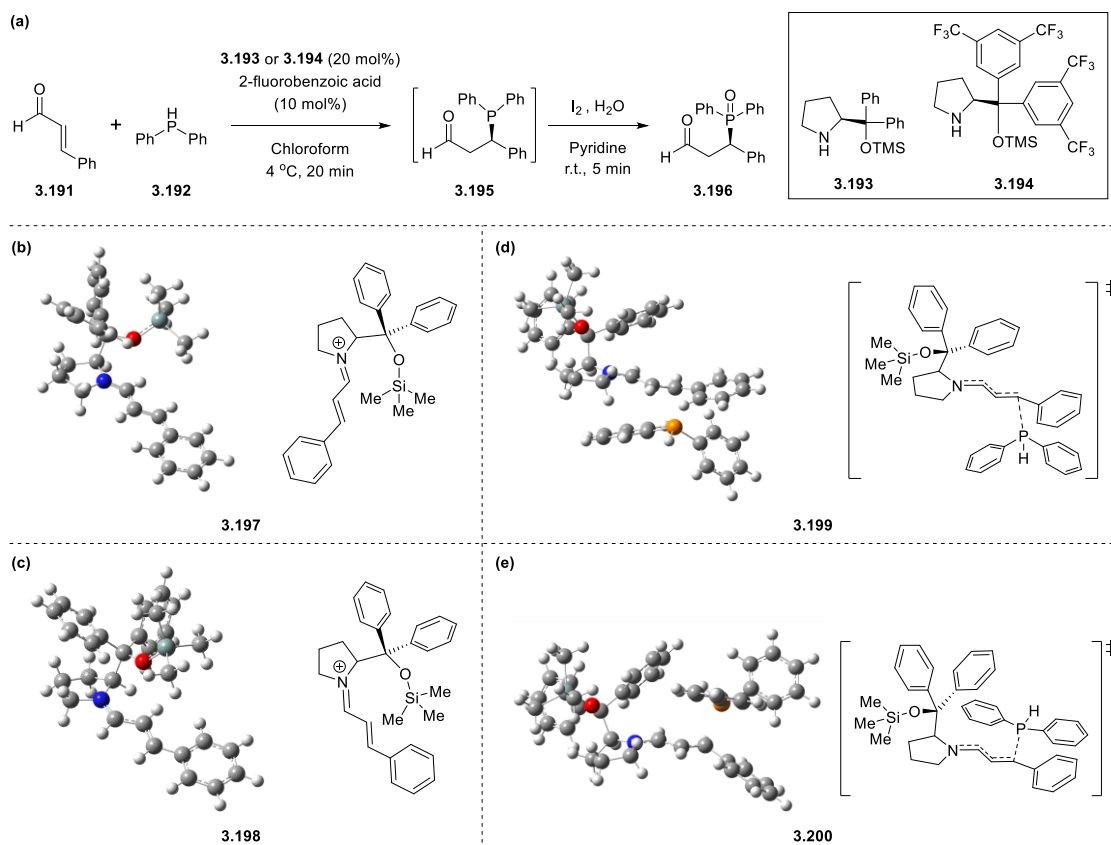
Scheme 3.35: (a) Organocatalytic synthesis of chiral phosphine **3.195** developed by Córdova *et al.*; optimised geometries of the (b) *trans-* (**3.197**) and (c) *cis-* (**3.198**) conformations of the reactive iminium intermediate; optimised transition state geometries for the phosphine attack from the (d) unshielded face **3.199** and (e) shielded face **3.200**.[92]

Still within the scope of investigating catalytic reaction mechanisms, Larhed *et al.* applied theoretical modelling to rationalise the reactivity observed in their terminal Heck arylation reactions. This reaction was then applied to generate **3.203**, a useful precursor which can be further reacted over three steps to yield the pharmaceutically-active Betaxolol **3.204** (Scheme 3.36a).[93] Following an initial investigation into their reaction conditions, those affording the greatest reactivity and selectivity were applied to a number of aryl chlorides. For their computational modelling, a number of *para*-substituted arenes (including those bearing electron-donating and electron-withdrawing groups) were studied. Optimisations were performed at the B3LYP/LANL2DZ level of theory, with a relativistic effective core potential employed for palladium. Single point energy calculations were subsequently performed using a triple-zeta basis set.
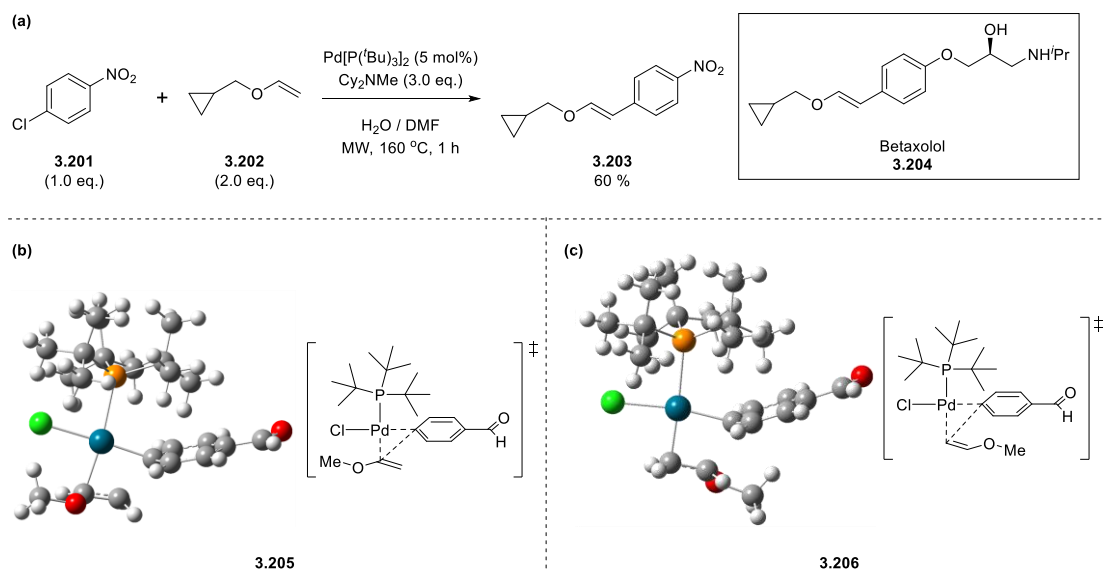
Scheme 3.36: (a) Terminal Heck arylation of 4-chloronitrobenzene **3.201** towards the Betaxolol precursor **3.203** as developed by Larhed *et al.*; optimised geometries of transition state complexes (b) **3.205** leading to the α-coupled by-product and (c) **3.206** leading to the desired β-coupled product of 4-chlorobenzaldehyde and methyl vinyl ether. [93]

When probing the origins of the regioselectivity of these reactions, they found that both steric and electronic factors were influential; an electron-withdrawing *para*-substituent on the aryl chloride increased the β-selectivity of the reaction, as did the use of a bulkier phosphine ligand. Looking firstly at the electronic factor, electron-deficient aromatic substrates led to stronger coordination between the chloride anion and the palladium centre. This was demonstrated by the difference in Pd—Cl bond strength of 5.0 kcal mol^{-1} for a complex containing 4-chlorobenzaldehyde relative to that containing the electron-rich 4-chloroanisole. With regards to the steric influence, it was noted that this will have a greater influence on the transition state towards the α-substituted product (Scheme 3.36b) relative to that leading to the desired β-substituted product (Scheme 3.36c). This effect was highlighted through comparison of the relative activation energies for a given system utilising the bulky P(^{t}Bu)$_3$ ligand and the non-bulky PH$_3$ ligand. The transition state complex of 4-chlorobenzaldehyde with the bulky phosphine ligand for the α-substitution was 3.8 kcal mol^{-1} higher in energy than the corresponding β-substitution complex, while for the non-bulky ligand complexes this energy difference was only 2.6 kcal mol^{-1}.

The group of Wang have used theory and experiment in parallel to explain the dual-activation mechanism of the cinchona alkaloid thiourea organocatalyst **3.209** (Scheme 3.37).[94] Extending on their previous experimental observations,[95] they applied NMR and DFT studies in an endeavour to probe the mechanism involved in these transformations. Computationally, optimisations were performed initially at the B3LYP/6-31G(d) level of theory in the gas phase, followed by optimisation using the 6-31G(d,p) basis set and conductor-like polarisable continuum (CPCM) solvation with the parameters for chloroform. Energetics were obtained using single point energy calculations at the B3LYP/6-31++G(d,p) level, including the previously used solvation parameters.
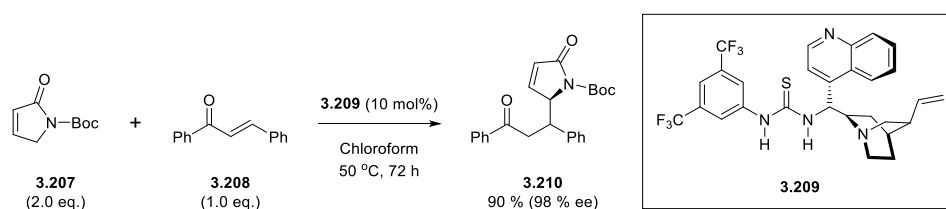
Scheme 3.37: Enantioselective vinylogous Michael addition affording **3.210** (5*R*,6*S*) catalysed by the thiourea organocatalyst **3.209**.[94, 95]

Mechanistic proposals were made by Takemoto[96] and Papai,[97] to rationalise this dual activation, which show only subtle differences when compared to the proposal of Wang. These mechanistic differences arise from the hydrogen bonding network established between the catalyst **3.209** and the two reagents **3.207** and **3.208** (Figure 3.2). The NMR studies carried out by Wang indicated that the catalyst had a greater binding affinity for the nucleophile relative to the electrophile. Based on the kinetic studies, it was predicted that the rate-determining step would be the C—C bond formation step, something later confirmed through their calculations. The calculated barrier for this bond formation, 8.8 kcal mol^{-1}, was in good agreement with the experimentally determined value of 10.2 kcal mol^{-1}. To investigate the diastereo- and enantioselectivity of their model, they calculated the three transition states leading to the potential by-products for comparison with that leading to the observed product **3.210** (5*R*,6*S*). The transition state leading to the (5*S*, 6*R*) enantiomer of **3.210** was found to be 3.9 kcal mol^{-1} higher in energy relative to that of the observed product,

while the two possible diastereomers (*5R,6R*) and (*5S,6S*) were 8.7 and 2.6 kcal mol^{-1} higher in energy respectively.
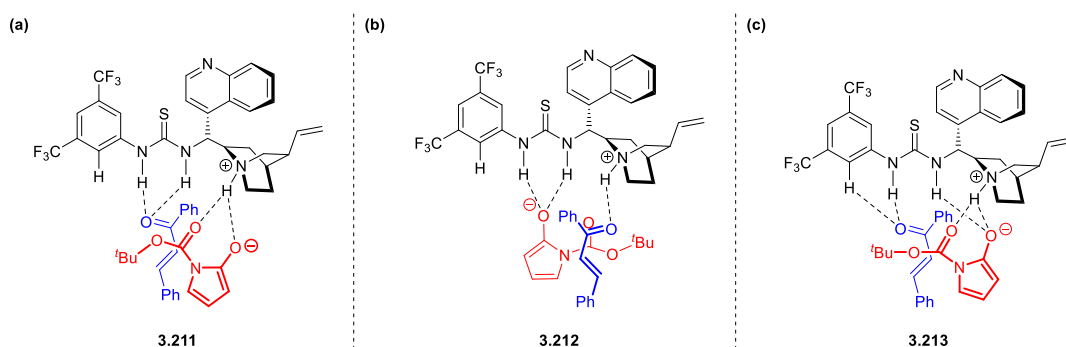
Figure 3.2: Key interactions between the thiourea organocatalyst **3.209** and reagents **3.207** and **3.208** proposed by (a) Takemoto *et al*.;[96] (b) Papai *et al*.[97] and (c) Wang *et al*.[94] to rationalise the dual-activation mechanism.

Schoenebeck *et al.* have successfully demonstrated the ability of computational investigations to design a palladium catalyst capable of performing the challenging reductive elimination of trifluoromethylated products.[98] Prior investigations into this reaction by Grushin[99] had shown that wide bite angle ligands such as Xantphos could afford the desired reactivity, while small-bite angle ligands were ineffective for this transformation.

Earlier computational studies by Schoenebeck[100] focussed on calculating the dissociation of complexes **3.214** and **3.216** to afford the desired product **3.215** (Scheme 3.38a). This initial work demonstrated that for **3.214**, both steric and electronic effects contributed favourably to give a lower activation free energy for **3.214a** (24.2 kcal mol^{-1}) relative to **3.214b** (27.6 kcal mol^{-1}). For complex **3.216**, the steric effects appear to dominate, leading to an activation free energy barrier for **3.216a** which was 5.4 kcal mol^{-1} higher than that for **3.216b**. Based on these outcomes, they proposed that the bite angle was not critical to the reactivity of the ligand, but rather the interactions of the ligand with the substrate were driving the elimination step forwards.

Taking this proposal forward, they subsequently designed a small bite angle ligand based on **3.216**, where trifluoromethyl groups were incorporated as the R group (Scheme 3.38b). This ligand benefits from having a decreased steric influence on the

reaction complex, already known to be detrimental to reactivity in small bite angle ligands. The inclusion of the polar trifluoromethyl groups, they proposed, would sufficiently destabilise the reactant complex through electrostatic repulsion of the species to be eliminated. Using the ONIOM (B3LYP / HF) method, they calculated an activation barrier of 24.8 kcal mol^{-1}, indicating that their designed complex **3.217** should sufficiently furnish the eliminated product **3.215**. Complex **3.217** was subsequently synthesised and heated in benzene with a second equivalent of the designed ligand, with quantitative elimination of trifluoromethylbenzene **3.215** confirming their prediction.
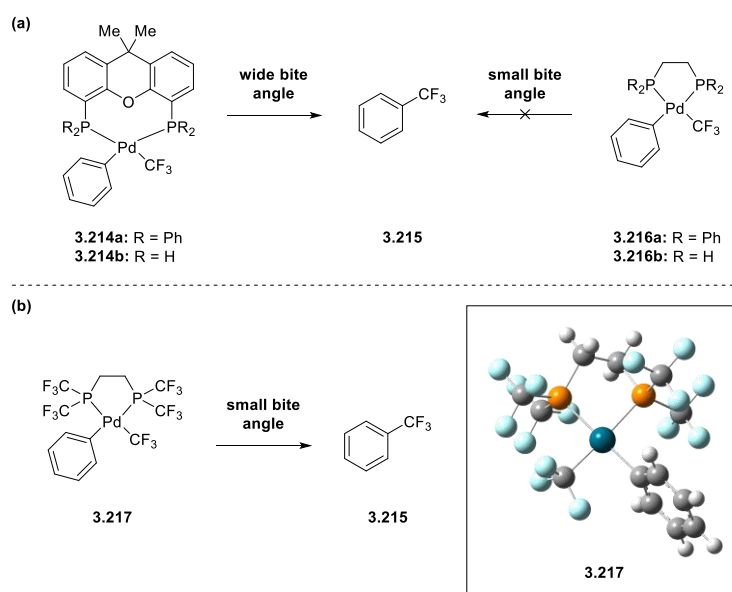
Scheme 3.38: (a) Examples of palladium complexes capable (**3.214**) and incapable (**3.216**) of reductive elimination to form trifluoromethylbenzene **3.215**; (b) computationally designed palladium complex **3.217** capable of performing desired reductive elimination to form **3.215**.[98]

Extensive research efforts have been committed to the idea of developing theoretical enzymes, or 'theozymes', as proposed by Houk *et al.* in 1996.[101] Previous experimental research from an independent group had shown that antibody 34E4, a metaboliser of haptens such as **3.220**, was proficient at promoting the elimination reaction of nitrobenzisoxazole **3.218** (Scheme 3.39a).[102] In an attempt to enhance this reactivity to enzymatic efficiency, Houk *et al.* sought to design a more efficient active site through computational modelling of the main interactions thought to be involved in this transformation. Due to the limited computing power at the time, truncated systems were used in performing this work, with Hartree-Fock optimisations being

complemented with MP2 single point energy calculations. Based on their results, the key proposals for future investigations were to design an active site capable of both forming suitable hydrogen bonds with the substrate and shielding of the isoxazole moiety from solvent hydrogen bonding (Scheme 3.39b).
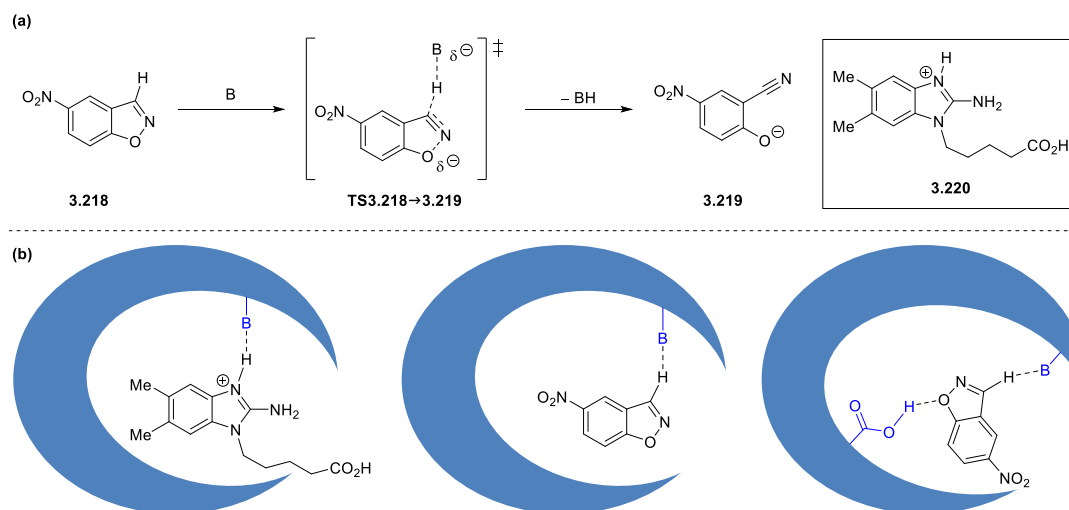
Scheme 3.39: (a) Concerted elimination reaction of **3.218** catalysed by antibody 34E4; (b) idealised active site for reaction with **3.220** [left], integration of **3.218** into this same active site [centre] and the idealised active site for **3.218**, avoiding solvent stabilisation of the substrate [right].

In later years, the same group expanded on this early work and designed two different idealised active sites for this transformation; one employing either an aspartate or glutamate moiety as the base, and another using a dyad comprised of the imidazole group of histidine polarised by either aspartate or glutamate (Figure 3.3).[103] Both of these proposed active sites included an aromatic residue to π-stack with the substrate and a hydrogen bond donor to stabilise the charge developing on the phenolic oxygen.

They then used a hashing algorithm (RosettaMatch) to search for proteins bearing these scaffolds, which led them towards the general TIM barrel structure. Following design of their active site based on this scaffold, 59 candidates were put forward; 39 using the carboxylate as the base and 20 using the histidine-containing dyad. Of the 59, 8 were found to be active experimentally, and targeted mutations to remove the active residues led to diminished activity, supporting their proposed mechanism of reaction. The same group later followed up this successful research by designing enzymes capable of catalysing the retro-aldol reaction[104] and a stereoselective bimolecular Diels-Alder reaction.[105]
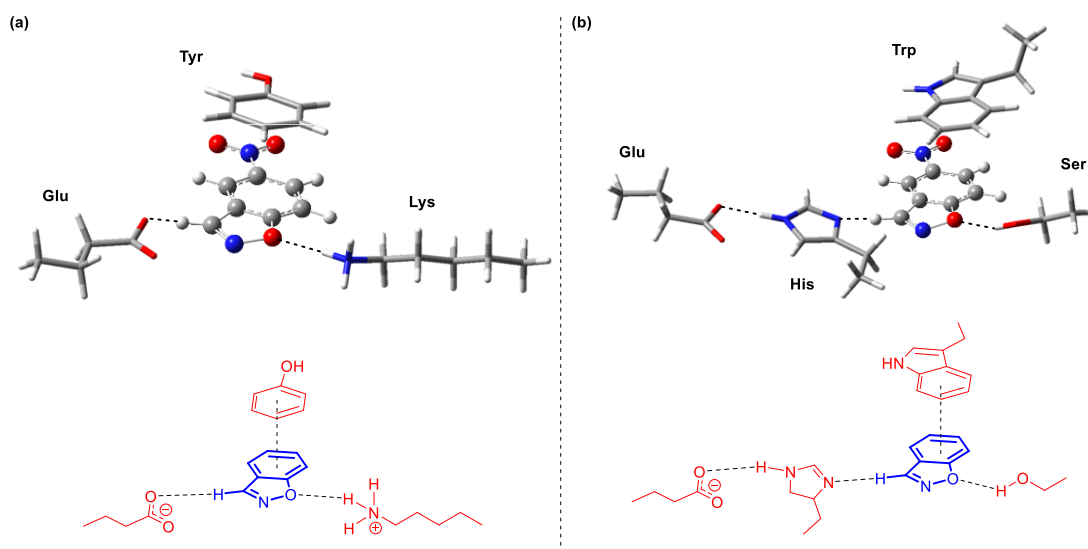
Figure 3.3: Idealised active sites proposed by Houk *et al.* for performing the Kemp elimination reaction of **3.218** using (a) glutamate or (b) the histidine-glutamate dyad as a base, along with a π−stacking residue and a hydrogen bond donor.[103]

These research outcomes, along with countless others that have not been covered within the scope of this discussion, clearly demonstrate the power of computational techniques to supplement and guide chemical research. That new programs and chemical models are being continually developed for more diverse areas of research suggests that computational modelling, alongside experimental chemistry, will continue to have an important role in scientific research. Such a combined approach has in fact been taken in order to understand and rationalise the chemistry discussed hereafter.

4

Computational Theory

4.1 Quantum Chemistry

In order to understand Density Functional Theory (DFT), which has been employed extensively throughout this research, it is necessary to introduce the basics of quantum mechanics. Quantum mechanics form the foundations on which DFT is built. The sections which follow will cover the fundamentals of this complex subject in a concise manner, based on two excellent texts[106, 107] which should be consulted for further reading if desired.

4.1.1 The Wavefunction

When considering a system composed of n particles in quantum theory, the system can be described by $3n$ coordinates (q_1, q_2, ... q_{3n}). This same system can therefore be described by a wavefunction $\psi(q_1, q_2, ... q_{3n}, t)$, where t is time, which contains all of the information about the system. The wavefunction cannot be measured directly, and so it must be interpreted physically (Eqn. 1), where V defines the volume of the region.

$$\int_0^\infty \psi^* \psi \, dV \qquad \text{(Eqn. 1)}$$

This represents the probability of finding the n particles with coordinates in the region defined by $q_1...q_{3n}$ and $(q_1 + dq_1)...(q_{3n} + dq_{3n})$. Since the particle must exist somewhere in space, we can introduce the normalisation condition and therefore giving a total probability of 1 (Eqn. 2).

$$\int_0^\infty \psi^* \psi \, dV = 1 \qquad \text{(Eqn. 2)}$$

To be physically acceptable, a wavefunction must meet four additional conditions as well as the normalisation condition. The wavefunction must: be single-valued; be continuous everywhere; possess a continuous first derivative and be finite over a finite range.

The extraction of information from a wavefunction such as the physical properties, known as an observable (o), requires the use of an operator ($\hat{O}$). This allows us to form what is termed an Eigenvalue equation. If we wish to extract the energy (E) as our observable, we must apply the Hamiltonian operator $\hat{H}$, which accounts for the combined kinetic and potential energy of all particles within a given system. This particular Eigenvalue equation is known as the Schrödinger equation (Eqn. 3).

$$\hat{H}\psi = E\psi \tag{Eqn. 3}$$

4.1.2 The Born-Oppenheimer Approximation

As mentioned previously, the Hamiltonian operator accounts for the total kinetic and potential energy contributions from all particles in a given system, i.e., the electrons and the nuclei, in the absence of an external field. The operator takes the form:

$$\hat{H} = -\frac{1}{2}\sum_{i=1}^{N}\nabla_i^2 - \frac{1}{2}\sum_{A=1}^{M}\frac{1}{M_A}\nabla_A^2 - \sum_{i=1}^{N}\sum_{A=1}^{M}\frac{Z_A}{r_{iA}} + \sum_{i=1}^{N}\sum_{j>i}^{N}\frac{1}{r_{ij}} + \sum_{A=1}^{M}\sum_{B>A}^{M}\frac{Z_A Z_B}{r_{AB}} \tag{Eqn. 4}$$

Where A and B refer to the M nuclei, and i and j refer to the N electrons that comprise the system; M_A is the mass of the nucleus A in atomic units; Z_A is the charge on nucleus A; r_{iA} is the nucleus-electron distance; r_{ij} is the interelectron distance and R_{AB} is the internuclear distance. The first two terms relate to the kinetic energies of the electrons and nuclei respectively and ∇^2 is the Laplacian operator (Eqn. 5), which is defined as the sum of the differential operators (in Cartesian coordinates)

$$\nabla_q^2 = \frac{\partial^2}{\partial x_q^2} + \frac{\partial^2}{\partial y_q^2} + \frac{\partial^2}{\partial z_q^2} \tag{Eqn. 5}$$

The last three terms in Eqn. 4 represent the potential energy terms. The first of these is the electrostatic attraction between the electrons and the nuclei, while the remaining two terms represent the electrostatic repulsions due to electron-electron and internuclear interactions respectively.

The Born-Oppenheimer approximation is derived based on the assumption that relative to the electrons, the nuclei are stationary due to the difference in mass between the two particles. As a consequence of this approximation, the Hamiltonian operator for a given system can be rewritten in the absence of the nuclear kinetic energy, and with a constant replacing the internuclear repulsion term. This is termed the electronic Hamiltonian (Eqn. 6).

$$\hat{H}_{elec} = -\frac{1}{2}\sum_{i=1}^{N}\nabla_i^2 - \sum_{i=1}^{N}\sum_{A=1}^{M}\frac{Z_A}{r_{iA}} + \sum_{i=1}^{N}\sum_{j>i}^{N}\frac{1}{r_{ij}} = \hat{T} + \hat{V}_{Ne} + \hat{V}_{ee} \qquad \text{(Eqn. 6)}$$

Solving the Schrödinger equation with the electronic Hamiltonian affords the electronic wavefunction ψ_{elec} and the electronic energy E_{elec}. The electronic wavefunction depends solely on the electron coordinates, with the nuclear coordinates considered to be constant. Therefore, the total energy E_{tot} is equal to the sum of the electronic energy and the constant nuclear repulsion term (Eqn. 7).

$$E_{tot} = E_{elec} + E_{nuc} \qquad \text{(Eqn. 7)}$$

Herein, references to E will refer only to the electronic properties, and so E_{elec} will cease to be used.

4.1.3 The Variational Principle

In solving the Schrödinger equation for a given system, the only system specific information is the number of electrons N and the external potential V_{ext}. Based on these, the eigenfunctions and corresponding eigenvalues of the Hamiltonian must be determined, thus allowing properties of interest to be extracted through application of an appropriate operator on the wavefunction. Excluding trivial systems such as the hydrogen atom, no strategy exists for solving the Schrödinger equation exactly. The Variational Principle (Eqn. 8) allows for a systematic approach towards determining the ground state wavefunction ψ_0 at which the energy minimum E_0 is observed. Normalising the wavefunction gives:

$$E_{trial} = \langle \psi_{trial} | \hat{H} | \psi_{trial} \rangle \geq E_0 \qquad \text{(Eqn. 8)}$$

To elucidate the ground state energy and wavefunction for a system, it is necessary to minimise *E[ψ]* . This is achieved by searching through all of the acceptable wavefunctions for an *N* electron system, as defined in Chapter 4.1.1. The function giving the lowest energy will hence be *ψ₀* , and the associated energy will be the ground state energy *E₀* . A search across every eligible function is not possible, so the Variational Principle is instead applied to subsets of all possible functions, resulting in a best approximation to the exact wavefunction based on the specified subset.

4.1.4 The Hartree-Fock Approximation

To generate a suitable subset of wavefunctions, Hartree-Fock approximates an *N* electron wavefunction as the anti-symmetrised product of *N* one-electron wavefunctions, referred to as a Slater determinant Φ_{SD} (Eqn. 9):

$$\psi_0 \approx \Phi_{SD} = \frac{1}{\sqrt{N!}} \begin{vmatrix} \chi_1(\vec{x}_1) & \chi_2(\vec{x}_1) & \cdots & \chi_N(\vec{x}_1) \\ \chi_1(\vec{x}_2) & \chi_2(\vec{x}_2) & & \chi_N(\vec{x}_2) \\ \vdots & \vdots & & \\ \chi_1(\vec{x}_N) & \chi_2(\vec{x}_N) & \cdots & \chi_N(\vec{x}_N) \end{vmatrix} \qquad \text{(Eqn. 9)}$$

The above equation can be written to give only the diagonal elements (Eqn. 10):

$$\Phi_{SD} = \frac{1}{\sqrt{N!}} \det\{\chi_1(\vec{x}_1) \quad \chi_2(\vec{x}_2) \quad \cdots \quad \chi_N(\vec{x}_N)\} \qquad \text{(Eqn. 10)}$$

Each one-electron function is referred to as a spin orbital, composed of both a spatial orbital $\phi_i(\vec{r})$ and one of two spin functions, denoted *σ*; *α(s)* or *β(s)* (Eqn. 11):

$$\chi(\vec{x}) = \phi(\vec{r})\sigma(s) \qquad \text{(Eqn. 11)}$$

The spin functions are orthonormal, such that $\langle \alpha | \alpha \rangle = \langle \beta | \beta \rangle = 1$ (Eqn. 12) and $\langle \alpha | \beta \rangle = \langle \beta | \alpha \rangle = 0$ (Eqn. 13). Similarly, the spin orbitals themselves are also taken to be orthonormal.

$$\langle \alpha | \alpha \rangle = \int \alpha^*(s)\alpha(s) \, ds = 1 \qquad \text{(Eqn. 12)}$$

and

$$\langle \alpha | \beta \rangle = \int \alpha^*(s)\beta(s)\, ds = 0 \qquad \text{(Eqn. 13)}$$

Following the choice of wavefunction form, the Variational Principle is applied to determine the lowest energy Slater determinant. Flexibility of the Slater determinant is dependent on the spin orbitals, and in the Hartree-Fock approach these are varied, under the constraint that they remain orthonormal, until the energy minimum is found. Expanding the Slater determinant allows the derivation of the expectation value of the Hamiltonian operator. The final energy is given by:

$$E_{HF} = \langle \Phi_{SD} | \hat{H} | \Phi_{SD} \rangle = \sum_i^N (i|\hat{h}|i) + \frac{1}{2}\sum_i^N \sum_j^N (ii|jj) - (ij|ji) \qquad \text{(Eqn. 14)}$$

The first term of this equation represents the kinetic energy and the electron-nucleus attraction contribution:

$$(i|\hat{h}|i) = \int \chi_i^*(\vec{x}_1)\, \hat{h}\, \chi_i(\vec{x}_1)d\vec{x}_1 = \int \chi_i^*(\vec{x}_1)\left\{ -\frac{1}{2}\nabla^2 - \sum_A^M \frac{Z_A}{r_{1A}} \right\} \chi_i(\vec{x}_1)d\vec{x}_1 \qquad \text{(Eqn. 15)}$$

The second term of Eqn. 14 refers to the Coulomb (Eqn. 16) and exchange (Eqn. 17) integrals respectively, representing the interactions between two electrons *i* and *j*.

$$(ii|jj) = \iint |\chi_i(\vec{x}_1)|^2 \frac{1}{r_{12}} |\chi_j(\vec{x}_2)|^2 \, d\vec{x}_1 d\vec{x}_2 \qquad \text{(Eqn. 16)}$$

$$(ij|ji) = \int \chi_i(\vec{x}_1)\, \chi_j^*(\vec{x}_1) \frac{1}{r_{12}} \chi_j(\vec{x}_2)\, \chi_i^*(\vec{x}_2) \, d\vec{x}_1 d\vec{x}_2 \qquad \text{(Eqn. 17)}$$

Since E_{HF} is a functional of the spin orbitals, the variational freedom associated with this expression arises in the choice of the orbitals. Addition of Lagrangian multipliers in the resulting equations ensures that the spin orbitals remain orthonormal throughout the minimization (Eqn. 18). These equations determine the optimal spin orbitals for which the minimum value of E_{HF} is obtained.

$$\hat{f}_i \chi_i = \varepsilon_i \chi_i \quad \text{where } i = 1, 2, \dots N \qquad \text{(Eqn. 18)}$$

These effective Eigenvalue equations employ the Lagrangian multipliers as the eigenvalues of the Fock operator $\hat{f}_i$. These multipliers can be physically interpreted as the orbital energies. The Fock operator is an effective one-electron operator, which can be defined as:

$$\hat{f}_i = -\frac{1}{2}\nabla^2 - \sum_A^M \frac{Z_A}{r_{iA}} + V_{HF}(i) \qquad \text{(Eqn. 19)}$$

The first two terms refer to the kinetic and potential energies resulting from the electron-nucleus interaction respectively. The Hartree-Fock potential $V_{HF}(i)$ is the average repulsive potential experienced by the ith electron due to the remaining *N-1* electrons in the system. This allows the two-electron repulsion operator of the Hamiltonian $\frac{1}{r_{ij}}$ to be replaced with a simpler one-electron operator that utilises averaged electron-electron repulsion:

$$V_{HF}(\vec{x}_1) = \sum_j^N \left(\hat{J}_j(\vec{x}_1) - \hat{K}_j(\vec{x}_1)\right) \qquad \text{(Eqn. 20)}$$

This operator contains two components; the Coulomb operator $\hat{J}$ and the exchange contribution to the Hartree-Fock potential $\hat{K}$. The Coulomb operator represents the potential that an electron at position $\vec{x}_i$ experiences as a result of the average charge distribution of another electron in spin orbital χ_j, and is defined as:

$$\hat{J}_j(\vec{x}_1) = \int \left|\chi_j(\vec{x}_2)\right|^2 \frac{1}{r_{12}} d\vec{x}_2 \qquad \text{(Eqn. 21)}$$

The Coulomb repulsion corresponding to a given distance between the reference electron at position $\vec{x}_1$ and another one at position $\vec{x}_2$ is weighted by the probability that the other electron is at this point in space. The interaction is integrated over all space and spin coordinates. Since the outcome of applying this operator depends solely on the value of χ_i at position $\vec{x}_1$, this operator and the corresponding potential are termed local.

The exchange operator can only be defined through its effect when operating on a spin orbital:

$$\hat{K}_j(\vec{x}_1)\chi_i(\vec{x}_1) = \int \chi_j^*(\vec{x}_2) \frac{1}{r_{12}} \chi_i(\vec{x}_2)\, d\vec{x}_2\, \chi_j(\vec{x}_1) \qquad \text{(Eqn. 22)}$$

In this equation, $\hat{K}_j(\vec{x}_1)$ leads to an exchange of the variables in the two spin orbitals concerned. Operation on $\chi_i(\vec{x}_1)$ by $\hat{K}_j(\vec{x}_1)$ depends on the value of χ_i at all points in space, thus relating χ_i to the position $\vec{x}_2$. Consequently, this operator and the corresponding exchange potential are termed non-local.

The exchange term can be considered a consequence of the anti-symmetry of the Slater determinant and is applicable to all fermions. Since the $\frac{1}{r_{12}}$ operator is spin-independent, integration over the spin coordinate in Eqn. 22 can be separated. This gives the integral over the product of the spin orbitals χ_i and χ_j, both of which depend on the coordinate $\vec{x}_2$. Due to the orthonormal nature of spin functions, exchange contributions only exist for electrons of like spin. As a consequence of terms such as $\langle \alpha | \beta \rangle$ and $\langle \beta | \alpha \rangle$, the integrand of antiparallel spins would equate to zero.

For instances where $i = j$ in Eqn. 14, the integral of Eqn. 16 then describes the Coulomb interaction of the charge distribution of a single electron with itself. Such a self-interaction term doesn't make sense physically, however this is remedied by the exchange term (Eqn. 22). For the case of $i = j$, the Coulomb and exchange integrals are identical, and so both reduce to:

$$\iint |\chi_i(\vec{x}_1)|^2 \frac{1}{r_{12}} |\chi_i(\vec{x}_2)|^2\, d\vec{x}_1\vec{x}_2 \qquad \text{(Eqn. 23)}$$

Since both integrals enter Eqn. 14 with opposite signs, the issue of self-interaction is negated.

The Fock operator is dependent on the Hartree-Fock potential of the spin orbitals, and so the eigenvalue problem to be solved requires an iterative approach. This pseudo-eigenvalue problem is solved using the Hartree-Fock self-consistent field (SCF)

procedure. An initial set of orbitals is guessed, with which the Hartree-Fock equations are solved. The set of orbitals resulting from this is then used in the next iteration, and this process continues until the energy difference between the input and output orbital set is lower than a predetermined threshold value.

New Iteration

No

Yes

| Input Nuclei Coordinates | Fock Matrix Formation | Is the SCF Converged? | Calculate System Properties |
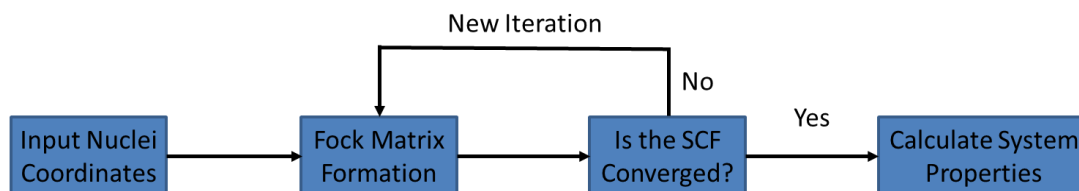
Figure 4.1: Simplified flow diagram representing the Hartree-Fock SCF cycle.

Most systems encountered in computational chemistry deal with an even number of electrons, all of which are paired. This is known as a closed-shell system, and is of singlet multiplicity. In these instances, two degenerate spin orbitals χ_p and χ_q occupy a single spatial orbital and therefore have the same orbital energy. This gives rise to the restricted Hartree-Fock approximation. Sometimes, a system may contain an odd number of electrons or an even number of electrons where not all electrons are paired. Two options exist for dealing with such systems; use restricted open-shell Hartree-Fock which doubly occupies all spatial orbitals except for the explicitly singly-occupied orbital(s), or use unrestricted Hartree-Fock which allows each spin orbital to have its own spatial orbital. More commonly, the latter option is preferred as the α and β orbitals in this method experience different effective potentials V_{HF}^{α} and V_{HF}^{β}. Consequently, each orbital has different spatial characteristics and orbital energies.

4.1.5 Electron Correlation

A single Slater determinant is a reasonably good approximation of the wavefunction of a many-electron system, but will never correspond to the exact wave function. As a consequence of the Variational Principle, the calculated Hartree-Fock energy will always be greater than the actual ground state energy of the system. The calculated difference between these two values is termed the correlation energy E_C^{HF} :

$$E_C^{HF} = E_0 - E_{HF}$$ <div align="right">(Eqn. 24)</div>

The correlation energy value represents an error value introduced through the Hartree-Fock scheme. The main contribution to this is the instantaneous repulsion of electrons, which is not accounted for in the effective Hartree-Fock potential. Since electrostatic repulsions are treated in an averaged manner, electrons will often get too close to each other, resulting in an over-estimation of the electron repulsion term. This is directly related to the $\frac{1}{r_{12}}$ term which controls the electron-electron repulsion of the Hamiltonian. This term will increase in value as the distance between the two electrons decreases. Since this term relates to the movement of electrons, it is known as dynamical electron correlation, and represents a short-range effect.

The correlation energy also contains a non-dynamical correlation term, which is a consequence of a poor approximation of the true ground state by the ground state Slater determinant. In some instances, an alternative Slater determinant might have energy more comparable to that of the true ground state. Considering the H_2 molecule as an illustrative example (Figure 4.2), at the equilibrium bond distance the Hartree-Fock scheme gives a good approximation of the system. Stretching the bond distance towards infinity, we give rise to two hydrogen atoms; each atom possesses a single electron which experiences no electron-electron interaction.
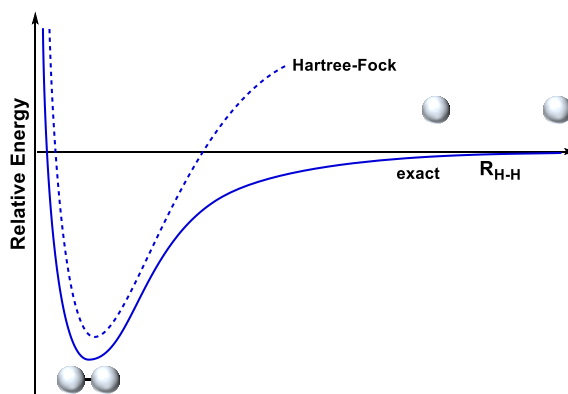
Figure 4.2: Comparison of the exact potential energy curve and Hartree-Fock potential energy curve for H_2.

The Hartree-Fock wavefunction for this scenario consists of two neutral terms, and two ionic terms (Eqn. 25, where s_L and s_R correspond to the 1s orbitals of the 'Left' and 'Right' hydrogen atom respectively), leading to an overestimation of the interaction energy and therefore an error in the dissociation energy. Additional errors in this term arise from the kinetic energy and nucleus-electron interaction terms of the Hamiltonian.

$$\Phi_{GS} = \frac{1}{2}[\det\{1s_L\alpha \; 1s_R\beta\} + \det\{1s_L\beta \; 1s_R\alpha\}$$
$$+ \det\{1s_L\alpha \; 1s_L\beta\} + \det\{1s_R\alpha \; 1s_R\beta\}]$$

(Eqn. 25)

4.2 Density Functional Theory

4.2.1 Electron Density

The electron density $\rho(\vec{r})$ can be derived from the probability interpretation of the wavefunction $\int |\psi(\vec{x}_1, \vec{x}_2, ... \vec{x}_N)|^2 \, dx_1, d\vec{x}_2, ..., d\vec{x}_N$ and takes the form of a multiple integral of all electron spin coordinates and all but one spatial variable:

$$\rho(\vec{r}) = N \int ... \int |\psi(\vec{x}_1, \vec{x}_2, ... \vec{x}_N)|^2 \, ds_1, d\vec{x}_2, ..., d\vec{x}_N$$

(Eqn. 26)

This determines the probability of finding any of the N electrons of a system with arbitrary spin within a volume $d\vec{r}_1$ whilst the remaining *N-1* electrons have arbitrary positions and spin in the state represented by ψ. Since electrons are indistinguishable, the probability of finding an electron at any given position is N times the probability for one particular electron. Electron density is a non-negative function of three spatial variables. It integrates to the total number of electrons N and also tends towards zero as $\vec{r}_1$ tends towards infinity. It is also an observable, and can be measured experimentally by means of X-ray diffraction. At any position, the electron density exhibits a finite value due to the attraction of electrons to the positive charge of the nucleus.

4.2.2 Pair Density

Pair density $\rho_2(\vec{x}_1, \vec{x}_2)$ represents an extension of the idea of electron density, and considers the probability of finding a pair of electrons with spins σ_1 and σ_2 in the volumes $d\vec{r}_1$ and $d\vec{r}_2$ whilst the remaining electrons have arbitrary spin and positions:

$$\rho_2(\vec{x}_1, \vec{x}_2) = N(N-1) \int \cdots \int |\psi(\vec{x}_1, \vec{x}_2, \dots, \vec{x}_N)|^2 \; d\vec{x}_3 \dots d\vec{x}_N \qquad \text{(Eqn. 27)}$$

The pair density contains all of the information about electron correlation and is a non-negative quantity. It is symmetric with respect to the spatial coordinates and is normalised to the number of non-distinct electron pairs. Since the electrons are not considered to have any volume, the possibility of both electrons occupying the same volume element arises. In such an instance, the pair density would reduce to the product of the individual probabilities:

$$\rho_2(\vec{x}_1, \vec{x}_2) = \frac{N-1}{N} \; \rho(\vec{x}_1)\rho(\vec{x}_2) \qquad \text{(Eqn. 28)}$$

Introducing the $\frac{N-1}{N}$ factor into the equation negates the paradox whereby the electron at $\vec{x}_1$ would simultaneously exist at $\vec{x}_2$. The probability of an electron existing at $\vec{x}_2$ whilst another exists at $\vec{x}_1$ is therefore $\frac{N-1}{N} \, \rho(\vec{x}_2)$.

Due to the anti-symmetry of the wavefunction, it is possible to derive a reduced density matrix for the two electrons as a generalisation of $\rho(\vec{x}_1, \vec{x}_2)$ known as γ_2 :

$$\begin{aligned} \gamma_2(\vec{x}_1, \vec{x}_2; \; \vec{x}_1', \vec{x}_2') \\ = N(N-1) \int \cdots \int \psi(\vec{x}_1, \vec{x}_2, \vec{x}_3, \dots, \vec{x}_N) \, \psi^*(\vec{x}_1', \vec{x}_2', \vec{x}_3, \dots, \vec{x}_N) \, d\vec{x}_3 \dots d\vec{x}_N \end{aligned} \qquad \text{(Eqn. 29)}$$

In converting from ρ_2 to γ_2, variables in the second factor which are included from the integration are primed. Interchanging two variables results in a change in the sign of γ_2 as a consequence of the antisymmetry of ψ :

$$\gamma_2\left(\vec{x}_1, \vec{x}_2; \vec{x}_1', \vec{x}_2'\right) = -\gamma_2\left(\vec{x}_2, \vec{x}_1; \vec{x}_1', \vec{x}_2'\right) \qquad \text{(Eqn. 30)}$$

On considering the situation where $\vec{x}_1 = \vec{x}_2$, i.e., the probability that two electrons of the same spin exist within the same volume element, the following arises:

$$\rho_2\left(\vec{x}_1, \vec{x}_1\right) = -\rho_2\left(\vec{x}_1, \vec{x}_1\right) \qquad \text{(Eqn. 31)}$$

which can only be true when $\rho_2\left(\vec{x}_1, \vec{x}_1\right)$ is equal to zero. As a consequence of the Pauli Exclusion Principle, two electrons of like spin cannot move independently of each other; this is not true however for cases where both electrons have opposite spin, which is termed the Fermi correlation.

Another factor influencing pair density is the charge of the electrons, since electrostatic repulsion will prevent electrons from coming too close to each other. This arises from the $\frac{1}{r_{12}}$ term of the Hamiltonian and is independent of the electron spin, termed Coulomb correlation. Although the Hartree-Fock approximation does account for Fermi correlation, it does not account for Coulomb correlation.

To better understand the influence of Fermi and Coulomb correlation on pair density, it is possible to separate the pair density into two terms; the simple product of independent densities and the contributions brought about by the Fermi and Coulomb effects:

$$\rho_2\left(\vec{x}_1, \vec{x}_2\right) = \rho(\vec{x}_1)\rho(\vec{x}_2)[1 + f(\vec{x}_1; \vec{x}_2)] \qquad \text{(Eqn. 32)}$$

Where $f(\vec{x}_1; \vec{x}_2)$ is referred to as the correlation factor. The probability of finding an electron at position $\vec{x}_1$ while one already exists at $\vec{x}_2$ is defined as a conditional probability:

$$\Omega(\vec{x}_2; \vec{x}_1) = \frac{\rho_2(\vec{x}_1, \vec{x}_2)}{\rho(\vec{x}_1)} \qquad \text{(Eqn. 33)}$$

Integration of this conditional density equates to *N-1* electrons due to the exclusion of the electron at position $\vec{x}_1$.

4.2.3 The Hohenberg-Kohn Theory

The Hohenberg-Kohn theory was the first to prove conclusively that the electron density can be used with the Hamiltonian operator to determine the properties of a molecular system.[108] It states that the external potential V_{ext} is a unique functional of electron density $\rho(\vec{r})$ and, in turn, the ground state is a unique functional of $\rho(\vec{r})$. Consequently, the ground state electron density can be used to determine the Hamiltonian, wavefunction and properties of a given system:

$$\rho \Rightarrow \{N, Z_A, R_A\} \Rightarrow \hat{H} \Rightarrow \psi_0 \Rightarrow E_0 \text{ (and all other properties)} \qquad \text{(Eqn. 34)}$$

If the ground state energy is a functional of the ground state electron density, so too must be its individual components. Thus it can be written:

$$E_0[\rho_0] = T[\rho_0] + E_{ee}[\rho_0] + E_{Ne}[\rho_0] \qquad \text{(Eqn. 35)}$$

where E_{Ne} refers to the external potential due to the attraction of electrons to the nuclei.

This energy expression can be rewritten as three terms, whereby the first of these depends on the actual system and the other two are universally valid, i.e., do not depend on *N*, R_A and Z_A:

$$E_0[\rho_0] = \int \rho_0(\vec{r}) V_{Ne} d\vec{r} + T[\rho_0] + E_{ee}[\rho_0] \qquad \text{(Eqn. 36)}$$

The two system-independent terms can be collectively termed as the Hohenberg-Kohn functional, $F_{HK}[\rho_0]$. This allows the ground energy state expression to be rewritten as:

$$E_0[\rho_0] = \int \rho_0(\vec{r}) V_{Ne} d\vec{r} + F_{HK}[\rho_0] \qquad \text{(Eqn. 37)}$$

Inputting an arbitrary electron density, , into the Hohenberg-Kohn functional affords the expectation value $\langle \psi | T + V_{ee} | \psi \rangle$. This is the sum of the kinetic energy and the electron-electron repulsion operator with the ground state wave function connected to this density. In other words, of all the possible wavefunctions that can afford the electron density ρ, this wavefunction delivers the lowest energy system.

$$F_{HK}[\rho] = T[\rho] + E_{ee}[\rho] = \langle \psi | T + V_{ee} | \psi \rangle \qquad \text{(Eqn. 38)}$$

If this functional were known exactly, it would allow for the exact solution of the Schrödinger equation. It is not possible to determine the kinetic energy or electron-electron repulsion exactly, however it is possible to expand the electron-electron repulsion energy term:

$$E_{ee}[\rho] = \frac{1}{2} \iint \frac{\rho(\vec{r}_1)\rho(\vec{r}_2)}{r_{12}} d\vec{r}_1 d\vec{r}_2 + E_{ncl} = J[\rho] + E_{ncl}[\rho] \qquad \text{(Eqn. 39)}$$

From this expression, it is possible to solve $J[\rho]$ which represents the classical Coulomb term. The $E_{ncl}[\rho]$ term represents non-classical contributions to the electron-electron interaction, those being self-interaction correction, Fermi and Coulomb correlation.

The second theory proposed by Hohenberg and Kohn applies the Variational Principle to their first theory, where $\tilde{\rho}$ represents a trial density:

$$E_0 \leq E[\tilde{\rho}] = T[\tilde{\rho}] + E_{Ne}[\tilde{\rho}] + E_{ee}[\tilde{\rho}] \qquad \text{(Eqn. 40)}$$

Only when the true ground state density is input to this expression is the ground state energy obtained.

4.2.4 The Kohn-Sham Approach

The Kohn-Sham approach[109] allows the kinetic energy contribution to be determined. Similar to Hohenberg-Kohn theory, the system-independent terms can be collectively represented by a single term $F[\rho]$:

$$F[\rho(\vec{r})] = T[\rho(\vec{r})] + J[\rho(\vec{r})] + E_{ncl}[\rho(\vec{r})] \qquad \text{(Eqn. 41)}$$

In their approach, Kohn and Sham used the Slater determinant to solve the kinetic energy term. This determinant can be considered as the exact wavefunction of a fictitious system comprised of N non-interacting electrons moving in the effective Hartree-Fock potential. In such a case, the kinetic energy can be expressed as:

$$T_{HF} = -\frac{1}{2} \sum_{i}^{N} \langle \chi_i | \nabla^2 | \chi_i \rangle \qquad \text{(Eqn. 42)}$$

The spin orbitals in this expression are chosen such that the Hartree-Fock energy value obtained is the minimum. Taking this expression along with the fictitious system allows for the determination of the kinetic energy of the interacting system. Introducing an effective local potential $V_S(\vec{r})$ permits the determination of a Hamiltonian for the non-interacting system:

$$\hat{H}_S = -\frac{1}{2} \sum_{i}^{N} \nabla_i^2 + \sum_{i}^{N} V_S(\vec{r}_i) \qquad \text{(Eqn. 43)}$$

The ground state wavefunction of this system can be represented using a Slater determinant, with the spin orbitals determined by the eigenvalue equation:

$$\hat{f}^{KS}\varphi_i = \varepsilon_i\varphi_i$$

(Eqn. 44)

Where φ_i represents the spin orbitals and ε_i represents the energy of these orbitals. $\hat{f}^{KS}$ is the one-electron Kohn-Sham operator, which is defined as:

$$\hat{f}^{KS} = -\frac{1}{2}\nabla^2 + V_s(\vec{r})$$

(Eqn. 45)

In order to connect the non-interacting and interacting systems, an effective potential is chosen which produces a calculated density equal to that of the ground state density of the interacting system:

$$\rho_S(\vec{r}) = \sum_i^N\sum_S|\varphi(\vec{r},s)|^2 = \rho_0(\vec{r})$$

(Eqn. 46)

Since the kinetic energy cannot be calculated explicitly, it was realised that the exact kinetic energy of the non-interacting system could be obtained by applying the density of the interacting system to Eqn. 42:

$$T_S = -\frac{1}{2}\sum_i^N\langle\varphi_i|\nabla^2|\varphi_i\rangle$$

(Eqn. 47)

Due to the difference in the non-interacting and the true kinetic energies, an additional separation of the functional was introduced:

$$F[\rho(\vec{r})] = T_S[\rho(\vec{r})] + J[\rho(\vec{r})] + E_{XC}[\rho(\vec{r})]$$

(Eqn. 48)

Where E_{XC} is the exchange correlation energy, defined as:

$$E_{XC}[\rho] = (T[\rho] - T_S[\rho]) + (E_{ee}[\rho] - J[\rho]) = T_C[\rho] + E_{ncl}[\rho] \qquad \text{(Eqn. 49)}$$

The above expression contains the non-classical electrostatic contributions and the residual part of the true kinetic energy. Collectively, the exchange correlation energy represents the unknown contributions to the true ground state electronic energy. Presently, significant research is dedicated to producing methods that can better approximate the exchange correlation functional.

4.2.5 Functionals and Basis Sets

4.2.5.1 Local Density Approximation (LDA)

The Local Density Approximation (LDA) lies at the heart of almost all approximate exchange correlation functionals. The central idea of this model is that of a uniform electron gas, where the electrons move on a positive background, making the system electronically neutral overall. The electron density value is constant throughout the system, and remains a finite value even as the gas volume or the number of electrons approach infinity. This model simplifies the exchange correlation function by using the assumption that:

$$E_{XC}^{LDA}[\rho] = \int \rho(\vec{r})\varepsilon_{XC}(\rho(\vec{r}))\, d\vec{r} \qquad \text{(Eqn. 50)}$$

In this expression, $\varepsilon_{XC}(\rho(\vec{r}))$ represents the exchange correlation energy per particle of a uniform electron gas of density $\rho(\vec{r})$. Writing the exchange correlation energy term in this way defines the local density approximation. Expanding $\varepsilon_{XC}(\rho(\vec{r}))$ allows the individual terms corresponding to the exchange $[\varepsilon_X(\rho(\vec{r}))]$ and correlation $[\varepsilon_C(\rho(\vec{r}))]$ contributions to be identified.

In situations where open-shell systems are to be calculated, it is useful to use the spin densities rather than the electron density. For instances involving an odd number of

electrons, functionals of the two spin densities frequently produce more accurate results. For unrestricted cases, LDA can be extended to afford the Local Spin Density Approximation (LSDA), which differs only slightly from the LDA approximation:

$$E_{XC}^{LSDA}[\rho_\alpha, \rho_\beta] = \int \rho(\vec{r})\varepsilon_{XC}\left(\rho_\alpha(\vec{r}), \rho_\beta(\vec{r})\right) d\vec{r} \qquad \text{(Eqn. 51)}$$

In situations where $\rho_\alpha(\vec{r}) \neq \rho_\beta(\vec{r})$, the energy can be expressed as spin-polarised. The extent of the spin polarisation is measured through the spin polarisation parameter ξ :

$$\xi = \frac{\rho_\alpha(\vec{r}) - \rho_\beta(\vec{r})}{\rho(\vec{r})} \qquad \text{(Eqn. 52)}$$

The value for this parameter lies between 0 (systems where there is equal population of both spin states) to 1 (for when all electrons are in the same spin state).

4.2.5.2 Generalised Gradient Approximation (GGA)

An improvement on the LDA model, the Generalised Gradient Approximation (GGA) allows for electron density to be more accurately described by accounting for the gradient of electron density $\nabla\rho(\vec{r})$, thus considering it to be heterogeneous. In general terms, these functionals are defined as:

$$E_{XC}^{GGA}[\rho_\alpha, \rho_\beta] = \int f(\rho_\alpha, \rho_\beta, \nabla\rho_\alpha, \nabla\rho_\beta,) d\vec{r} \qquad \text{(Eqn. 53)}$$

Rather than looking at the exchange correlation energy as a single entity, it is better to consider the exchange and correlation terms individually in order to obtain better approximations of each. The exchange contribution to this term can be rewritten to include the LDA approximation:

$$E_X^{GGA} = E_X^{LDA} - \sum_\sigma \int F(s_\sigma) \, \rho_\sigma^{4/3} \, (\vec{r}) \, d\vec{r} \qquad \text{(Eqn. 54)}$$

The argument of the function F is the reduced density gradient for spin σ and is expressed as:

$$s_\sigma(\vec{r}) = \frac{|\nabla \rho_\sigma(\vec{r})|}{\rho_\sigma^{4/3}(\vec{r})} \qquad \text{(Eqn. 55)}$$

The parameter s_σ ensures that the system remains heterogeneous. It regulates this by producing large values not only in cases with a large gradient, but also for those that have small densities. Conversely, small values are produced in both the case where a small gradient, or a large density is present. A homogeneous gas such as that used in the LDA will produce a s_σ value of zero.

4.2.5.3 Hybrid Functionals

Hybrid functionals are a combination of pure density functionals for exchange and exact Hartree-Fock exchange. They contain different weightings of other functionals, for example the B3LYP functional[110-113] comprises a combination of the Becke 3-parameter exchange functional[110] and the Lee, Yang and Parr correlation functional:[111]

$$E_{XC}^{B3LYP} = 0.80 E_X^{LSDA} + 0.20 E_X^{HF} + 0.72\Delta E_X^{B88} + 0.81 E_C^{LYP} + 0.19 E_C^{LSDA} \qquad \text{(Eqn. 56)}$$

where E_X^{HF} is the exact Hartree-Fock exchange energy, ΔE_X^{B88} is Becke's 1988 gradient correction to the LSDA for exchange and E_C^{LYP} is Lee, Yang and Parr's correlation functional.

The M06 functional suite is a combination of hybrid and meta-GGA functionals suitable for the calculation of a variety of systems.[114, 115] This suite includes the M06 functional, which has good "across the board" performance; the M06-L functional, which is a local functional best suited to moderately sized to large systems; the M06-2X functional

which is suited for main group thermochemistry and kinetics and the M06-HF functional, which uses full Hartree-Fock exchange, is useful for systems where long-range self-interaction might be an issue.

4.2.5.4 Basis Sets

A basis set is a collection of functions that describes the molecular orbitals used to approximate the wavefunction. There are two main types of basis set; Gaussian-type orbitals (GTO's) and Slater-type orbitals (STO's). GTO's are generally chosen for Hartree-Fock and related methods as they are advantageous for calculating the large number of four-centre-two-electron integrals of the Coulomb and Hartree-Fock exchange terms. They assume the general form:

$$\eta^{GTO} = N \, x^l \, y^m \, z^n \, e^{-\alpha r^2} \qquad \text{(Eqn. 57)}$$

In this expression, N is a normalisation factor included to ensure that $\langle \eta_\mu | \eta_\mu \rangle = 1$, and α is the orbital exponent which determines the size of the function (a large value of α results in a compact function, while a small value of α results in a diffuse function). The integers l, m and n are components which equate to L when summed, which determines the nature of the orbitals as s-functions ($L = 0$), p-functions ($L = 1$), d-functions ($L = 2$) etc.

STO's are simple exponentials, which exhibit the correct cusp behaviour as $r \rightarrow 0$, with a discontinuous derivative and also the correct exponential decay in tail regions as $r \rightarrow \infty$. The general expression of an STO is:

$$\eta^{STO} = N \, r^{n-1} \, e^{-r\zeta} \, Y_{lm}(\Theta, \phi) \qquad \text{(Eqn. 58)}$$

Where n corresponds to the principal quantum number, ζ is the orbital exponent and Y_{lm} describes the angular part of the functional. STO basis sets become problematic when many-centre integrals are to be computed, and so GTO basis sets have become

more prominent in modern quantum chemistry programs. Although typically three times more GTO's than STO's are required to obtain similar accuracy, it is possible to use a reduced set of GTO's known as a contracted GTO basis set. For a contracted GTO, several primitive Gaussian functions are combined linearly to give a single contracted Gaussian function (CGF):

$$\eta_\tau^{CGF} = \sum_\alpha^A d_{\alpha\tau}\eta_{\alpha\tau}^{GTO}$$

(Eqn. 59)

The quality of results extracted from a DFT calculation is dependent on the basis set chosen. The simplest expansion of the molecule's orbital uses only a single basis function to describe each atomic orbital. This is the least accurate expansion and is termed a minimal set, for example the STO-3G basis set. Improving on this, we reach what is termed a double-ζ basis set, which has two functions to describe each atomic orbital. This can be extended further to obtain triple- and quadruple-ζ basis sets which, along with offering more accuracy to calculations, have a higher computational cost associated.

To reduce computational cost, it is possible to treat the inert core electrons using a minimal set. This allows the valence electrons, known to be central to chemical reactions, to be the focus of the calculation. This is known as a split valence which can be exemplified by basis sets such as 3-21G and 6-31G. If we consider the latter of these examples, the first number corresponds to the number of primitive Gaussian functions used to describe the core electrons. The numbers which follow this indicate that the valence electrons are described by two GTO's consisting of 3 and 1 primitive Gaussian functions respectively. Such basis sets are typically accompanied by polarisation functions, which describe functions of higher angular momentum than those occupied in the atom. This allows for orbital distortion, thus making the system more able to adapt to changes in the molecular environment during, for example, the calculation of a transition state. Similarly, diffuse functions can be used if the system to be computed contains anions or heavy atoms with electrons that are far from the nucleus. Since the choice of basis set has implications both on the accuracy of results and the

computational cost, it is often beneficial to carry out a comparison of the performance of a number of these in order to optimise accuracy and efficiency.

As mentioned previously, the core electrons don't play a significant role in chemical reactivity, and so for elements of the lower part of the periodic table it is beneficial to be able to model these using a suitable function, while considering only the valence electrons explicitly. This function is referred to as an effective core potential (ECP), or in some instances a pseudopotential (PP). This allows suitably accurate results to be obtained for such systems in a more efficient manner. When using Gaussian functions, the ECP is determined by the number of electrons to be modelled in this manner. The use of an ECP is important for dealing with elements where relativistic effects are significant. ECP's do exist for lighter elements; however the benefits of using these are minimal in comparison to their use for heavier elements. For elements such as iodine, we can envisage that there are three options for modelling this computationally: i) an all electron method; ii) using a small core ECP or iii) using a large core ECP. Each of these is illustrated below with explicitly modelled electrons indicated in bold (and totalled in brackets), and electrons replaced by an ECP indicated in italics:

i) **$(1s)^2, (2s)^2, (2p)^6, (3s)^2, (3p)^6, (4s)^2, (3d)^{10}, (4p)^6, (4d)^8, (5s)^2, (5p)^5$** (53 explicit)

ii) *$(1s)^2, (2s)^2, (2p)^6, (3s)^2, (3p)^6,$* **$(4s)^2,$** *$(3d)^{10},$* **$(4p)^6, (4d)^8, (5s)^2, (5p)^5$** (23 explicit)

iii) *$(1s)^2, (2s)^2, (2p)^6, (3s)^2, (3p)^6, (4s)^2, (3d)^{10}, (4p)^6,$* **$(4d)^8, (5s)^2, (5p)^5$** (15 explicit)

4.3 Continuum Solvation Models

An important factor to be considered in theoretical calculations is the chemical environment of the system being investigated, that is, the solvent. By default, quantum mechanical calculations are performed in the gas phase. However, it is desirable to incorporate the effect of solvation as this is likely to have a significant effect on the calculated energetics. The solvation of a chemical system can be modelled in one of two ways; explicitly through the inclusion of individual solvent molecules, or implicitly through modelling of a continuum parameterised according to the solvent in question. The continuum solvation model considers the solvent as a uniform polarisable medium with a cavity, inside which the solute is placed. Cavity generation can be achieved by using a simple shape such as a sphere or an ellipsoid, or in more complex models a molecule-shaped cavity, based on the van der Waals radii of the solute atoms, can be used (Figure 4.3). For the conductor-like polarisable continuum model (CPCM),[116, 117] the cavity is formed using spheres centred on the atoms comprising the solute. This cavity has a dielectric constant of 1, while the outside of the cavity has a dielectric constant corresponding to the solvent chosen.

Figure 4.3: Graphical representation of a continuum solvation model using an ellipsoid cavity [left] and a molecule-shaped cavity [right] such as that used in the CPCM model.[116, 117]

For the implicit solvation model, the free energy of solvation, ΔG_{solv}, is calculated as:

$$\Delta G_{solv} = \Delta G_{elec} + \Delta G_{vdW} + \Delta G_{cav} \qquad \text{(Eqn. 60)}$$

where ΔG_{elec} is the electrostatic contribution arising from the polarisation of the solvent by the solute, ΔG_{vdW} is the contribution due to van der Waals interactions between the solute and solvent, and ΔG_{cav} is the free energy required to form a

cavity in the solvent. In computing the contributions of the van der Waals and cavitation free energy to the solvation free energy, the following can be used:

$$\Delta G_{vdW} + \Delta G_{cav} = \sum_{i=1}^{N} a_i \, S_i + c \qquad \text{(Eqn. 61)}$$

where S_i is the solvent accessible area contributions of the different atom types to the overall solute molecule, and a_i and c are constants. For calculation of the electrostatic contribution to the solvation free energy, a number of methods exist. The conductor-like polarisable continuum model (CPCM) applies the Poisson-Boltzmann model to derive this value. The Poisson equation describes the relationship between the electrostatic potential ϕ, the charge distribution ρ and the dielectric constant ε:

$$\nabla \cdot \left(\varepsilon(r) \nabla \phi(r) \right) = -4\pi\rho(r) \qquad \text{(Eqn. 62)}$$

Extending this equation to account for the movement of charged particles in solution affords the Poisson-Boltzmann equation which, written in terms of a reduced potential u affords:

$$\nabla \cdot \left(\varepsilon(r) \nabla u(r) \right) - \kappa^2 \, sinh\left(u(r) \right) = -4\pi\rho(r) \qquad \text{(Eqn. 63)}$$

Solving this equation gives information about the electrostatic potential at a given point in space. This can be used to generate the reaction field ϕ_{react}, which is the difference between the potential in the presence of a solvent and in vacuum. Multiplying by the solute charge, using the partial charge description, gives:

$$\Delta G_{elec} = \frac{1}{2} \sum_{i} Q(r_i) \phi_{react}(r_i) \qquad \text{(Eqn. 64)}$$

4.4 Transition State Theory

The calculation of potential energy surfaces for particular reactions requires not only optimised reactant and product geometries, but also transition state geometries. In order to comprehend the significance of energetics obtained from such calculations, an understanding of transition state theory itself is required. When considering a chemical reaction, a potential energy surface (PES) can be envisioned, across which a reactant passes via the lowest energy pathway in order to reach the corresponding product state. Both the reactant and product species represent reaction minima, and these are joined by a transition state. On the PES, the transition state is a 1st–order saddle point; that is a maximum with respect to the reaction coordinate direction and a minimum with respect to the remaining coordinates (represented visually in Figure 4.4 below).
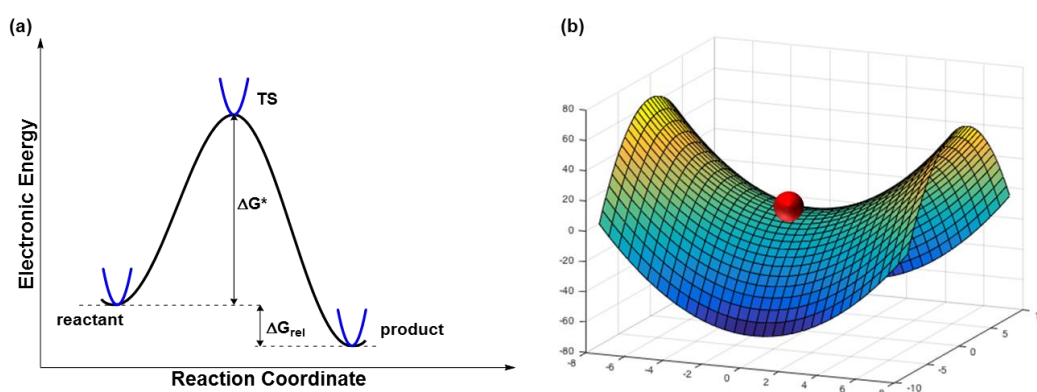
Figure 4.4: (a) 2D representation of a PES; (b) 3D representation of a PES highlighting the 1st–order saddle point [red sphere].

Transition state theory is a semi-classical theory, which assumes an equilibrium energy distribution among all possible quantum states at all points along the reaction coordinate. Within this theory, it is assumed that the transition state molecules are at equilibrium with the reactant state. The rate constant can be expressed using the Eyring equation:[118]

$$k_{rate} = \frac{k_B T}{h} \, e^{-\frac{\Delta G^*}{RT}} \qquad \text{(Eqn. 65)}$$

where k_B is the Boltzmann constant, T is the temperature (Kelvin), h is Planck's constant, ΔG^* is the free energy of activation and R is the universal gas constant. Similarly, the equilibrium constant for the overall reaction can be expressed as:

$$K_{eq} = e^{-\frac{\Delta G_{rel}}{RT}}$$
(Eqn. 66)

When the activation free energy is known, inputting this value along with the relevant reaction temperature into Eqn. 65 allows for the rate constant for a specific reaction to be computationally predicted. Alternatively, predictions about the rate constant can be made experimentally through kinetic investigations. Rearranging Eqn. 65, the activation free energy can subsequently be calculated. Utilising these two approaches, it is therefore possible to allow comparison between theory and experiment to assess the accuracy of computational methods. Through similar means, the calculated relative free energy of reaction can be used to obtain the equilibrium constant.

With this theory, there are a number of associated limitations. In multi-step reactions for example, it is assumed that each intermediate is sufficiently long-lived that it can reach a Boltzmann energy distribution before progressing further along the potential energy surface. In addition to this, the theory cannot always easily be applied to the prediction of the activation free energies for electron transfer reactions. To overcome this latter problem, Rudolph Marcus developed a theory by which these reactions could be described.

4.5 Marcus Theory of Electron Transfer

The study of electron transfer reactions using computational techniques is possible largely due to the work of Rudolph Marcus,[119] who formulated his theory for the calculation of electron transfer reaction activation free energies in the 1960's. Calculation of the activation free energy is based on two factors; the total reorganisation energy of the system λ and the relative free energy ΔG_{rel}:

$$\Delta G^* = \frac{\lambda}{4}\left(1 + \frac{\Delta G_{rel}}{\lambda}\right)^2 \qquad \text{(Eqn. 67)}$$

The PES of two half reactions can be considered as separate parabolas, and thus Marcus Theory can be illustrated as per Figure 4.5. The intersection of these parabolas represents the activation free energy, while the energy difference between the two minima represents the relative free energy. The reorganisation energy is interpreted as the vertical energy difference between the minimum of the product curve and the point where the reactant curve overlaps with this on the PES.
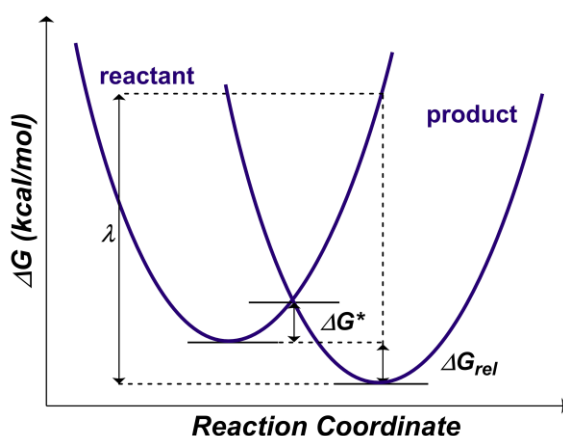
Figure 4.5: Energy diagram for the calculation of electron transfer reactions by Marcus Theory.

The total reorganisation energy of the system is comprised of the internal reorganisation λ_i (electron donor and acceptor molecules) and the external reorganisation energy λ_o (solvent reorganisation in response to the electron transfer). Research published by Kochi[120-122] and Banerjee[123] has demonstrated that in calculating the overall reorganisation energy, the internal reorganisation energy has a more significant influence on the total reorganisation energy relative to the external reorganisation energy. The opposite of this was observed by Blumberger;[124] however this work was focussed on biological systems. The systems investigated in this research exist in a non-strongly coordinated medium, and as such are more akin to those studied by Kochi and Banerjee. With this in mind, Eqn. 67 can be reduced to the following, accounting only for the internal reorganisation energy contribution:

$$\Delta G^* = \frac{\lambda_i}{4}\left(1 + \frac{\Delta G_{rel}}{\lambda_i}\right)^2 \qquad \text{(Eqn. 68)}$$

The internal reorganisation energy is calculated as follows:

$$\lambda_i = \frac{\lambda_i(D) + \lambda_i(A)}{2} \qquad \text{(Eqn. 69)}$$

where $\lambda_i(D)$ represents the internal reorganisation energy for the electron donor and $\lambda_i(A)$ represents the internal reorganisation energy for the acceptor. The internal reorganisation energy for a given species is typically calculated using Nelsen's four-point method,[125] which for the electron donor yields:

$$\lambda_i(D) = \left(E_S(R_P) - E_S(R_S)\right) + \left(E_P(R_S) - E_P(R_P)\right) \qquad \text{(Eqn. 70)}$$

An analogous equation can be written for the electron acceptor. In the above equation, $E_S(R_P)$ is the energy of the species with the starting electronic configuration and the product geometry; $E_S(R_S)$ is the energy of the optimised starting species; $E_P(R_S)$ is the energy of the species with the product electronic configuration and the starting geometry and $E_P(R_P)$ is the energy of the optimised product species.

5

Discovery of the *in situ* Formation of Organic Super Electron Donors

5.1 Introduction

Our group became interested the idea of transition metal-free coupling reactions following the results of Charette's studies,[51] which mirrored the observations of Itami[1] where biaryl coupling could be afforded through the combination of high temperature, potassium *tert*-butoxide and pyridine as solvent. My investigation into this chemistry began with the reproduction of the results observed by Charette under his additive-free reaction conditions.[51] The simple substrate 2-(benzyloxy)iodobenzene **5.3**, used in his work, was synthesised by reaction of 2-iodophenol **5.1** with benzyl bromide **5.2** as per literature procedure,[126] affording the target in excellent yield (Scheme 5.1a).
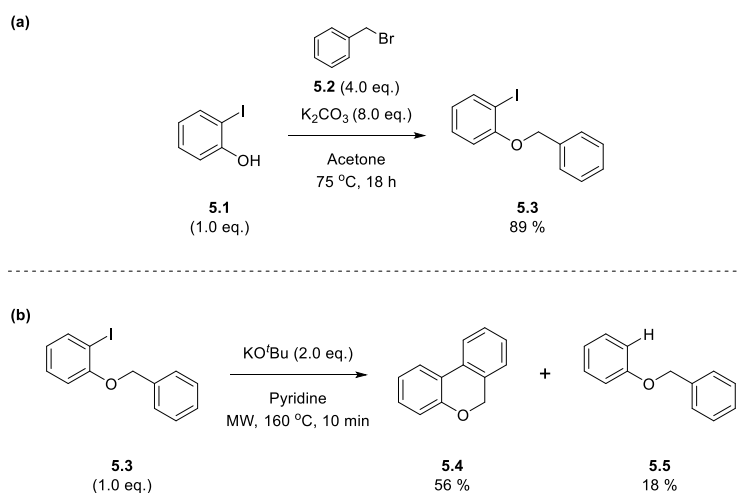
Scheme 5.1: (a) Synthesis of substrate **5.3** used by Charette;[126] (b) reaction of substrate **5.3** under Charette's transition metal-free coupling conditions.[51]

Taking the chemistry forward, the next step was to subject substrate **5.3** to Charette's reaction conditions. Similar to their results, the coupled product **5.4** was obtained in 56 % yield, along with 18 % of the reduced starting material **5.5** (Scheme 5.1b). Interestingly, the reaction was accompanied by a distinct colour change from an initial yellow to a deep red which, to us, was indicative of the formation of a highly conjugated system. Satisfied with the reproduction of this chemistry, we began to speculate on the nature of the mechanism by which a radical process could be initiated under these reaction conditions.

Within our own research group, a set of highly-conjugated organic molecules, aptly named Super Electron Donors (SED), have been developed (Scheme 5.2a).[127,128] These

neutral organic reagents have a broad scope of reactivity based on their ability to donate one or two electrons. The reductive ability of these SEDs is best illustrated as per Scheme 5.2b. Using **5.7** as an illustrative example, we see that upon loss of a single electron to form **5.9**, aromaticity is generated in one of the two imidazole rings, with the radical generated on the other ring being stabilised by the neighbouring nitrogen atoms. Subsequent loss of a second electron affords the dicationic species **5.10** which, as before, is a facile reaction due to the generation of aromaticity on the second imidazole ring.
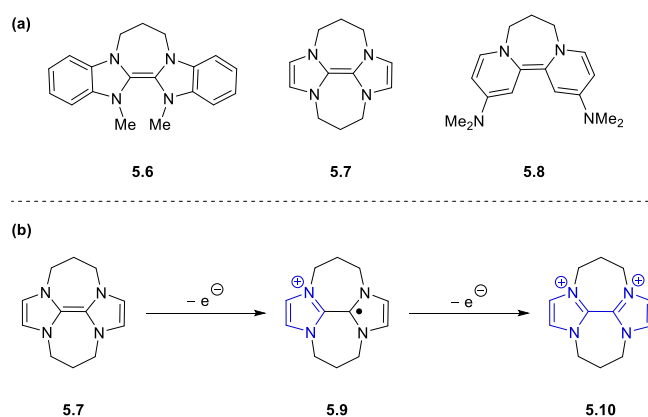
Scheme 5.2: (a) Structures of organic Super Electron Donors **5.6-5.8** developed in the Murphy group; (b) generation of aromaticity (shown in blue) following loss of two electrons from **5.7**.[127, 128]

Typically, SEDs **5.6** and **5.7** are generated *in situ* from reaction of the corresponding precursor disalt with a base such as sodium hydride.[129, 130] In line with the chemistry discussed so far, it is worth noting that C—C bond formations are indeed achievable using these reagents. For example donor **5.6**, generated from the disalt **5.12**, has been shown to reduce aryl iodides such as **5.11** to their corresponding aryl radical.[129] Following an intramolecular radical cyclisation, the *N*-protected indoline product **5.13** is obtained in excellent yield (Scheme 5.3).

Scheme 5.3: Synthesis of *N*-protected indolines via a radical intramolecular cyclisation reaction.[129]

These reagents are not restricted to the generation of radical intermediates; in fact donor **5.7** has been demonstrated to mediate reactions that require an anionic pathway.[130] To determine if these donors were donating one or two electrons, the iodoester **5.14** was synthesised; a carbon radical will not react with the ester group in this molecule, however a carbanion will. First to be tested was donor **5.6**, which afforded only the dehalogenated product **5.15**, expected to form via an aryl radical intermediate. Using donor **5.7** for the same reaction gave the dehalogenated species **5.15** as the major product; however the cyclised product **5.16**, formed by attack of an aryl anion on the ester, was also obtained in 16 % yield (Scheme 5.4).

Scheme 5.4: Demonstration of a double-electron transfer from donor **5.7**.[130]

It was discovered that the DMAP-derived donor **5.8**, developed within our group, has a broad absorption peak at 345 nm, making it a suitable candidate to undergo photoactivation. This has indeed been achieved using commercially available UV lamps (typically with a wavelength of 365 nm), and has allowed for more challenging transformations, including the reduction of aryl chlorides such as **5.17** under mild conditions, to be within the scope of our donors.[131] This enhanced reactivity is best demonstrated by a comparison of thermal versus photoactivation reaction conditions; no dehalogenation is observed upon heating the reaction mixture to 100 $^\circ$C. Using appropriate photoactivation (365 nm), however, afforded the dehalogenated product **5.18** in excellent yield even at room temperature (Scheme 5.5).[131]

Scheme 5.5: Reduction of aryl chloride **5.17** by photoactivated organic SED **5.8**.[131]

Considering the nature of the chemistry discussed, we began to speculate that during the course of these reactions, an organic super electron donor formed *in situ* might be

responsible for the conversion of **5.3** to **5.4**. Expanding on this idea, we tentatively proposed the mechanism outlined in Scheme 5.6.

Scheme 5.6: Pathway for the formation of neutral organic electron donor **5.26** proposed to form under Charette's reaction conditions.

It has previously been discussed that precedent exists for the formation of benzyne intermediates from aryl halides at elevated temperatures.[15-17, 33, 34] With this in mind, we proposed this as a starting point for our computations. In order to reduce computational cost, iodobenzene **5.19** was studied rather than **5.3** as the benzyloxy substituent was not vital to our proposed mechanism (Scheme 5.6). Accepting at this point that a purely benzyne-mediated mechanism was not affording the observed coupling, the idea of forming an electron donor *in situ* was pursued. Literature focussed on the reaction of benzyne has noted that in the absence of a sufficiently reactive coupling partner, an external nucleophile can attack the benzyne intermediate to form a substituted product.[19, 39] Reaction of a *tert*-butoxide anion with benzyne might lead to the formation of an electron donor; aryl Grignard[132] and arylzinc[133] reagents have been speculated to afford such reactivity. However, the reaction of pyridine with benzyne offered a more promising outlet. Literature precedent exists for the nucleophilic attack of benzynes by pyridine,[21] giving us confidence in our proposal that intermediate **5.22** could be formed from such an attack.

Intermediate **5.22**, we proposed, could undergo one of two reaction pathways; intramolecular proton abstraction to give carbene **5.24** directly, or a *tert*-butanol mediated pathway involving protonation to give **5.23** and a subsequent deprotonation of this to afford carbene **5.24**. From here, reaction with a molecule of the preceding

intermediate **5.23** would afford the dimer **5.25** which, following deprotonation, yields the candidate neutral electron donor **5.26**. Structurally, this bears some resemblance to the DMAP-derived electron donor **5.8** used extensively within our own research group.[131, 134, 135] Experimentally, it was demonstrated by Dr Eswararao Doni in our research group that using the chloride salt of **5.23** as an additive in these reactions could lead to synthesis of biaryls. This positive result was encouraging, as it supported our proposal that a donor such as **5.26** could in fact be formed in the presence of a suitable base (Scheme 5.7).
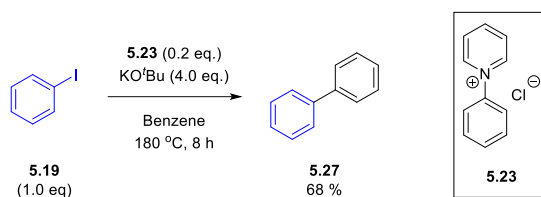
Scheme 5.7: Experimental investigation carried out by Dr Eswararao Doni in support of the proposed formation of donor **5.26**.

5.2 Computational Methods

DFT calculations were performed using the Gaussian 09 software package.[136] All reaction species were optimised using the M06L functional[115, 137] with the triple-ζ 6-311G(d,p) basis set.[138-140] Density fitting was specified using the 'auto' keyword.[141, 142] Implicit solvation of the reaction systems was modelled using the CPCM model with the associated parameters for pyridine.[116, 117] Frequency calculations were performed on all optimised structures in order to characterise them as minima (zero imaginary frequencies) or saddle points (single imaginary frequency) and to obtain thermochemical data. All calculations were modelled at a temperature of 298 K. Throughout this chapter, unless stated otherwise, the reactant and product state for each transformation was taken to be the reaction complex rather than the separated reactant and product species. As an approximation to improve computational efficiency, potassium *tert*-butoxide has been modelled as a monomeric entity, despite being a tetrameric species.

5.3 Results and Discussion

In our initial studies looking at the formation of benzyne **5.20**, we were unable to locate a transition state for the concerted deprotonation-loss of iodide; however a stepwise pathway affording the same outcome was identified (Figure 5.1). Looking at the reaction free energies, we see that for the initial deprotonation step the product complex **5.29** is 1.5 kcal mol^{-1} higher in energy than the transition state. When the electronic energies are considered instead, the transition state does in fact represent a true reaction maximum and, similarly, the product complex is a reaction minimum. With respect to the electronic energy, the reverse reaction has a 1.3 kcal mol^{-1} energy barrier. These energetics indicate that the reverse reaction is favoured in this instance, affording the starting complex predominantly. Due to the endergonic nature of the forward reaction, and in keeping with Le Chatelier's principle, it is expected that benzyne could form in this manner under the conditions employed in these reactions.
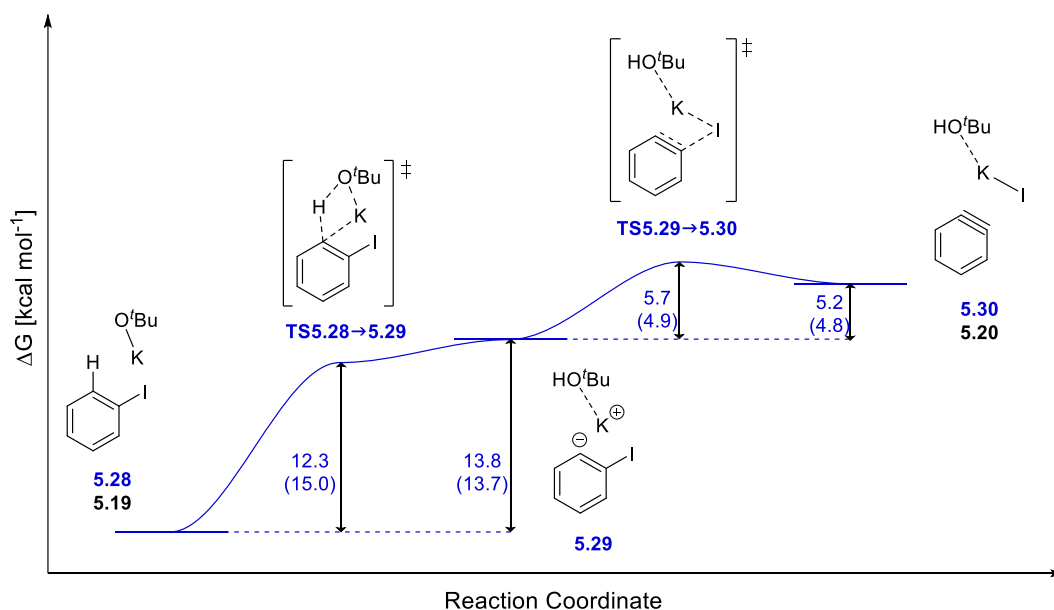
Figure 5.1: Gibbs free energy (ΔG) profile for the formation of benzyne **5.20** from reaction of iodobenzene **5.19** with potassium *tert*-butoxide. Values in parentheses correspond to the change in electronic energy (ΔE). Structure numbers in blue correspond to the reaction complex modelled computationally, while structure numbers in black represent the separate species involved.

The geometries obtained from these calculations also highlight the stepwise manner of this pathway. Following the initial deprotonation, no significant decrease in the C—C bond length of the forming aryne is observed in **5.29** (0.02 Å difference between

reactant complex **5.28** and intermediate complex **5.29**). The C—I bond is beginning to extend, but does not appear to be cleaved following an increase in the C—I distance of 0.11 Å in **5.29** relative to **5.28**. Looking at the transition state **TS5.28→5.29**, the O—H distance of 1.15 Å is only marginally greater than the 1.02 Å bond length of intermediate **5.29**, indicative of a late transition state (Figure 5.2). Based on the Hammond Postulate,[143] such transition states are associated with endothermic processes, in good agreement with experimental observations for benzyne formation by this method.
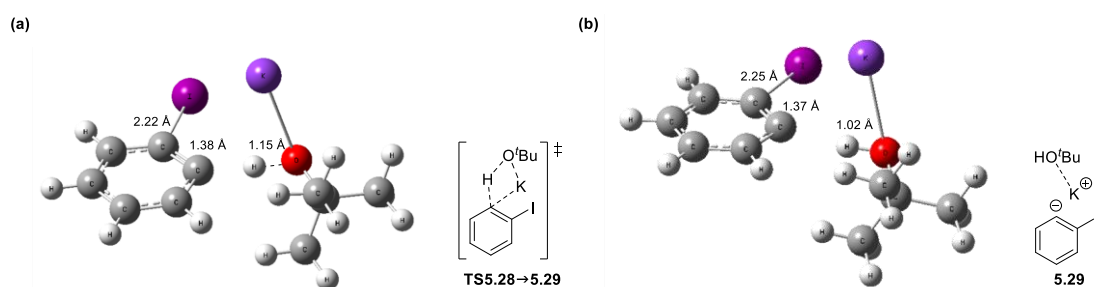
Figure 5.2: Optimised geometries of (a) the transition state complex **TS5.28→5.17** and (b) the product complex **5.29** for the initial deprotonation of iodobenzene.

In the second step of this transformation, transition state **TS5.29→5.30** was identified in which both the C—I bond extension and C—C bond contraction could be observed (Figure 5.3a). This transformation had an activation barrier of 5.7 kcal mol^{-1} which, in addition to the relative free energy of the initial step, gives the overall formation of benzyne by this method a total barrier of 19.5 kcal mol^{-1}. Once again, a low barrier for the reverse reaction is observed, equal to 0.5 kcal mol^{-1} on the free energy scale. Subsequent dissociation of the product complex into its individual components is exergonic by a value of 8.8 kcal mol^{-1}. Thus it can reasonably be expected that in the absence of an alternative nucleophile, the product complex **5.30** will collapse to the initial reactant state **5.28**.
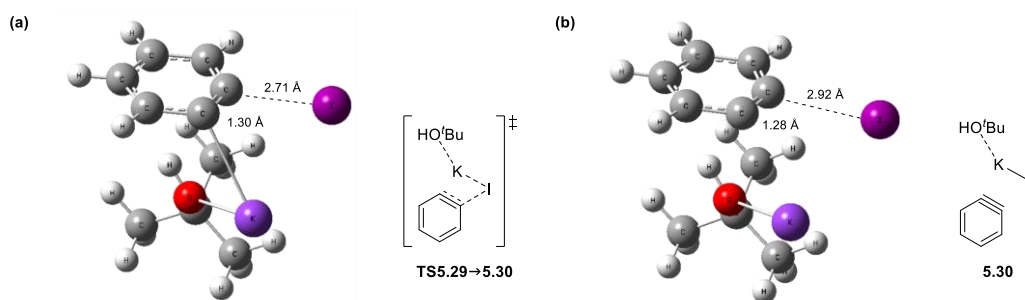
Figure 5.3: Optimised geometries of (a) the transition state complex **TS5.29→5.30** and (b) the product complex **5.30** for the loss of iodide from **5.29** to generate benzyne **5.20**.

Following the generation of benzyne, the next step was the nucleophilic attack on this intermediate by a molecule of pyridine, resulting in **5.22**. Expectedly, the reactant complex **5.31** took the form of a π-stack. Location of the transition state for this transformation required a manual transition state scan, which was performed by stretching the C—N bond of the product **5.22** initially over 0.1 Å increments between 1.48 and 2.18 Å, followed by smaller 0.02 Å increments between 1.86 and 2.06 Å. Frequency calculations were performed on each of these in order to identify the structure with a single imaginary frequency corresponding to the C—N bond formation (Figure 5.4). Looking at the energetics for this step, we note a minimal activation barrier of 4.0 kcal mol^{-1} (Figure 5.5). The overall coupling of these two reactants is significantly exergonic, with a relative free energy of -16.4 kcal mol^{-1}. With the reverse reaction now requiring a 20.4 kcal mol^{-1} barrier to be overcome, it is likely that from this point on the potential energy surface, the reaction coordinate will proceed in the forward direction.
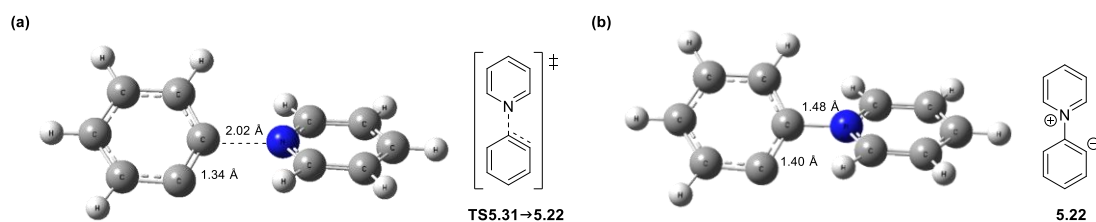
Figure 5.4: Optimised geometries of (a) the transition state complex **TS5.31→5.22** and (b) the product complex **5.22** for the coupling of pyridine with benzyne.

As discussed earlier, species **5.22** has two potential pathways by which it can form **5.24**. Considering firstly the *tert*-butanol-mediated pathway, a minimal activation energy of 0.1 kcal mol^{-1} is observed for the initial deprotonation of *tert*-butanol by the

phenyl anion moiety of **5.22**, with the intermediate complex **5.33** being energetically favoured by 8.6 kcal mol^{-1}. Subsequent deprotonation of the pyridinium moiety of **5.23** has a negative activation free energy; inspection of the electronic energies for this reaction step once again confirm that the calculated geometries represent true minima (reactant and product complexes) and maxima (transition state complex). This reaction is also exergonic by 5.7 kcal mol^{-1}, giving the overall transformation from **5.31** to **5.34** a net energetic loss of 30.7 kcal mol^{-1}.
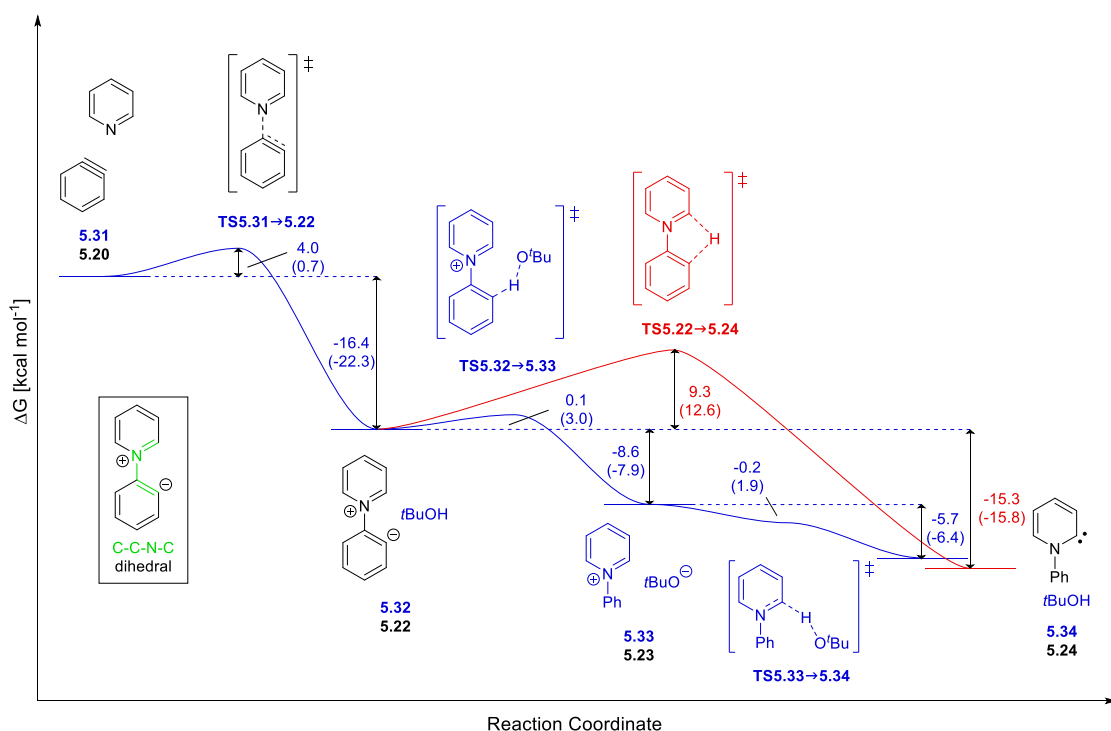
Figure 5.5: Gibbs free energy (ΔG) profile for the formation of the carbene intermediate **5.24** from the reaction of benzyne **5.20** with pyridine followed by proton transfer. Structures specific to the *tert*-butanol mediated pathway are shown in blue; structures in red are associated with the intramolecular proton transfer. Values in parentheses correspond to the change in electronic energy (ΔE). Structure numbers in blue or red correspond to the reaction complex modelled computationally, while structure numbers in black represent the separate species involved.

Looking towards the alternative intramolecular proposal, an activation energy of 9.3 kcal mol^{-1} is required for this transformation to proceed. While this is a feasible barrier to overcome, and one which leads to an energetically favoured product, it is substantially higher than those calculated in the *tert*-butanol-mediated route. This can be rationalised by the disfavoured planarity required (dihedral angle = 0.1 °) to form the transition state relative to a ground state dihedral of 35.2 °.

The final steps towards the formation of our proposed electron donor involve the coupling of carbene **5.24** with the preceding phenylpyridinium species **5.23**, and the subsequent deprotonation of the resulting intermediate **5.25** by potassium *tert*-butoxide to afford **5.26** (Figure 5.6). The reaction of **5.24** with **5.23** proceeded with an activation energy of only 2.6 kcal mol^{-1}, with intermediate **5.25** being 16.0 kcal mol^{-1} lower in energy than the reactant complex **5.35**. Similar to the previous step, the activation energy for the deprotonation of **5.25** is only 3.9 kcal mol^{-1}, with product complex **5.37** being energetically favoured by -30.1 kcal mol^{-1} relative to **5.36**.
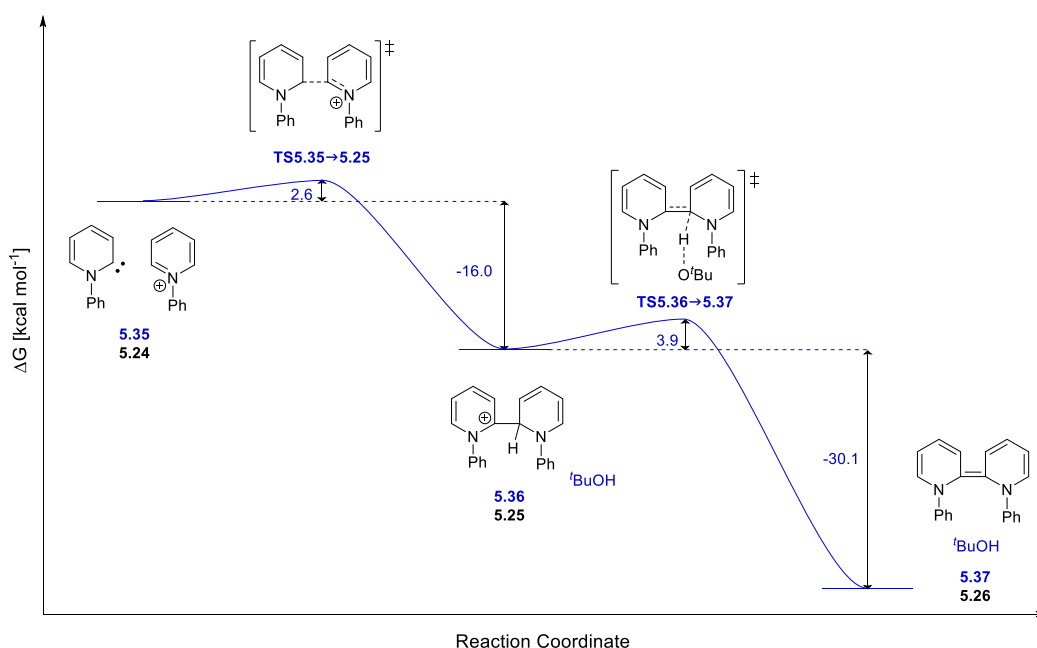
Figure 5.6: Gibbs free energy (ΔG) profile for the formation of the proposed neutral organic donor **5.26** from the reaction of carbene **5.24** with the pyridinium species **5.23**, followed by deprotonation by potassium *tert*-butoxide. Structure numbers in blue correspond to the reaction complex modelled computationally, while structure numbers in black represent the separate species involved.

On initial observation of the structure of the proposed donor **5.26**, it's reasonable to expect that its formation might be ill-affected by the steric bulk of the two phenyl groups. Interestingly, however, looking at the optimised geometry we see that the two phenyl groups are angled slightly away from each other. In addition to this, it is reasonable to expect that there is, to some extent, favourable π—π interactions between these two substituents (Figure 5.7). Structure **5.26** assumes a relatively planar conformation about the two pyridine moieties, which are in a *cis*-conformation about the bridging alkene. To confirm that this was in fact the more stable

conformation, the *trans*-isomer **5.38** was also modelled. Comparing the two structures, the *trans*-isomer is energetically disfavoured by 4.3 kcal mol^{-1} relative to the *cis*-isomer, confirming that we were investigating the more stable product.

Table 5.1: Summary of the calculated Gibbs free energies (ΔG) and electronic energies (ΔE) [kcal mol^{-1}] of intermediate and product complexes relative to **5.28** for the overall transformation **5.28→5.37**.

Reaction Complex	5.28	5.29	5.30	5.22	5.33
ΔG$_{rel}$	0	13.8	19.0	2.6	-6.0
ΔE$_{rel}$	0	13.7	18.5	-3.8	-11.7
Reaction Complex	5.34	5.24	5.36	5.37	
ΔG$_{rel}$	-11.7	-12.7	-28.7	-58.8	
ΔE$_{rel}$	-18.1	-19.6	-37.3	-66.2	
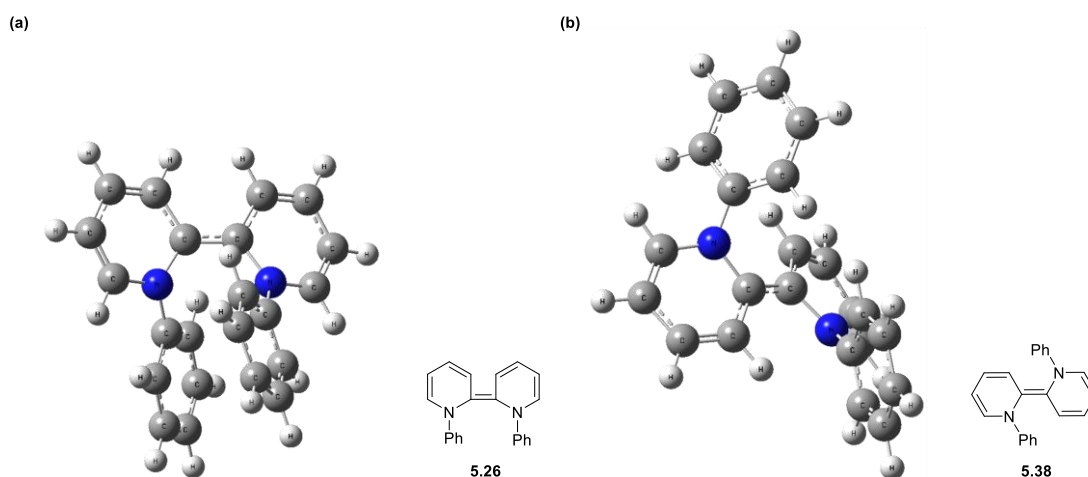
Figure 5.7: Optimised geometry of (a) the energetically favoured *cis*-isomer **5.26** and (b) the energetically disfavoured *trans*-isomer **5.38**.

In order to demonstrate the requirement for benzyne formation to afford the observed coupling, it was necessary to attempt the reaction with a substrate from which benzyne cannot be generated. For this purpose, 2,6-bis(benzyloxy)iodobenzene **5.41** was synthesised in a two-step procedure starting from resorcinol **5.39** (Scheme 5.8a). Subjecting this substrate to Charette's conditions, we were intrigued to observe evidence for a radical coupling reaction (Scheme 5.8b). Although in lower yields relative to those observed when using 2-(benzyloxy)iodobenzene **5.3**, we were able to

identify the coupled product 1-(benzyloxy)-*6H*-benzo[*c*]chromene **5.42** as well as some reduced starting material **5.43**. The lower yield of **5.42** relative to **5.43** can potentially be attributed to steric effects about the radical centre generated following the initial electron transfer.
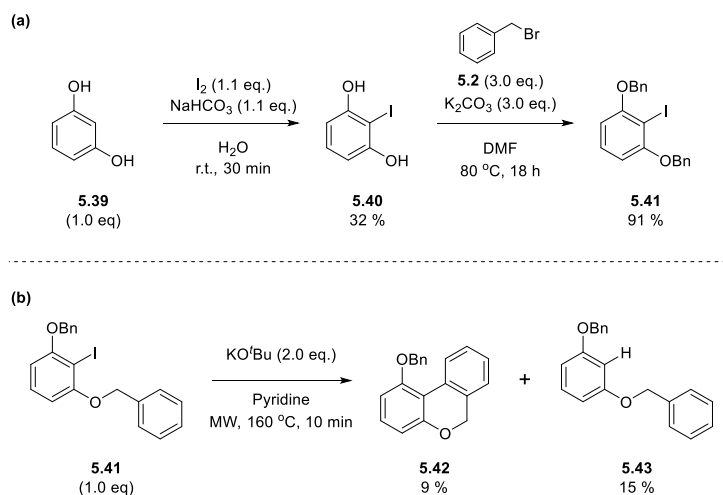
Scheme 5.8: (a) Synthetic route towards substrate **5.41**; (b) reaction of substrate **5.41** under Charette's reaction conditions.

With this unexpected result in hand, we turned our attention to the reactions which utilise 1,10-phenanthroline **5.44** as an additive in an attempt to gain mechanistic insight into these transformations and explain these curious observations. This reagent has featured substantially in the early publications in this area[39, 40, 46, 51] and is largely believed to act as a bidentate ligand, chelating the base to give rise to a complex such as **5.45**. The proposal was that this complex would then donate an electron to the substrate to afford its corresponding radical cation **5.46** plus the substrate radical anion, which would subsequently dissociate to the substrate radical plus iodide (Scheme 5.9). To test the viability of this proposal, the relative energetics for the process illustrated in Scheme 5.9 were investigated computationally. Employing both sodium and potassium *tert*-butoxide as the base, and benzene as the solvent, we obtained relative free energies of 63.9 and 59.5 kcal mol^{-1} respectively. Based on the temperatures typically employed in these reactions (100 – 150 $^{\circ}$C), it is difficult to envisage a thermodynamically accessible mechanism involving this particular electron transfer.
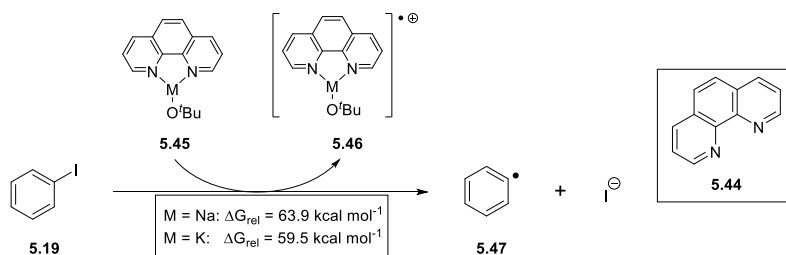
Scheme 5.9: Calculated reaction free energy for the radical initiation process, in benzene as solvent, proposed widely within the literature when 1,10-phenanthroline **5.44** is used as an additive.

Knowing that an electron donor must be formed *in situ* in order to initiate these reactions, we began to speculate as to how a donor could be formed from 1,10-phenanthroline in the presence of potassium *tert*-butoxide. A colleague within the group, Dr Shengze Zhou, was also investigating this chemistry. He subjected 1,10-phenanthroline **5.44** to reaction with potassium *tert*-butoxide in benzene with heating in a sealed pressure tube. Upon exposure to air, the reaction mixture was found to be pyrophoric, and so the experiment was repeated incorporating an oxidative work up using iodine. Purification by column chromatography allowed for the isolation of the product 2,3'-bis-1,10-phenanthroline **5.48**, which was identified by NMR (Scheme 5.10).
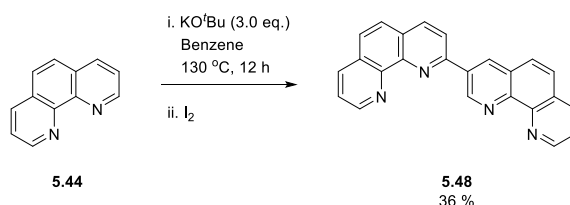
Scheme 5.10: Synthesis of 2,3'-bis-1,10-phenanthroline **5.48** as performed by Dr Shengze Zhou.

With such an intriguing result at hand, it was necessary to explore the energetics for the formation of this compound, since such a transformation had not previously been reported in the literature. Based on the isolated product **5.48**, we proposed the following pathway for its formation (Scheme 5.11). Deprotonation at the 2-position of 1,10-phenanthroline **5.44** would produce the anion **5.49** which could react at the 3-position of a second molecule of 1,10 phenanthroline via an *S$_N$Ar* reaction to form **5.50**. Deprotonation of this species by a second equivalent of potassium *tert*-butoxide produces the dianionic species **5.51** which, upon oxidative quenching by iodine, would afford the observed product **5.48**. Of course, formation of this species could equally

arise from initial deprotonation at the 3-position followed by attack at the 2-position and subsequent deprotonation of the anionic dimer. However, this deprotonation should be less favourable.
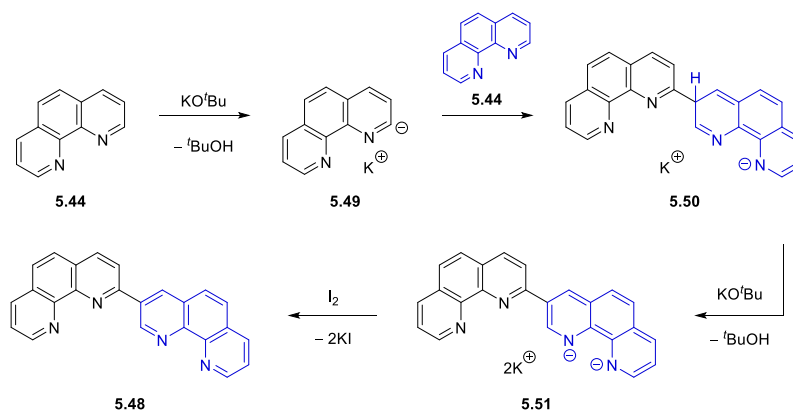
Scheme 5.11: Proposed mechanism for the formation of 2,3′-bisphenanthroline **5.48** via the proposed organic electron donor **5.51**.

Our investigation began by looking at the possibility of deprotonating 1,10-phenanthroline **5.44** with potassium *tert*-butoxide, a reaction which could happen at one of four positions. Due to the non-polar nature of the solvent in these reactions (benzene), we proposed that the potassium counter-ion would have an important role in the overall transformation. To demonstrate this, the binding free energies of the base with 1,10-phenanthroline were calculated for both the inclusion (Figure 5.8) and exclusion of the potassium ion (Table 5.2). From these values, it is clear that when potassium is included, the formation of the reactant complex is only energetically favoured when the base is chelated by the 1,10-phenanthroline, as observed for deprotonation at the 2-position (Figure 5.8a). For the three remaining positions, there is a small energetic cost associated with the formation of the reactant complex of between 2.2 – 5.6 kcal mol^{-1}. In these systems, it can be seen that the base is only loosely associated with the 1,10-phenanthroline, and that no cation − π interactions exist (Figure 5.8b-d). Interestingly, when the potassium cation is excluded in these systems, the binding energy associated with forming the reactant complex for deprotonation at the 2-position has an energetic demand of 1.6 kcal mol^{-1}, while the three remaining reactant complexes have favourable binding free energies of between 1.5 – 6.4 kcal mol^{-1}.

Table 5.2: Calculated binding free energies (ΔG_{bind}) and relative free energies (ΔG_{rel}) [kcal mol^{-1}] for potassium *tert*-butoxide and the *tert*-butoxide anion with 1,10-phenanthroline **5.44**.

Deprotonation Position	ΔG_{bind} (KO^{t}Bu)	ΔG_{bind} (^{t}BuO$^-$)	$\Delta\Delta G_{bind}$ [b]
2 [a]	-4.3	1.6	-5.9
3	5.6	-1.5	7.1
4	2.2	-6.4	8.6
5	2.5	-5.8	8.3

[a] in the presence of the potassium cation, the base is chelated by the substrate
[b] calculated relative to the binding free energy in the presence of the potassium cation
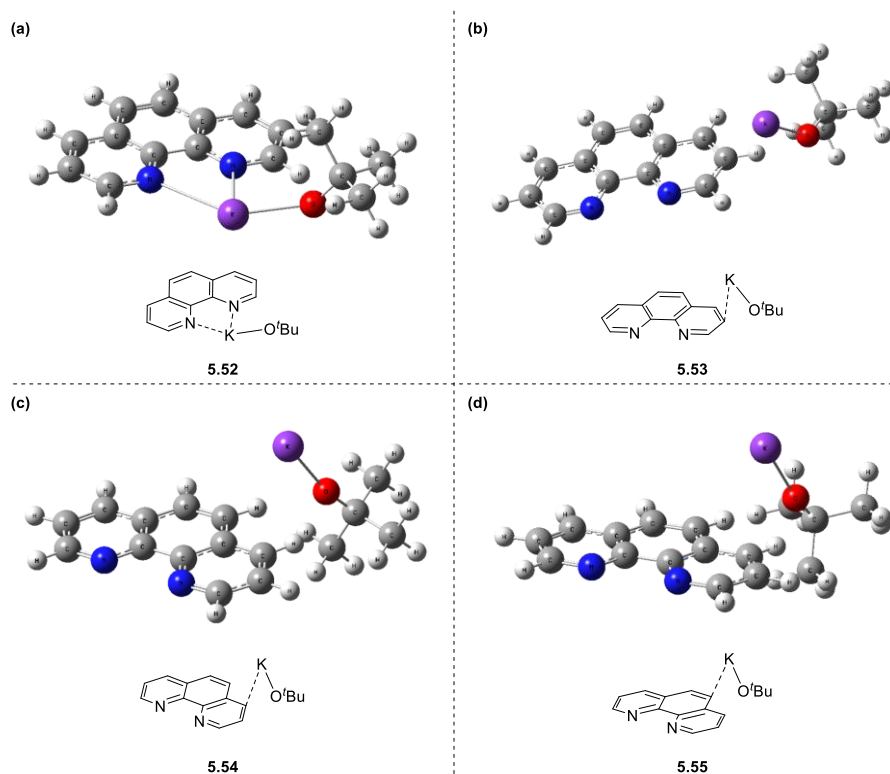
Figure 5.8: Optimised geometries of the reactant complexes for the deprotonation of 1,10-phenanthroline **5.44** at the (a) 2-; (b) 3-; (c) 4- and (d) 5-positions by potassium *tert*-butoxide.

From these reactant complexes, the corresponding transition state and product complexes were calculated for each possible deprotonation (Table 5.3). Energetically, the free energy barrier for deprotonation at the 2-position is 6.8 kcal mol^{-1} lower in the absence of the cation. Visual comparison of the transition states for this deprotonation in both the presence and absence of the potassium cation highlights key structural differences (Figure 5.9). In the absence of the cation, it is possible for the 1,10-

phenanthroline and the base to assume a more favourable electrostatic alignment, giving a C—H—O bond angle of 178.6 $^{\circ}$. This same level of pre-organisation is not possible when the chelated cation is included, which results in this bond angle decreasing to 163.5 $^{\circ}$. The C—O distance between the carbon of the 1,10-phenanthroline and the oxygen of the *tert*-butoxide is approximately equal both in the presence and the absence of potassium (2.69 Å and 2.66 Å respectively). The O—H bond distance, however, is slightly shorter in the presence of potassium, indicating a later transition state relative to that obtained in the absence of potassium (Figure 5.9).

Table 5.3: Calculated Gibbs free energies (ΔG) and electronic energies (ΔE) [kcal mol^{-1}] relative to reactant complexes **5.52**-**5.55** for deprotonation of 1,10-phenanthroline **5.44** at various positions.

Deprotonation Position	ΔG^*	ΔG_{rel}	ΔE^*	ΔE_{rel}
2^a	15.6 (8.8)	15.8 (10.2)	17.10 (10.7)	17.09 (9.6)
3^b	15.5 (6.7)	16.0 (7.6)	16.6 (8.8)	16.1 (7.4)
4	16.6 (8.7)	17.9 (10.0)	18.3 (10.6)	18.2 (9.5)
5	18.0 (9.3)	19.4 (10.6)	19.63 (11.9)	19.59 (11.1)

^{a} denotes systems where the potassium cation was chelated.
^{b} in the absence of a potassium cation, this system relaxed to the structures observed in entry 1.
Values in brackets were obtained in the absence of a potassium counter ion.
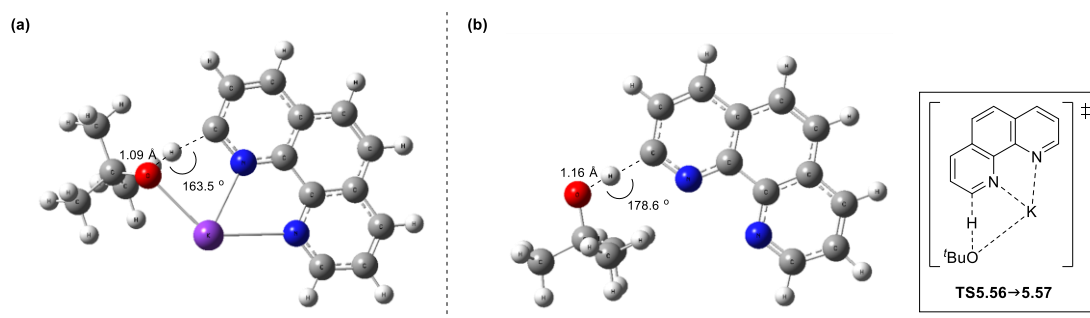
Figure 5.9: Optimised geometries of the transition state **TS5.56→5.57** (a) in the presence and (b) in the absence of a potassium counter ion.

For the deprotonations at the 3-, 4- and 5 positions, transition states where the base is not chelated were obtained in both the presence and absence of the potassium cation. In all cases, the favourable alignment of the C, H and O atoms involved in these deprotonations was observed. As with the deprotonation at the 2-position, inclusion of the potassium cation raised the activation free energy by between 7.9 – 8.8 kcal mol^{-1}. For each possible deprotonation, the electronic potential energy surface was probed

to confirm that the optimised geometries represented true reaction maxima and minima. The challenging nature of these deprotonations is best highlighted by considering the energetics for the reverse reactions, with the highest calculated barrier being a mere 1.4 kcal mol^{-1}. Based on the endergonic nature of this first reaction step, the subsequent reaction steps would need to be sufficiently exergonic that the forward pathway is more favourable than the reverse of the deprotonation.

Following deprotonation, anion **5.49** reacts with a second molecule of 1,10-phenanthroline (Scheme 5.11). Similar to the deprotonation step, this second step offers a number of options for where the addition could occur. In order to determine if any selectivity exists for this process, the attacks onto the 2-, 3-, 4- and 5-positions of the second phenanthroline molecule were modelled (Figure 5.10). In all cases, the dimer formed subsequently underwent deprotonation by a molecule of potassium *tert*-butoxide to give the proposed electron donor. The energetics for these transformations are summarised in Figures 5.11 – 5.14.
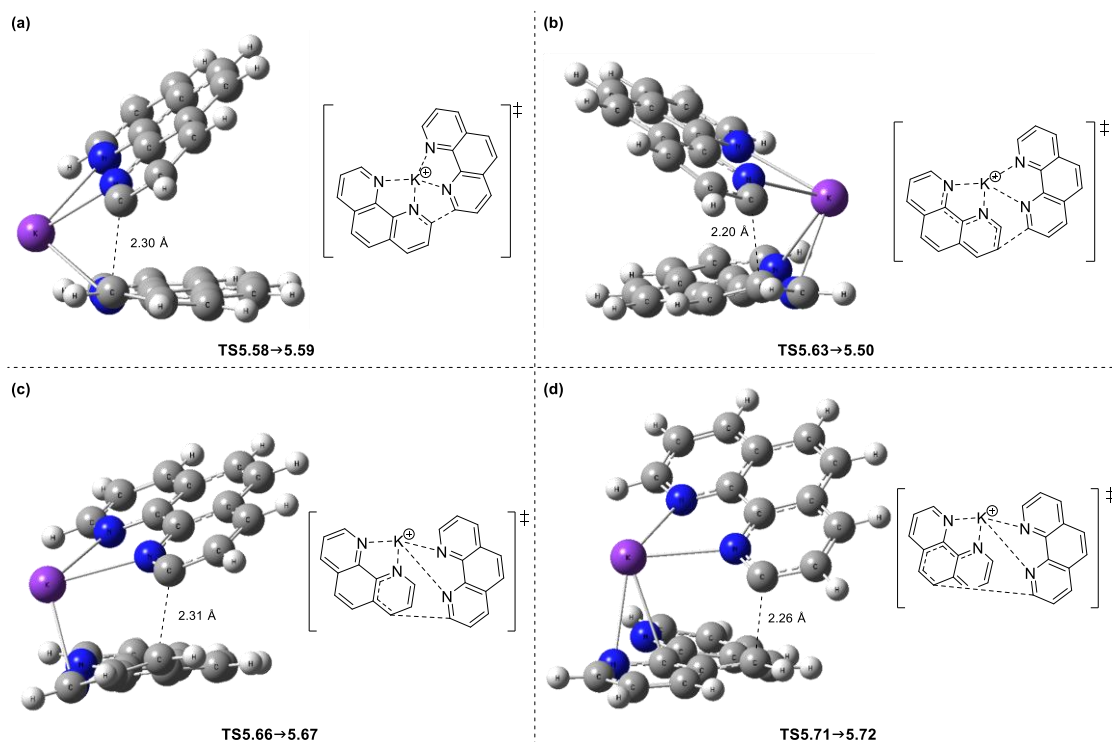
Figure 5.10: Optimised geometries of the transition states for the coupling of anion **5.49** to a second molecule of 1,10-phenanthroline **5.44** at the (a) 2-; (b) 3-; (c) 4- and (d) 5-positions.
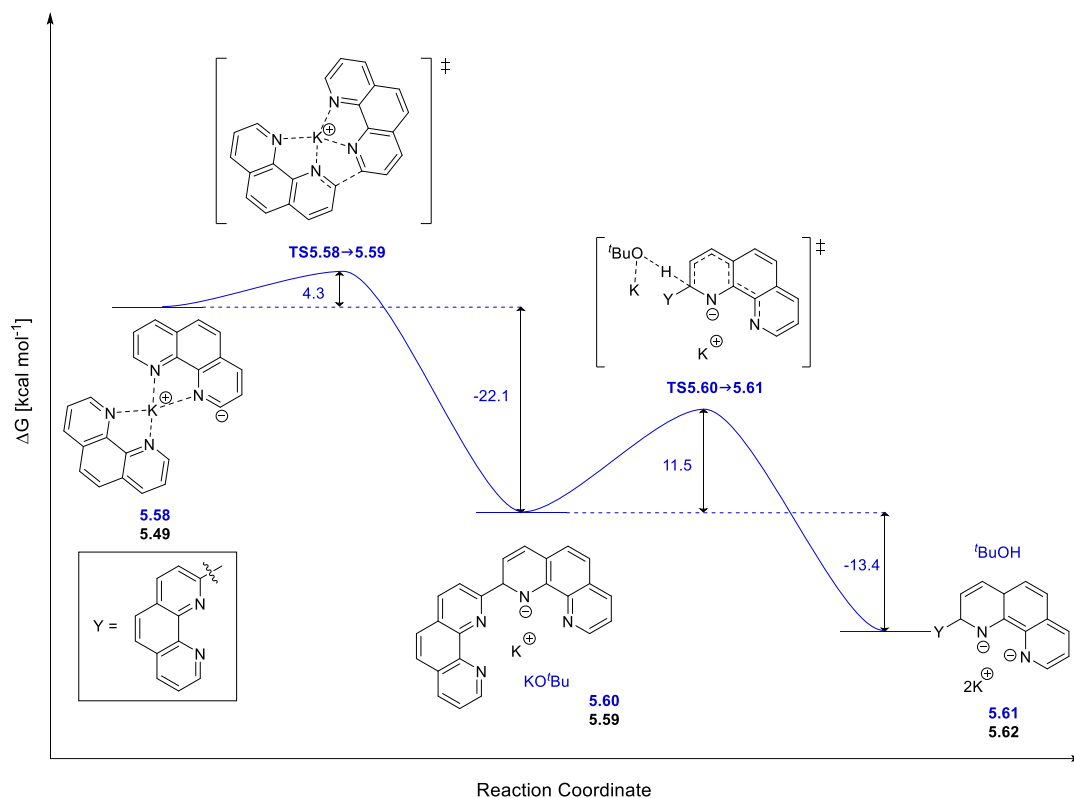
Figure 5.11: Gibbs free energy (ΔG) profile for the formation of the proposed 2,2'-bisphenanthroline donor **5.62**. Structure numbers in blue correspond to the reaction complex modelled computationally, while structure numbers in black represent the separate species involved.

Considering firstly the formation of donor **5.62** upon the addition of anion **5.49** to the 2-position of a second molecule of 1,10-phenanthroline, only a small activation barrier must be overcome in order to afford dimer **5.59**. This intermediate is significantly exergonic relative to the starting complex, and would compensate energetically for the endergonic deprotonation which precedes it. Donor **5.62** is formed following deprotonation of intermediate **5.59**, a reaction which has an 11.5 kcal mol^{-1} barrier associated with it. The product complex **5.61** is exergonic by 13.4 kcal mol^{-1} relative to **5.60**, giving a net energetic loss of 35.5 kcal mol^{-1} from **5.58** to **5.61**.
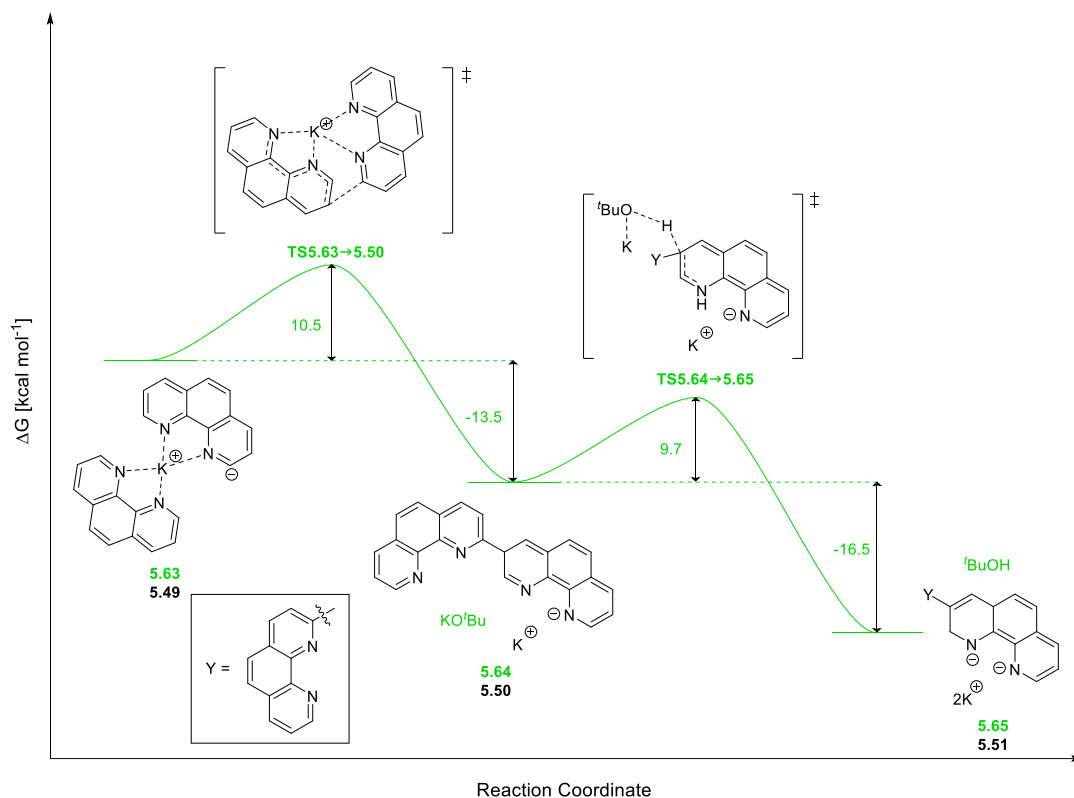
Figure 5.12: Gibbs free energy (ΔG) profile for the formation of the proposed 2,3'-bisphenanthroline donor **5.51**. Structure numbers in green correspond to the reaction complex modelled computationally, while structure numbers in black represent the separate species involved.

The formation of donor **5.51**, proposed to form based on the experimental isolation of its oxidised analogue **5.48**, follows a similar energetic pathway. Formation of dimer **5.50** requires a slightly higher activation barrier of 10.5 kcal mol^{-1} to be overcome in order to afford dimer **5.50**, which is found to be 13.5 kcal mol^{-1} lower in energy than the reactant complex **5.63**. The deprotonation of **5.50** by potassium *tert*-butoxide proceeds with an activation free energy of 9.7 kcal mol^{-1}, and the product complex **5.65** is then 16.5 kcal mol^{-1} downhill relative to **5.64**, giving an overall energetic loss of 29.0 kcal mol^{-1} relative to **5.63**.
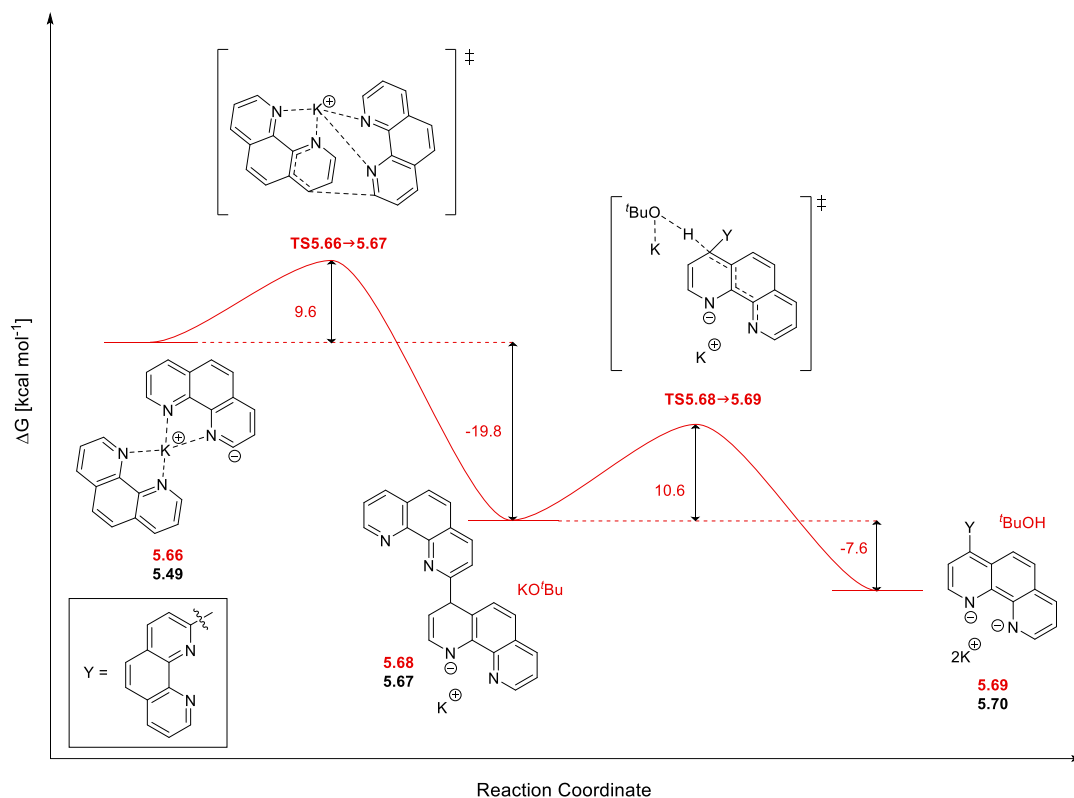
Figure 5.13: Gibbs free energy (ΔG) profile for the formation of the proposed 2,4'-bisphenanthroline donor **5.70**. Structure numbers in red correspond to the reaction complex modelled computationally, while structure numbers in black represent the separate species involved.

The pathway towards donor **5.70** consists of two exergonic reactions for both the initial coupling to form intermediate **5.67** and the subsequent deprotonation of this by potassium *tert*-butoxide. The first step proceeds following an accessible barrier of 9.6 kcal mol^{-1} to give **5.67**, which is 19.8 kcal mol^{-1} downhill of the preceding complex **5.66**. The deprotonation step has a slightly higher barrier of 10.6 kcal mol^{-1} that must be overcome in order to yield the product complex **6.69** with an energetic loss of 7.6 kcal mol^{-1}. Overall, this pathway has a net loss of 27.4 kcal mol^{-1}, which is comparable to that for the pathway towards donor **5.51**.
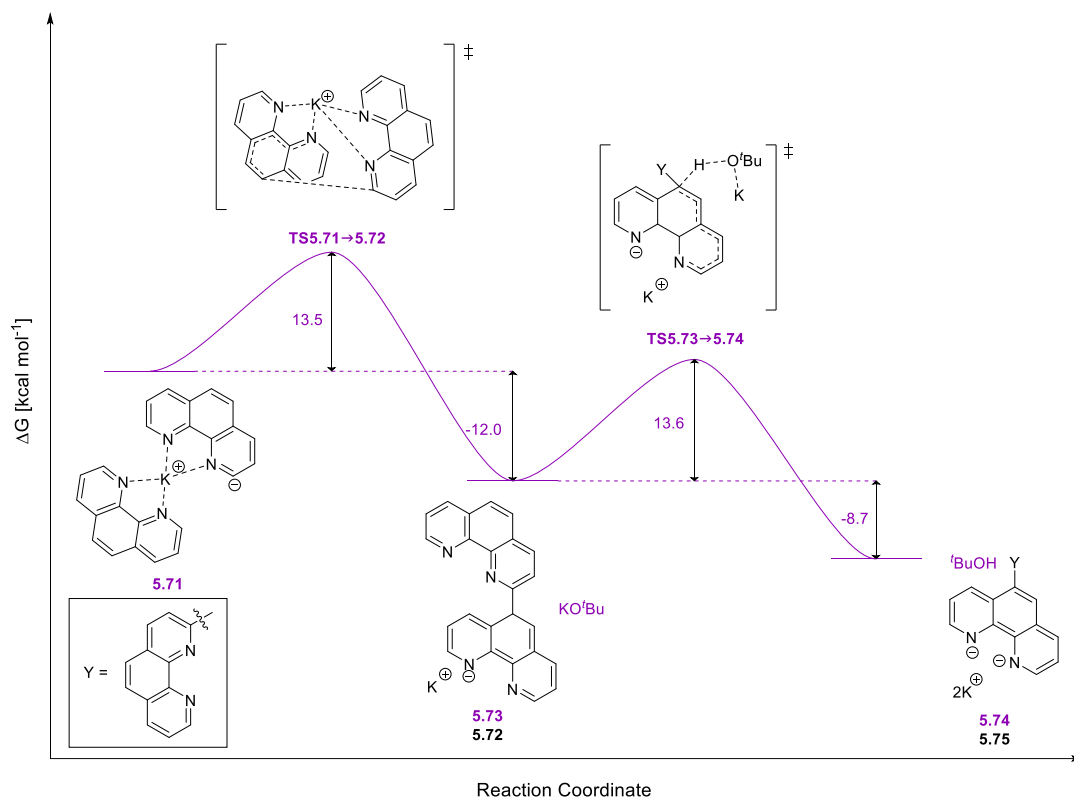
Figure 5.14: Gibbs free energy (ΔG) profile for the formation of the proposed 2,5'-bisphenanthroline donor **5.75**. Structure numbers in purple correspond to the reaction complex modelled computationally, while structure numbers in black represent the separate species involved.

The final possible dimerization pathway was predicted to be the most energetically-challenging. Indeed, this pathway was found to have activation free energies of 13.5 kcal mol^{-1} and 13.6 kcal mol^{-1} for the formation of **5.72** and **5.74** respectively. Overall, this pathway is stabilised by 20.7 kcal mol^{-1}, which is the least stabilisation observed in the four possible pathways.

A number of interesting observations can be made from these calculated reaction pathways. In all four cases, the net energetic loss from the steps following the initial deprotonation to form anion **5.49** is sufficient to make the formation of each donor exergonic overall. This deprotonation represents the rate-determining step for all three pathways, however if anion **5.49** is taken as the starting point, the rate determining step for the remaining two steps is not consistent across all pathways. In forming donor **5.62**, the rate-determining step is the deprotonation of intermediate **5.59**, with a barrier of 11.5 kcal mol^{-1}. This is also true for donors **5.70** and **5.75**, which require barriers of 10.6 kcal mol^{-1} and 13.6 kcal mol^{-1} to be overcome respectively. For

donor **5.51**, the formation of intermediate **5.50**, rather than the final deprotonation, is rate determining with an activation free energy of 10.5 kcal mol^{-1}. The two activation barriers towards donor **5.75** are the greatest observed across the series, and are approximately equal in value. Despite these differences, the energetic similarity of these barrier heights suggests that experimentally it is very likely that these proposed pathways will be in competition with each other, ultimately affording a mixture of products. This is in good agreement with experimental observations, where a number of products were found to have similar retention factors in the purification that ultimately led to the isolation of **5.48**.

Table 5.4: Summary of the calculated Gibbs free energies (ΔG) and electronic energies (ΔE) [kcal mol^{-1}] of intermediate and product complexes relative to **5.52** for the formation of bis-phenanthroline-based organic electron donors.

Reaction Complex	5.52	5.49	5.60	5.61
ΔG_{rel}	0.0	15.8	-6.2	-19.6
ΔE_{rel}	0.0	17.1	-5.8	-18.1
Reaction Complex	5.52	5.49	5.64	5.65
ΔG_{rel}	0.0	15.8	2.3	-14.2
ΔE_{rel}	0.0	17.1	1.8	-14.1
Reaction Complex	5.52	5.49	5.64	5.65
ΔG_{rel}	0.0	15.8	-4.0	-11.8
ΔE_{rel}	0.0	17.1	-4.6	-11.1
Reaction Complex	5.52	5.49	5.64	5.65
ΔG_{rel}	0.0	15.8	3.9	-4.8
ΔE_{rel}	0.0	17.1	2.6	-3.6

This understanding of the underlying mechanism for transition metal-free coupling reactions mediated by 1,10-phenanthroline **5.44** suggests that it is necessary to consider the possibility of a similar pathway affording the reactivity observed in the work of Itami[1] and Charette.[51] These transformations were both performed in the absence of an organic additive with pyridine as the solvent, which could indeed react

analogously to 1,10-phenanthroline. Similar to the previous experiment (Scheme 5.10), a substrate-free reaction was performed by Dr Shengze Zhou where pyridine **5.76** was heated with potassium *tert*-butoxide in benzene as solvent (Scheme 5.12). Unlike the 1,10-phenanthroline case, only a limited amount of product was formed from this reaction. Spiking the crude reaction mixture with reference standards allowed for the products 2,2'-bispyridine **5.77** and 4,4'-bispyridine **5.78** to be identified by GC-MS and ^{1}H NMR analysis. Interestingly, we note that the mixed product 2,4'-bispyridine **5.85** was not identified in the product mixture.
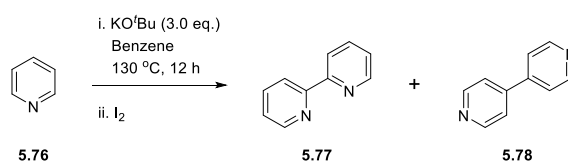
Scheme 5.12: Synthesis of 2,2'-bispyridine **5.72** and 4,4'-bispyridine **5.73** as performed by Dr Shengze Zhou.

By revising the mechanism proposed for the formation of the electron donor **5.51** from 1,10-phenanthroline, we proposed the following to rationalise the formation of the two bispyridine compounds **5.77** and **5.78** (Scheme 5.13). Initial deprotonation of pyridine **5.76** by potassium *tert*-butoxide at the 2- or 4-position[144] gives rise to the anions **5.79** and **5.82** respectively. These species can then act as nucleophiles and react with a second molecule of pyridine to form anions **5.80** and **5.83**. Deprotonation of each of these by a second equivalent of potassium *tert*-butoxide yields the proposed electron donors **5.81** and **5.84** which, upon oxidative work-up, afford the observed products **5.77** and **5.78**.
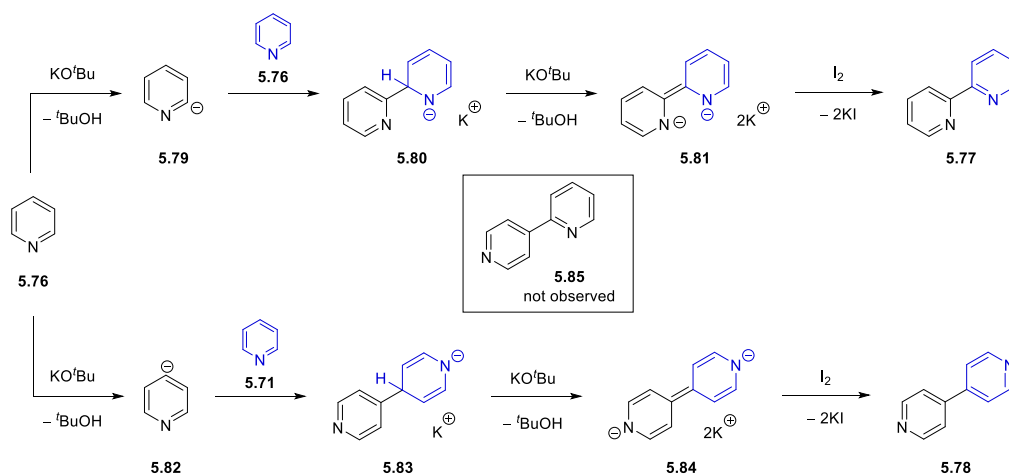
Scheme 5.13: Proposed mechanism for the formation of 2,2'-bispyridine **5.72** and 4,4'-bispyridine **5.73** via the proposed organic electron donors **5.76** and **5.79** respectively.

Although the experimentally observed products suggest that deprotonation only occurs at the 2- and 4-positions, computationally we considered the possibility of deprotonating at all three positions. Once again, unfavourable energetics were predicted for this first deprotonation and, as was observed previously with 1,10-phenanthroline **5.44**, the reaction barriers were slightly lower in the absence of the potassium cation (Table 5.5). The relative free energies show that deprotonation at the 4-position proceeds with the lowest energetic demand (1.9 and 2.0 kcal mol^{-1} less than for deprotonation at the 2- and 3-positions respectively). Inspection of the optimised reactant complex geometries reveals that of the three complexes, only **5.86** has the potassium cation interacting with the nitrogen of pyridine (Figure 5.15). The result of this is a stabilisation of 4.6 and 5.7 kcal mol^{-1} for complex **5.86** relative to complexes **5.87** and **5.88** respectively.
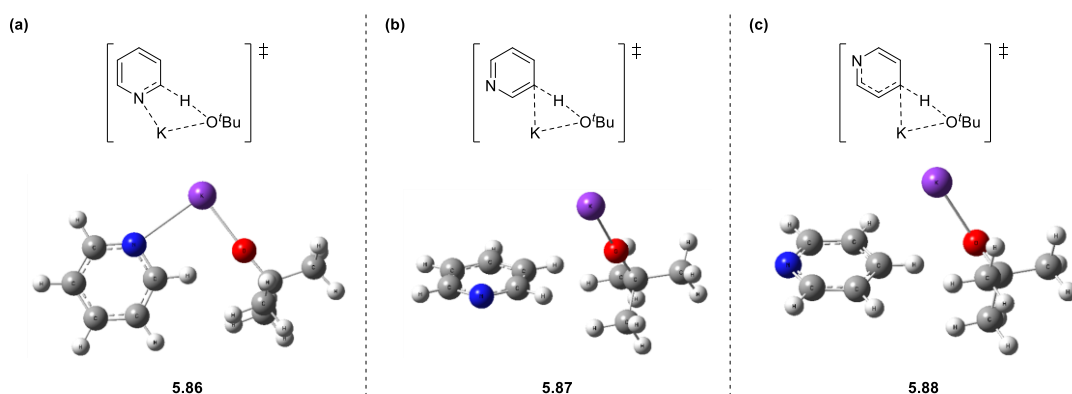
Figure 5.15: Optimised geometries of the reactant complexes (a) **5.86**, (b) **5.87** and (c) **5.88** for the deprotonation of pyridine **5.76** at the 2-, 3- and 4-positions respectively.

Table 5.5: Calculated Gibbs free energies and electronic energies [kcal mol^{-1}] relative to the reactant complexes **5.86**-**5.88** for deprotonation of pyridine by potassium *tert*-butoxide at different positions.

Deprotonation Position	ΔG^*	ΔG_{rel}	ΔE^*	ΔE_{rel}
2	18.5 (13.9)	18.6 (14.9)	19.6 (14.3)	19.5 (14.1)
3	17.3 (8.1)	18.7 (9.9)	18.0 (10.5)	17.8 (10.0)
4	16.3 (9.5)	16.7 (10.4)	17.2 (10.0)	17.0 (9.2)

Values in brackets were obtained for the same reaction step in the absence of a potassium counter ion.

Based on experimental observations, only the donor formation pathways involving deprotonation and / or nucleophilic attack at the 2- and 4-positions were investigated further through computational modelling. For the formation of 2,4-bispyridine **5.85**, two pathways required consideration here; one mediated via anion **5.79** and another via anion **5.82**. The calculated free energy profiles for these pathways are illustrated in Figures 5.16 – 5.19.

Following the endergonic formation of anion **5.79**, the coupling of this species with a second molecule of pyridine proceeds via an activation barrier of 15.0 kcal mol^{-1}, with product complex **5.80** forming following an energetic loss of 11.2 kcal mol^{-1} (Figure 5.15). The deprotonation of this intermediate by potassium *tert*-butoxide requires a barrier of 10.8 kcal mol^{-1} to be overcome, yielding **5.91** in a mildly exergonic reaction. The transformation from **5.89** to **5.91** has a total energetic loss of 14.4 kcal mol^{-1} which, taking into account the energetics for the initial deprotonation of pyridine **5.76** (ΔG_{rel} = 18.6 kcal mol^{-1}), gives an overall endergonic process.
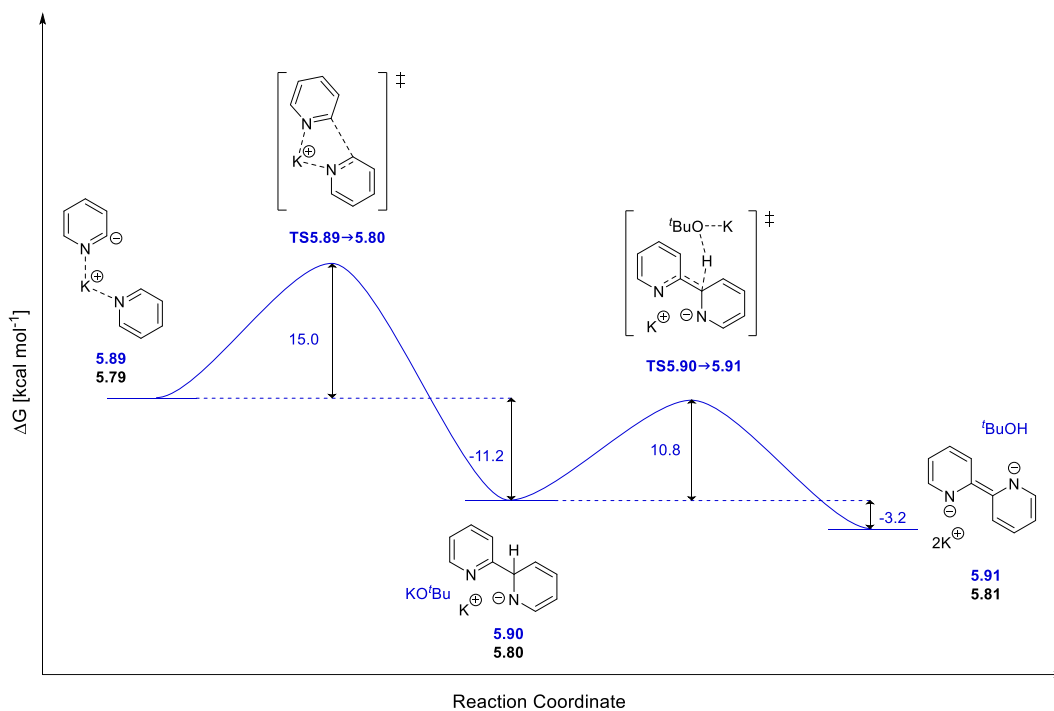
Figure 5.16: Gibbs free energy (ΔG) profile for the formation of proposed 2,2'-bispyridine donor **5.81**. Structure numbers in blue correspond to the reaction complex modelled computationally, while structure numbers in black represent the separate species involved.
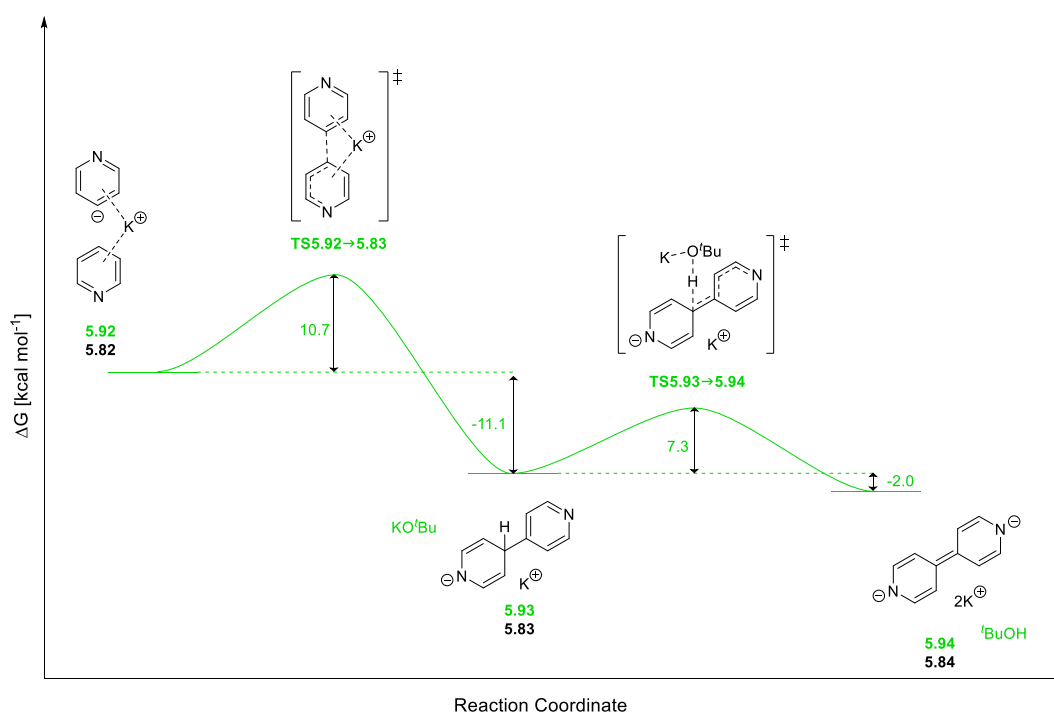
Figure 5.17: Gibbs free energy (ΔG) profile for the formation of proposed 4,4'-bispyridine donor **5.84**. Structure numbers in green correspond to the reaction complex modelled computationally, while structure numbers in black represent the separate species involved.

Considering the formation of the 4,4'-bispyridine donor **5.84**, the coupling of anion **5.82** with a second molecule of pyridine at the 4-position has an activation free energy of 10.7 kcal mol^{-1} to be overcome prior to the formation of **5.83**, found to be downhill of the reactant complex **5.92** by 11.2 kcal mol^{-1}. Following the accessible barrier of 7.3 kcal mol^{-1} the deprotonation of intermediate **5.83** can be achieved, affording **5.94** in a mildly exergonic reaction as was observed in the formation of **5.91**. Similar to the previous reaction pathway, the overall energetic loss of 13.1 kcal mol^{-1} is not sufficient to offset the endergonic nature of the initial deprotonation (ΔG_{rel} = 16.7 kcal mol^{-1}), again resulting in an overall endergonic process.
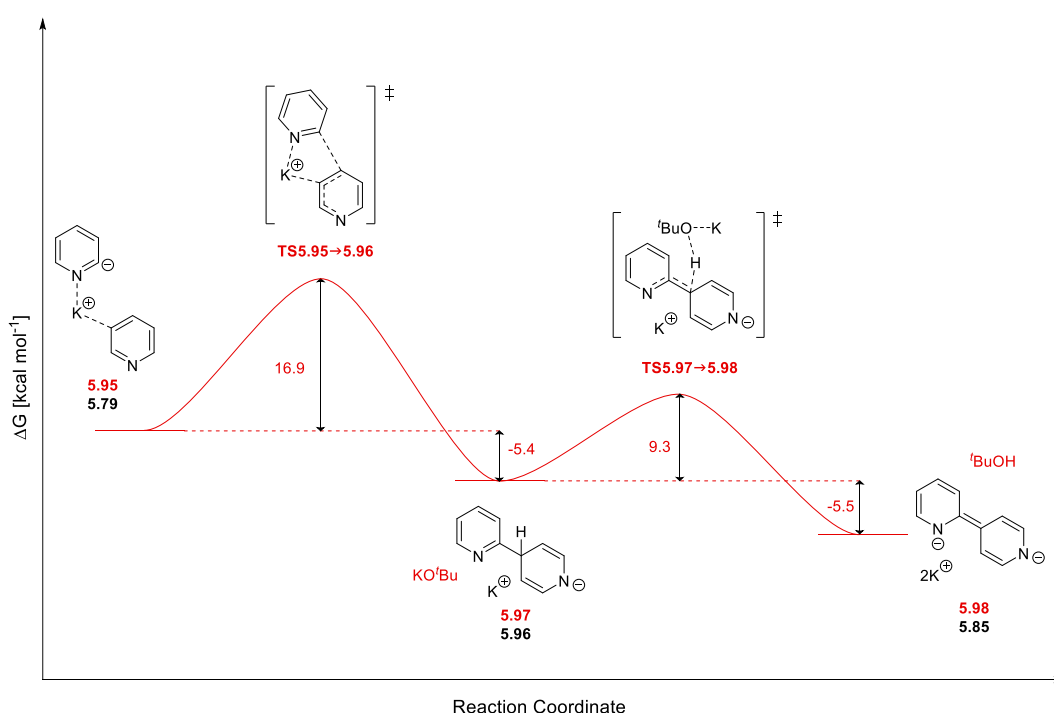
Figure 5.18: Gibbs free energy (ΔG) profile for the formation of proposed 2,4'-bispyridine donor **5.85** using anion **5.79** as the nucleophile. Structure numbers in red correspond to the reaction complex modelled computationally, while structure numbers in black represent the separate species involved.

For the first of the two possible pathways to the formation of the mixed 2,4'-bispyridine donor **5.85**, the attack of the second molecule of pyridine at the 4-position by anion **5.79** was investigated. For this reaction step a barrier of 16.9 kcal mol^{-1} must be overcome to yield intermediate **5.96**, which is only stabilised by 5.4 kcal mol^{-1} relative to the preceding reactant complex **5.95**. The deprotonation step has a similar energetic profile to that found in the formation of donors **5.81** and **5.84**, and is once again only slightly exergonic. This pathway bears an energetic loss of 10.9 kcal mol^{-1},

again resulting in an endergonic process overall. The alternative pathway towards **5.85** involving the attack of a pyridine molecule at the 2-position by anion **5.82** again has a similar energetic profile, albeit with slightly lower activation barriers relative to those in Figure 5.18. Noteworthy of this route is that the overall energetic loss is slightly higher at 14.4 kcal mol^{-1}.
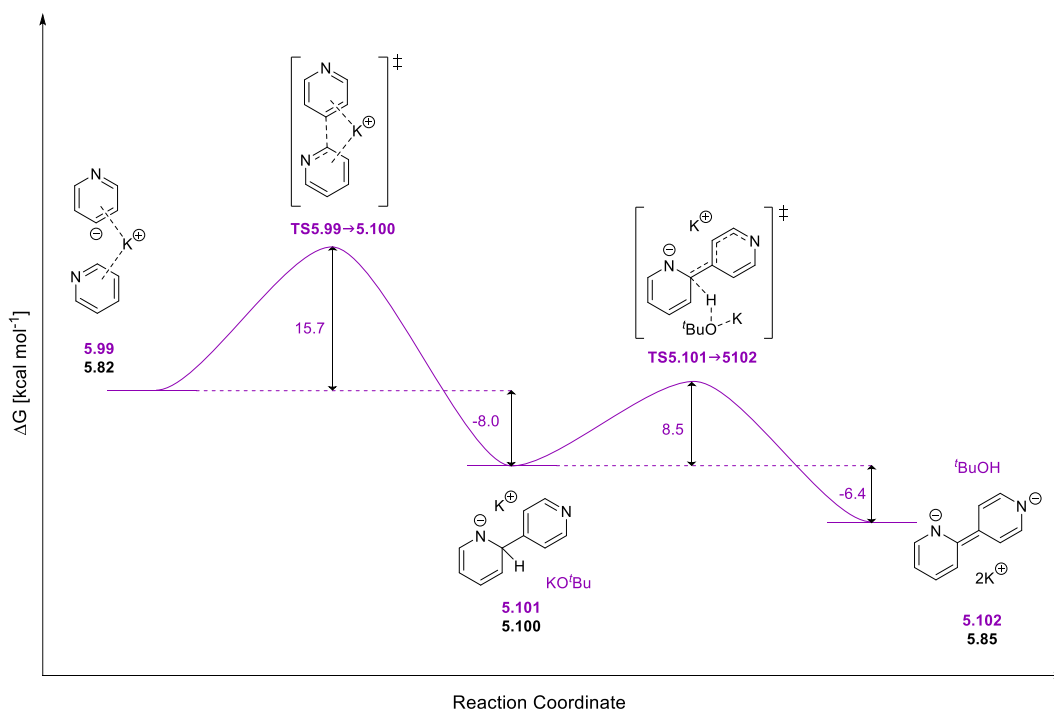
Figure 5.19: Gibbs free energy (ΔG) profile for the formation of proposed 2,4'-bispyridine donor **5.85** using anion **5.82** as the nucleophile. Structure numbers in purple correspond to the reaction complex modelled computationally, while structure numbers in black represent the separate species involved.

Comparing the energetics for these possible reaction pathways, the initial deprotonation of pyridine to afford anions **5.79** and **5.82** is the rate-determining step in all four cases. All four pathways are endergonic overall, which can explain why only trace quantities of the oxidised products could be obtained from the reaction mixture. The reaction pathways for the possible donors derived from 1,10-phenanthroline **5.44** on the other hand are all exergonic, even upon the inclusion of the initial deprotonation energetics.

Table 5.6: Summary of the calculated Gibbs free energies (ΔG) and electronic energies (ΔE) [kcal mol^{-1}] of intermediate and product complexes relative to **5.86** and **5.88** for the formation of bis-pyridine-based organic electron donors.

Reaction Complex	5.86	5.79	5.90	5.91
ΔG_{rel}	0.0	18.6	4.9	1.7
ΔE_{rel}	0.0	19.5	2.1	-2.5
Reaction Complex	5.88	5.82	5.93	5.94
ΔG_{rel}	0.0	16.7	5.6	3.6
ΔE_{rel}	0.0	17.0	3.5	0.6
Reaction Complex	5.86	5.79	5.97	5.98
ΔG_{rel}	0.0	18.6	13.2	7.7
ΔE_{rel}	0.0	19.5	9.5	3.4
Reaction Complex	5.88	5.82	5.101	5.102
ΔG_{rel}	0.0	16.7	8.7	2.3
ΔE_{rel}	0.0	17.0	4.8	-1.6

The difference in energetics observed when forming an organic donor from 1,10-phenanthroline **5.44** versus pyridine **5.76** could be explained by the difference in ability to bind to the potassium cation of the base. In the case of 1,10-phenanthroline, this has been shown to facilitate the initial deprotonation step (Figure 5.9) and, upon chelation by a second molecule of 1,10-phenanthroline, hold the reaction complex together for the nucleophilic aromatic substitution step (Figure 5.10). For the nucleophilic aromatic substitution steps in the four pyridine pathways, the second molecule of pyridine is bound through a cation – π interaction in most cases (Figure 5.20).
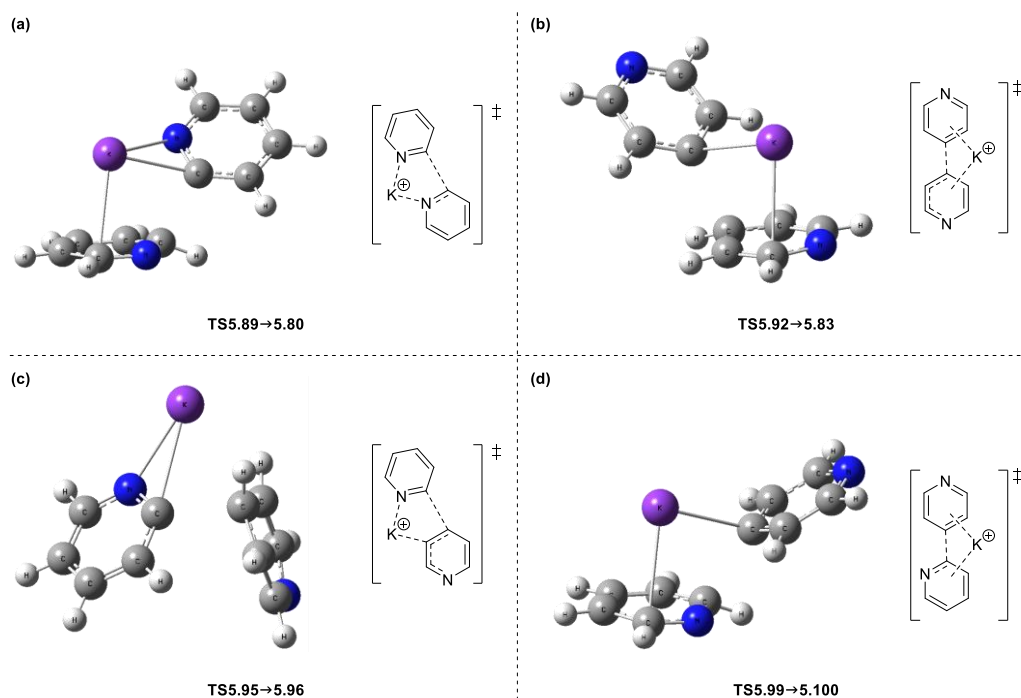
Figure 5.20: Optimised geometries of the transition states for the nucleophilic aromatic substitution reaction towards the formation of bispyridine intermediates (a) **5.80**, (b) **5.83**, (c) **5.96** and (d) **5.100**.

The binding strengths of a number of reaction complexes involved in the formation of donors from 1,10-phenanthroline **5.44** and pyridine **5.76** were calculated to determine if chelation has a positive effect on these transformations (Figure 5.20). For the initial deprotonation, it is known from earlier work that forming reactant complex **5.52** from 1,10-phenanthroline and potassium *tert*-butoxide is energetically favourable (ΔG_{bind} = -4.2 kcal mol^{-1}, Figure 5.21a). Formation of the related pyridine complex **5.86** is less favourable, but still mildly exergonic (ΔG_{bind} = -0.4 kcal mol^{-1}, Figure 5.21b) while the formation of complex **5.88** has an energetic penalty of 5.2 kcal mol^{-1} (Figure 5.21c). Similar energetic differences were found to be involved in the subsequent formation of reaction complexes **5.58**, **5.89** and **5.92**. Forming the 1,10-phenanthroline complex **5.58** was found to be energetically favourable with a binding free energy of -5.1 kcal mol^{-1} (Figure 5.21d). Conversely, complexes **5.89** (Figure 5.21e) and **5.92** (Figure 5.21f) were found to have small energetic penalties of 2.4 and 3.4 kcal mol^{-1} respectively.
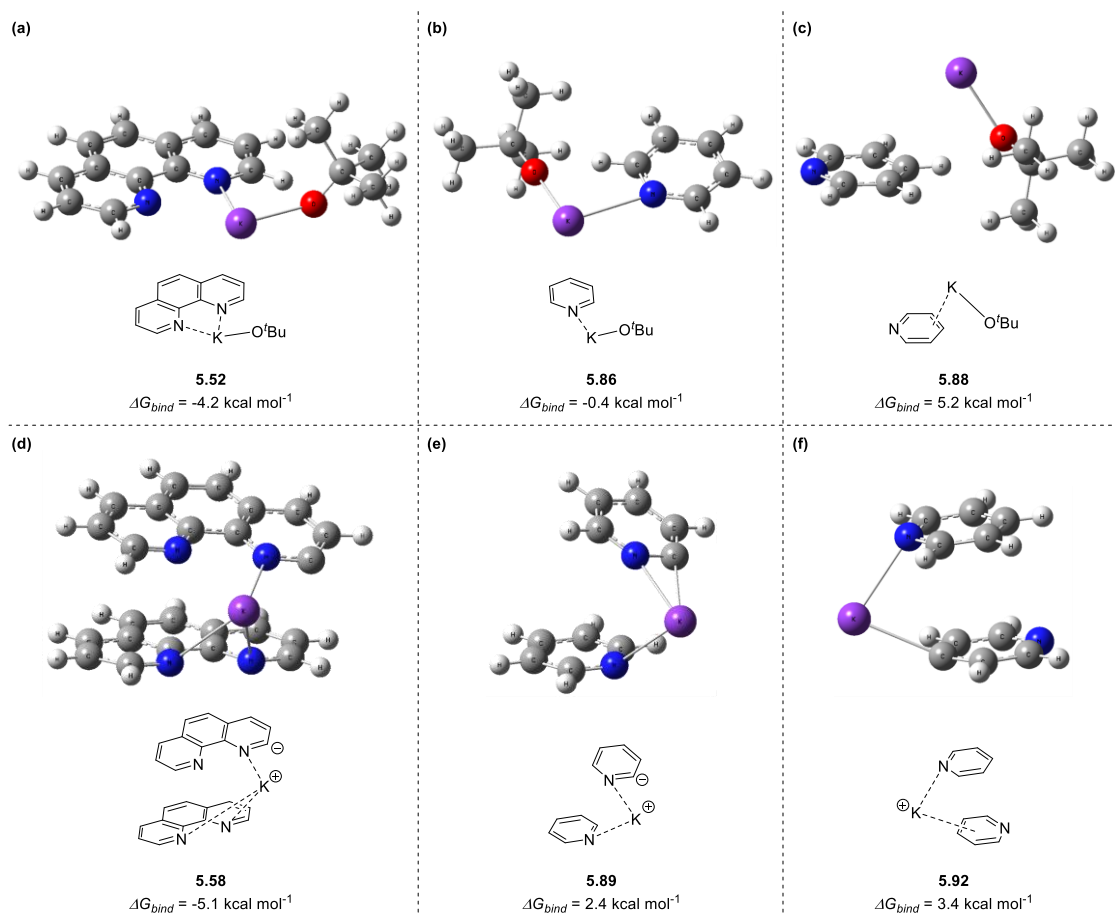
Figure 5.21: Optimised geometries of the reactant complexes (a) **5.52**, (b) **5.86**, (c) **5.88**, (d) **5.58**, (e) **5.89** and (f) **5.92**, including the binding free energies (ΔG_{bind}, kcal mol^{-1}) associated with their formation.

These initial findings demonstrate the ability to form powerful reducing agents following a number of simple transformations, namely deprotonations and the formation of dimeric intermediates. Based on the molecules studied, the electron-rich alkene moiety bearing adjacent anionic heteroatoms is likely to represent the reactive centre of the electron donor (Figure 5.22). This, along with the generation of aromaticity upon the loss of two electrons, aligns well with the neutral organic super electron donors developed within our research group. The ability to effectively bind to the cation of the base appears to have a positive influence on the formation of these organic electron donors. Experimentally, this has been demonstrated through the higher yield of **5.48** obtained relative to **5.77** and **5.78**. Computationally, investigation of the binding free energies associated with the formation of key reaction complexes supports this hypothesis.
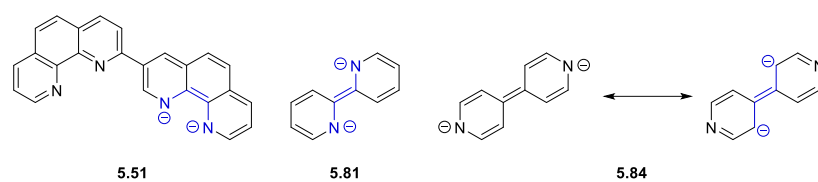
Figure 5.22: Structure of proposed organic super electron donors **5.51**, **5.81** and **5.84**, highlighting the electron-rich alkene moiety present in each.

6

Expanding the Scope for the *in situ* Formation of Organic Super Electron Donors

6.1 Introduction

Returning to the proposals within the literature of a chelate complex forming between the organic additive and the base, and this complex then acting as an electron donor, the results discussed in Chapter 5 suggest that the first step is likely to happen. The ability of this complex to transfer an electron to an iodoarene, however, has been ruled out through computation of the relative energetics for such a reaction. It became of interest, therefore, to extend the scope of our understanding beyond these two additives and investigate the possibility of forming analogous organic electron donors upon treatment of other small organic molecules with potassium *tert*-butoxide. For this study, two sub-categories of organic additives were addressed: Chapter 6.3 discusses possible electron donors derived from amino acids and their related compounds, while Chapter 6.4 discusses those derived from diols and diamines.

Research by Tanimori has already demonstrated the ability of the amino acids sarcosine **6.3** and proline **6.4** to efficiently promote the coupling of 4-iodoanisole **6.1** with benzene (Scheme 6.1a).[47] Given the evidence for the formation of dimeric electron donors such as **5.51** discussed in Chapter 5, the possibility of amino acid dimerization was considered. Such a reaction, if it were to happen, would result in the formation of a cyclic dipeptide, or 2,5-diketopiperazine (DKP), with structures **6.5** and **6.6** representing the DKP's of amino acids **6.3** and **6.4** respectively (Scheme 6.1b). Within the literature, DKP's of the form **6.8** have been successfully synthesised in moderate-to-excellent yields under microwave irradiation using the ester of the corresponding linear dipeptide **6.7** as the starting material (Scheme 6.1c).[145] In 2011, however, an article published by Nonappa *et al.* demonstrated the ability to synthesise DKP's using single amino acids as precursors, again under microwave irradiation (Scheme 6.1d).[146]
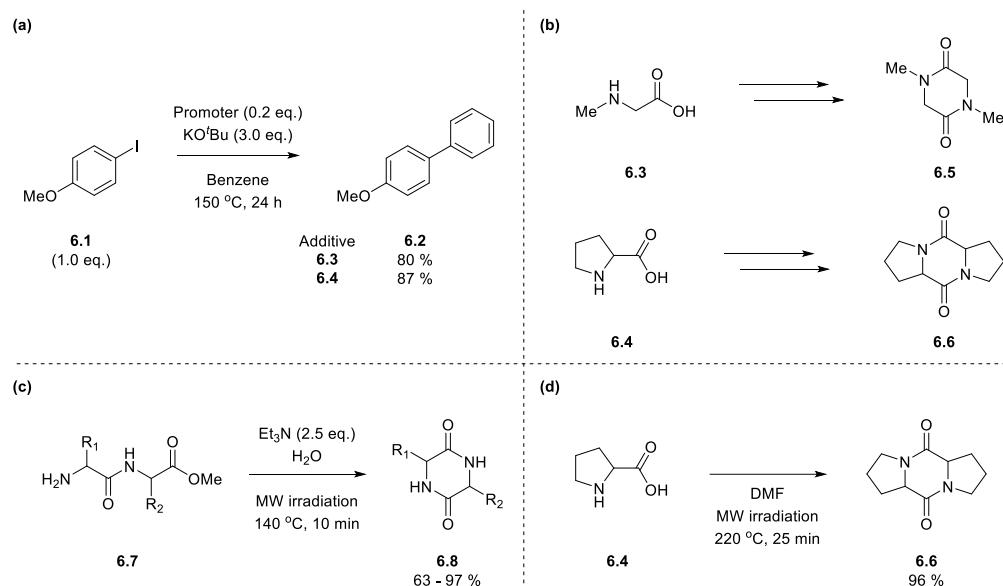
Scheme 6.1: (a) Biaryl coupling of 4-iodoanisole **6.1** with benzene promoted by amino acids as demonstrated by Tanimori;[47] (b) structures of DKP's **6.5** and **6.6** proposed to form from amino acids **6.3** and **6.4** respectively; (c) synthesis of DKP's of the general form **6.8** from the corresponding linear dipeptide ester **6.7**[145] and (d) synthesis of DKP **6.6** from **6.4** performed by Nonappa.[146]

The work detailed in this chapter begins by studying possible reaction pathways by which organic electron donors might be derived from amino acids, with both calculations and experimental results aiding in the acceptance or rejecting of proposed mechanisms. Following a thorough investigation of how donors might be formed from simple diols, these principles are extended to rationalise the analogous formation of donors from diamines.

6.2 Computational Methods

DFT calculations were performed using the Gaussian 09 software package.[136] All reaction species were optimised using the M06-2X functional[115] with a double-ζ basis set. With the exceptions of potassium and iodine, all elements were modelled using the aug-cc-pVDZ basis set.[147] Potassium was modelled using the 6-31++G(d,p) basis set.[148] For systems that included iodine, the small-core energy consistent relativistic pseudopotential was implemented.[149, 150] Implicit solvation of the reaction systems was modelled using the CPCM model with the associated parameters for benzene.[116,

[117] Frequency calculations were performed on all optimised structures in order to characterise them as minima (zero imaginary frequencies) saddle points (single imaginary frequency) and to obtain thermochemical data. All calculations were modelled at a temperature of 298 K. Throughout this chapter, unless stated otherwise, the reactant and product state for each transformation was taken to be the reaction complex rather than the separated reactant and product species. As an approximation to improve computational efficiency, potassium *tert*-butoxide has been modelled as a monomeric entity, despite being a tetrameric species.

6.3 Amino Acids and Related Compounds as Additives

The starting point for this investigation was to test a number of amino acids to determine their relative ability to promote this same coupling reaction (Scheme 6.2a). Extending on the idea of DKP's forming *in situ* from amino acids, DKP **6.14** was synthesised via the route shown in Scheme 6.2b, and subsequently tested under the same reaction conditions.
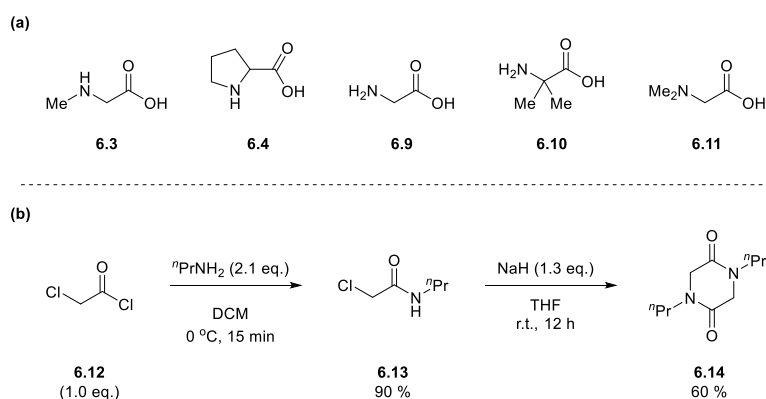
Scheme 6.2: (a) Amino acids investigated within this study and (b) the synthetic route towards DKP **6.14**.

Based on literature precedent, it is expected that at higher reaction temperatures the benzyne-mediated pathway will compete to a greater extent with the electron transfer pathway. Due to the greater nucleophilicity of the *tert*-butoxide anion relative to benzene, the formation of the *meta*- and *para*-(*tert*-butoxy)anisole side products **6.16** and **6.17** is expected to increase at higher reaction temperatures (Scheme 6.3). For this

reason, a reaction temperature of 130 ^{o}C was chosen instead of the 150 ^{o}C used by Tanimori.[47] The results of these investigations are summarised in Table 6.1.
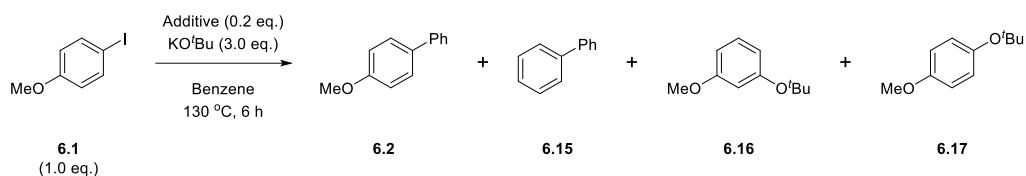
Scheme 6.3: Possible products arising from the transition metal-free coupling reaction of 4-iodoanisole **6.1** with benzene promoted by amino acid and DKP additives.

Table 6.1: Comparison of the effectiveness of amino acid and DKP additives to promote the transition metal-free coupling of 4-iodoanisole **6.1** with benzene.

Organic Additive	% Yield of 6.2	% Yield of 6.15	% Yield of 6.16 and 6.17 (1:1 mixture)
--	30	1	46
6.3	90	4	--
6.4	92	3	--
6.9	88	3	--
6.10	19	1	27
6.11	30	1	30
6.14	89	3	--

From these results, it is clear that additives **6.3**, **6.4** and **6.9** are the most effective of the amino acids tested for this chemistry, with respective yields of 90 %, 92 % and 88 % of the desired product **6.2** obtained. In addition to this, small amounts of the side-product biphenyl **6.15** were also obtained in these reactions. This side-product forms when phenyl radicals are generated as a result of hydrogen atom abstraction from the solvent by the substrate aryl radical. This would afford small quantities of anisole, which is then lost upon work-up due to its volatility.

The two dimethylated derivatives of glycine **6.10** and **6.11** produced significantly lower yields of the desired product, furnishing 19 % and 30 % of **6.2** respectively. In addition to **6.2** and trace amounts of **6.15**, these two additives also gave rise to a moderate quantity of the (*tert*-butoxy)anisole products **6.16** and **6.17**, obtained as a 1:1 mixture

of the *meta-* and *para-*isomers. Comparing these results with those from the blank reaction under the same reaction conditions, it is interesting to note that the yield of **6.2** obtained using **6.10** (19 %) is in fact less than that obtained in the absence of additive (30 %). This echoes the observation of Tanimori when the amino acid valine **3.105** (Chapter 3, page 20) was used as an additive, which also gave less effective coupling relative to the blank reaction (Scheme 3.18).[47] A possible explanation is that amino acids **3.105** and **6.10** are in fact suppressing the competing reaction pathway(s) that dominate in the absence of an additive. Pleasingly, the use of the DKP additive **6.14** afforded the desired product **6.2** in a yield comparable to those obtained with amino acids **6.3**, **6.4** and **6.9**.

If the *in situ* formation of DKP intermediates via the dimerization of amino acids was indeed occurring, it is proposed that in the presence of a sufficiently strong base such as potassium *tert*-butoxide, deprotonation of the α-carbon would afford enolate **6.18**. Analogous deprotonation of the second α-carbon would then afford dianion **6.19**, which is predicted to be an extremely powerful electron donor due to its anti-aromaticity. Loss of two electrons from this species would subsequently afford the zwitterionic disalt **6.20** (Scheme 6.4).
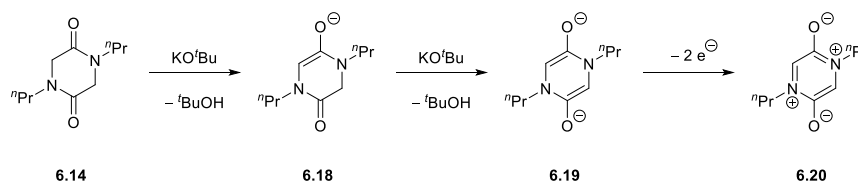
Scheme 6.4: Structure of the proposed organic electron donors **6.18** and **6.19** derived from DKP **6.14**, demonstrating how loss of two electrons can generate the zwitterionic disalt **6.20**.

To investigate the possibility of forming intermediates such as **6.19**, the deprotonations of **6.14** and **6.18** by potassium *tert*-butoxide were modelled computationally (Figure 6.1). The calculated reaction energetics show that the first C—H deprotonation proceeds via a small activation barrier of 3.6 kcal mol^{-1}, with the product complex **6.22** being only slightly uphill of the reactant complex **6.21** (0.2 kcal mol^{-1}). The energetics for the deprotonation of **6.18** to afford **6.19** exhibit the same unfavourable profile that has been observed previously for the deprotonations of 1,10-phenanthroline **5.44** and pyridine **5.71**. The electronic surface confirms that the

optimised geometry for **TS6.23→6.24** represents a true reaction maximum, while **6.23** and **6.24** represent reaction minima. Despite the unfavourable energetics, the overall energetic demand of 12.8 kcal mol^{-1} to form dianion **6.19** should allow for it to form, if only in small amounts.
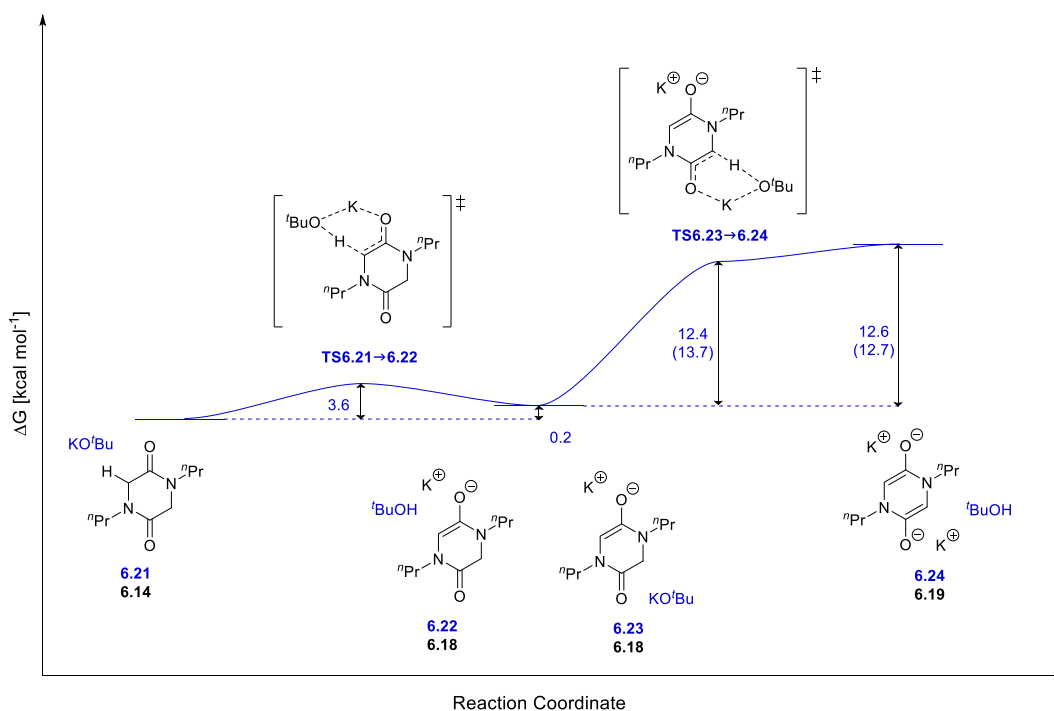
Figure 6.1: Gibbs free energy (ΔG) profile for the formation of proposed electron donors **6.18** and **6.19** following deprotonation of DKP **6.14** by potassium *tert*-butoxide. Values in parentheses correspond to the change in electronic energy (ΔE). Structure numbers in blue correspond to the reaction complex modelled computationally, while structure numbers in black represent the separate species involved.

Extending this proposed mechanism of reactivity, it is possible to begin to rationalise the experimental observations outlined in Table 6.1. The effectiveness of sarcosine **6.3** and proline **6.4** to promote this chemistry could arise from the secondary nature of these amino acids. Upon formation of their respective DKP's, only C—H deprotonations would be possible, thus allowing for the formation of **6.26**, analogous to **6.19**, with no competing pathways (Scheme 6.5a). While glycine **6.9** has been shown to be equally effective at promoting this chemistry relative to amino acids **6.3** and **6.4**, there remains the possibility that, upon formation of its respective DKP **6.27**, competition between the C—H and N—H deprotonation could afford a less effective electron donor such as **6.28** instead of **6.29** (Scheme 6.5b). Amino acids **6.10** and **6.11**, the *C,C*- and *N,N*-dimethylated derivatives of glycine **6.9** respectively, produced lower

yields of the desired product **6.2** in these reactions. Based on this reactivity model, while amino acid **6.10** can react to form the corresponding DKP **6.30**, this species has no C—H bonds available for deprotonation to form an intermediate analogous to **6.19** (Scheme 6.5c). For amino acid **6.11**, the formation of a DKP such as **6.32** is not likely to occur as a consequence of the absence of N—H bonds for deprotonation (Scheme 6.5d).
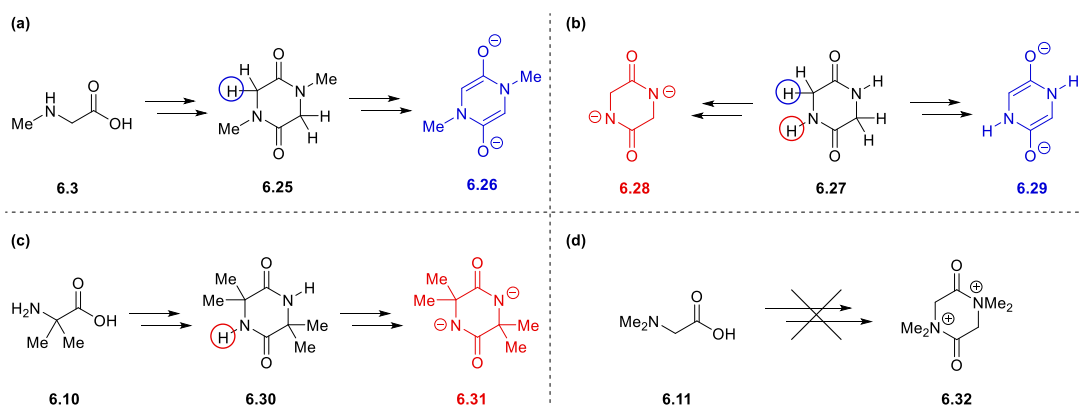
Scheme 6.5: Explanation of observed amino acid reactivity based on the proposal that DKP intermediates are formed *in situ*. (a) Formation of DKP **6.25** from sarcosine **6.3** and deprotonation to form the proposed electron donor **6.26**. (b) Possible deprotonations of DKP **6.27**, formed from glycine **6.9**, giving the dianionic species **6.28** or the proposed electron donor **6.29**. (c) Formation of DKP **6.30** from *C,C*-dimethylglycine **6.10** and subsequent deprotonation to afford the dianionic species **6.31**. (d) Inability of *N,N*-dimethylglycine **6.11** to form a DKP such as **6.32** due to the tertiary nature of the amine group.

While this mechanistic proposal can explain some of the experimental results obtained when using amino acids as additives, there remain a number of anomalous observations this model cannot explain. Firstly, the decreased yield of **6.2** obtained when using amino acid **6.10** relative to the blank reaction; this might arise as a result of the zwitterionic species **6.38** forming, which would be lost upon aqueous work up. Carboxylate **6.33**, derived from amino acid **6.10**, could undergo deprotonation by potassium *tert*-butoxide to afford **6.34**. This could react as a nucleophile with the aryne intermediate **6.35** to afford **6.36**, with subsequent reactions yielding the bisarylated species **6.37** and the trisarylated zwitterion **6.38** (Scheme 6.6a). Precedent for such a reaction has recently been detailed within the literature by Diesendruck *et al.*, who have used benzyne chemistry to synthesise a number of quaternary ammonium salts, including the structurally similar **6.41** and **6.42** (Scheme 6.6b).[151]

(a)

(b)
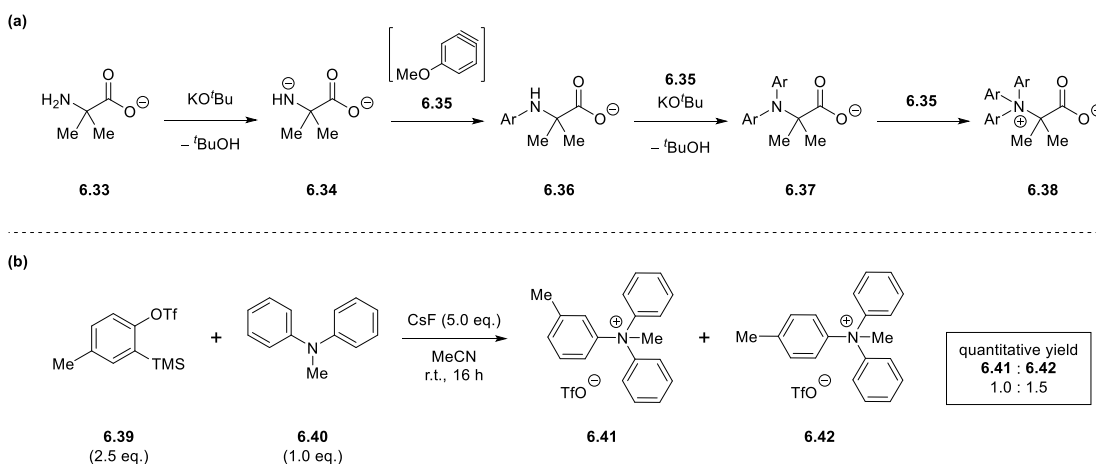
Scheme 6.6: (a) Proposed side reaction of amino acid additives with benzyne when the electron transfer pathway is inactive; (b) formation of the quaternary ammonium salts from the reaction of the tertiary amines with aryne intermediates.[151]

The next issue arises from the reaction efficiencies of amino acids **6.10** and **6.11** relative to the blank reaction; due to the significant amount of product forming in the absence of additive, it is difficult to definitively compare the relative abilities of these two species. This might arise due to a greater propensity for 4-iodoanisole **6.1** to generate an aryne intermediate due to the inductive effect of the methoxy group. To allow for a better comparison, reactions were performed by Dr Eswararao Doni using 4-iodotoluene **6.43** as the substrate (Scheme 6.7).
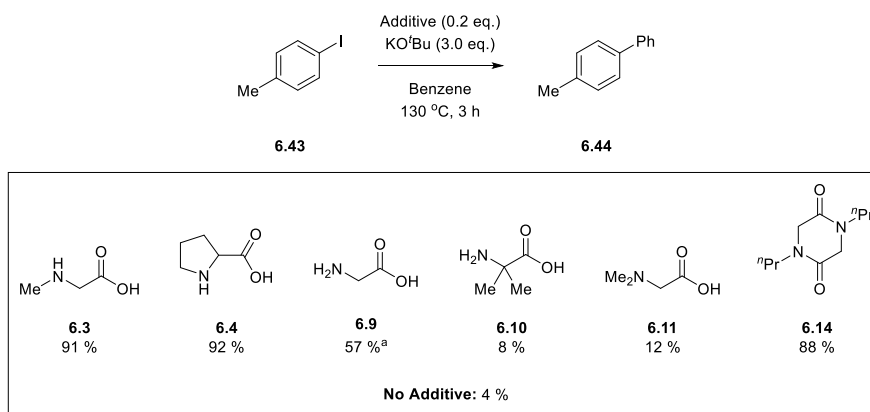
Scheme 6.7: Transition metal-free coupling reaction of 4-iodotoluene **6.43** with benzene, using amino acids and related compounds as organic additives, performed by Dr Eswararao Doni.[152] [a] Increasing the reaction time to 5 h afforded **6.44** in 89 % yield.

Organic additives **6.3**, **6.4** and **6.14** are once again efficient promoters of this chemistry, even at a reaction time of 3 hours. In this series of reactions, it was found that glycine **6.9** produced only a yield of 57 % in the 3 hour reaction time. Extending

this to 5 hours, however, afforded the desired product **6.44** in comparable yields to **6.3**, **6.4** and **6.14**. In addition to this, the competing benzyne-mediated pathway appears to be suppressed in these reactions, with the blank reaction only producing 4 % of the product **6.44**. This allows for a better comparison of additives **6.10** and **6.11**, which afforded the coupled product in yields of 8 % and 12 % respectively. Based on these results, it is clear that neither of these additives can effectively promote this chemistry. The fact that amino acid **6.11** appears to be slightly more effective than **6.10** is contradictory to the DKP reaction model, suggesting an alternative pathway is likely to be responsible for the observed reactivity. However, this reactivity may just be an artefact of a competing side reaction, such as the benzyne-mediated process proposed to occur in the blank reaction.

A final set of experiments performed by Dr Shengze Zhou utilised the substrate 2-iodo-*meta*-xylene **6.45**, from which an aryne intermediate cannot be generated due to the substituents *ortho*- to the iodine. Consequently, any coupling chemistry observed with this substrate must arise solely from electron transfer chemistry. Based on the outcomes for experiments involving substrate **5.41** discussed previously, it is expected that the products from this reaction will include the desired coupling product **6.46**, biphenyl **6.15** and the reduced starting material **6.47**, which is expected to be lost upon work-up (Scheme 6.8).
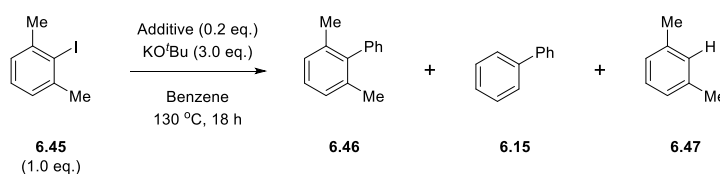
Scheme 6.8: Transition metal-free coupling reaction of 2-iodo-*meta*-xylene **6.45** with benzene, using amino acids and related compounds as organic additives, performed by Dr Shengze Zhou.[152]

Table 6.2: Comparison of the effectiveness of different amino acid and DKP additives to promote the transition metal-free coupling of 2-iodo-*meta*-xylene **6.45** with benzene.

Organic Additive	Mass Recovered (mg) of Coupled Product mixture (6.46 + 6.15)[a]	% Recovery of 6.45
--	< 0.5	88
6.3	44	25
6.4	32	54
6.9	16	70
6.10	< 0.5	92
6.11	< 0.5	94
6.14	45	22

[a] an inseparable mixture of **6.46** and **6.15** is obtained at an approximate ratio of 1.0:4.0.

These results confirm the initial observations made using substrates **6.1** and **6.43** in that, of the additives tested, **6.3**, **6.4** and **6.14** are the most effective promoters of this chemistry. Amino acid **6.9** shows modest effectiveness when using substrate **6.45**, but has comparable effectiveness to **6.3**, for example, for substrates **6.1** and **6.43.** With the possibility of benzyne chemistry eliminated in the reactions of **6.45**, amino acids **6.10** and **6.11** are conclusively shown to be poor promoters of this chemistry, with yields comparable to that from the blank reaction. In the blank reaction, the fact that trace amounts of the coupling products are observed suggests the possible presence of an as yet unidentified minor initiation pathway. The absence of a potential electron donor precursor and the inability to generate an aryne from **6.45** eliminate the possibility of the two known initiation pathways affording this reactivity.

Based on the results across the three substrates **6.1**, **6.43** and **6.45**, a revised model of reactivity was proposed (Scheme 6.9a). Using glycine **6.9** as an illustrative example, deprotonation of the carboxylic acid group yields **6.48**. This intermediate then has two types of proton available for reaction; N—H deprotonation can generate dianion **6.49** which is predicted to be a weaker electron donor due to the localised charge. Alternatively, C—H deprotonation would yield dianion **6.50**, which is expected to be a stronger electron donor due to the formation of the electron-rich alkene moiety observed in previous organic electron donors.
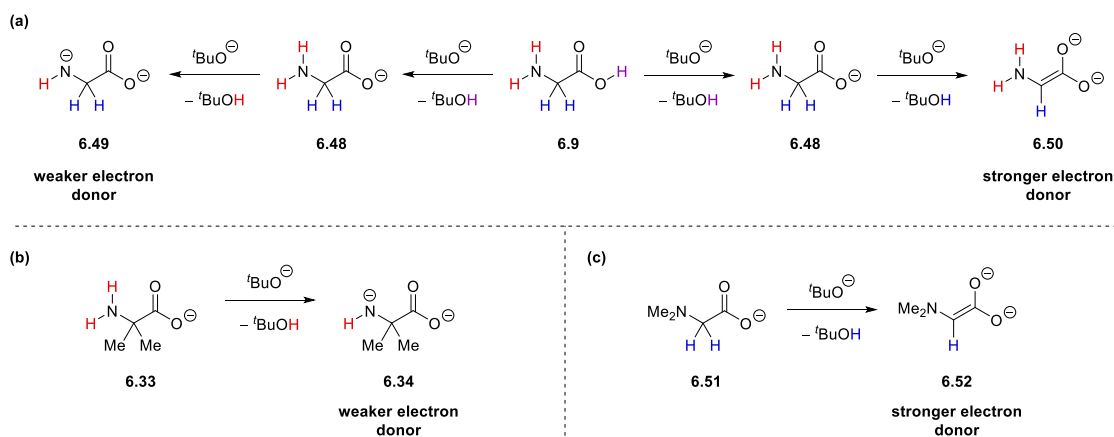
Scheme 6.9: (a) Alternative mechanism proposed to rationalise the relative effectiveness of amino acid additives to promote transition metal-free coupling reactions via possible electron donors analogous to **6.49** or **6.50**. Formation of (b) the weaker electron donor **6.34** from carboxylate **6.33** and (c) the stronger electron donor **6.52** from carboxylate **6.51**.

This new proposed pathway is more capable of rationalising the relative efficiencies of amino acids **6.10** and **6.11** to promote the biaryl coupling reactions. Considering firstly amino acid **6.10**: the corresponding carboxylate **6.33** can only undergo N—H deprotonation to dianion **6.34**, a structure expected to be a weaker electron donor (Scheme 6.9b). On the other hand carboxylate **6.51**, formed from **6.11**, can undergo a C—H deprotonation to dianion **6.52** (Scheme 6.9c). While this should represent a stronger electron donor, capable of reaction efficiencies comparable to amino acid **6.3** for example, the additional steric bulk of the tertiary nitrogen might inhibit the formation of **6.52** and hence the ability for **6.11** to effectively promote the coupling reaction.

Building on this proposal, theoretical calculations were performed to investigate the possibility of forming these species. For the deprotonation of the neutral amino acids to afford their respective carboxylates, it was not possible to locate a transition state or reactant complex; attempts at optimising the reactant complex led to exclusive formation of the product complex. Given the acidity of this proton and hence the unlikelihood of this step being rate-determining, the amino acid carboxylates were chosen as the starting point for this investigation (Scheme 6.10).

Using potassium *tert*-butoxide as the base, the deprotonation of the N—H groups could not be achieved computationally. To overcome this obstacle, an approximation

of the product complex energy was made through summation of the free energies of the dianions (including potassium counter ions) and *tert*-butanol. Based on this value, and estimation of the relative free energy for the product formation was made. Such an approach was not required for the C—H deprotonation pathways, which could be calculated through standard optimisation protocols. The results of these calculations are summarised in Table 6.3.
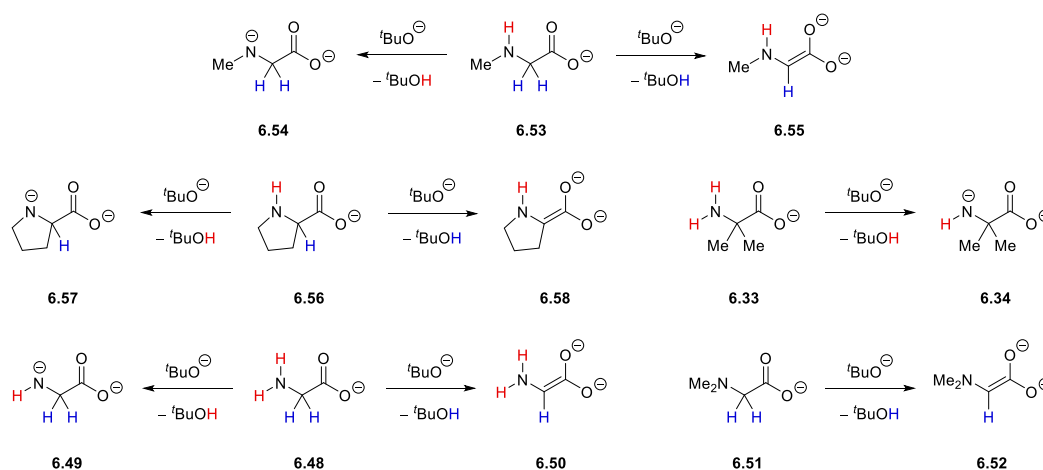
Scheme 6.10: Summary of the reactions studied for the formation of candidate organic electron donors following deprotonation of amino acid carboxylates by potassium *tert*-butoxide.

Table 6.3: Calculated Gibbs free energies (ΔG) and electronic energies (ΔE) [kcal mol^{-1}] for the deprotonation of amino acid carboxylates by potassium *tert*-butoxide.

Parent Amino Acid	Deprotonation Reaction	ΔG*	ΔG$_{rel}$	ΔE*	ΔE$_{rel}$
6.3	6.53 → 6.54	--	31.4	--	46.6
	6.53 → 6.55	13.6	15.7	16.1	15.1
6.4	6.56 → 6.57	--	29.1	--	43.8
	6.56 → 6.58	14.3	15.4	15.2	14.4
6.9	6.48 → 6.49	--	22.2	--	36.5
	6.48 → 6.50	14.7	16.2	17.1	16.2
6.10	6.33 → 6.34	--	31.5	--	46.0
6.11	6.51 → 6.52	24.4	23.2	26.7	25.6

From the results in Table 6.3, it is clear that the C—H deprotonation of the amino acid carboxylates is energetically favoured relative to the N—H deprotonation. The fact that attempts at optimising the product complex of this reaction led to exclusive

formation of the reactant complex suggests that the reverse reaction would be barrierless on the electronic energy surface. While the C—H deprotonations are disfavoured energetically on both the electronic and free energy surfaces, there is a small activation barrier predicted for the reverse reaction, indicating that product **6.55**, for example, would have a longer lifetime relative to **6.54**. Considering the pK_a values involved in these possible transformations, it is not surprising that the N—H deprotonation cannot be performed using potassium *tert*-butoxide (approximately 37.0[153] for a secondary amine proton versus 17.0[154] for the O—H proton of *tert*-butanol). On the other hand, the C—H proton would have an approximate pK_a of 19.0[153] which, although is not favoured, would occur to a greater extent than the N—H deprotonation. Of the four amino acids that could undergo a C—H deprotonation, it was found that the deprotonation of **6.51** to afford **6.52** had the most challenging barrier to overcome at 24.4 kcal mol^{-1}, which is approximately 10.0 kcal mol^{-1} greater than the barriers associated with the formation of dianions **6.50**, **6.55** and **6.58**. This energy difference is proposed to arise due to the allylic strain imposed on the double-bond formed as a result of the tertiary nature of the amine in **6.52**.

Based on these observations we predict that, under the standard conditions for these reactions, there would be no competition between the N—H and C—H deprotonation pathways. The exception to this scenario would be if the amino acids were reacting to generate DKP intermediates *in situ*; the amide proton would have an approximate pK_a of 15.0, and consequently deprotonation at this position would be favoured over the desired C—H deprotonation.

6.4 Diols and Diamines as Additives

Expanding the scope beyond amino acids, the diol and diamine additives discussed herein have also been proposed to form electron-transfer complexes with the potassium *tert*-butoxide base (Scheme 6.11a). Applying the mechanistic insight gained from the amino acid study, it is proposed that through a series of deprotonation reactions, electron donors could be generated *in situ* from these additives. Lei *et al.*

have proposed that *N,N'*-dimethylethylenediamine (DMEDA) **6.61** might undergo a series of reactions to afford a radical anion such as **6.65**, which could act as a powerful electron donor (Scheme 6.11b).[41] This suggestion does hold literature precedent; investigations by Wotiz have demonstrated that reaction of ethylenediamine (EDA) **6.66** with a strong base produces an EPR signal identical to that observed in the reduction of pyrazine by potassium metal, corresponding to the pyrazine radical anion **6.67** (Scheme 6.11c).[155]
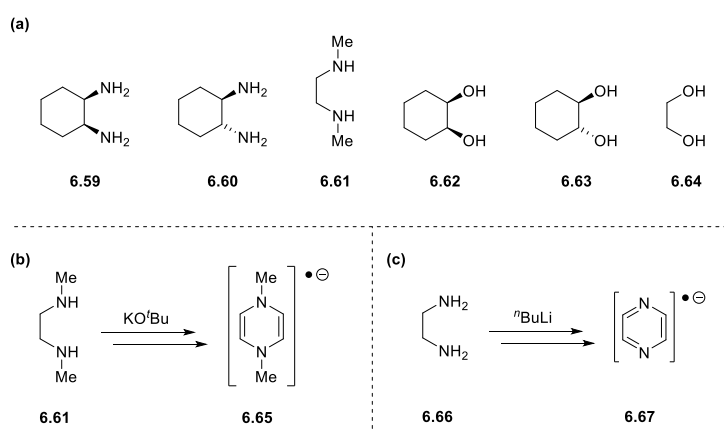
Scheme 6.11: (a) Structures of diamine and diol additives shown within the literature to promote transition metal-free coupling reactions; (b) structure of the radical anion **6.65** proposed to form upon reaction of DMEDA **6.61** with potassium *tert*-butoxide;[41] (c) formation of the pyrazine radical anion **6.67** from the reaction of EDA **6.66** with ^{n}BuLi, as shown by Wotiz.[155]

A number of these additives were tested for their relative ability to promote biaryl coupling reactions through electron transfer chemistry. The reactions were performed by Dr Shengze Zhou in our research group, using 2-iodo-*meta*-xylene **6.45** as the substrate (Table 6.4). Interestingly, all three additives afforded complete consumption of the starting material which, given the significant recovery of **6.45** in the blank reaction, is a clear indication of highly efficient electron transfer chemistry occurring. For the *cis*- and *trans*-isomers of cyclohexane-1,2-diol, **6.62** and **6.63** respectively, it appears that both are equally capable of initiating the electron transfer reaction, albeit that **6.63** produced a greater yield of the coupling products **6.46** and **6.15**.

Table 6.4: Comparison of the effectiveness of different diamine and diol additives to promote the transition metal-free coupling of 2-iodo-*meta*-xylene **6.45** with benzene.

Organic Additive	Mass Recovered (mg) of Coupled Product mixture (6.46 + 6.15)[a]	% Recovery of 6.45
--	< 0.5	93
6.61	46	0
6.62	32	0
6.63	64	0

[a] an inseparable mixture of **6.46** and **6.15** is obtained at an approximate ratio of 1.0:4.0.

The formation of electron donors from the cyclohexane-1,2-diols **6.62** and **6.63** was chosen as the starting point for computational investigation. The mechanism by which this is proposed to occur is outlined in Scheme 6.12a using **6.62** as an example. Initial deprotonation of one of the hydroxyl groups by potassium *tert*-butoxide would afford alkoxide **6.68**. Through the elimination of hydride, 2-hydroxycyclohexanone **6.69** could form as an intermediate; such reactivity is typically associated with the Oppenauer oxidation, with the hydride being delivered to an electrophilic species such as a ketone. Woodward has demonstrated the ability of potassium *tert*-butoxide, in benzene as solvent, to effect the analogous oxidation of quinine **6.75** to quininone **6.77** with benzophenone **6.76** as the oxidant (Scheme 6.12b).[156]

In the absence of an appropriate electrophile, however, the elimination of hydride will be an energetically disfavoured process. This would be true of the proposed pathway in Scheme 6.12a, where the potassium cation is tentatively proposed as a hydride acceptor. The reverse of this reaction, reduction of a ketone by a metal hydride, has limited literature precedence,[157] further highlighting the limitations of this proposal. Subsequent C—H deprotonation of **6.69** would yield either **6.71** or **6.73**, both of which might represent strong candidates for the active electron donor in these reactions. Alternatively, each of these could undergo a final O—H deprotonation to afford their respective dianions **6.72** and **6.74**.

(a)

(b)
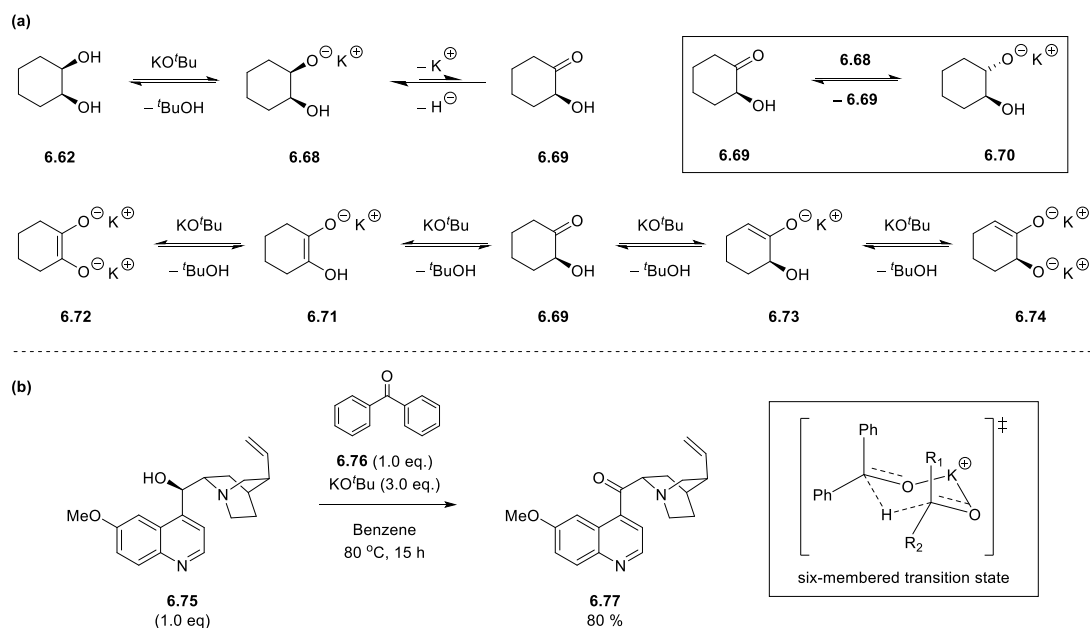
Scheme 6.12: (a) Proposed mechanism for the formation of proposed organic electron donors **6.71** − **6.74** from *cis*-cyclohexane-1,2-diol **6.62** as a demonstrative example; (b) Woodward's modification of the Oppenauer oxidation.[156]

An interesting possibility in this reaction is that in the presence of **6.68**, 2-hydroxycyclohexanone **6.69** can act as the hydride acceptor and perhaps afford **6.70**. To probe the possibility of this stereochemical scrambling, *cis*-4-*tert*-butylcyclohexanol **6.78** was treated with an excess of potassium *tert*-butoxide in benzene at 170 °C, affording a mixture of *cis*-4-*tert*-butylcyclohexanol **6.78**, *trans*-4-*tert*-butylcyclohexanol **6.79** and *cis*-4-*tert*-butylcyclohexanone **6.80** in a ratio of 1.0:6.5:0.3 (Scheme 6.13). An activation free energy of 10.0 kcal mol^{-1} was calculated for this reaction, with the *trans*-isomer **6.78** being energetically favoured over the *cis*-isomer **6.77** by 3.6 kcal mol^{-1}.
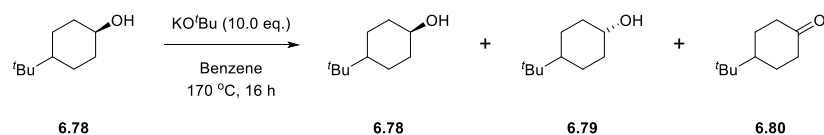
Scheme 6.13: Experimental support for the Woodward modification of the Oppenauer oxidation operating in the reaction of *cis*-4-*tert*-butylcyclohexanol **6.78** with potassium *tert*-butoxide performed by Dr Eswararao Doni.

In light of this result, all three possible stereoisomers of cyclohexane-1,2-diol were investigated (Scheme 6.14). To begin with, the initial deprotonation and subsequent hydride elimination pathways were modelled (Table 6.5). With the exception of isomer

6.63a, all of the initial deprotonations produced negative activation energies on the free energy surface. Probing the electronic energy surfaces for these reactions, the transition state complexes were found to represent true saddle points and the product complexes true minima. Overall, this first reaction step is effectively thermoneutral; all product complexes are approximately equal in energy to their respective reactant complex.
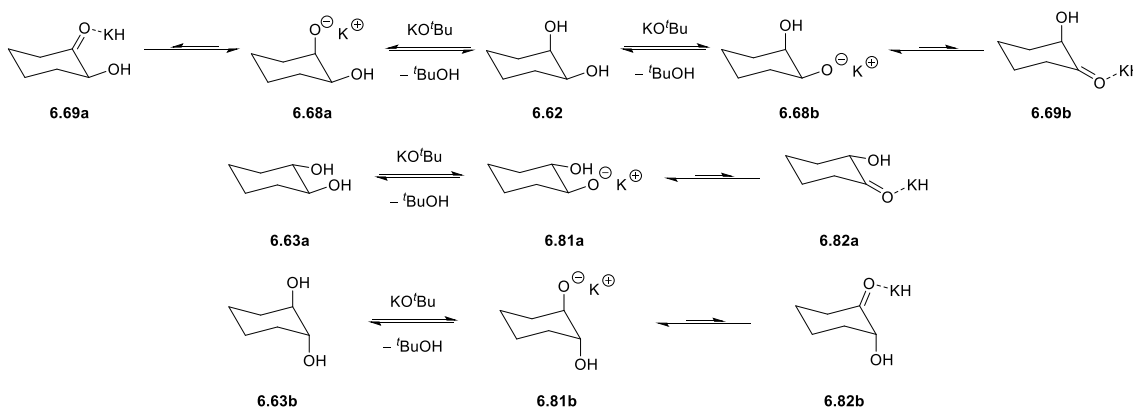
Scheme 6.14: Summary of the reaction pathways investigated to afford intermediates **6.69a**, **6.69b**, **6.82a** and **6.82b** from the three isomers of cyclohexane-1,2-diol **6.62**, **6.63a** and **6.63b** respectively.

Table 6.5: Calculated Gibbs free energies (ΔG) and electronic energies (ΔE) [kcal mol^{-1}] for the four potential reaction pathways towards intermediates **6.69a**, **6.69b**, **6.76a** and **6.76b**.

Parent Diol	Reaction Step	ΔG^*	ΔG_{rel}	ΔE^*	ΔE_{rel}
6.62	6.62 → 6.68a	-1.1	-0.4	0.1	-0.4
	6.68a → 6.69a	32.5	19.4	36.8	25.6
6.62	6.62 → 6.68b	-1.4	-0.7	0.2	-1.6
	6.68b → 6.69b	36.6	22.3	41.1	28.9
6.63a	6.63a → 6.81a	5.2	-0.3	6.2	-0.8
	6.75a → 6.82a	33.3	22.0	37.2	27.1
6.63b	6.63b → 6.81b	-1.4	-1.5	0.2	-1.4
	6.75b → 6.82b	26.3	22.8	28.9	27.4

As was expected, the subsequent elimination of hydride was found to be an endergonic reaction with activation free energies in the range of 26.3 – 36.6 kcal mol^{-1}. Upon visual inspection of the product complexes associated with these reactions, an

interesting observation was made; the eliminated hydride in all cases becomes suitably aligned with the remaining O—H bond for a subsequent deprotonation to occur (Figure 6.2).
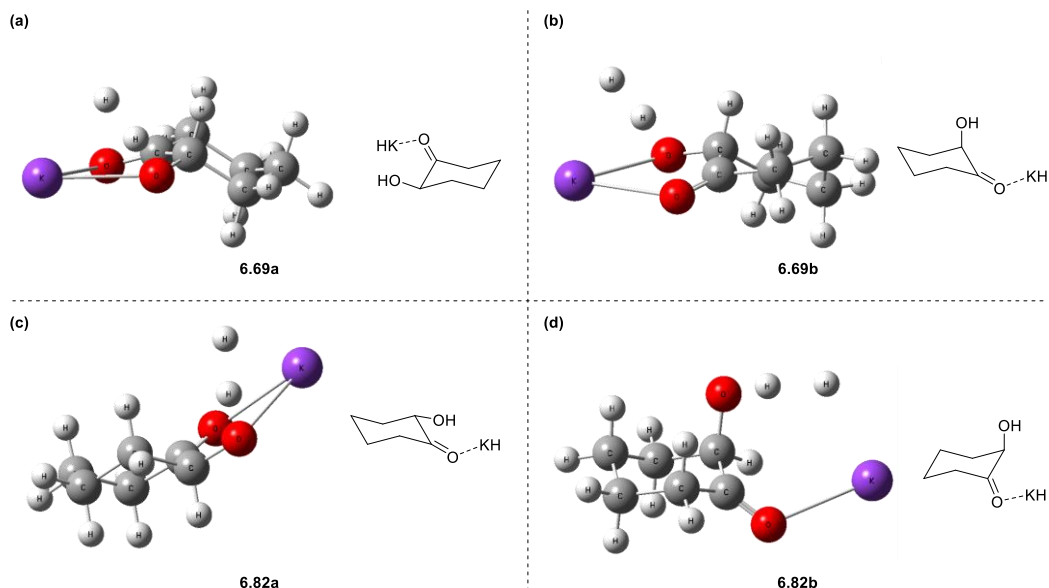
Figure 6.2: Optimised geometries of the product complexes (a) **6.69a**, (b) **6.69b**, (c) **6.82a** and (d) **6.82b** following hydride elimination.

This result prompted the proposal of a revised mechanism as outlined in Scheme 6.15, using **6.62** as an illustrative example. Upon deprotonation and subsequent hydride elimination to afford intermediate **6.69**, deprotonation of the remaining hydroxyl group by the hydride generated *in situ* affords anion **6.83**. This can undergo one of two possible deprotonations to yield the dianionic donor candidates **6.72** and **6.74**. Given that the transformation **6.69→6.83** should be non-reversible due to the loss of hydrogen gas, this revised pathway benefits from eliminating the potential for the reverse reaction **6.77→6.68**. The potential energy surfaces associated with the formation of candidate donors **6.72** and **6.74** derived from **6.62** by this revised pathway have been plotted, with noteworthy observations from the possible *trans*-pathways discussed at each stage.
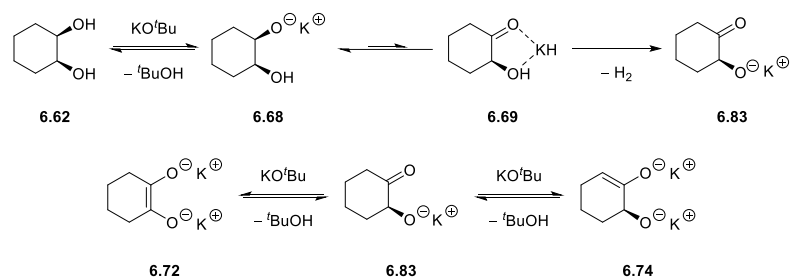
Scheme 6.15: Alternative mechanism proposed for the formation of the dianionic organic electron donors **6.72** and **6.74** involving the deprotonation of an OH group by the expelled hydride.
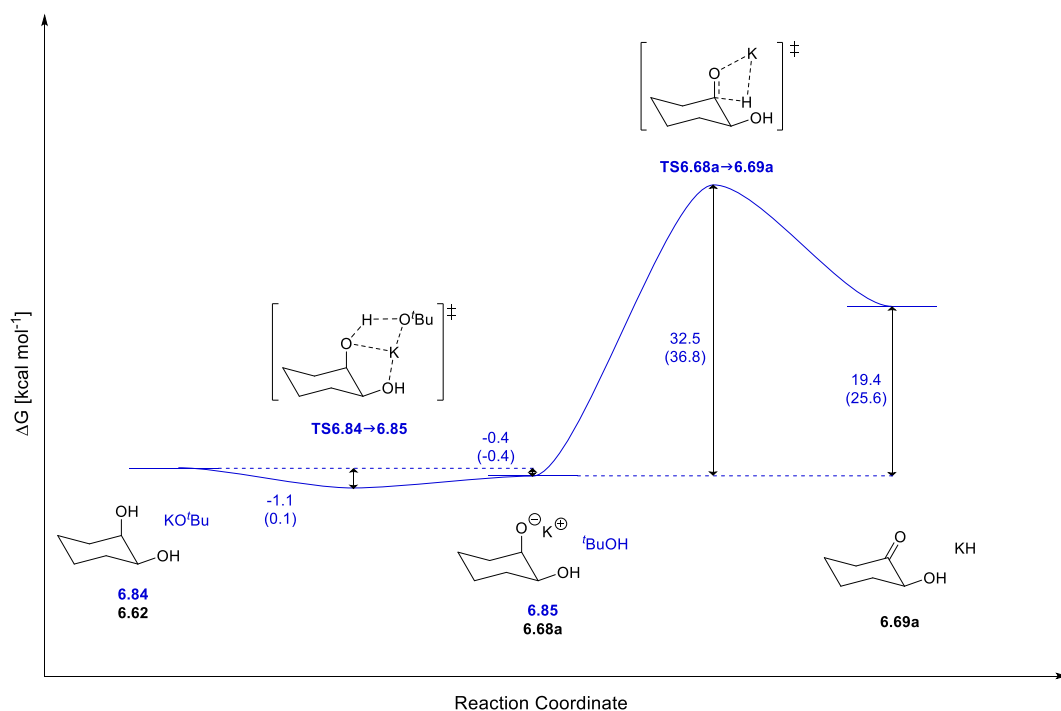
Figure 6.3: Gibbs free energy (ΔG) profile for the formation of **6.69a** following axial deprotonation of **6.62** by potassium *tert*-butoxide and subsequent hydride elimination from **6.68a**. Values in parentheses correspond to the change in electronic energy (ΔE). Structure numbers in blue correspond to the reaction complex modelled computationally, while structure numbers in black represent the separate species involved.

The energetics of the initial deprotonations have been addressed previously, as have those associated with the subsequent hydride elimination step. Figures 6.3 and 6.4 summarise the formations of **6.69a** and **6.69b** respectively. Noteworthy at this stage is the relative energy difference between the deprotonation pathways; the axial deprotonation pathway was found to be stabilised by between 6 – 7 kcal mol^{-1}, a consequence of the orientation of the bulky potassium *tert*-butoxide base (Figure 6.5a and b). Interestingly, due to the position of the potassium cation in **6.68b** relative to

the hydride to be eliminated, the cyclohexane structure must distort from the stable chair conformation (Figure 6.5c) to the less stable twisted boat conformation in order to facilitate the hydride elimination (Figure 6.5d).
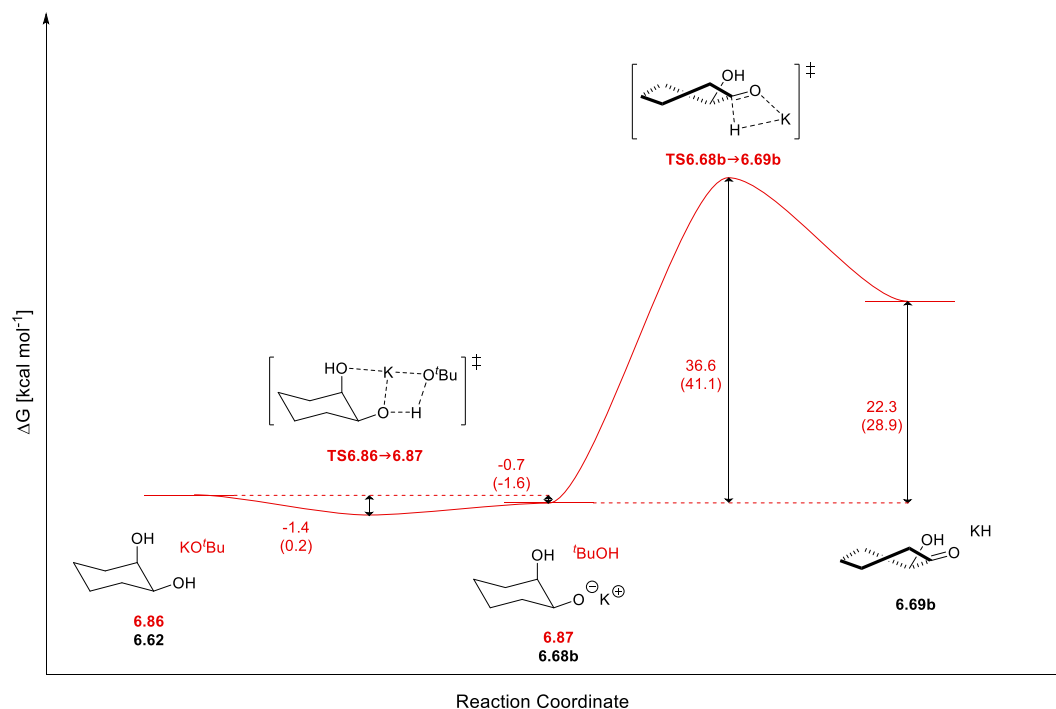
Figure 6.4: Gibbs free energy (ΔG) profile for the formation of **6.69b** following equatorial deprotonation of **6.62** by potassium *tert*-butoxide and subsequent hydride elimination from **6.68b**. Values in parentheses correspond to the change in electronic energy (ΔE). Structure numbers in blue correspond to the reaction complex modelled computationally, while structure numbers in black represent the separate species involved.
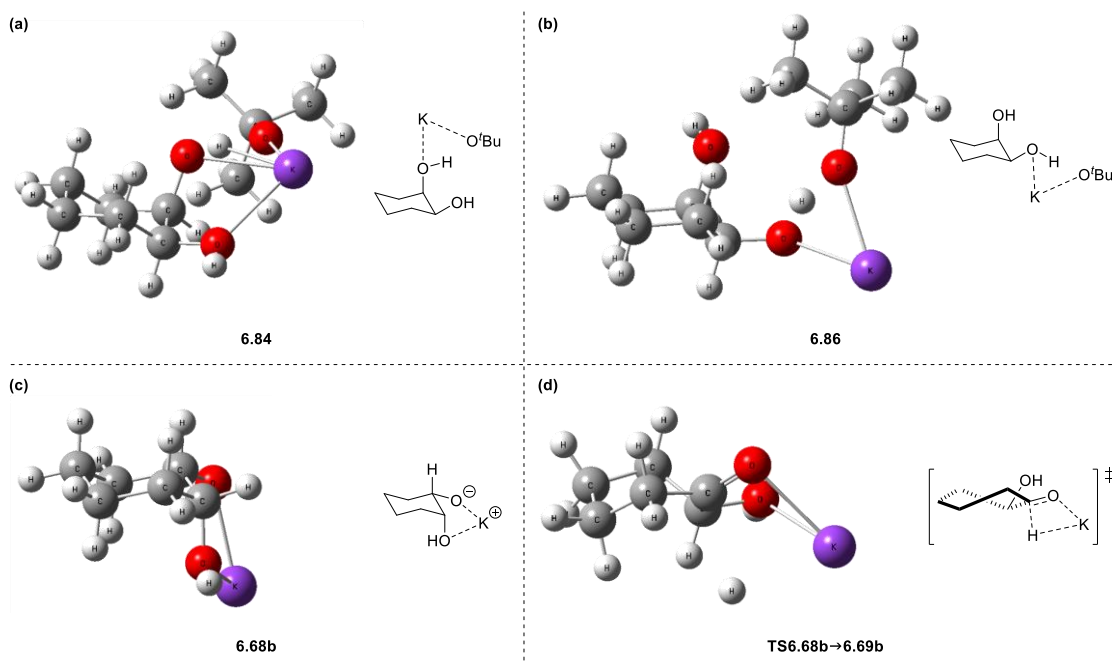
Figure 6.5: Optimised geometries of reaction complexes (a) **6.78**, (b) **6.80** and (c) **6.68b**. (d) Optimised geometry of the transition state complex **TS6.68b→6.69b** highlighting ring distortion.

From intermediate **6.69**, the next step is the formation of hydrogen gas through deprotonation by the potassium hydride formed *in situ*. Although intermediates **6.82b** and **6.88b** were optimised as true minima, a transition state linking these two geometries could not be located (Scheme 6.16). For the remaining three possible reaction pathways, the respective reaction maxima and minima were located. These calculations highlight the facile nature of this reaction, with negligible activation energies and overall exergonic profiles observed across all possible pathways (Table 6.6). As mentioned previously, the non-reversibility of this reaction will provide a driving force towards the formation of an *in situ* electron donor upon subsequent deprotonation of these intermediates.
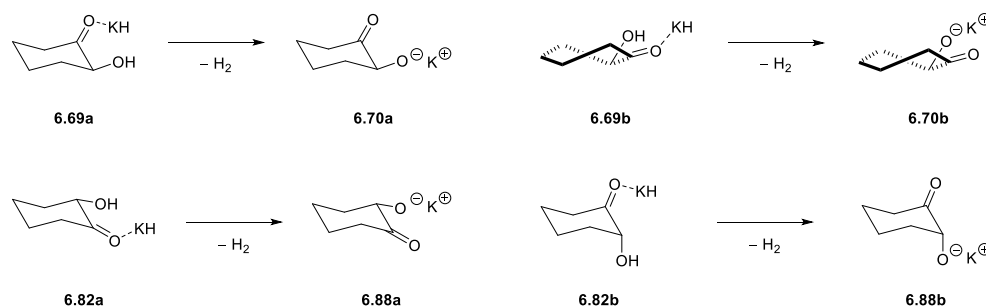
Scheme 6.16: Summary of the OH deprotonation reactions mediated by the expelled hydride.

Table 6.6: Calculated Gibbs free energies (ΔG) and electronic energies (ΔE) [kcal mol^{-1}] for the four potential reaction pathways towards intermediates **6.70** and **6.82** from different isomers of cyclohexane-1,2-diol.

Parent Diol	Reaction Step	ΔG*	ΔG$_{rel}$	ΔE*	ΔE$_{rel}$
6.62	**6.69a → 6.70a**	-1.4	-10.8	0.1	-8.7
6.62	**6.69b → 6.70b**	-1.5	-10.5	0.1	-9.4
6.63a	**6.76a → 6.82a**	-1.5	-11.6	0.4	-9.8
6.63b	**6.76b → 6.82b^a**	--	-11.7	--	-10.4

^{a} the transition state for this reaction could not be located.

Based on the retention of a chair conformation of the cyclohexane ring in the formation of **6.70a** relative to **6.70b**, it is expected that the former of these two pathways will dominate overall. This structural difference manifests itself in an energetic bias for **6.70a** of 3.7 kcal mol^{-1}. Nevertheless, the two possible deprotonations of each of these intermediates to generate candidate electron donors have been calculated, in addition to the two possible *trans*-isomers (Table 6.7). An interesting observation from this series of calculations is the inability to form the candidate donor **6.91** from the *trans*-diaxial isomer of cyclohexane-1,2-diol **6.88b**. For this pathway, it was not possible to locate a transition state due to geometric constraints imposed by the relative positions of the two oxygens. Attempts at aligning the base in order to perform the desired C—H deprotonation afforded only the reactant complex **6.93** (Figure 6.6a). Encouragingly, however, for this substrate it was possible to locate the transition state which ultimately affords **6.92b**. In addition to this, the subsequent deprotonations of **6.70b** show an energetic bias of 7.5 kcal mol^{-1} for the formation of dianion **6.89b** over **6.90b**. This is anomalous to the observations for precursors **6.70a** and **6.82a**, where the formation of the proposed weaker electron donors **6.90a** and **6.92a** respectively is energetically favoured. This can be rationalised by the favourable change in the cyclohexane ring geometry associated with the formation of **6.89b**, which does not occur in the formation of **6.90b** (Figure 6.6b and c).
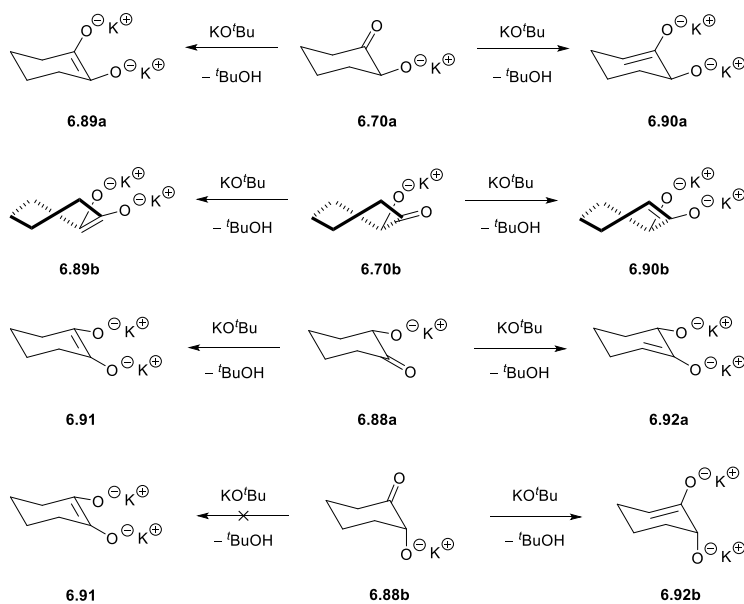
Scheme 6.17: Summary of the final deprotonations of intermediates **6.70** and **6.82** by potassium *tert*-butoxide

Table 6.7: Calculated Gibbs free energies (ΔG) and electronic energies (ΔE) [kcal mol^{-1}] for the final deprotonation reactions affording the proposed organic electron donors **6.89**, **6.90**, **6.91** and **6.92** from different isomers of cyclohexane-1,2-diol.

Parent Diol	Reaction Step	ΔG*	ΔG$_{rel}$	ΔE*	ΔE$_{rel}$
6.62	**6.70a → 6.89a**	13.7	-4.5	15.4	-6.4
	6.70a → 6.90a	7.2	-9.4	8.7	-10.9
6.62	**6.70b → 6.89b**	7.2	-12.4	8.1	-13.9
	6.70b → 6.90b	4.3	-4.9	6.2	-5.8
6.63a	**6.88a → 6.91**	14.0	-4.2	16.2	-5.6
	6.88a → 6.92a	8.6	-8.2	9.0	-10.4
6.63b	**6.88b → 6.91**	--	--	--	--
	6.88b → 6.92b	4.9	-3.7	7.0	-4.1
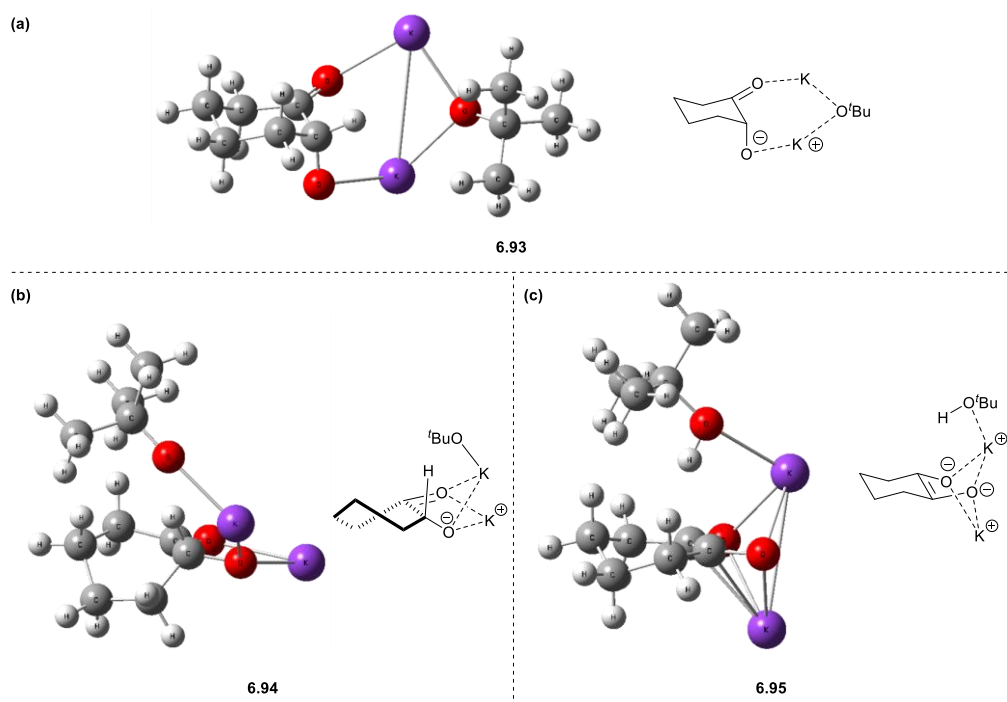
Figure 6.6: (a) Optimised geometry of the complex **6.93** obtained when attempting to locate a transition state for the deprotonation of **6.88b** to afford **6.91**. Optimised geometries of the (b) reactant complex **6.94** and (c) product complex **6.95** associated with the formation of **6.89b** from **6.70b**.
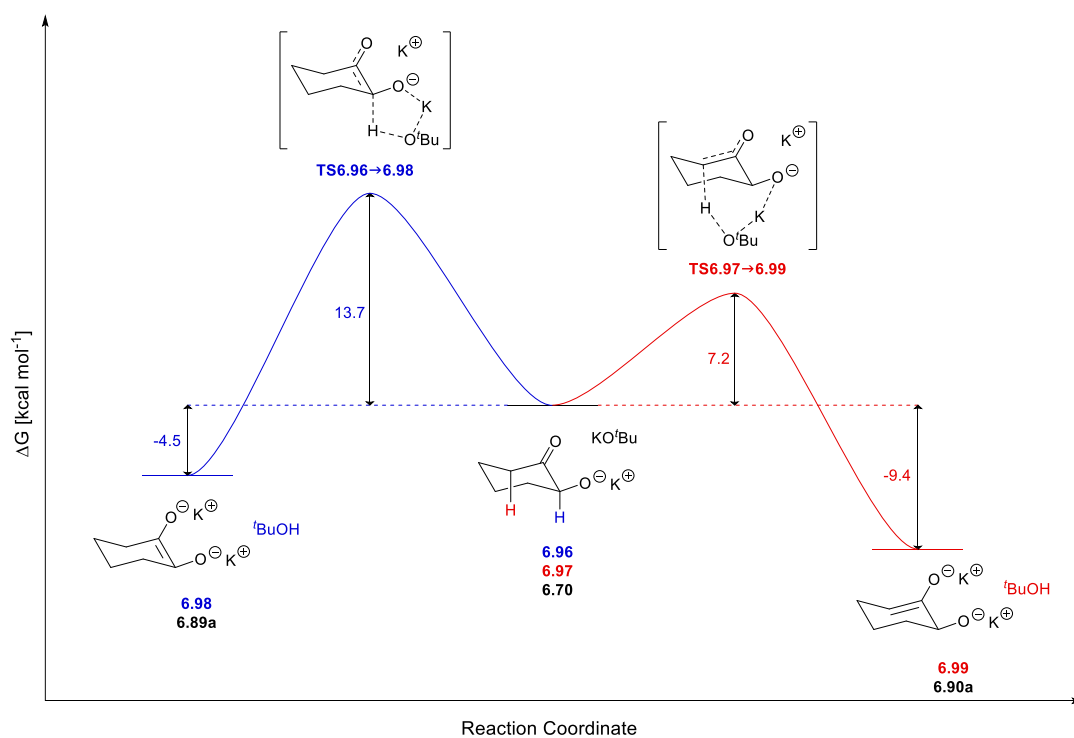
Figure 6.7: Gibbs free energy (ΔG) profile for the formation of **6.89a** (blue reaction pathway) and **6.90a** (red reaction pathway) following deprotonation of intermediate **6.70** by potassium *tert*-butoxide.

Structure numbers in blue or red correspond to the reaction complex modelled computationally, while structure numbers in black represent the separate species involved.
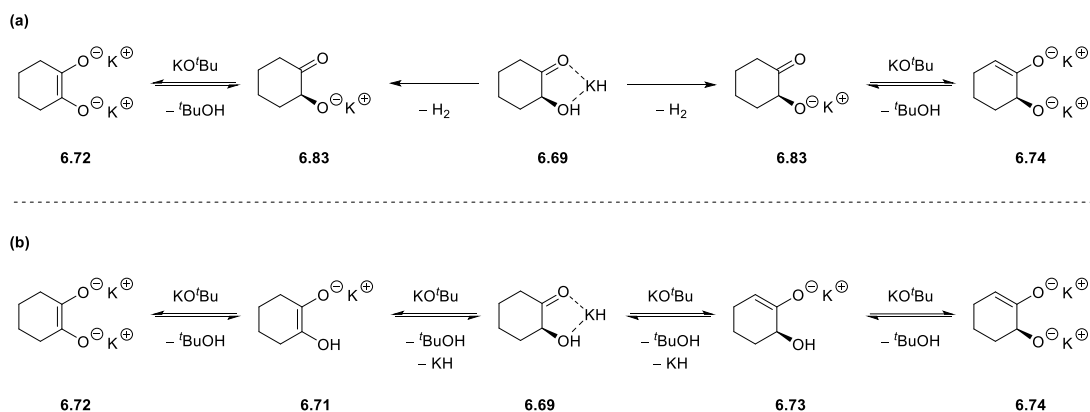
Scheme 6.18: Comparison of (a) the initial reaction mechanism and (b) the present proposed mechanism towards the formation of the proposed organic electron donors **6.71 – 6.74**.

One of the major differences between the present mechanism and the initial proposal is that following the formation of intermediate **6.69**, the current mechanism does not proceed via intermediates **6.71** and **6.73** (Scheme 6.18). Given that these structures are proposed to represent candidate electron donors, the initial reaction pathway was revisited to determine the energetics associated with the deprotonation of intermediate **6.69** by potassium *tert*-butoxide (Table 6.8). In keeping with the format of the earlier deprotonation investigations, each of the possible deprotonations outlined in Scheme 6.19 was investigated.
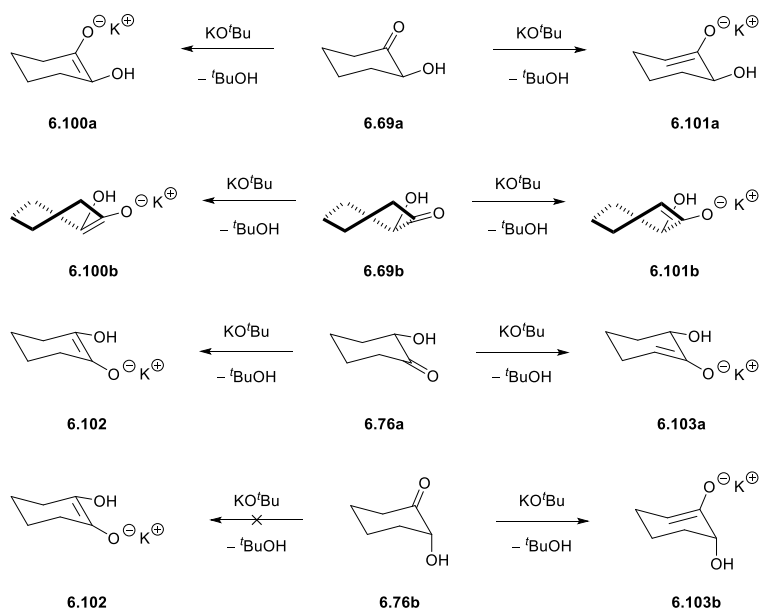
Scheme 6.19: Summary of the deprotonations of intermediates **6.94** and **6.97** by potassium *tert*-butoxide investigated for the formation of the proposed monoanionic donors **6.95**, **6.96**, **6.98** and **6.99**.

Table 6.8: Calculated Gibbs free energies (ΔG) and electronic energies (ΔE) [kcal mol^{-1}] for the final deprotonation reactions affording the proposed organic electron donors **6.95**, **6.96**, **6.98** and **6.99** from different isomers of cyclohexane-1,2-diol.

Parent Diol	Reaction Step	ΔG*	ΔG$_{rel}$	ΔE*	ΔE$_{rel}$
6.62	**6.69a → 6.100a**	2.8	-6.4	6.1	-5.5
	6.69a → 6.101a	3.4	-11.2	4.9	-12.4
6.62	**6.69b → 6.100b**	2.8	-8.6	5.5	-8.8
	6.69b → 6.101b	2.3	-7.8	3.3	-9.4
6.63a	**6.76a → 6.102**	3.4	-5.7	6.1	-5.5
	6.76a → 6.103a	2.5	-8.4	5.1	-8.6
6.63b	**6.76b → 6.102**	--	--	--	--
	6.76b → 6.103b	2.0	-10.7	2.0	-13.5

The formation of singly anionic electron donors of the general form **6.71** or **6.73** is found to proceed via lower activation barriers than for the formation of the analogous dianions (of the general form **6.72** and **6.74**). As was noted for the dianionic donor formations, the weaker donors **6.101a** and **6.102** are energetically favoured over **6.100a** and **6.103a** respectively. Due to the decrease in the twist of the cyclohexane ring, the formation of **6.100b** is more stabilising than the formation of **6.101b**, as was

noted for the deprotonation of **6.70b**. Once again, a transition state for the formation of the electron donor **6.102** from the *trans*-diaxial diol **6.76b** could not be located, as was observed for the attempted formation of **6.91** from **6.88b**.

From these calculations, we can conclude that for each of the possible cyclohexane-1,2-diol isomers it is possible to generate at least one candidate electron donor *in situ* following reaction with potassium *tert*-butoxide. With the exception of the *trans*-diaxial isomer **6.63b**, all isomers can undergo either of two possible C—H deprotonations to afford enolate anions and dianions, depending on which pathway is followed. The fact that transition states could not be located for the formation of **6.102** from **6.76b** or **6.91** from **6.88b** suggests that **6.63b** can only give rise to the weaker donor candidates **6.92b** and **6.103b**, which might ultimately lead to it being a less effective promoter of the biaryl coupling chemistry.

The principles covered in the formation of electron donors from diols can be extended to rationalise the possible donors derived from diamines such as **6.61**, leading to the mechanisms outlined in Scheme 6.20. Each of the three pathways begin with an N—H deprotonation of the starting diamine **6.61**, followed by subsequent hydride elimination to afford imine **6.105**. N—H deprotonation of **6.105** by the potassium hydride generated *in situ*, followed by a C—H deprotonation by potassium *tert*-butoxide, would afford the proposed donor structure **6.107** (Scheme 6.20a). Alternating the order of these reactions, i.e. C—H deprotonation by potassium hydride, followed by N—H deprotonation by potassium *tert*-butoxide, ultimately affords the same product (Scheme 6.20b). It should be noted that this second route is mediated via intermediate **6.108**, which represents another candidate for the active electron donor in reactions mediated by DMEDA. The final proposed route resembles that outlined in Scheme 6.20b, except the C—H deprotonation is performed using potassium *tert*-butoxide, followed by N—H deprotonation by the potassium hydride (Scheme 6.20c). A possible side reaction, the deprotonation of *tert*-butanol by potassium hydride to regenerate potassium *tert*-butoxide, is not addressed in this study as it is not believed to contribute towards our proposed reaction pathways.
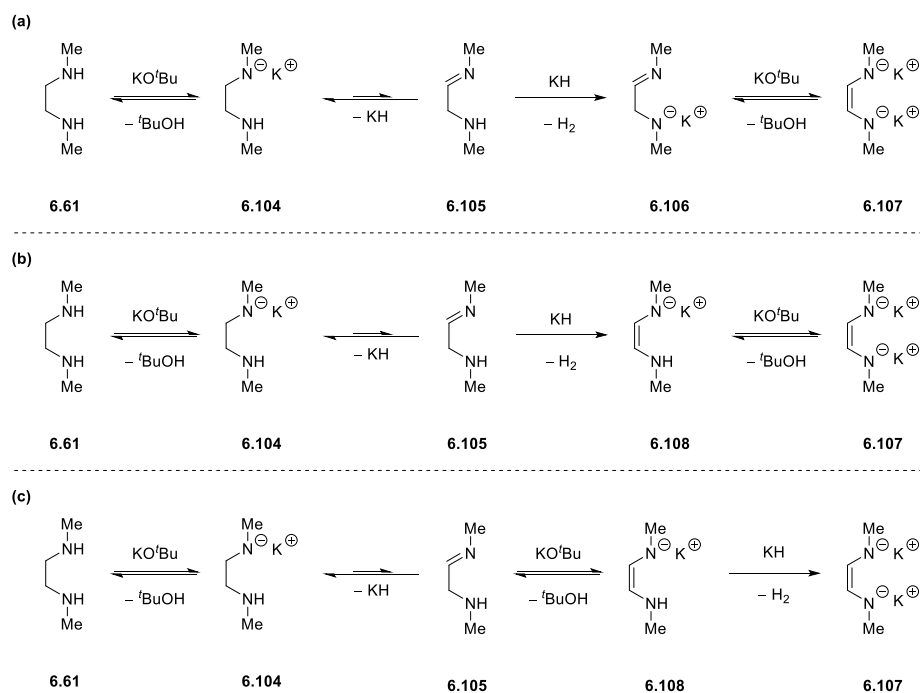
Scheme 6.20: Proposed mechanisms for the formation of electron donors **6.107** and **6.108** from the reaction of DMEDA **6.61** with potassium *tert*-butoxide.

For this series of reactions, optimisation of the transition state and product complex geometries for N—H deprotonations by potassium *tert*-butoxide could not be achieved through standard protocols. Initially, bond scan calculations were performed for the N—H bond under investigation using the 'opt=modredundant' keyword and an initial step size of 0.05 Å. This approach produced a scan energy curve with no determinable reaction maximum or minimum, corresponding to the desired transition state and product geometries respectively (Figure 6.8a). The bond scan calculations were repeated with the N—O bond distance frozen at the distance found in the reactant complex geometry. Pleasingly, using the same initial 0.05 Å step size, a scan energy curve with a defined reaction maximum and minimum was obtained (Figure 6.8b).

To create a more accurate scan curve, subsequent bond scan calculations were performed using a smaller step size of 0.02 Å. For these calculations, a geometry more closely resembling that of the putative transition state was chosen as the start point. The geometries corresponding to the transition state and product complexes for each bond scan calculation were subjected to frequency calculations in order to characterise them as true reaction maxima (one imaginary frequency) and minima (zero imaginary frequencies). For the initial deprotonation of DMEDA **6.61**, the corresponding

transition state and product geometries obtained from this protocol are shown in Figure 6.9.
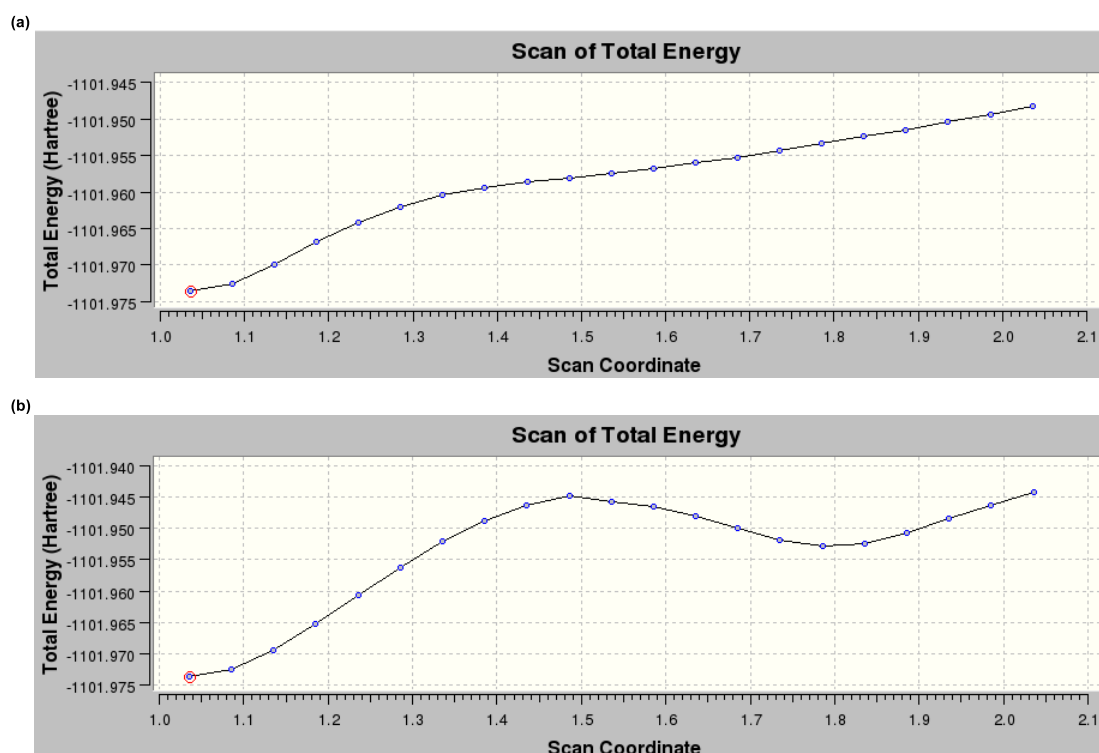
Figure 6.8: Scan energy curves obtained (a) without and (b) with a frozen N—O bond distance for the initial deprotonation of DMEDA **6.61** using potassium *tert*-butoxide (0.05 Å step size).
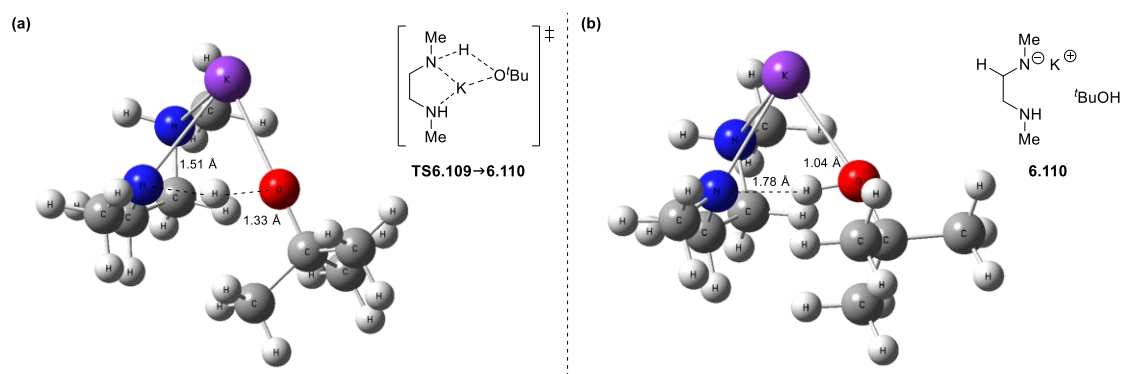
Figure 6.9: Calculated geometries of (a) the transition state complex **TS6.109→6.110** and (b) the product complex **6.110** obtained from bond scan calculation.
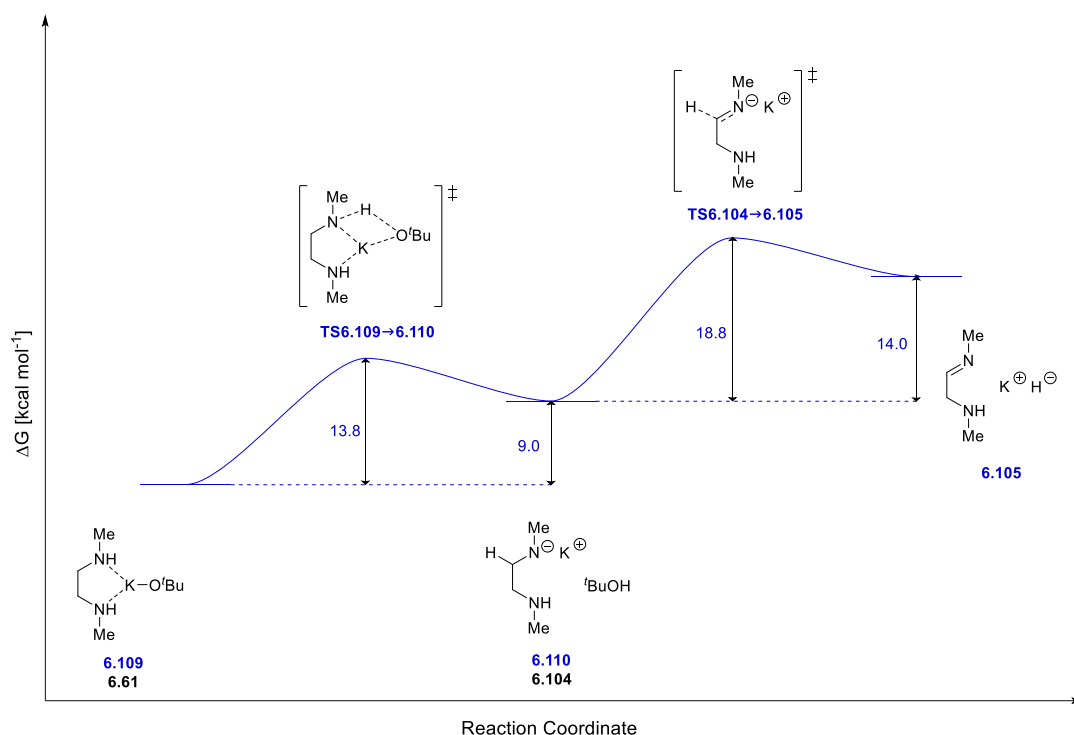
Figure 6.10: Gibbs free energy (ΔG) profile for the formation of **6.105** following deprotonation of DMEDA **6.61** by potassium *tert*-butoxide and subsequent hydride elimination from **6.104**. Structure numbers in blue correspond to the reaction complex modelled computationally, while structure numbers in black represent the separate species involved.

From these calculations, an activation free energy of 13.8 kcal mol^{-1} was predicted for the initial N—H deprotonation. The product complex of this reaction **6.110** was uphill of the reactant complex by 9.0 kcal mol^{-1}, giving a reverse barrier of only 4.8 kcal mol^{-1} (Figure 6.10). The elimination of hydride from **6.104** was found to be energetically challenging with an activation barrier of 18.8 kcal mol^{-1} to be overcome for the reaction to proceed. Once again this is an endergonic process, with a 4.8 kcal mol^{-1} reverse barrier highlighting the unfavourable nature of the transformation. It should be noted here that the energetics obtained through the bond scan calculations represent only an estimate of the reaction energetics. An interesting observation was made when the hydride elimination reaction was modelled in the presence of the *tert*-butanol formed from the first deprotonation. Upon location of the transition state for this reaction, relaxation of this to the reactant geometry afforded complex **6.109** rather than the anticipated **6.110** (Figure 6.11). For this transformation an activation free energy of 37.7 kcal mol^{-1} was calculated, with a relative free energy of 35.3 kcal mol^{-1} again demonstrating the unfavourable nature of this reaction.
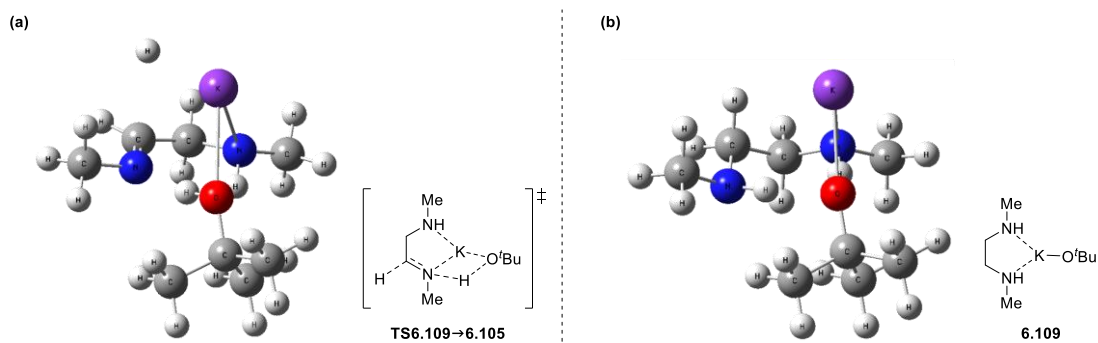
Figure 6.11: Optimised geometry of (a) the pseudo-concerted transition state **TS6.109→6.105** and (b) the optimised reactant complex **6.109** associated with this transition state.

A number of possible deprotonations of the intermediate imine **6.105** have been outlined, ultimately affording a candidate electron donor. Utilising the potassium hydride generated *in situ*, **6.105** can undergo two possible reactions; N—H deprotonation to afford **6.106** (Scheme 6.20a) or C—H deprotonation to afford **6.108** (Scheme 6.20b). Comparing the energetics for these pathways, both reactions have accessible activation free energies. The formation of the electron donor candidate **6.108** is found to be energetically more favourable by 7.6 kcal mol^{-1} relative to the formation of **6.106** (Figure 6.12). Further deprotonation of intermediates **6.106** and **6.108** by potassium *tert*-butoxide can generate the dianion **6.107**. The formation of this species is found to be energetically feasible by both possible pathways; deprotonation of **6.106** is found to be mildly exergonic while deprotonation of **6.108** is mildly endergonic, with a reverse barrier of only 3.6 kcal mol^{-1} (Figure 6.13).
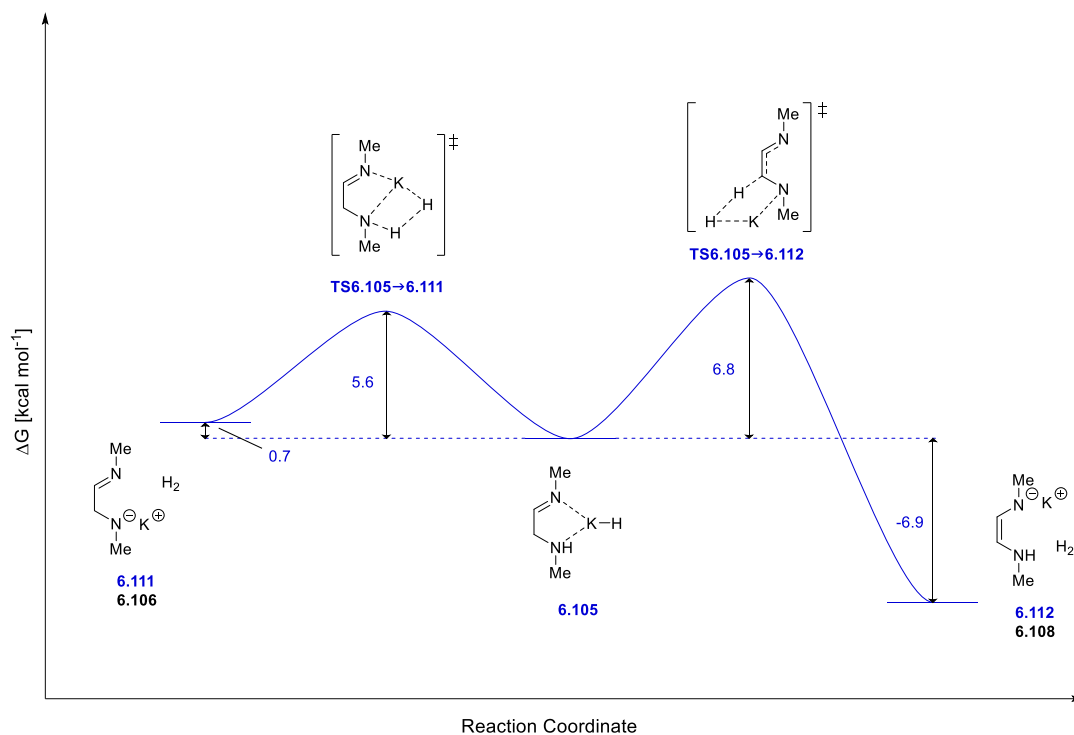
Figure 6.12: Gibbs free energy (ΔG) profile for the two possible deprotonations of **6.105** by the potassium hydride formed *in situ*. Structure numbers in blue correspond to the reaction complex modelled computationally, while structure numbers in black represent the separate species involved.
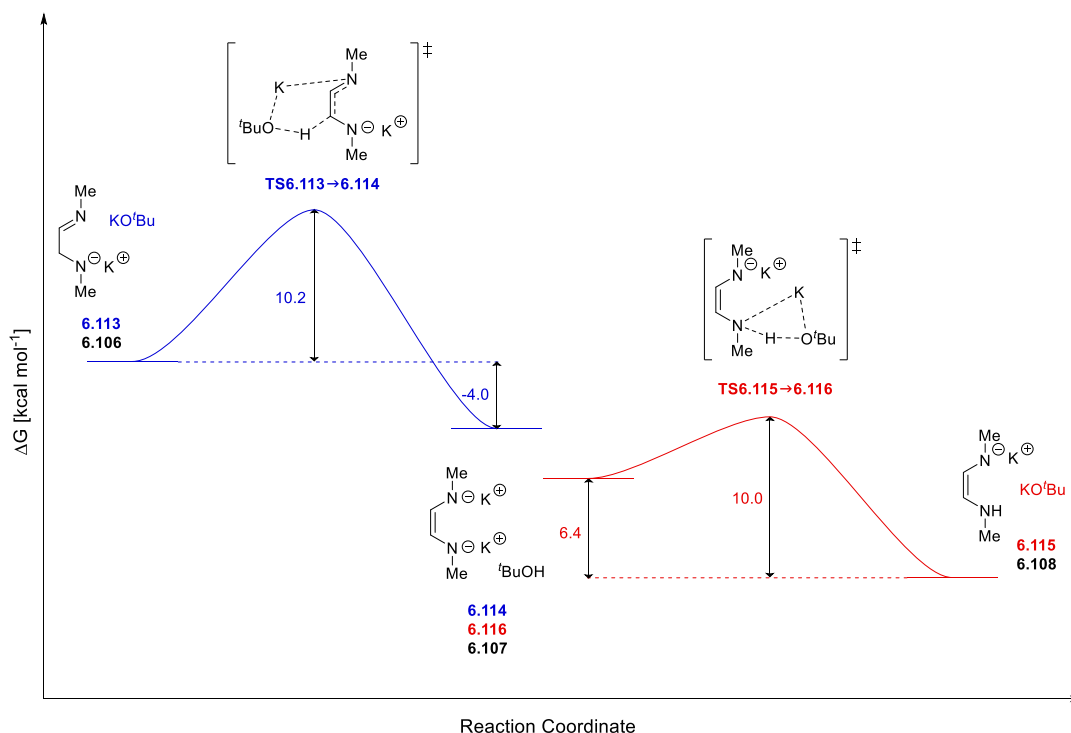
Figure 6.13: Gibbs free energy (ΔG) profile for the formation of **6.107** following deprotonation of intermediates **6.106** (blue pathway) and **6.108** (red pathway) by potassium *tert*-butoxide. Structure numbers in blue or red correspond to the reaction complex modelled computationally, while structure numbers in black represent the separate species involved.

In the reaction pathway outlined in Scheme 6.20c, the imine intermediate **6.105** undergoes a C—H deprotonation by potassium *tert*-butoxide to afford **6.108**. This anion is then deprotonated by the potassium hydride generated in the imine formation step, yielding the dianionic species **6.107**. Modelling this reaction pathway, it was found that both reaction steps are slightly endergonic, with the product complex **6.120** uphill of the reactant complex **6.117** by 5.3 kcal mol^{-1} (Figure 6.14).
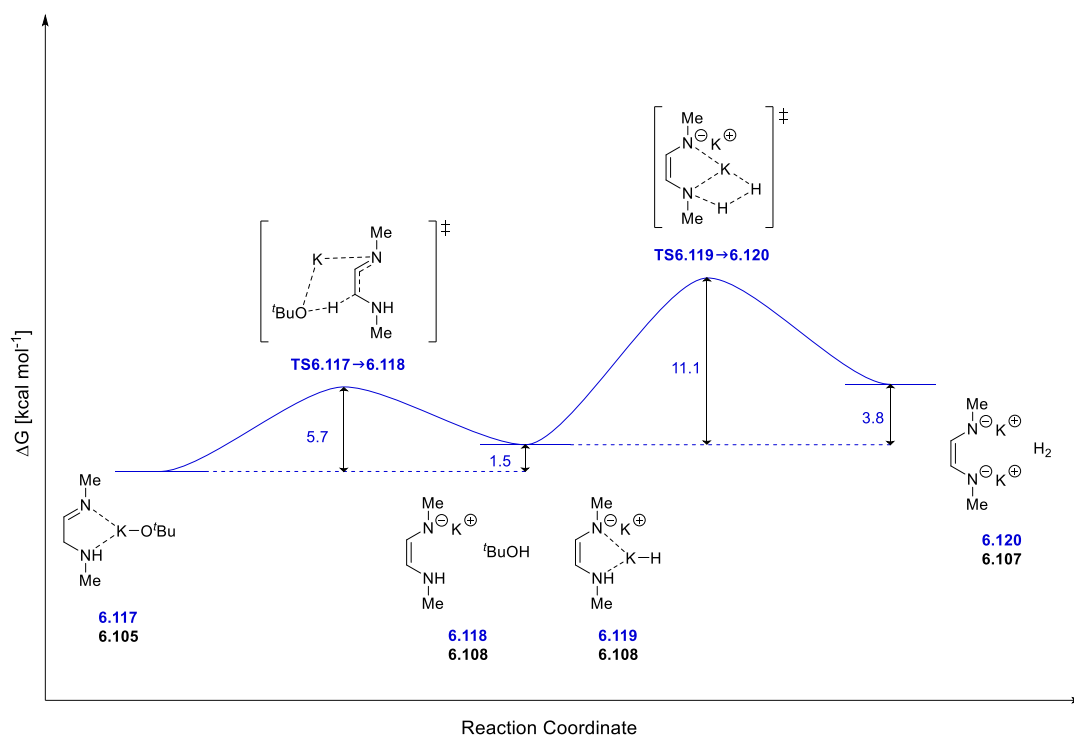
Figure 6.14: Gibbs free energy (ΔG) profile for the formation of the proposed organic electron donor **6.108** following deprotonation of intermediate **6.105** by potassium *tert*-butoxide, and subsequent deprotonation of this by the potassium hydride formed *in situ* to afford **6.107**. Structure numbers in blue correspond to the reaction complex modelled computationally, while structure numbers in black represent the separate species involved.

In considering the overall energetic profiles for the proposed reaction pathways outlined in Scheme 6.20, a number of key observations can be made. In all three cases, the rate-determining step is the unfavourable hydride elimination step, with an activation free energy of 18.8 kcal mol^{-1}. For the formation of the proposed donor species **6.107** via the route described in Scheme 6.20a, this route is found to be endergonic with an overall relative free energy of 19.7 kcal mol^{-1}. The alternative electron donor candidate **6.108** can be formed by the route described in Scheme 6.20b, with this mechanism calculated to be endergonic by only 16.1 kcal mol^{-1}. To

form **6.107** by this route, the overall relative free energy increases to 22.5 kcal mol^{-1}. The final proposed pathway (Scheme 6.20c) was found to have the greatest energetic demand for the formation of **6.107** with an overall relative free energy of 28.3 kcal mol^{-1}. Furthermore, the formation of **6.108** by this route is found to be significantly less favourable than by the route outlined in Scheme 6.20b with a relative free energy of 24.5 kcal mol^{-1}. Based on these energetic observations, it is herein proposed that the formation of the proposed electron donor **6.107** is most likely to proceed via the reaction mechanism outlined in Scheme 6.20a. The pathway described in Scheme 6.20b represents the energetically most favoured route towards the proposed electron donor **6.108**, however the formation of **6.107** is less favourable by this route relative to that described in Scheme 6.20a. The final proposed route (Scheme 6.20c) is the most energetically demanding route towards both **6.107** and **6.108**, therefore it is proposed that this route is not likely to be responsible for donor formation in these reactions.

While the formation of a number of candidate electron donors derived from simple organic molecules has been investigated through computational means, the relative reducing ability of these species has not yet been addressed. The energetics for the formation of these donors has imparted some rationale for the relative ability of the respective parent molecules to mediate transition metal-free coupling reactions. It is of interest, however, to determine if the structures proposed throughout the present chapter do in fact represent electron donors. To that end, it was decided to apply the Marcus-Hush theory for electron transfer to understand the reaction energetics involved in the reduction of a simple iodoarene by these species.

7

Computational Application of Marcus Theory

7.1 Introduction

The calculations of reaction energetics for electron transfer processes is a challenging task, which has been made possible through the development of a theory for electron transfer by Rudolph Marcus.[119] The prediction of these energetics using computational techniques was first demonstrated in 1987 by Nelsen *et al.*, who were investigating the self-electron transfer between bis-*N,N'*-sesquibicyclichyrazines such as **7.1** (Scheme 7.1).[125] Ultimately this led to the development of what has become known as the Nelsen four-point method. This methodology has since been utilised both within the literature[120-123] and within our own research group[130] to calculate the reaction free energies for various electron transfer chemistries using quantum mechanics.
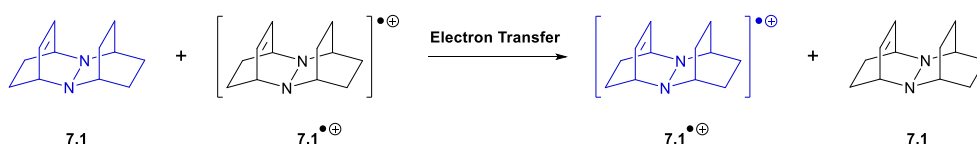
Scheme 7.1: Self-electron transfer reaction of **7.1** and its related radical cation investigated by Nelsen *et al.* using Marcus theory.[125]

Comparing the systems investigated previously to those currently being investigated, a number of key differences are noted. First of these is the choice of solvent; the present work uses the non-polar solvent benzene, while the earlier work was performed in DMF. In addition to this, the electron donors currently under investigation are proposed to be singly- or doubly-anionic in their active state rather than neutral. Taking these factors into consideration, it is expected that the reaction profiles calculated for the current electron donors are likely to differ from those in the earlier work.

This Chapter begins with the calculation of activation free energies for electron transfer reactions for a variety of small organic electron donors. Revisions of the methodology are subsequently introduced in order to produce a more representative model of the reactions predicted to occur under reaction conditions. Combining these results with those outlined in Chapter 6, observed experimental results can begin to be rationalised.

7.2 Computational Methods

DFT calculations were performed using the Gaussian 09 software package.[136] All reaction species were optimised using the M06-2X functional[115] with a double-ζ basis set. With the exceptions of potassium and iodine, all elements were modelled using the aug-cc-pVDZ basis set.[147] Potassium was modelled using the 6-31++G(d,p) basis set.[148] For systems that included iodine, the small-core energy consistent relativistic pseudopotential was implemented.[149, 150] Implicit solvation of the reaction systems was modelled using the CPCM model with the associated parameters for benzene.[116, 117] Frequency calculations were performed on all optimised structures in order to characterise them as minima (zero imaginary frequencies) or saddle points (single imaginary frequency) and to obtain thermochemical data. All calculations were modelled at a temperature of 298 K. Throughout this chapter, unless stated otherwise, the reactant and product state for each transformation was taken to be the reaction complex rather than the separated reactant and product species. As an approximation to improve computational efficiency, potassium *tert*-butoxide has been modelled as a monomeric entity, despite being a tetrameric species.

7.3 Application of Marcus Theory to Proposed Organic Electron Donors

The formation of charged organic electron donors following reaction of simple organic additives with potassium *tert*-butoxide has been investigated and discussed throughout Chapter 6. Figure 7.1 summarises the various structures which are i) proposed candidates for the active electron donor in transition metal-free coupling reactions or ii) intermediates formed en route to the final electron donor. The neutral organic precursors to these species have been coloured to illustrate whether they represent effective (blue, Figure 7.1) or ineffective (red, Figure 7.1) promotors of biaryl coupling reactions. Marcus theory was utilised to determine the free energy profiles associated with the reduction of the substrate 4-iodoanisole **7.32**.
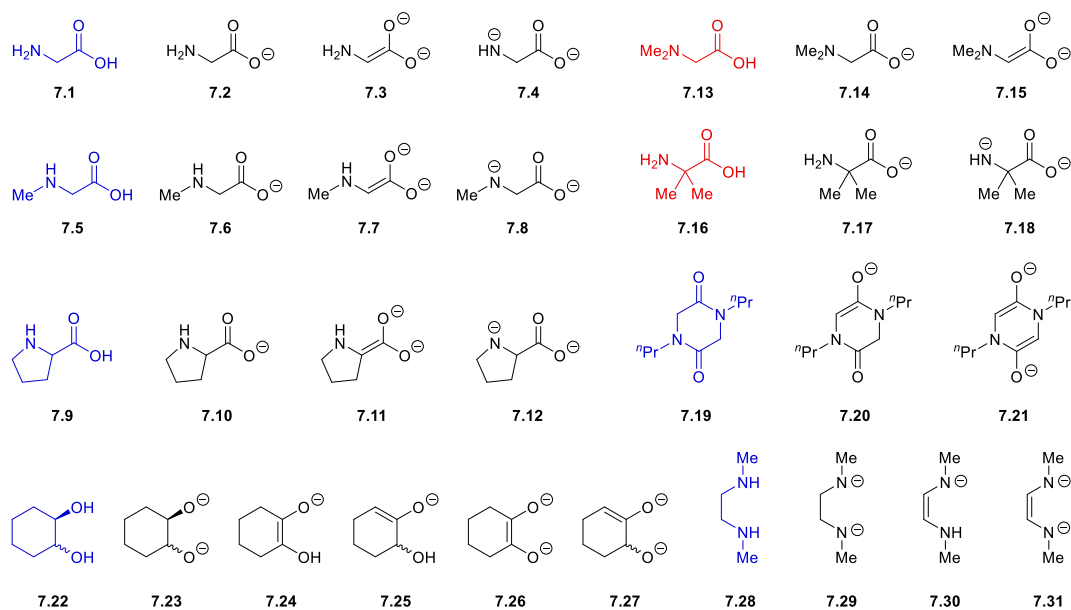
Figure 7.1: Structures of organic additives and their related electron donors (as discussed in Chapter 6) investigated in this work. Precursors are coloured blue to indicate those shown experimentally to give rise to efficient coupled product formation and red to indicate those which result in inefficient coupled product formation.

The activation and relative free energies calculated for the reduction of **7.32** by the singly anionic species investigated in Chapter 6 are summarised in Figure 7.2b. From these energetics it is clear that the amino acid carboxylates are unlikely to be able to transfer an electron, with activation free energies in excess of 49.0 kcal mol^{-1}. The singly anionic species **7.20**, formed by single deprotonation of the DKP additive **7.19**, is predicted to be an effective electron donor for the reduction of **7.32**, with an accessible activation free energy of 26.2 kcal mol^{-1} for this reaction. Comparing the calculated energetics for the structurally-related anions **7.24** and **7.25**, the former is predicted to represent a stronger reducing agent. Relative to **7.25**, the activation free energy for **7.24** is 6.3 kcal mol^{-1} lower, and the relative free energy is significantly more favourable (11.2 kcal mol^{-1} versus 21.9 kcal mol^{-1}). Of the anionic structures investigated, **7.30** is predicted to be the most powerful reducing agent with an activation free energy of 15.3 kcal mol^{-1}. What's more, this is the only anionic species predicted to have an exergonic reaction profile.

(a)

7.32   **7.33**

(b)

7.2	**7.6**	**7.10**	**7.14**	**7.17**	**7.20**	**7.24**	**7.25**	**7.30**

ΔG^* : 53.6	ΔG^* : 50.3	ΔG^* : 49.6	ΔG^* : 49.9	ΔG^* : 51.5	ΔG^* : 26.2	ΔG^* : 22.2	ΔG^* : 28.5	ΔG^* : 15.3
ΔG_{rel} : 43.4	ΔG_{rel} : 38.7	ΔG_{rel} : 43.5	ΔG_{rel} : 44.1	ΔG_{rel} : 39.8	ΔG_{rel} : 16.9	ΔG_{rel} : 11.2	ΔG_{rel} : 21.9	ΔG_{rel} : -4.0
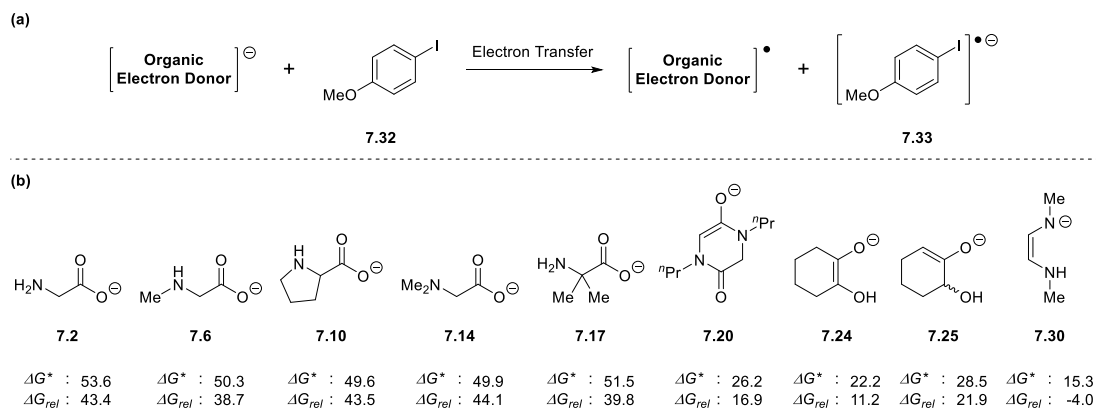
Figure 7.2: (a) Summary of the electron transfer reaction being investigated in this work; (b) structure of the proposed anionic electron donors investigated, with their associated reaction free energies (ΔG) [kcal mol^{-1}] obtained from the computational application of Marcus Theory.

The predicted energetics for the reduction of **7.32** by the various dianionic species investigated showed unusual results, with the maximum activation free energy for these species calculated at 5.6 kcal mol^{-1} for **7.27**. In addition to this, each reduction was predicted to be significantly exergonic, with relative free energies for this series of transformations ranging between -25.7 and -71.8 kcal mol^{-1} (Figure 7.3b). This suggests that all possible dianions are highly effective reducing agents, which is not observed experimentally in the cases of **7.15** and **7.18**, for example.

(a)

7.32   **7.33**

(b)

7.3	**7.4**	**7.7**	**7.8**	**7.11**	**7.12**	**7.15**

ΔG^* : 0.2	ΔG^* : 1.8	ΔG^* : 0.2	ΔG^* : 1.8	ΔG^* : 0.6	ΔG^* : 2.7	ΔG^* : 0.7
ΔG_{rel} : -64.5	ΔG_{rel} : -39.1	ΔG_{rel} : -62.3	ΔG_{rel} : -41.7	ΔG_{rel} : -60.2	ΔG_{rel} : -39.7	ΔG_{rel} : -54.9

7.18	**7.21**	**7.23**	**7.26**	**7.27**	**7.29**	**7.31**

ΔG^* : 1.9	ΔG^* : 1.1	ΔG^* : 4.3	ΔG^* : 0.1	ΔG^* : 5.6	ΔG^* : 2.0	ΔG^* : 0.3
ΔG_{rel} : -40.8	ΔG_{rel} : -53.6	ΔG_{rel} : -41.0	ΔG_{rel} : -68.0	ΔG_{rel} : -25.8	ΔG_{rel} : -41.6	ΔG_{rel} : -71.8
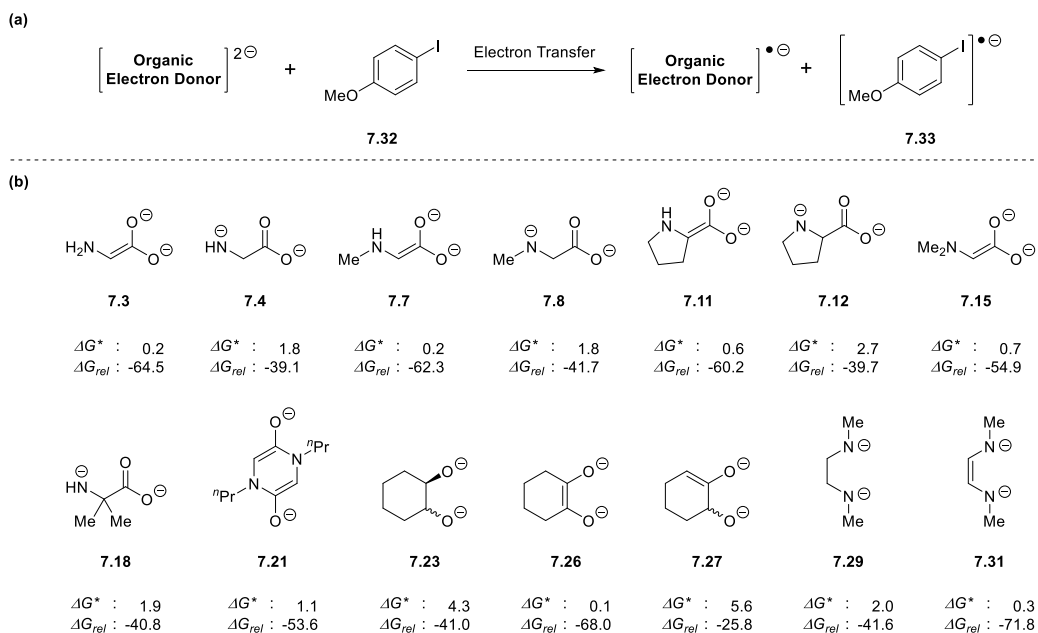
Figure 7.3 (a) Summary of the electron transfer reaction being investigated in this work; (b) structure of the proposed dianionic electron donors investigated, with their associated reaction free energies (ΔG) [kcal mol^{-1}] obtained from the computational application of Marcus Theory.

Despite these curious results, some interesting observations can be made. For the amino acid-derived dianions, the activation free energies for dianions resulting from C—H deprotonation of the preceding carboxylate (**7.3**, **7.7**, **7.11** and **7.15**) were lower than those dianions formed from the alternative N—H deprotonation (**7.4**, **7.8**, **7.12** and **7.18**). In addition to lower activation free energies, their relative free energies were also predicted to be more favourable by approximately $14.0 - 25.4$ kcal mol^{-1}. Of dianions **7.26** and **7.27**, we initially predicted that **7.26** would represent a greater reducing agent, and indeed these initial predictions appear to support this. While both species have low activation free energies, the respective relative free energies of -68.0 and -25.8 kcal mol^{-1} do indeed support this hypothesis. Similarly, comparing the DMEDA-derived dianions **7.29** and **7.31**, the presence of an alkene moiety between the two anionic nitrogen atoms appears to enhance the reducing power significantly. This structural difference accounts for a difference in the relative free energies of 30.2 kcal mol^{-1}.

With all dianionic species predicted to be highly effective electron donors, we became sceptical of the validity of these predicted energetics. To determine if this methodology was suitably able to predict the reaction energetics for electron transfer under the transition metal-free coupling conditions, the reduction by neutral organic super electron donors **7.34** – **7.36** was investigated. To our surprise, the lowest activation free energy obtained for these species was 39.5 kcal mol^{-1} for **7.36**. Furthermore, donor **7.34** was predicted to have an activation free energy of 54.2 kcal mol^{-1}, which would be inaccessible under the current reaction conditions. This is in disagreement with previous experimental observations, where **7.34** has efficiently facilitated the coupling of **7.32** with benzene.

(a)

7.32   **7.33**

(b)

| **7.34** | **7.35** | **7.36** |

ΔG^* : 54.2 ΔG^* : 40.2 ΔG^* : 39.5
ΔG_{rel} : 53.2 ΔG_{rel} : 36.1 ΔG_{rel} : 33.9
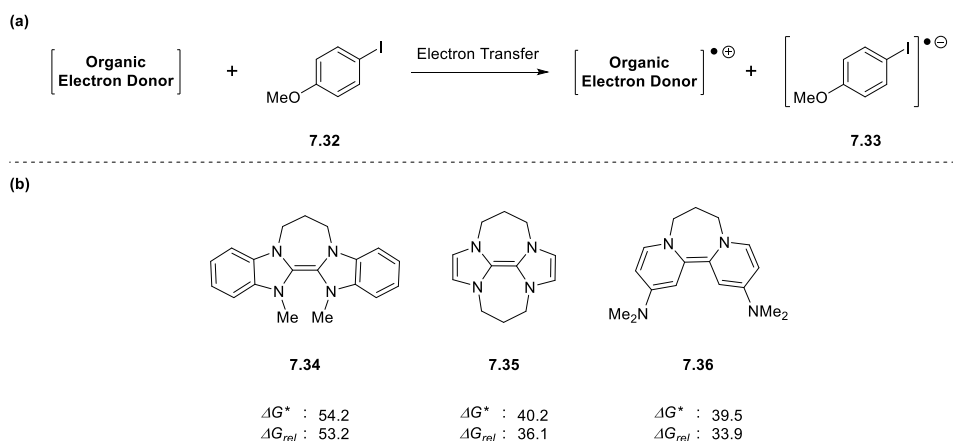
Figure 7.4: (a) Summary of the electron transfer reaction being investigated in this work; (b) structure of the neutral organic super electron donors investigated, with their associated reaction free energies (ΔG) [kcal mol^{-1}] obtained from the computational application of Marcus Theory.

Given this disagreement between experiment and theory, we began to speculate if the present theoretical model for calculating electron transfer energetics was sufficient for the investigation of systems in non-polar reaction medium. This would become especially problematic for the charged electron donors formed *in situ*, which would most likely not exist in solution as 'naked' anions. To resolve these issues, we sought to develop a new protocol by which these reactions could be more accurately modelled.

7.4 Refining the Electron Transfer Model

In the current protocol for calculation the activation free energies for electron transfer reactions, the donor and acceptor molecules are considered as separate entities. For the charged electron donors being investigated in this research, the energetic difference associated with the loss of an electron in non-polar solvent will be considerably greater than that for loss of an electron in a polar solvent. As a consequence, these charged species are likely to be portrayed as significantly stronger electron donors when modelled in non-polar solvents. To more accurately represent these reactions, we propose the use of an electron transfer complex. Through inclusion of the potassium counter-ions, it would be possible to model the electron transfer reaction with a net neutral charge; something we predict will give more accurate reaction energetics.

Through the course of this chapter, three reaction Models will be discussed. The use of the standard Nelsen four-point method, as implemented in the previous sub-chapter, will herein be referred to as Model 1. For the charged electron donors, Model 2 will refer to the implementation of Model 1 with the inclusion of potassium cations in the donor structure to give the reactant species a neutral charge (single cation for anionic species, two cations for dianionic species). Finally, the use of an electron transfer complex to model the electron transfer reaction will be referred to as Model 3 (Figure 7.5). This model uses a modified version of the Nelsen four-point method, and hence the equations outlined in Chapter 4.5 require small alterations. The current proposed model consists of only a single reaction system, whereas the original protocol has a 'donor' and an 'acceptor' system. Accounting for this difference, Eqn. 69 can be reduced to Eqn. 71:

$$\lambda_i = \frac{\lambda_i(D) + \lambda_i(A)}{2} \qquad \text{(Eqn. 69)}$$

$$\lambda_i = \lambda_i(DA) \qquad \text{(Eqn. 71)}$$

where $\lambda_i(DA)$ is calculated in the same manner as $\lambda_i(D)$. In these complex systems, the starting complex is taken to be in the singlet state, while the product complex is modelled as a triplet; thus there is no net change in the overall system charge. Through the use of this new reaction model, we expect to be able to determine the effect on the internal reorganisation energy of having a reaction partner in the system.
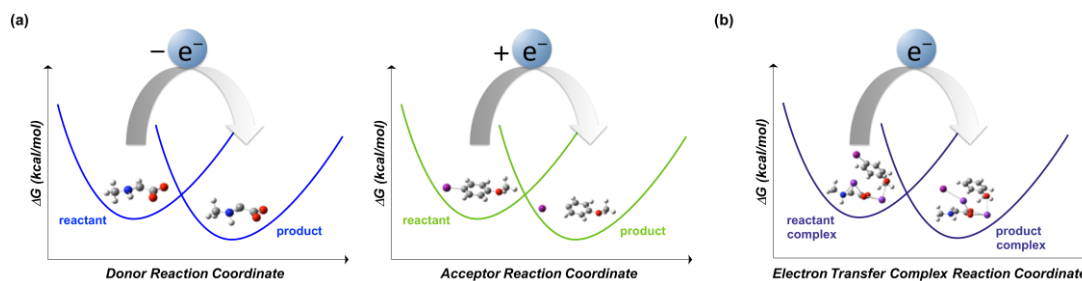
Figure 7.5: Graphical representation of (a) the Nelsen four-point method and (b) the electron transfer complex model developed.

To establish a baseline for calculated reaction energies, we chose the reduction of **7.32** by neutral organic super electron donors **7.34 – 7.36** as a starting point (Table 7.1). The

results for Model 3 show that the use of an electron transfer complex produces a significant change in the electron transfer energetics relative to those obtained using Model 1. For the three donors modelled, there is a notable decrease in the relative free energy of the electron transfer. Although the reaction is still endergonic, the barrier corresponding to the reverse reaction is higher than that obtained using Model 1 (13.0 – 19.3 kcal mol^{-1} vs. 1.0 – 5.6 kcal mol^{-1}), thus making the reverse reaction more challenging. Furthermore, a significant decrease in the activation free energy is observed when using a donor-acceptor complex to perform these calculations. Taking donor **7.35** as an example, the activation free energy is decreased by 16.3 kcal mol^{-1}, with the relative energy decreasing by 31.5 kcal mol^{-1} relative to Model 1. This results in an electron transfer reaction which is only mildly endergonic (4.6 kcal mol^{-1}), suggesting that the reorganisation of the electron transfer complex is more favourable than the reorganisation of the individual components.

Table 7.1: Comparison of the activation and relative free energies (ΔG) [kcal mol^{-1}] calculated for neutral organic electron donors **7.34**-**7.36** using Models 1 and 3.

Organic Electron Donor	Model 1		Model 3	
	ΔG^*	ΔG_{rel}	ΔG^*	ΔG_{rel}
7.34	54.2	53.2	34.1	20.3
7.35	40.2	36.1	23.9	4.6
7.36	39.5	33.9	27.2	14.2

We sought to ensure that calculated energetics did indeed represent the transfer of an electron from the donor molecule to the acceptor, and not a singlet-to-triplet excitation localised on the electron donor. To do this, we probed the HOMO and LUMO of the reactant complex and the spin density of the product complex as shown in Figure 7.6 for the complex of donor **7.35** and 4-iodoanisole **7.32**. Figure 7.6a shows that, despite the formation of a stable electron transfer complex, the HOMO is localised on the donor molecule, while Figure 7.6b shows that the LUMO is localised on the acceptor. For the product complex (Figure 7.6c), the spin density (2) is distributed relatively evenly across both the donor and acceptor components of the complex (Figure 6.2d). A decomposition of the atomic contributions to the spin densities shows

that 1.06 electrons are localised to the acceptor and 0.94 are localised across the donor molecule.
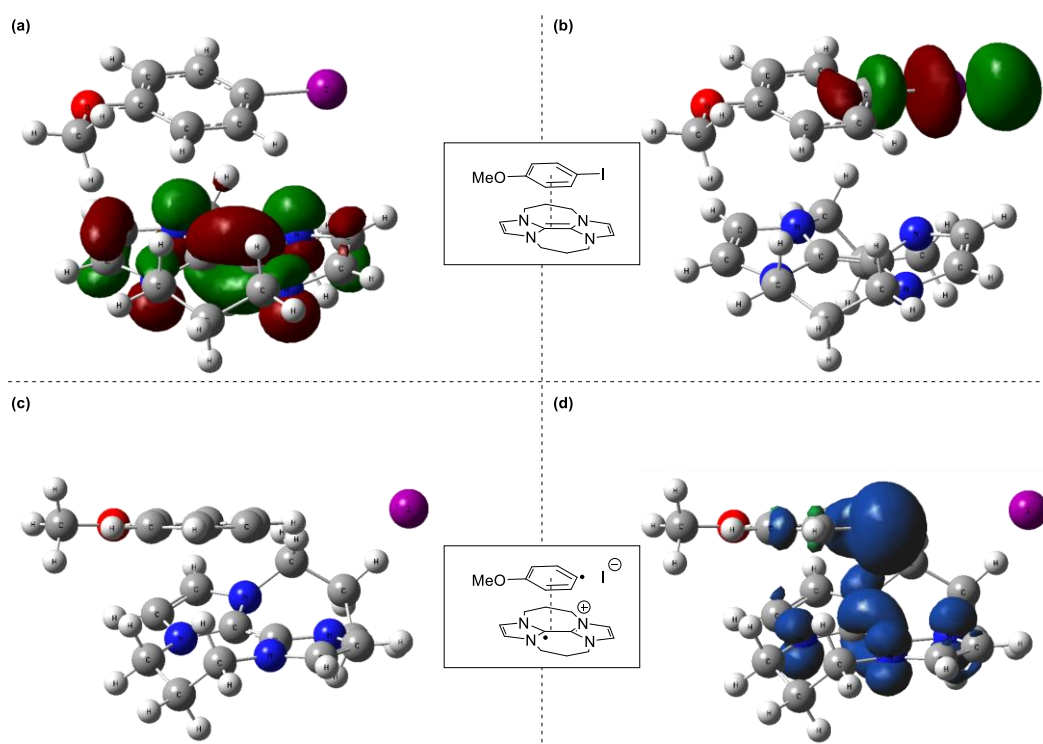
Figure 7.6: Calculated (a) HOMO and (b) LUMO for the reactant complex; (c) the optimised geometry and (d) calculated spin density for the product complex of donor **7.35** with 4-iodoanisole **7.32**.

Extending this approach to the charged organic electron donors, the reduction of 4-iodoanisole **7.32** by the singly anionic candidates was investigated to begin with. Calculating the reaction energetics using Model 2, we note that the inclusion of the potassium counter ions in the 'donor' systems results in all singly anionic systems having inaccessible reaction free energy barriers, the lowest of these being 46.7 kcal mol^{-1} for donor **7.30** (Table 7.2). This reaction model can almost be considered an intermediate between Models 1 and 3, and is not believed to produce accurate representation of electron transfer reaction energetics.

It has already been established through the use of Model 1 that the amino acid carboxylates **7.2**, **7.6**, **7.10**, **7.14** and **7.17** are ineffective at reducing 4-iodoanisole **7.32**; this trend is again using Model 3, where the calculated activation free energies for these species are all in excess of 64.0 kcal mol^{-1}. From these results, we can confidently conclude that these carboxylates do not represent the active electron

donor in coupling reactions promoted by amino acids. The DKP-derived donor candidate **7.20** has been predicted through Model 1 to be an effective reducing agent with an activation free energy of 26.2 kcal mol^{-1}. Using Model 3, an activation free energy of 33.5 kcal mol^{-1} is predicted for this donor candidate. Despite the fact that this is a more challenging barrier to overcome, the relative free energy calculated by this Model is more favourable than that calculated by Model 1.

Table 7.2: Summary of the activation and relative free energies (ΔG) [kcal mol^{-1}] calculated for anionic organic electron donors using Models 1, 2 and 3.

Organic Electron Donor	Model 1		Model 2		Model 3	
	ΔG^*	ΔG_{rel}	ΔG^*	ΔG_{rel}	ΔG^*	ΔG_{rel}
7.2	53.6	43.4	99.5	99.2	64.7	58.3
7.6	50.3	38.7	92.0	91.6	64.9	58.8
7.10	49.6	43.5	89.7	89.6	65.7	59.5
7.14	49.9	44.1	85.8	85.6	65.1	58.9
7.17	51.5	39.8	95.0	94.9	64.3	58.3
7.20	26.2	16.9	53.8	52.2	33.5	11.7
7.24	22.2	11.2	55.7	54.6	31.6	8.6
7.25	28.5	21.9	63.2	63.2	43.3	21.7
7.30	15.3	-4.0	46.7	44.8	25.5	2.9

The predicted relative effectiveness of donor candidates **7.24** and **7.25** has been addressed through the predictions obtained using Model 1, and is again demonstrated through the energetics obtained from Model 3. The difference between the activation free energies for these two related structures is only 6.3 kcal mol^{-1} using Model 1; considering these donors as part of an electron transfer complex, this difference increases to 11.7 kcal mol^{-1}. The calculated activation free energy for **7.25** (43.3 kcal mol^{-1}) would be inaccessible under the employed reaction conditions, whereas the barrier of 31.6 kcal mol^{-1} predicted for **7.24** should allow for the reduction of **7.32**. Of all the anionic structures investigated in this research, the DMEDA-derived anion **7.30** represents the strongest reducing agent, with an activation free energy of only 25.5 kcal mol^{-1} calculated using Model 3. Similar to donors **7.20** and **7.24**, **7.30** would

therefore be expected to be capable of efficiently reducing an iodoarene under standard reaction conditions.

As was performed for the neutral electron donors, the reactant complex orbitals and product complex spin densities were investigated in order to confirm the calculation of a single electron transfer. For the amino acid carboxylates this produced an unusual result, which can provide rationale for the inaccessible barriers calculated for these structures (Figure 7.7). Rather than the expected spin density corresponding to the product complex of an electron transfer reaction, approximately half of the total spin was localised on the iodine atom (Figure 7.7a). Rather than the cleavage of the radical anion of an iodoarene, this spin distribution is representative of the homolytic bond scission of a neutral iodoarene, thus suggesting that an electron transfer reaction has not occurred in this system. This was not the case for the remaining anions **7.20** (Figure 7.7b), **7.24**, **7.25** and **7.30**, all of which displayed the expected spin distribution in their respective product complexes.
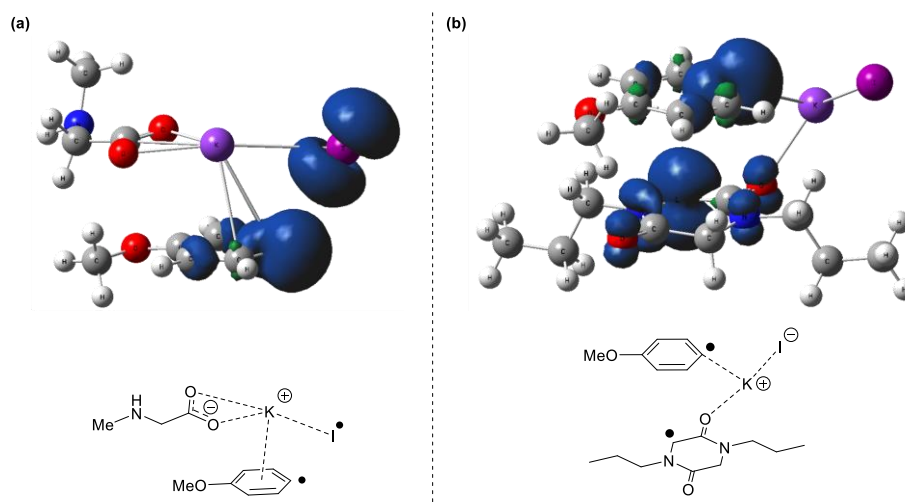
Figure 7.7: Calculated spin densities for the product complexes associated with the reduction of 4-iodoanisole **7.32** by (a) carboxylate **7.6** and (b) the DKP anion **7.20**.

Knowing that a monoanionic species was not responsible for the observed reactivity when using amino acids as additives in these coupling reactions, we focussed on the investigation of the dianionic species using Models 1-3 (Table 7.3). While four of the monoanionic species are predicted to be able to initiate these reactions (**7.20**, **7.24**, **7.25** and **7.30**), their related dianionic derivatives were still considered in this work. As

discussed previously, Model 1 predicts that the dianionic amino acid derivatives **7.15** and **7.18** should be sufficiently able to promote the coupling of 4-iodoanisole **7.32** with benzene. Experimentally, when their respective precursor compounds **7.14** and **7.17** are used as the organic additive, poor reactivity is observed. From our perspective, this suggests a deficiency in the existing protocol to accurately model highly charged systems.

Table 7.3: Summary of the activation and relative free energies (ΔG) [kcal mol^{-1}] calculated for dianionic organic electron donors using Models 1, 2 and 3.

Organic Electron Donor	Model 1		Model 2		Model 3	
	ΔG^*	ΔG_{rel}	ΔG^*	ΔG_{rel}	ΔG^*	ΔG_{rel}
7.3	0.2	-64.5	33.0	22.9	15.2	-14.9
7.4	1.8	-39.1	43.9	42.3	25.9	1.3
7.7	0.2	-62.3	35.7	28.3	19.1	-8.8
7.8	1.8	-41.7	38.9	35.7	25.4	-1.5
7.11	0.6	-60.2	31.5	23.2	11.3	-14.0
7.12	2.7	-39.7	40.0	36.5	25.5	-4.9
7.15	0.7	-54.9	36.2	27.7	20.3	-8.0
7.18	1.9	-40.8	43.2	41.4	30.5	3.9
7.21	1.1	-53.6	31.6	18.5	15.0	-11.8
7.23	4.3	-41.0	53.7	50.7	31.7	4.8
7.26	0.1	-68.0	36.9	31.9	12.7	-13.7
7.27	5.6	-25.8	53.1	51.7	35.4	9.4
7.29	2.0	-41.6	40.6	37.6	24.2	-6.0
7.31	0.3	-71.8	27.7	18.8	3.0	-25.6

Using Model 2, a number of differences become more apparent when comparing the potential dianionic donors derived from amino acid additives. The dianions derived from C—H deprotonation of the carboxylate species (**7.3**, **7.7**, **7.11** and **7.15**) have predicted activation free energies between 3.0 – 10.0 kcal mol^{-1} lower than those formed upon N—H deprotonation (**7.4**, **7.8**, **7.12** and **7.18**). This offers further support for our early proposals for the relative effectiveness of these two subsets of amino acid derivatives, favouring those where an alkene moiety is formed between the electron-

rich heteroatoms. The calculated energetics using Model 3 for these candidates again highlight the stronger reducing ability of dianions derived from C—H deprotonation of the amino acid carboxylates. This model also predicts the reduction of 4-iodoanisole **7.32** by the amino acid-derived dianions to be exergonic in all but two cases (**7.4** and **7.18**). The DKP-derived dianion **7.21**, by Model 2, has an accessible barrier of 31.6 kcal mol^{-1} for the electron transfer reaction. This barrier decreases to 15.0 kcal mol^{-1} when calculated using Model 3 and, as was noted for most of the amino acid dianions, the electron transfer is exergonic when this model is used.

Comparison of the three dianions **7.23**, **7.26** and **7.27**, derived from cyclohexane-1,2-diol **7.22**, allows the effect of the alkene moiety to be probed. By Model 2, the lowest activation energy is obtained for **7.26** at 36.9 kcal mol^{-1}; however under the reaction conditions, it is unlikely that this would produce efficient reactivity. The alternative dianions, **7.23** and **7.27**, were predicted to have activation energies in excess of 57.0 kcal mol^{-1}, as well as less favourable relative free energies. Using Model 3, the respective activation free energies for **7.23**, **7.26** and **7.27** are calculated at 31.7, 12.7 and 35.4 kcal mol^{-1}, reaffirming the greater reducing ability of **7.26**. The comparable energetics for dianions **7.23** and **7.27** are a surprising result, which is believed to be a consequence of the C—C bond cleavage observed in **7.23** upon loss of an electron (Figure 7.8). This same bond cleavage is also observed in Models 1 and 2, but is not observed in the reactions of dianions **7.26** or **7.27**. The difference in barrier height of 23.3 kcal mol^{-1} for the electron transfer by **7.26** relative to **7.27** signifies the difference in reactivity arising from the position at which the enolate is formed.
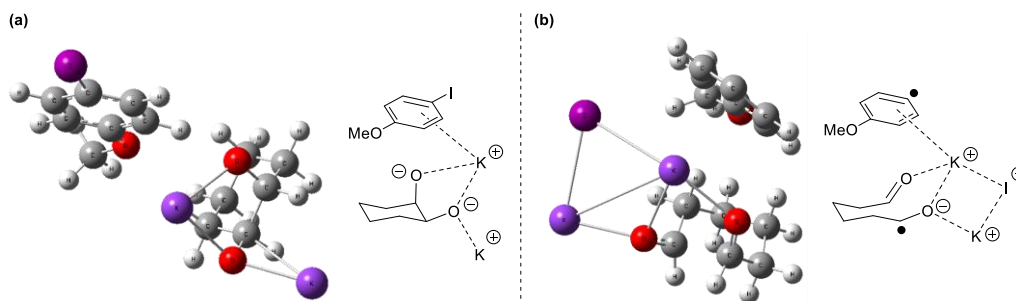
Figure 7.8: Optimised geometries of (a) the reactant complex and (b) the product complex for the reduction of 4-iodoanisole **7.32** by dianion **7.23**, illustrating the C—C bond cleavage observed upon electron transfer.

When diamines are used in place of diols, a significant increase in reducing strength is observed. The DMEDA-derived dianion **7.31** is predicted to have an activation free energy of 27.7 kcal mol^{-1} by Model 2, the lowest barrier observed across the structures investigated in this study. The related structure **7.29**, with no alkene moiety linking the heteroatoms, is predicted to be significantly less reducing, with an activation free energy of 40.7 kcal mol^{-1}. When Model 3 is used, the difference in barrier height between **7.29** and **7.31** is found to be 21.2 kcal mol^{-1}, with the activation free energy when using **7.31** being a mere 3.0 kcal mol^{-1}. As observed in Model 2, this species exhibits the lowest calculated activation energy of all the structures investigated. Comparing **7.31** with the related diol **7.26**, the difference in activation energy of 9.7 kcal mol^{-1} (Model 3) demonstrates the effect of changing the heteroatom on the strength of the electron donor.

7.5 Rationalising the Relative Effectiveness of Small Organic Molecules as Promoters of Transition Metal-Free Coupling Reactions

Upon comparison of the calculated energetics for the reduction of 4-iodoanisole **7.32** by the structurally-related amino acid dianions **7.7** and **7.15**, derived from amino acids **7.5** and **7.13** respectively, a difference of only 1.2 kcal mol^{-1} is noted between their respective activation free energies (Table 7.3). Experimentally, we recall that using their respective amino acid precursors as organic additives produced significantly different levels of reactivity (Scheme 7.2). Based on these observations, we believe that the predicted energetics for the electron transfer step cannot be considered exclusively when determining the effectiveness of a candidate organic electron donor. Rather, full consideration should be given to the entire initiation pathway, including the formation of the electron donor from its respective precursor.
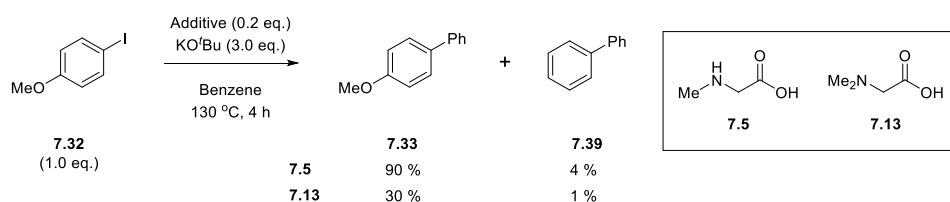
Scheme 7.2: Comparison of the relative effectiveness of amino acids **7.5** and **7.13** to promote the biaryl coupling reaction between 4-iodoanisole **7.32** and benzene.

Taking into consideration both the energetics for the formation of donors **7.7** and **7.15** from their respective carboxylates **7.6** and **7.14** (known to form exergonically from the neutral precursors), and the predicted energetics for the electron transfer to 4-iodoanisole **7.32**, pseudo potential energy surfaces can be obtained as shown in Figures 7.9 and 7.10.
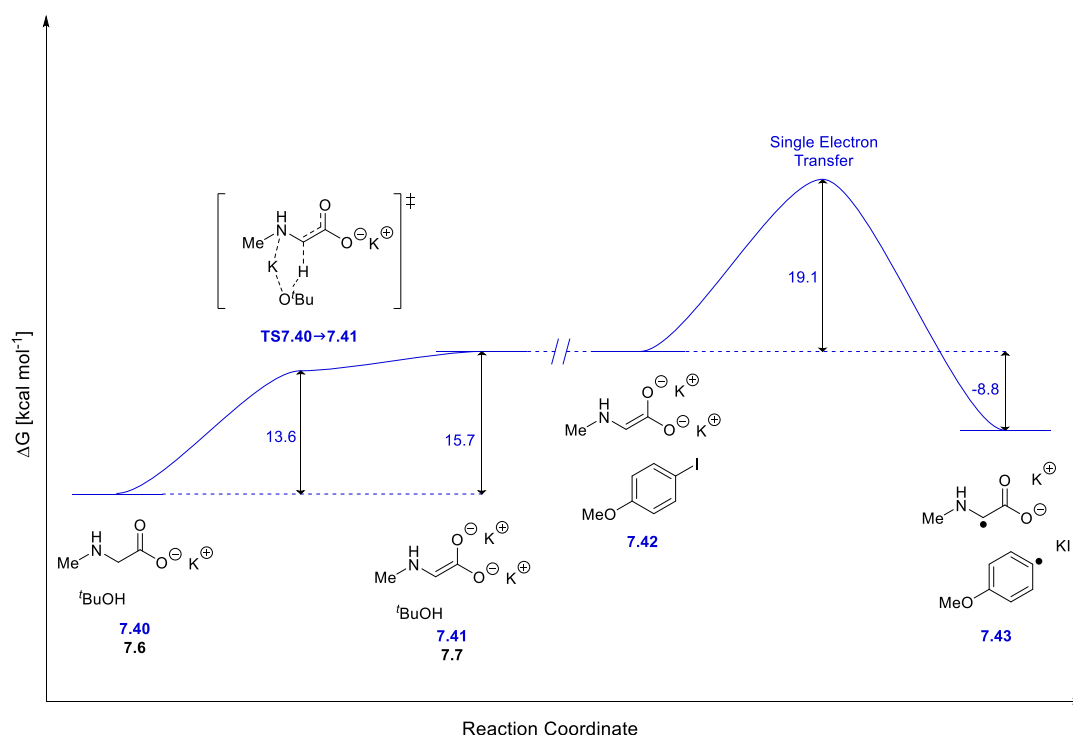
Figure 7.9: Gibbs free energy (ΔG) profile for the formation of the proposed organic electron donor **7.7** following deprotonation of **7.6** by potassium *tert*-butoxide, and subsequent electron transfer from this to 4-iodoanisole **7.32**. Structure numbers in blue correspond to the reaction complex modelled computationally, while structure numbers in black represent the separate species involved.

Due to the endergonic nature of the deprotonations affording **7.7** and **7.15**, the overall barrier height for the electron transfer can more accurately be considered as a combination of the barrier for donor formation and the barrier for electron transfer. For amino acid **7.5**, this produces an overall barrier to electron transfer of 34.8 kcal

mol^{-1} whereas for **7.15** this barrier is equal to 43.5 kcal mol^{-1}. This difference in barrier height of 8.7 kcal mol^{-1} would be sufficient to produce the experimentally-observed difference in reactivity.
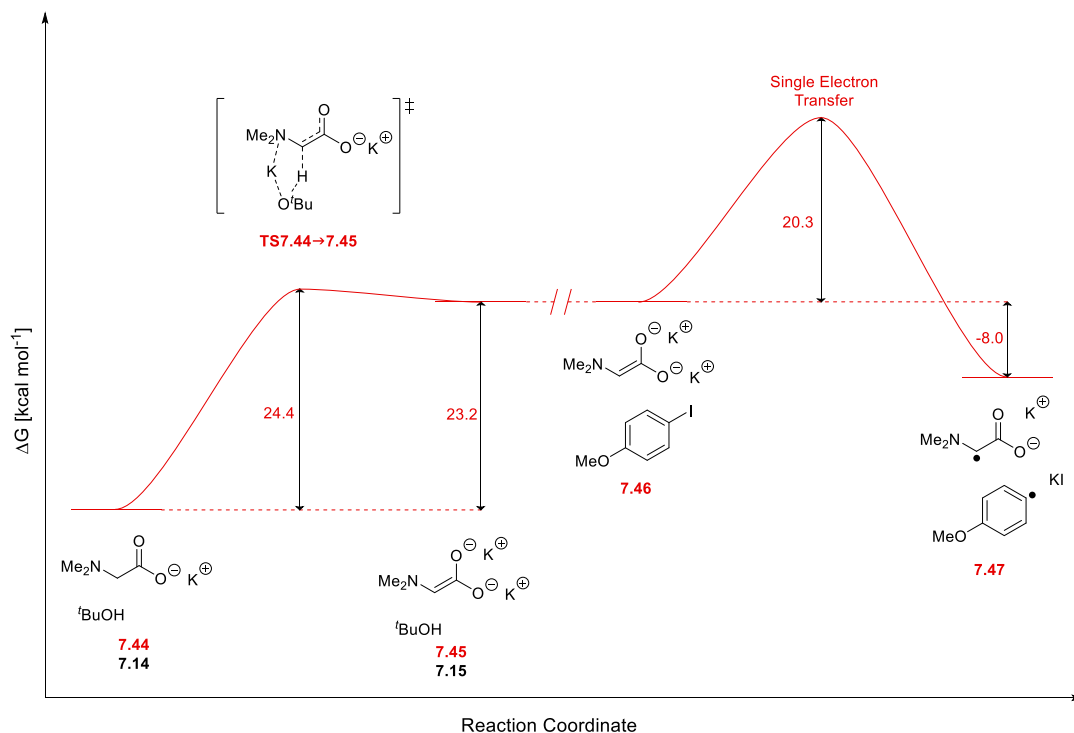
Figure 7.10: Gibbs free energy (ΔG) profile for the formation of the proposed organic electron donor **7.15** following deprotonation of **7.14** by potassium *tert*-butoxide, and subsequent electron transfer from this to 4-iodoanisole **7.32**. Structure numbers in red correspond to the reaction complex modelled computationally, while structure numbers in black represent the separate species involved.

Extending this principle to the remaining donor candidates, we can begin to paint a clearer picture of the relative effectiveness of their respective organic additives to promote transition metal-free coupling reactions. Beginning with the anionic candidate donors (Table 7.4), the amino acid carboxylates have already been ruled out based on the calculated energetics for the electron transfer reaction. The monoanionic candidate **7.20**, derived from **7.19**, has a predicted total barrier of 33.7 kcal mol^{-1} when considering both the formation and electron transfer steps. We predict this barrier to be accessible under the reaction conditions employed. Considering anions **7.24** and **7.25**, when the donor formation is taken into account, it is predicted that both species would be unable to promote this chemistry. Based on the electron transfer energetics alone, **7.24** would be expected to promote this chemistry while **7.25** would be

ineffective. For **7.30**, a similar observation is made in that the electron transfer energetics alone suggest that this species could act as an electron donor. Due to the endergonic nature of the formation of this from **7.28**, however, the predicted total barrier increases from 25.5 kcal mol^{-1} to 41.6 kcal mol^{-1}.

Table 7.4: Proposed total activation free energies (ΔG) [kcal mol^{-1}] for proposed anionic donors, based on the inclusion of the relative energy of formation.

Parent Additive	Organic Electron Donor	ΔG_{rel} for Donor Formation	Electron Transfer Energetics		Total Barrier for Electron Transfer
			ΔG^*	ΔG_{rel}	
7.1	7.2	-32.1	64.7	58.3	64.7
7.5	7.6	-32.1	64.9	58.8	64.9
7.9	7.10	-31.0	65.7	59.5	65.7
7.13	7.14	-32.0	65.1	58.9	65.1
7.16	7.17	-33.6	64.3	58.3	64.3
7.19	7.20	0.2	33.5	11.7	33.7
7.22	7.24	13.0	31.6	8.6	44.6
	7.25	8.2	43.3	21.7	51.5
7.28	7.30	16.1	25.5	2.9	41.6

For the dianionic electron donors (Table 7.5), a number of structures can be ruled out as candidates for the active species in these reactions. The total barriers for dianions formed upon N—H deprotonation of the amino acid carboxylate (**7.4**, **7.8**, **7.12** and **7.18**) are in excess of 48.0 kcal mol^{-1} and therefore energetically inaccessible. For the dianions formed from C—H deprotonation (**7.3**, **7.7**, **7.11** and **7.15**) these barriers are lower and, with the exception of **7.15**, are energetically accessible under standard reaction conditions. For **7.15**, the C—H deprotonation reaction is more energetically demanding relative to the formations of **7.3**, **7.7** and **7.11**, resulting in the ineffectiveness of **7.13** as an additive. Whilst anion **7.20** has been demonstrated computationally to be an effective electron donor, the related dianion **7.21** is also expected to have an accessible barrier for electron transfer, equal to 27.8 kcal mol^{-1} on inclusion of the formation energetics.

Table 7.5: Proposed total activation free energies (ΔG) [kcal mol^{-1}] for proposed dianionic donors, based on the inclusion of the relative energy of formation.

Parent Additive	Organic Electron Donor	ΔG$_{rel}$ for Donor Formation	Electron Transfer Energetics		Total Barrier for Electron Transfer
			ΔG*	*ΔG$_{rel}$*	
7.1	**7.3**	16.2	15.2	-14.9	31.4
	7.4	22.2	25.9	1.3	48.1
7.5	**7.7**	15.7	19.1	-8.8	34.8
	7.8	31.4	25.4	-1.5	56.8
7.9	**7.11**	15.4	11.3	-14.0	26.7
	7.12	29.1	25.5	-4.9	54.6
7.13	**7.15**	23.2	20.3	-8.0	43.5
7.16	**7.18**	31.5	30.5	3.9	62.0
7.19	**7.21**	12.8	15.0	-11.8	27.8
7.22	**7.23**[a]	-4.2	31.7	4.8	31.7
	7.26	4.1	12.7	-13.7	16.8
	7.27	-0.8	35.4	9.4	35.4
7.28	**7.29**	18.2	24.2	-6.0	42.4
	7.31	19.7	3.0	-25.6	22.7

[a] not taking this result as genuine, may exclude.

The total predicted barriers for the reduction of 4-iodoanisole by **7.26** and **7.27** support our initial proposal that **7.26** represents the more effective electron donor. The calculated total barrier of 16.8 kcal mol^{-1} for **7.26** is significantly lower than that calculated for **7.27** (35.4 kcal mol^{-1}), despite the fact that the formation of **7.27** is energetically favoured by 4.9 kcal mol^{-1}. Under the reaction conditions, **7.27** might still be capable of initiating the reaction, albeit at a lesser rate than **7.26**. For the structurally-related dianions **7.29** and **7.31**, a significant difference in reducing power has already been highlighted from their calculated electron transfer energetics alone. Although the formation of each species is similarly endergonic, their relative reductive abilities result in only **7.31** having an accessible total barrier of 22.7 kcal mol^{-1}.

8

Prediction of New Organic Super Electron Donors

8.1 Introduction

The computational framework developed in Chapter 7 allows for better rationalisation of the relative efficiencies of various organic additives to promote transition metal-free coupling reactions. It has been established that this is based on both the energetics involved in the formation of the active electron donor *in situ* and those associated with the subsequent reduction of the substrate by electron transfer. In progressing this research from a supportive to a predictive tool, two further goals are envisioned: the ability to design more powerful electron donors *in silico*, and the ability to do so at lower computational cost.

The computational design of novel electron donors has the potential to be a powerful tool in overcoming the current limitations of transition metal-free coupling chemistry. As has been discussed in Chapter 7, both the relative free energy of formation of the active species and the electron transfer energetics must be considered when determining the effectiveness of a candidate electron donor. From an experimental standpoint, the synthetic feasibility must also be considered; while a structure can be built through a computational interface, its synthesis and / or isolation may be experimentally impossible. Taking these factors into consideration, novel ligand design should meet the following requirements:

- The active donor must be sufficiently reactive to reduce the intended substrate

- The formation of the active donor from its respective precursor must be energetically feasible

- The precursor to the electron donor must be synthetically viable

The chapter begins with a computational study of the formation of novel organic electron donors from simple precursor molecules. The synthetic feasibility of these species is investigated and, following refinement, literature-precedented synthetic pathways are identified for the proposed synthesis of analogous species.

8.2 Computational Methods

DFT calculations were performed using the Gaussian 09 software package.[136] All reaction species were optimised using the M06-2X functional[115, 137] with a double-ζ basis set. With the exceptions of potassium and iodine, all elements were modelled using the aug-cc-pVDZ basis set.[147] Potassium was modelled using the 6-31++G(d,p) basis set.[148] For systems that included iodine, the small-core energy consistent relativistic pseudopotential was implemented.[149, 150] Implicit solvation of the reaction systems was modelled using the CPCM model with the associated parameters for benzene.[116, 117] Frequency calculations were performed on all optimised structures in order to characterise them as reaction minima (zero imaginary frequencies) or maxima (single imaginary frequency) and to obtain thermochemical data. All calculations were modelled at a temperature of 298 K. Throughout this chapter, unless stated otherwise, the reactant and product state for each transformation was taken to be the reaction complex rather than the separated reactant and product species. As an approximation to improve computational efficiency, potassium *tert*-butoxide has been modelled as a monomeric entity, despite being a tetrameric species.

8.3 Computational Design of Novel Organic Electron Donors

Work within our research group from 2005 has already demonstrated the ability to form powerful reducing agents from simple organic frameworks.[129] Integral to their chemical properties is the formation of an electron-rich alkene in the active species, and the ability to generate aromaticity upon the loss of two electrons. The present research has demonstrated the ability to generate powerful reducing agents from smaller, more readily available starting materials. These species are predicted to contain similarly electron-rich moieties in their active form. Typically, there are two or more heteroatoms, in neutral or anionic charge states, adjoined to this alkene which can enhance reducing power through resonance effects. In our attempt at designing new compounds similar in structure to those discussed throughout Chapters 5 and 6,

we propose the following five structures (Scheme 8.1, structures coloured blue) along with their respective neutral precursors (Scheme 8.1, structures coloured black).
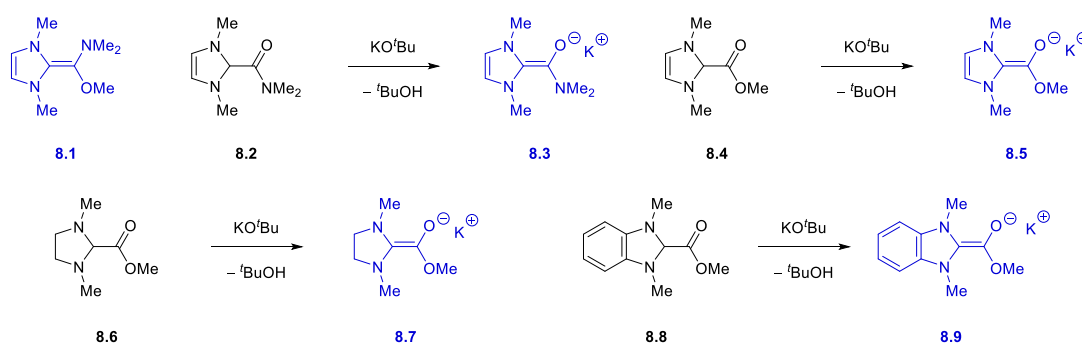
Scheme 8.1: Structures of the computationally designed organic electron donors (blue structures) and the associated precursor compounds for charged electron donors (black structures).

The first factor to be investigated with these donor candidates was the energetics for their formation (excluding **8.1**). The results in Table 8.1 illustrate the facile nature of all deprotonations investigated, with the highest barrier found to be 7.5 kcal mol^{-1} for the formation of **8.5**. This reaction also represents the least favourable transformation. However, it should be noted that with a relative free energy of 2.1 kcal mol^{-1}, this reaction is only mildly endergonic. The remaining three candidates **8.3**, **8.7** and **8.9** were found to form in an exergonic manner, with the formation of **8.9** (Figure 8.1) being most notable as it was exergonic by 12.4 kcal mol^{-1}.

Table 8.1: Calculated Gibbs free energies (ΔG) and electronic energies (ΔE) [kcal mol^{-1}] for the formation of the computationally-designed anionic organic electron donors **8.2**, **8.4**, **8.6** and **8.9** from their respective neutral precursors.

Parent Compound	Reaction Step	ΔG*	ΔG$_{rel}$	ΔE*	ΔE$_{rel}$
8.2	**8.2 → 8.3**	4.6	-2.3	7.0	-2.6
8.4	**8.4 → 8.5**	7.5	2.1	11.2	3.6
8.6	**8.6 → 8.7**	2.8	-4.8	5.7	-5.2
8.8	**8.8 → 8.9**	1.3	-12.3	2.4	-12.4
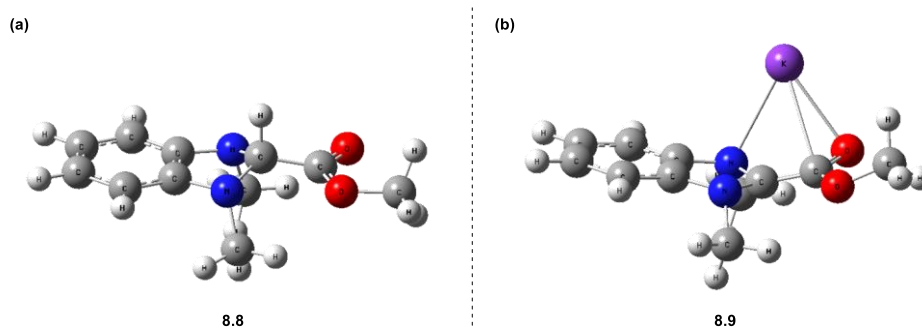
Figure 8.1: Optimised geometry of (a) the neutral precursor **8.8** and (b) the anionic electron donor **8.9**.

With the knowledge that these donors could be formed upon deprotonation of their respective precursors, our next objective was to predict the energetics for the electron transfer step. As with the investigations performed in Chapter 7, 4-iodoanisole **8.10** was chosen as the electron acceptor (Scheme 8.2a). For the neutral donor **8.1**, an activation free energy of 44.8 kcal mol^{-1} was predicted, making this donor weaker than the neutral donors previously designed within our group. The lowest predicted activation free energy was for donor **8.5** at 15.4 kcal mol^{-1}. This donor also gave rise to the most exergonic free energy profile with the product complex, following electron transfer, being 7.7 kcal mol^{-1} lower in energy than the reactant complex. Comparable to this was donor **8.3**, which had a slightly higher activation barrier of 17.1 kcal mol^{-1}. With the exception of donor **8.1**, the remaining donor candidates were found to have accessible activation free energies for the electron transfer reaction. With the incorporation of the preceding deprotonation step into the overall energetic requirement for reaction, the highest barrier was for the reduction of 4-iodoanisole **8.10** by **8.7** at 24.0 kcal mol^{-1} when considering only the charged electron donors.
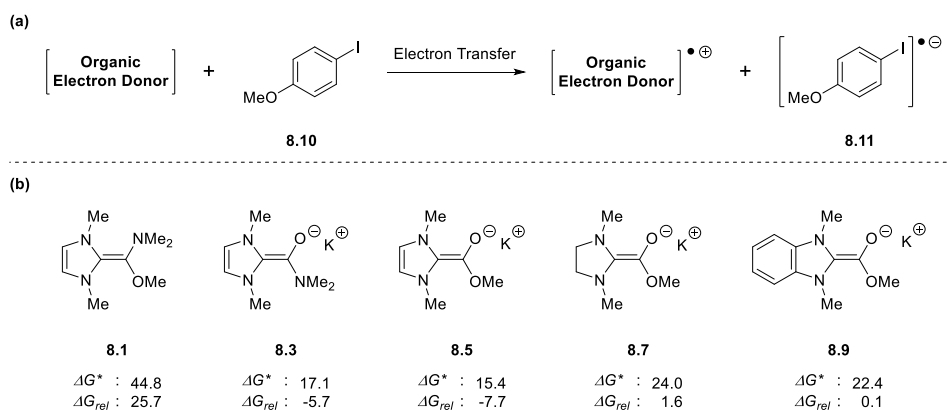
Scheme 8.2: (a) Summary of the electron transfer reaction being investigated in this work; (b) structure of the computationally designed electron donors investigated, with their associated reaction free energies (ΔG) [kcal mol^{-1}] obtained from the computational application of Marcus Theory (Model 3).

Table 8.3: Proposed total activation free energies (ΔG) [kcal mol^{-1}] for the computationally designed organic electron donors, based on the inclusion of the relative energy of formation.

Parent Additive	Organic Electron Donor	ΔG_{rel} for Donor Formation	Electron Transfer Energetics		Total Barrier for Electron Transfer
			ΔG^{*}	ΔG_{rel}	
8.1	8.1	--	44.8	25.7	44.8
8.2	8.3	-2.3	17.1	-5.7	17.1
8.4	8.5	2.1	15.4	-7.7	17.5
8.6	8.7	-4.8	24.0	1.6	24.0
8.8	8.9	-12.3	22.4	0.1	22.4

Having calculated the energetics associated with the donor formation and subsequent electron transfer, the only factor to be considered was the synthetic viability of the precursor compounds. In the current literature, there is no indication that any of the neutral precursors shown in Scheme 8.1 have been synthesised or characterised. Expanding the literature search to include structurally-related compounds identified two promising candidates in **8.12**[158] and **8.16**[159, 160] (Scheme 8.3). Retrosynthesis of these species allows for the possibility of generating a greater variety of structures through adaptation of the reaction conditions, starting from proline **8.15** (Scheme 8.3a) or cyclohexane-1,2-diamine **8.20** (Scheme 8.3b).

(a)
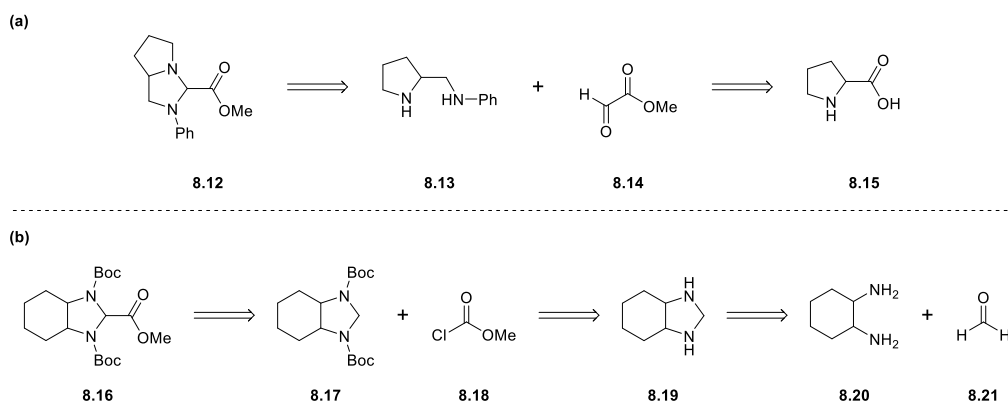
Scheme 8.3: Retrosynthetic analysis of (a) **8.12** and (b) **8.16**, identifying proline **8.15** and cyclohexane-1,2-diamine **8.20** as respective starting materials.

In 2007, Dunina *et al.* published a five-step synthesis affording diamine **8.13** using proline **8.15** as the starting material (Scheme 8.4a).[161] Following Boc-protection of **8.15**, **8.22** is reacted with ethyl chloroformate in the presence of *N*-methylmorpholine (NMM) to afford **8.23**, which is subsequently reacted with aniline to give the Boc-protected prolinanilide **8.24**. Boc-deprotection of **8.24** followed by reduction then affords the diamine **8.13**. Research by Warren and O'Brien has shown that diamine **8.13** can undergo reaction with methyl glyoxylate **8.14** to afford the target compound **8.12**.[158]
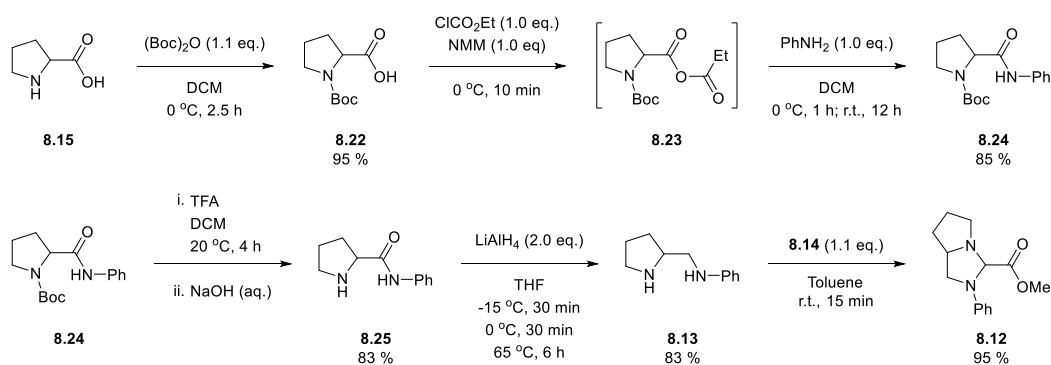
Scheme 8.4: Synthetic route towards diamine **8.13** and subsequent formation of the proposed donor precursor **8.12**.[158, 161]

Adaptations that could be made to these reaction conditions to give additional donor precursors include the use of alternative amines in place of aniline in the synthesis of **8.24**. This would give the general Boc-protected prolinamine **8.26**, and ultimately compounds of the general structure **8.27**. Alternatively, the final step in Scheme 8.4 could be replaced with a formylation of **8.13** followed by reaction with

dimethylcarbamyl chloride **8.30** in the presence of a suitable base to afford compounds of general structure **8.31**.
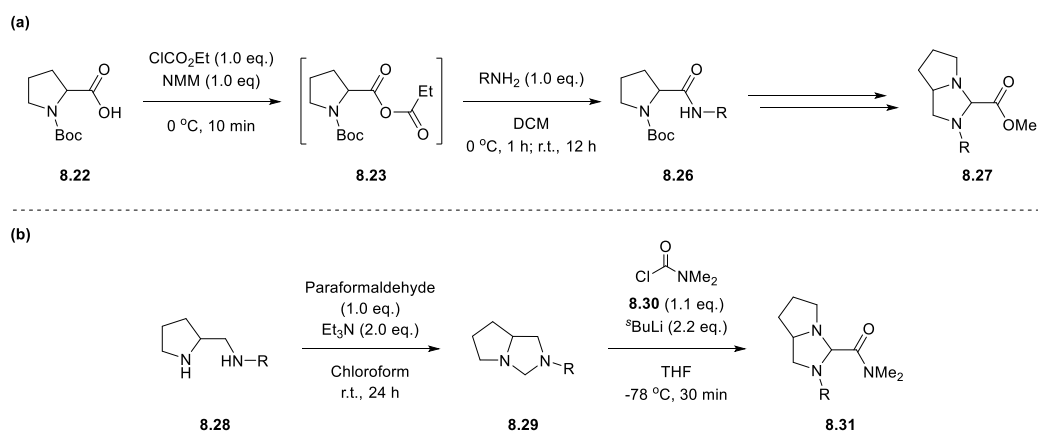
Scheme 8.5: Possible adaptations to the synthetic route proposed in Scheme 8.5, allowing for the synthesis of precursors of the general structure (a) **8.27** or (b) **8.31**.

The synthesis of both **8.16** and the precursor imidazolidine **8.17** was demonstrated by Coldham *et al.*,[159, 160] and based on the retrosynthesis outlined in Scheme 8.3b a number of synthetic pathways can be envisioned. Using cyclohexane-1,2-diamine **8.32** (Scheme 8.6a) or 1,2-phenylenediamine **8.36** (Scheme 8.6b) as the starting material, reaction with ethyl chloroformate[162] followed by reduction[163] could yield the *N,N'*-dimethylated diamines **8.34** or **8.38** respectively. Reaction of these with methyl glyoxylate **8.14** would then afford the respective donor precursor candidates **8.35** and **8.8**. Similar to the pathway described in Scheme 8.5b, diamines **8.34** and **8.38** could undergo reaction with paraformaldehyde to yield intermediates analogous to **8.29**, with subsequent reaction with dimethylcarbamyl chloride **8.30** yielding **8.39** or **8.40**. Furthermore, simply replacing the synthesised diamine **8.34** with DMEDA **8.41** presents a route towards the originally proposed precursor **8.6**.
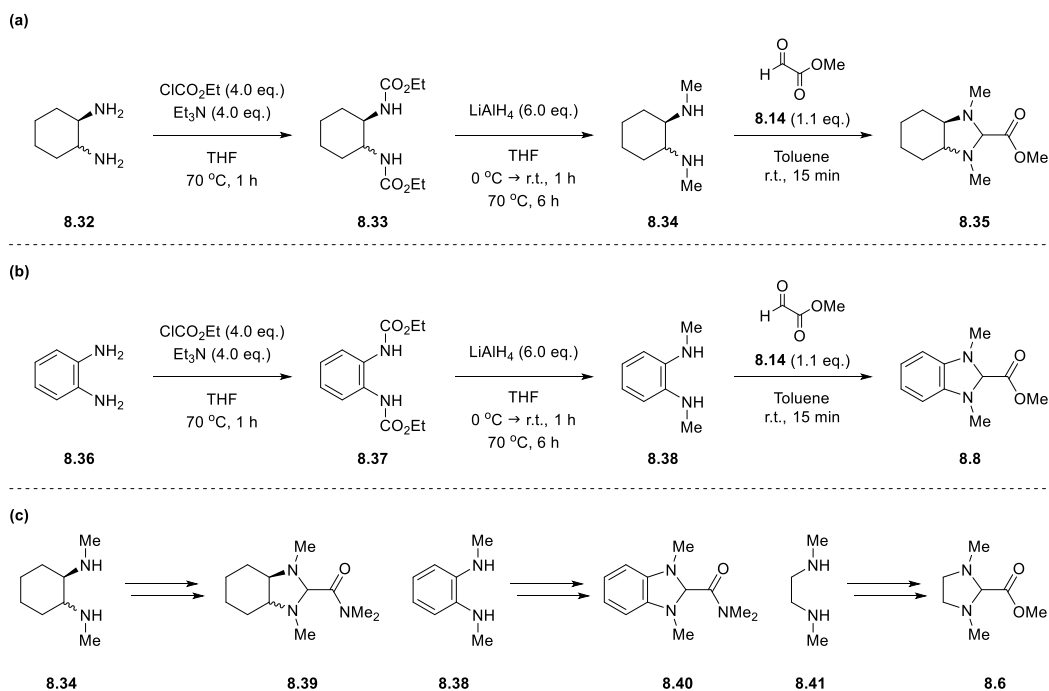
Scheme 8.6: Synthetic route towards the formation of (a) the donor precursor **8.35** from **8.32** and (b) the donor precursor **8.8** from **8.36**. (c) Possible adaptations allowing for the formation of electron donor precursors **8.39**, **8.40** and **8.6** from **8.34**, **8.38** and **8.41** respectively.

The synthesis of the computationally-designed donor precursors **8.1**, **8.2** and **8.4** appears to be challenging, while synthesis of **8.6** and **8.8** and the structurally similar precursor compounds **8.27**, **8.31**, **8.35**, and **8.39**-**8.41** seems to be achievable (Scheme 8.7). Importantly, these structures all contain a reactive pro-enolate core which, upon deprotonation, can afford donors analogous in structure to **8.7** and **8.9**. Although the additional desaturation such as that observed in **8.2** could not be incorporated into these compounds, predicted electron transfer activation free energies for **8.7** and **8.9** lower than 25.0 kcal mol^{-1} suggest that this should not hinder their ability to effectively promote the transition metal-free coupling chemistry.
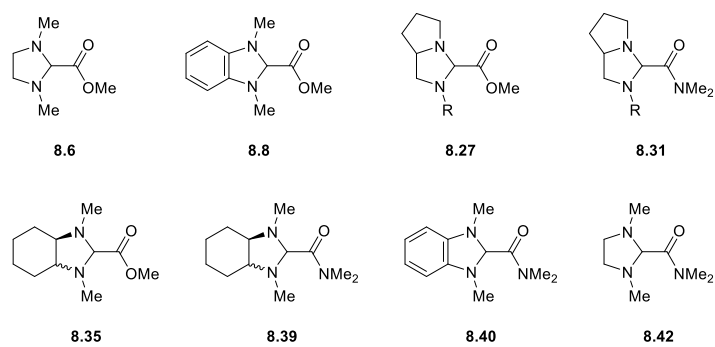
Scheme 8.7: Summary of the proposed electron donor precursors expected to be synthetically-feasible based on current literature precedent.

9 Conclusions and Future Work

The research conducted within this project has demonstrated the benefits of executing both experimental and theoretical studies in tandem in order to understand as yet unexplained chemical phenomena. This thesis began in Chapter 5 with the initial discovery of the ability to form organic super electron donors *in situ* upon reaction of simple organic molecules with the strong base potassium *tert*-butoxide. This discovery was made possible through the isolation of 2,3'-bisphenanthroline **5.48** experimentally, and the identification of the 2,2'- and 4,4'-bispyridines **5.72** and **5.73**. Computationally, the free energy profiles for the formation of all possible isomers of donors derived from 1,10-phenanthroline **5.44** and pyridine **5.71** were calculated. These results have shown that the formation of donors from **5.44** is energetically more favourable than from **5.71**, in good agreement with experiment.

Expanding on these initial findings, we sought to understand the underlying mechanism involved for other organic additives shown to promote transition metal-free coupling reactions. A number of possible reaction pathways were investigated computationally in Chapter 6 in order to elucidate the structure of the active electron donors derived from small organic molecules such as amino acids, diols and diamines. Early proposals for the amino acid mechanism led to the discovery that DKP's such as **6.14** were effective promoters of this chemistry. The inability to form DKP's from amino acids under our reaction conditions prompted a revision to our initial proposal, ultimately leading us to the idea that dianionic species such as **6.55** could represent the active electron donor in these reactions. We then applied the idea of forming electron-rich alkenes *in situ* upon reaction of amino acids with potassium *tert*-butoxide to diols and diamines. This resulted in our proposal that structures such as **6.71** and **6.104** could represent plausible candidates for the active species involved when diols and diamines respectively are used as organic additives.

The results presented in Chapter 6 prompted the question of whether the monoanionic donor candidates were strong enough electron donors to reduce an iodoarene, or if their dianionic counterparts were required in order to initiate the

BHAS cycle. This was the focus of Chapter 7, where Marcus theory was applied to investigate the free energy profiles for the electron transfer step. Initial results from this study using Model 1 provided no meaningful insight into the relative ability of candidate electron donors. This prompted the development of an alternative model, involving electron transfer complexes (Model 3), by which these reactions could be more accurately investigated computationally. Model 3 provided free energy profiles which were in stronger agreement with experimental observations, with the exception of **7.13**. It was noted in Chapter 6 that the relative energy for formation of **7.15** was significantly higher than for the formation of **7.7**, for example. Lending consideration to both the relative energy for donor formation and the predicted electron transfer energetics, we rationalised the likely ability of different electron donor candidates to initiate the BHAS cycle through reduction of 4-iodoanisole **7.32**.

At this stage in the project, computational investigation had solely been used in tandem with experiment. However, it became desirable to determine if the framework outlined in Chapter 7 could be used in a predictive manner. A number of simple electron donors and their respective precursor compounds were proposed, solely from a theoretical perspective, in the beginning of Chapter 8. The energetics for donor formation and electron transfer to 4-iodoanisole **8.10** were predicted for these structures, identifying the anionic donors **8.3**, **8.5**, **8.7** and **8.9** as effective reducing agents. From an experimental perspective, synthesis of the precursors **8.2** and **8.4** did not appear to be a feasible task. Pleasingly, synthetic routes to **8.6** and **8.8** were identified, as were routes to analogues of these compounds.

Granted the opportunity to continue this research, the synthesis of the precursor species through the routes detailed in Chapter 8 would represent a top priority. Should these compounds successfully promote the desired coupling chemistry, it would represent the ability of our computational model to accurately predict the reducing power of novel electron donors. In addition to this, the design of electron donors capable of reducing bromo- and chloroarenes to their respective aryl radicals would be of interest.

Due to the computational expense of calculating the electron transfer complexes involved in Model 3, it would be desirable to investigate the possibility of using computationally less expensive basis sets and pseudopotentials to accurately predict electron transfer energetics. This would allow for an improvement on the throughput of this model, making it more suitable for the screening of future donor candidates.

Associated with the vast scope of additives demonstrated to effect transition metal-free coupling chemistry is an equally vast range of reaction conditions, which are deemed optimal for certain systems. The two interesting factors in these reactions are the reaction temperature and the base employed, which tends to show the most variation. Experimental screening of the different additives under different reaction conditions, coupled with computational investigation of donor formations using different bases, might bring to light factors affecting this chemistry that have not yet been addressed explicitly.

10

Experimental Details

10.1 General Information

All reagents used were obtained from commercial supplies. Column chromatography was performed using Prolabo 35-70 μm particle size silica gel 60 (200-400 mesh). Reaction progress was determined using thin layer chromatography (TLC) using Merck silica gel 60 F_{254} pre-coated aluminium plates. Visualisation of TLC plates was achieved under a UVP mineralight UVG-11 lamp, followed by development using ethanolic vanillin or phosphomolybdic acid. Melting points were recorded using a Gallenkamp "Griffen Melting Point Apparatus". Microwave reactions were performed using a CEM Discover® SP instrument.

^{1}H-NMR spectra were obtained at 400.03 MHz and ^{13}C-NMR spectra were obtained at 100.59 MHz on a Bruker AV3 400 instrument using broadband decoupled mode. Spectra were recorded in deuterated chloroform ($CDCl_3$). Chemical shifts are recorded in parts per million (ppm) and coupling constants J are reported in Hertz (Hz). The following abbreviations are used to denote peak multiplicities: s, singlet; d, doublet; t, triplet; q, quartet; qu, quintet; sx, sextet; dd, doublet of doublets; dt, doublet of triplets; td, triplet of doublets; tt, triplet of triplets; m, multiplet; bs, broad singlet.

GC-MS data were recorded using an Agilent Technologies 7890A GC System coupled to a 5975C inert XL EI/CI MS detector. Separation was performed on a DB5MS-UI column (30 m x 0.25 mm x 0.25 μm) at a temperature of 320 °C with helium as the carrier gas. Positive Chemical Ionisation (PCI+) was used with methane as the ionisation gas and a voltage of 952.941 V.

High-resolution mass spectrometry (HRMS) was performed at the University of Wales, Swansea in the EPSRC National Mass Spectrometry Centre. Accurate mass was obtained using nanospray ionisation (NSI) or atmospheric pressure chemical ionisation (APCI) with a LTQ Orbitrap XL mass spectrometer. Low-resolution mass spectrometry was performed at the University of Strathclyde using electrospray ionisation (ESI) on a Finnigan LCQ duo ESI mass spectrometer.

10.2 Experimental Procedures Chapter 5

Synthesis of 2-(benzyloxy)iodobenzene **5.3**

In an oven-dried round-bottomed flask, 2-iodophenol **5.1** (1.0 eq., 4.0 g, 18.2 mmol) and potassium carbonate (8.0 eq., 20.1 g, 145.4 mmol) were dissolved in acetone (100 mL) and stirred prior to addition of benzyl bromide **5.2** (4.0 eq., 12.4 g, 72.7 mmol). The reaction mixture was stirred overnight under reflux at 75 ^{o}C. The cooled reaction mixture was filtered to remove potassium carbonate, and the organic phase was dried over anhydrous sodium sulfate before concentrating under vacuum. The crude product was purified by column chromatography on silica gel (100 % petroleum ether, increasing to 10 % ethyl acetate in petroleum ether) to elute the product 2-(benzyloxy)iodobenzene **5.3** as an orange oil (5.1 g, 16.3 mmol, 90 %). δ_H (400 MHz, CDCl$_3$): 5.19 (2H, s, -CH_2-), 6.76 (1H, td, J = 7.6, 1.3 Hz, ArH), 6.90 (1H, dd, J = 8.2, 1.2 Hz, ArH), 7.28-7.38 (2H, m, ArH), 7.42-7.46 (2H, m, ArH), 7.53-7.56 (2H, m, ArH), 7.84 (1H, dd, J = 7.8, 1.6 Hz, ArH). δ_C (100 MHz, CDCl$_3$): 70.4, 86.4, 112.3, 122.4, 126.5, 127.4, 128.1, 136.1, 139.1, 156.8. m/z (APCI): found 310.9926, C$_{13}$H$_{12}$OI$^+$ [M+H]$^+$ requires 310.9927.

Reaction of 2-(benzyloxy)iodobenzene **5.3** under microwave conditions

To a microwave reaction vial was added 2-(benzyloxy)iodobenzene **5.3** (1.0 eq., 0.15 g, 0.5 mmol), potassium *tert*-butoxide (2.0 eq., 0.12 g, 1.0 mmol) and pyridine (4 mL) under inert atmosphere. The reaction mixture was stirred for 1 min at room temperature prior to reaction at 160 ^{o}C under microwave irradiation for 10 min. The cooled reaction mixture was partitioned between ethyl acetate (25 mL) and 2 N HCl (25 mL) to remove residual pyridine. The aqueous phase was washed with two further portions of ethyl acetate (2 x 25 mL) and the combined organic phases were then washed with brine (30 mL), dried over anhydrous sodium sulfate and concentrated under vacuum. The crude product was purified by column chromatography on silica gel (10 % DCM in petroleum ether), affording an inseparable mixture of the products 6*H*-benzo[*c*]chromene **5.4** and (benzyloxy)benzene **5.5** as a yellow oil (66 mg). Analysis of

this mixture by ^{1}H NMR shows this to equate to 6*H*-benzo[*c*]chromene **5.4** (50.3 mg, 0.28 mmol, 56 %) and (benzyloxy)benzene **5.5** (15.7 mg, 0.09 mmol, 18 %). Representative signals due to 6*H*-benzo[*c*]chromene **5.4**: δ_H (400 MHz, CDCl$_3$): 5.18 (2H, s, -C*H*$_2$-). m/z (APCI): found 183.0803, C$_{13}$H$_{11}$O$^+$ [M+H]$^+$ requires 183.0804. Representative signals due to (benzyloxy)benzene **5.5**: δ_H (400 MHz, CDCl$_3$): 5.13 (2H, s, -C*H*$_2$-). m/z (APCI): found 185.0958, C$_{13}$H$_{13}$O$^+$ [M+H]$^+$ requires 185.0961.

Synthesis of 2-iodoresorcinol **5.40**

To an oven-dried round-bottomed flask, resorcinol **5.39** (1.0 eq., 3.3 g, 30 mmol) and iodine (1.1 eq., 8.16 g, 32 mmol) were added and dissolved in water (50 mL). Sodium hydrogen carbonate (1.1 eq., 2.82 g, 33.6 mmol) was added gradually before allowing the reaction mixture to stir at room temperature for 30 min. The reaction mixture was extracted into diethyl ether (3 x 50 mL), and the combined organics were dried over sodium sulfate before concentrating under vacuum. The crude product was purified by column chromatography on silica gel (50 % DCM in hexane, increasing to 75 % DCM in hexane). This afforded the product 2-iodoresorcinol **5.40** as an off-white solid (2.30 g, 9.72 mmol, 32 %). M.Pt. 90-92 ^{o}C (lit. 91 ^{o}C)[164] δ_H (400 MHz, CDCl$_3$): 5.36 (2H, s, -O*H*), 6.58 (2H, d, *J* = 8.1 Hz, Ar*H*), 7.13 (1H, t, *J* = 8.1 Hz, Ar*H*). δ_C (100 MHz, CDCl$_3$): 77.2, 106.9, 130.0, 155.2. m/z (APCI): found 236.9406, C$_6$H$_6$O$_2$I$^+$ [M+H]$^+$ requires 236.9407.

Synthesis of 2,6-bis(benzyloxy)iodobenzene **5.41**

To an oven-dried round-bottomed flask under argon, 2-iodoresorcinol **5.40** (1.0 eq., 0.6 g, 2.54 mmol) benzyl bromide **5.2** (3.0 eq., 0.9 mL, 7.62 mmol) and anhydrous potassium carbonate (3.0 eq., 1.1 g, 7.62 mmol) were added, dissolved in DMF (30 mL) and stirred overnight at 80 ^{o}C. The cooled reaction mixture was partitioned between water (30 mL) and ethyl acetate (30 mL), with the aqueous phase washed with two further portions of ethyl acetate (2 x 30 mL). The combined organics were washed with brine (50 mL), dried over anhydrous sodium sulfate and concentrated under vacuum.

The crude product was purified by column chromatography on silica gel (20 % ethyl acetate in petroleum ether), affording the product 2,6-bis(benzyloxy)iodobenzene **5.40** as a white solid (0.97 g, 2.32 mmol, 91 %). M.Pt. 88-90 ^{o}C (lit. 90-92 ^{o}C)[165] δ_H (400 MHz, CDCl$_3$): 5.20 (4H, s, -CH_2-), 6.58 (2H, d, J = 8.3 Hz, ArH), 7.23 (1H, t, J = 8.2 Hz, ArH), 7.35-7.39 (2H, m, ArH), 7.45 (4H, td, J = 7.2, 1.7 Hz, ArH), 7.58 (4H, d, J = 7.4 Hz, ArH). δ_C (100 MHz, CDCl$_3$): 70.5, 79.0, 105.6, 126.5, 127.4, 128.1, 129.3, 136.3, 158.3. m/z (APCI): found 417.0344, C$_{20}$H$_{18}$O$_2$I$^+$ [M+H]$^+$ requires 417.0346.

Reaction of 2,6-bis(benzyloxy)iodobenzene **5.40** under microwave conditions

To a microwave reaction vial was added 2,6-bis(benzyloxy)iodobenzene **5.40** (1.0 eq., 0.21 g, 0.5 mmol), potassium *tert*-butoxide (2.0 eq., 0.12 g, 1.0 mmol) and pyridine (4 mL) under inert atmosphere. The reaction mixture was stirred for 1 min at room temperature prior to reaction at 160 ^{o}C under microwave irradiation for 10 min. The cooled reaction mixture was partitioned between ethyl acetate (25 mL) and 2 N HCl (25 mL) to remove residual pyridine. The aqueous phase was washed with two further portions of ethyl acetate (2 x 25 mL) and the combined organic phases were then washed with brine (30 mL), dried over anhydrous sodium sulfate and concentrated under vacuum. The crude product was purified by column chromatography on silica gel (10 % DCM in petroleum ether), affording an inseparable mixture of the products 1-(benzyloxy)-6H-benzo[c]chromene **5.41** and 2,6-bis(benzyloxy)benzene **5.42** as a yellow oil (34 mg). Analysis of this mixture by ^{1}H NMR shows this to equate to 1-(benzyloxy)-6H-benzo[c]chromene **5.41** (12.7 mg, 0.04 mmol, 9 %) and 2,6-bis(benzyloxy)benzene **5.42** (21.3 mg, 0.07 mmol, 15 %).

Representative signals due to 1-(benzyloxy)-6H-benzo[c]chromene **5.41**: δ_H (400 MHz, CDCl$_3$): 5.06 (2H, s, -CH_2-), 5.25 (2H, s, -CH_2-), 6.76 (2H, d, J = 8.1 Hz, ArH). m/z (APCI): found 289.1218, C$_{20}$H$_{17}$O$_2$$^+$ [M+H]$^+$ requires 289.1223.

Representative signals due to 2,6-bis(benzyloxy)benzene **5.42**: δ_H (400 MHz, CDCl$_3$): 5.09 (2H, s, -CH_2-), 6.66 (2H, dd, J = 8.2, 2.4 Hz, ArH), 6.70 (1H, t, J = 2.3 Hz, ArH). m/z (APCI): found 291.1374, C$_{20}$H$_{19}$O$^+$ [M+H]$^+$ requires 291.1380.

10.3 Experimental Procedures Chapter 6

<u>Synthesis of 2-chloro-*N*-propylacetamide **6.13**</u>

To an oven-dried round-bottomed flask, DCM (40 mL) was added and cooled to 0 $^{\circ}$C in an ice bath. To this, chloroacetyl chloride **6.12** (1.0 eq., 5.65 g, 50 mmol) and propylamine (2.1 eq., 8.64 mL, 105 mmol) were added alternately in small portions (vigorous reaction). Upon complete addition of both reagents, the reaction mixture was allowed to react for 15 min at 0 $^{\circ}$C. The reaction mixture was diluted with diethyl ether (30 mL) and filtered to remove any solids. The solids were rinsed with a further portion of diethyl ether (30 mL) and the combined organics were concentrated under vacuum. The product 2-chloro-*N*-propylacetamide **6.13** was obtained as a pale yellow liquid, was used without further purification (6.1 g, 44.9 mmol, 90 %). δ_H (400 MHz, CDCl$_3$): 0.95 (3H, t, *J* = 7.4 Hz, -C*H*$_3$), 1.58 (2H, sx, *J* = 7.4 Hz, -C*H*$_2$-), 3.27 (2H, q, *J* = 6.76 Hz, -NC*H*$_2$-), 4.05 (2H, s, -C*H*$_2$-), 6.64 (1H, bs, -N*H*C(O)-). δ_C (100 MHz, CDCl$_3$): 10.8, 22.1, 41.0, 42.2, 165.3.

<u>Synthesis of *N,N'*-dipropyl-2,5-diketopiperazine **6.14**</u>

Sodium hydride (1.3 eq., 1.15 g, 47.9 mmol) was added to an oven-dried three-necked flask and washed with two portions of anhydrous hexane (2 x 40 mL) under argon. The washed sodium hydride was then suspended in anhydrous THF (40 mL), to which a solution of 2-chloro-*N*-propylacetamide **6.13** in THF (20 mL) was added dropwise at room temperature. The reaction mixture was allowed to stir overnight. The reaction was quenched by slow addition of water (10 mL), and the reaction mixture was partitioned between water (50 mL) and diethyl ether (50 mL). The aqueous phase was washed with further portions of diethyl ether (2 x 50 mL) and the combined organics were dried over anhydrous sodium sulfate before concentrating under vacuum. The crude product was purified by column chromatography on silica gel (50 % ethyl acetate in petroleum ether, increasing to 100 % ethyl acetate), affording the product *N,N'*-dipropyl-2,5-diketopiperazine **6.14** as a white solid (2.18 g, 11.0 mmol, 60 %). M.Pt. 40-42 $^{\circ}$C δ_H (400 MHz, CDCl$_3$): 0.92 (6H, t, *J* = 5.9 Hz, -C*H*$_3$), 1.58 (4H, sx, *J* = 6.0 Hz, -C*H*$_2$-),

3.35 (4H, t, J = 6.0 Hz, -NCH_2-), 3.95 (4H, s, -CH_2-). δ_C (400 MHz, CDCl$_3$): 10.6, 19.4, 47.0, 49.4, 163.0. m/z (ESI): found 199.1, C$_{10}$H$_{19}$N$_2$O$_2^+$ [M+H]$^+$ requires 199.14.

<u>General procedure for the coupling of 4-iodoanisole **6.1** with benzene</u>

To an oven-dried high pressure reaction vessel, 4-iodoanisole (1.0 eq., 0.234 g, 1.0 mmol) and the organic additive (0.2 eq., 0.2 mmol) were added. This was taken into the glovebox where, under inert atmosphere, potassium *tert*-butoxide (3.0 eq., 0.337 g, 3.0 mmol) and anhydrous benzene (6 mL) were added. The reaction vessel was sealed and transferred to a fume hood where the reaction mixture was heated to 130 ^{o}C in an oil bath and stirred for 6 h. The cooled reaction mixture was partitioned between water (30 mL) and a 1:1 mixture of diethyl ether and hexane (30 mL). The aqueous phase was washed with a further portion of the organic solvent mixture (30 mL) and the combined organics were washed with brine, dried over anhydrous sodium sulfate and concentrated under vacuum. The crude product was purified by column chromatography on silica gel (100 % hexane).

Representative signals due to 4-methoxybiphenyl **6.2**: δ_H (400 MHz, CDCl$_3$): 3.94 (3H, s, -OCH_3), 7.11 (2H, dt, J = 9.7, 3.0 Hz, ArH), 7.44 (1H, tt, J = 6.8, 1.2 Hz, ArH), 7.53-7.56 (2H, m, ArH), 7.66-7.71 (4H, m, ArH). δ_C (100 MHz, CDCl$_3$): 54.8, 113.8, 126.1, 126.2, 127.7, 128.2, 133.4, 140.4, 158.8.

Representative signals due to biphenyl **6.15**: δ_H (400 MHz, CDCl$_3$): 7.37 (2H, tt, J = 7.4, 13 Hz, ArH), 7.47 (4H, m, ArH), 7.62 (4H, m, ArH). δ_C (100 MHz, CDCl$_3$): 126.6, 126.7, 128.2, 140.8.

Representative signals due to *meta*-(*tert*-butoxy)anisole **6.16**: δ_H (400 MHz, CDCl$_3$): 1.43 (9H, s, -CH_3), 3.83 (3H, s, -OCH_3), 6.63 (1H, t, J = 2.0 Hz, ArH), 6.69 (2H, m, ArH), 7.22 (1H, t, J = 8.0 Hz, ArH).

Representative signals due to *para*-(*tert*-butoxy)anisole **6.17**: δ_H (400 MHz, CDCl$_3$): 1.37 (9H, s, -CH_3), 3.82 (3H, s, -OCH_3), 6.86 (2H, dd, J = 6.8, 2.4 Hz, ArH), 6.99 (2H, dd, J = 6.8, 2.4 Hz, ArH).

11 References

1.   S. Yanagisawa, K. Ueda, T. Taniguchi and K. Itami, *Org. Lett.*, 2008, **10**, 4673-4676.

2.   A. Studer and D. P. Curran, *Angew. Chem. Int. Ed.*, 2011, **50**, 5018-5022.

3.   T. Mizoroki, K. Mori and A. Ozaki, *Bull. Chem. Soc. Jpn.*, 1971, **44**, 581-581.

4.   R. F. Heck and J. P. Nolley, *J. Org. Chem.*, 1972, **37**, 2320-2322.

5.   N. Miyaura and A. Suzuki, *J. Chem. Soc., Chem. Commun.*, 1979, 866-867.

6.   A. F. Littke, C. Dai and G. C. Fu, *J. Am. Chem. Soc.*, 2000, **122**, 4020-4028.

7.   Y. Takeda, Y. Ikeda, A. Kuroda, S. Tanaka and S. Minakata, *J. Am. Chem. Soc.*, 2014, **136**, 8544-8547.

8.   http://www.nobelprize.org/nobel_prizes/chemistry/laureates/2010/, (accessed 06, 2016).

9.   N. E. Leadbeater and M. Marco, *Angew. Chem. Int. Ed.*, 2003, **42**, 1407-1409.

10.   N. E. Leadbeater and M. Marco, *Org. Lett.*, 2002, **4**, 2973-2976.

11.   N. E. Leadbeater and M. Marco, *J. Org. Chem.*, 2003, **68**, 5660-5667.

12.   R. K. Arvela, N. E. Leadbeater, M. S. Sangi, V. A. Williams, P. Granados and R. D. Singer, *J. Org. Chem.*, 2005, **70**, 161-168.

13.   A. H. M. de Vries, J. M. C. A. Mulders, J. H. M. Mommers, H. J. W. Henderickx and J. G. de Vries, *Org. Lett.*, 2003, **5**, 3285-3288.

14.   A. H. M. de Vries, F. J. Parlevliet, L. Schmieder-van de Vondervoort, J. H. M. Mommers, H. J. W. Henderickx, M. A. M. Walet and J. G. de Vries, *Adv. Synth. Catal.*, 2002, **344**, 996-1002.

15.   G. B. Bajracharya and O. Daugulis, *Org. Lett.*, 2008, **10**, 4625-4628.

16.   T. Truong and O. Daugulis, *J. Am. Chem. Soc.*, 2011, **133**, 4243-4245.

17.   T. Truong and O. Daugulis, *Org. Lett.*, 2012, **14**, 5964-5967.

18.   J. I. G. Cadogan and P. G. Hibbert, *Proc. Chem. Soc.*, 1964, 338-339.

19.   D. J. Cram and A. C. Day, *J. Org. Chem.*, 1966, **31**, 1227-1232.

20.   Z. Liu and R. C. Larock, *J. Org. Chem.*, 2006, **71**, 3198-3209.

21.   M. Jeganmohan and C.-H. Cheng, *Chem. Commun.*, 2006, 2454-2456.

22.   A. V. Dubrovskiy and R. C. Larock, *Org. Lett.*, 2010, **12**, 3117-3119.

23. T. Pirali, F. Zhang, A. H. Miller, J. L. Head, D. McAusland and M. F. Greaney, *Angew. Chem. Int. Ed.*, 2012, **51**, 1006-1009.

24. S. S. Bhojgude, A. Bhunia, R. G. Gonnade and A. T. Biju, *Org. Lett.*, 2014, **16**, 676-679.

25. S. S. Bhojgude, T. Kaicharla and A. T. Biju, *Org. Lett.*, 2013, **15**, 5452-5455.

26. F.-L. Liu, J.-R. Chen, Y.-Q. Zou, Q. Wei and W.-J. Xiao, *Org. Lett.*, 2014, **16**, 3768-3771.

27. V. G. Pandya and S. B. Mhaske, *Org. Lett.*, 2014, **16**, 3836-3839.

28. S. K. Aithagani, S. Dara, G. Munagala, H. Aruri, M. Yadav, S. Sharma, R. A. Vishwakarma and P. P. Singh, *Org. Lett.*, 2015, **17**, 5547-5549.

29. C. E. Hendrick and Q. Wang, *J. Org. Chem.*, 2015, **80**, 1059-1069.

30. A. F. C. Rossini, A. C. A. Muraca, G. A. Casagrande and C. Raminelli, *J. Org. Chem.*, 2015, **80**, 10033-10040.

31. Y. Himeshima, T. Sonoda and H. Kobayashi, *Chem. Lett.*, 1983, **12**, 1211-1214.

32. S. M. Bronner and N. K. Garg, *J. Org. Chem.*, 2009, **74**, 8842-8843.

33. T. Truong, M. Mesgar, K. K. A. Le and O. Daugulis, *J. Am. Chem. Soc.*, 2014, **136**, 8568-8576.

34. S. Yang, C. Wu, M. Ruan, Y. Yang, Y. Zhao, J. Niu, W. Yang and J. Xu, *Tetrahedron Lett.*, 2012, **53**, 4288-4292.

35. Z. Liu and R. C. Larock, *Org. Lett.*, 2004, **6**, 99-102.

36. Z. Liu and R. C. Larock, *Org. Lett.*, 2003, **5**, 4673-4675.

37. A. Studer and M. Bossart, in *Radicals in Organic Synthesis*, Wiley-VCH Verlag GmbH, 2008, pp. 62-80.

38. J. F. Bunnett, *Acc. Chem. Res.*, 1978, **11**, 413-420.

39. E. Shirakawa, K.-i. Itoh, T. Higashino and T. Hayashi, *J. Am. Chem. Soc.*, 2010, **132**, 15537-15539.

40. C.-L. Sun, H. Li, D.-G. Yu, M. Yu, X. Zhou, X.-Y. Lu, K. Huang, S.-F. Zheng, B.-J. Li and Z.-J. Shi, *Nature Chem.*, 2010, **2**, 1044-1049.

41. W. Liu, H. Cao, H. Zhang, H. Zhang, K. H. Chung, C. He, H. Wang, F. Y. Kwong and A. Lei, *J. Am. Chem. Soc.*, 2010, **132**, 16737-16740.

42. Y. Qiu, Y. Liu, K. Yang, W. Hong, Z. Li, Z. Wang, Z. Yao and S. Jiang, *Org. Lett.*, 2011, **13**, 3556-3559.

43.   S. Sharma, M. Kumar, V. Kumar and N. Kumar, *Tetrahedron Lett.*, 2013, **54**, 4868-4871.

44.   Y. Wu, P. Y. Choy and F. Y. Kwong, *Org. Biomol. Chem.*, 2014, **12**, 6820-6823.

45.   W.-C. Chen, Y.-C. Hsu, W.-C. Shih, C.-Y. Lee, W.-H. Chuang, Y.-F. Tsai, P. P.-Y. Chen and T.-G. Ong, *Chem. Commun.*, 2012, **48**, 6702-6704.

46.   Y. Wu, S. M. Wong, F. Mao, T. L. Chan and F. Y. Kwong, *Org. Lett.*, 2012, **14**, 5306-5309.

47.   K. Tanimoro, M. Ueno, K. Takeda, M. Kirihata and S. Tanimori, *J. Org. Chem.*, 2012, **77**, 7844-7849.

48.   I. Thomé and C. Bolm, *Org. Lett.*, 2012, **14**, 1892-1895.

49.   I. Thomé, C. Besson, T. Kleine and C. Bolm, *Angew. Chem. Int. Ed.*, 2013, **52**, 7509-7513.

50.   Y. S. Ng, C. S. Chan and K. S. Chan, *Tetrahedron Lett.*, 2012, **53**, 3911-3914.

51.   D. S. Roman, Y. Takahashi and A. B. Charette, *Org. Lett.*, 2011, **13**, 3242-3245.

52.   J. E. Baldwin, *J. Chem. Soc., Chem. Commun.*, 1976, 734-736.

53.   L. Benati, G. Calestani, R. Leardini, M. Minozzi, D. Nanni, P. Spagnolo, S. Strazzari and G. Zanardi, *J. Org. Chem.*, 2003, **68**, 3454-3464.

54.   W.-t. Wei, X.-j. Dong, S.-z. Nie, Y.-y. Chen, X.-j. Zhang and M. Yan, *Org. Lett.*, 2013, **15**, 6018-6021.

55.   W.-j. Wang, X. Zhao, L. Tong, J.-h. Chen, X.-j. Zhang and M. Yan, *J. Org. Chem.*, 2014, **79**, 8557-8565.

56.   M. Pichette Drapeau, I. Fabre, L. Grimaud, I. Ciofini, T. Ollevier and M. Taillefer, *Angew. Chem. Int. Ed.*, 2015, **54**, 10587-10591.

57.   A. Studer and D. P. Curran, *Nature Chem.*, 2014, **6**, 765-773.

58.   E. Shirakawa, X. Zhang and T. Hayashi, *Angew. Chem. Int. Ed.*, 2011, **50**, 4671-4674.

59.   S. Wertz, D. Leifert and A. Studer, *Org. Lett.*, 2013, **15**, 928-931.

60.   H. Zhang, R. Shi, A. Ding, L. Lu, B. Chen and A. Lei, *Angew. Chem. Int. Ed.*, 2012, **51**, 12542-12545.

61.   C. K. Prier, D. A. Rankic and D. W. C. MacMillan, *Chem. Rev.*, 2013, **113**, 5322-5363.

62.   H. Cano-Yelo and A. Deronzier, *J. Chem. Soc. Perkin Trans. 2*, 1984, 1093-1098.

63.   H. Kim and C. Lee, *Angew. Chem. Int. Ed.*, 2012, **51**, 12303-12306.

64.   M. Neumann, S. Füldner, B. König and K. Zeitler, *Angew. Chem. Int. Ed.*, 2011, **50**, 951-954.

65.   D. P. Hari and B. König, *Org. Lett.*, 2011, **13**, 3852-3855.

66.   D. P. Hari, T. Hering and B. König, *Org. Lett.*, 2012, **14**, 5334-5337.

67.   D. P. Hari, P. Schroll and B. König, *J. Am. Chem. Soc.*, 2012, **134**, 2958-2961.

68.   I. Ghosh, T. Ghosh, J. I. Bardagi and B. König, *Science*, 2014, **346**, 725-728.

69.   S. Fukuzumi, H. Kotani, K. Ohkubo, S. Ogo, N. V. Tkachenko and H. Lemmetyinen, *J. Am. Chem. Soc.*, 2004, **126**, 1600-1601.

70.   H. Kotani, K. Ohkubo and S. Fukuzumi, *J. Am. Chem. Soc.*, 2004, **126**, 15999-16006.

71.   K. Ohkubo, K. Mizushima, R. Iwata, K. Souma, N. Suzuki and S. Fukuzumi, *Chem. Commun.*, 2010, **46**, 601-603.

72.   D. J. Wilger, N. J. Gesmundo and D. A. Nicewicz, *Chem. Sci.*, 2013, **4**, 3160-3165.

73.   S. Fukuzumi and K. Ohkubo, *Org. Biomol. Chem.*, 2014, **12**, 6059-6071.

74.   D. A. Nicewicz and D. W. C. MacMillan, *Science*, 2008, **322**, 77-80.

75.   D. S. Hamilton and D. A. Nicewicz, *J. Am. Chem. Soc.*, 2012, **134**, 18577-18580.

76.   W. J. Kerr, M. Reid and T. Tuttle, *ACS Catal.*, 2015, **5**, 402-410.

77.   P. W. J. M. Frederix, G. G. Scott, Y. M. Abul-Haija, D. Kalafatovic, C. G. Pappas, N. Javid, N. T. Hunt, R. V. Ulijn and T. Tuttle, *Nature Chem.*, 2015, **7**, 30-37.

78.   C. Orofino-Pena, D. Cortizo-Lacalle, J. Cameron, M. T. Sajjad, P. P. Manousiadis, N. J. Findlay, A. L. Kanibolotsky, D. Amarasinghe, P. J. Skabara, T. Tuttle, G. A. Turnbull and I. D. W. Samuel, *Beilstein J. Org. Chem.*, 2014, **10**, 2704-2714.

79.   C. A. Lipinski, F. Lombardo, B. W. Dominy and P. J. Feeney, *Adv. Drug Delivery Rev.*, 2012, **64**, 4-17.

80.   R. Lonsdale, K. T. Houghton, J. Żurek, C. M. Bathelt, N. Foloppe, M. J. de Groot, J. N. Harvey and A. J. Mulholland, *J. Am. Chem. Soc.*, 2013, **135**, 8001-8015.

81.   P. Rydberg, R. Lonsdale, J. N. Harvey, A. J. Mulholland and L. Olsen, *J. Mol. Graphics Modell.*, 2014, **52**, 30-35.

82.   K. J. Bonney and F. Schoenebeck, *Chem. Soc. Rev.*, 2014, **43**, 6609-6638.

83.   A. S. K. Tsang, I. A. Sanhueza and F. Schoenebeck, *Chem. Eur. J.*, 2014, **20**, 16432-16441.

84.   C. Allemann, R. Gordillo, F. R. Clemente, P. H.-Y. Cheong and K. N. Houk, *Acc. Chem. Res.*, 2004, **37**, 558-569.

85.   C. L. McMullin, B. Rühle, M. Besora, A. G. Orpen, J. N. Harvey and N. Fey, *J. Mol. Catal. A: Chem.*, 2010, **324**, 48-55.

86.   C. L. McMullin, N. Fey and J. N. Harvey, *Dalton Trans.*, 2014, **43**, 13545-13556.

87.   J. P. Reid, L. Simón and J. M. Goodman, *Acc. Chem. Res.*, 2016.

88.   Q. Peng and R. S. Paton, *Acc. Chem. Res.*, 2016.

89.   R. Robiette, J. Richardson, V. K. Aggarwal and J. N. Harvey, *J. Am. Chem. Soc.*, 2006, **128**, 2394-2409.

90.   M. J. Hesse, S. Essafi, C. G. Watson, J. N. Harvey, D. Hirst, C. L. Willis and V. K. Aggarwal, *Angew. Chem. Int. Ed.*, 2014, **53**, 6145-6149.

91.   T. Sperger, I. A. Sanhueza and F. Schoenebeck, *Acc. Chem. Res.*, 2016.

92.   I. Ibrahem, P. Hammar, J. Vesely, R. Rios, L. Eriksson and A. Córdova, *Adv. Synth. Catal.*, 2008, **350**, 1875-1884.

93.   G. K. Datta, H. von Schenck, A. Hallberg and M. Larhed, *J. Org. Chem.*, 2006, **71**, 3896-3903.

94.   J.-L. Zhu, Y. Zhang, C. Liu, A.-M. Zheng and W. Wang, *J. Org. Chem.*, 2012, **77**, 9813-9825.

95.   Y. Zhang, Y.-L. Shao, H.-S. Xu and W. Wang, *J. Org. Chem.*, 2011, **76**, 1472-1474.

96.   T. Okino, Y. Hoashi, T. Furukawa, X. Xu and Y. Takemoto, *J. Am. Chem. Soc.*, 2005, **127**, 119-125.

97.   A. Hamza, G. Schubert, T. Soós and I. Pápai, *J. Am. Chem. Soc.*, 2006, **128**, 13151-13160.

98.   M. C. Nielsen, K. J. Bonney and F. Schoenebeck, *Angew. Chem. Int. Ed.*, 2014, **53**, 5903-5906.

99.   V. V. Grushin and W. J. Marshall, *J. Am. Chem. Soc.*, 2006, **128**, 12644-12645.

100.   P. Anstaett and F. Schoenebeck, *Chem. Eur. J.*, 2011, **17**, 12340-12346.

101.   J. Na, K. N. Houk and D. Hilvert, *J. Am. Chem. Soc.*, 1996, **118**, 6462-6471.

102.   S. N. Thorn, R. G. Daniels, M.-T. M. Auditor and D. Hilvert, *Nature*, 1995, **373**, 228-230.

103. D. Rothlisberger, O. Khersonsky, A. M. Wollacott, L. Jiang, J. DeChancie, J. Betker, J. L. Gallaher, E. A. Althoff, A. Zanghellini, O. Dym, S. Albeck, K. N. Houk, D. S. Tawfik and D. Baker, *Nature*, 2008, **453**, 190-195.

104. L. Jiang, E. A. Althoff, F. R. Clemente, L. Doyle, D. Röthlisberger, A. Zanghellini, J. L. Gallaher, J. L. Betker, F. Tanaka, C. F. Barbas, D. Hilvert, K. N. Houk, B. L. Stoddard and D. Baker, *Science*, 2008, **319**, 1387-1391.

105. J. B. Siegel, A. Zanghellini, H. M. Lovick, G. Kiss, A. R. Lambert, J. L. St.Clair, J. L. Gallaher, D. Hilvert, M. H. Gelb, B. L. Stoddard, K. N. Houk, F. E. Michael and D. Baker, *Science*, 2010, **329**, 309-313.

106. W. Koch and M. C. Holthausen, *A Chemist's Guide to Density Functional Theory*, John Wiley & Sons, 2001.

107. F. Jensen, *Introduction to Computational Chemistry*, John Wiley & Sons, 2006.

108. P. Hohenberg and W. Kohn, *Phys. Rev.*, 1964, **136**, B864-B871.

109. W. Kohn and L. J. Sham, *Phys. Rev.*, 1965, **140**, A1133-A1138.

110. A. D. Becke, *J. Chem. Phys.*, 1993, **98**, 5648-5652.

111. C. Lee, W. Yang and R. G. Parr, *Phys. Rev. B*, 1988, **37**, 785-789.

112. S. H. Vosko, L. Wilk and M. Nusair, *Can. J. Phys.*, 1980, **58**, 1200-1211.

113. P. J. Stephens, F. J. Devlin, C. F. Chabalowski and M. J. Frisch, *J. Phys. Chem.*, 1994, **98**, 11623-11627.

114. Y. Zhao and D. Truhlar, *Theor. Chem. Acc.*, 2008, **120**, 215-241.

115. Y. Zhao and D. G. Truhlar, *Acc. Chem. Res.*, 2008, **41**, 157-167.

116. V. Barone and M. Cossi, *J. Phys. Chem. A*, 1998, **102**, 1995-2001.

117. M. Cossi, N. Rega, G. Scalmani and V. Barone, *J. Comput. Chem.*, 2003, **24**, 669-681.

118. H. Eyring, *J. Chem. Phys.*, 1935, **3**, 107-115.

119. R. A. Marcus, *J. Chem. Phys.*, 1965, **43**, 679-701.

120. S. V. Rosokha, J.-M. Lü, M. D. Newton and J. K. Kochi, *J. Am. Chem. Soc.*, 2005, **127**, 7411-7420.

121. S. V. Rosokha, M. D. Newton, M. Head-Gordon and J. K. Kochi, *Chem. Phys.*, 2006, **324**, 117-128.

122. S. V. Rosokha, S. M. Dibrov, T. Y. Rosokha and J. K. Kochi, *Photochem. Photobiol. Sci.*, 2006, **5**, 914-924.

123. S. Kazemiabnavi, P. Dutta and S. Banerjee, *J. Phys. Chem. C*, 2014, **118**, 27183-27192.

124. J. Blumberger, *Phys. Chem. Chem. Phys.*, 2008, **10**, 5651-5667.

125. S. F. Nelsen, S. C. Blackstock and Y. Kim, *J. Am. Chem. Soc.*, 1987, **109**, 677-682.

126. S. P. Cakir, S. Stokes, A. Sygula and K. T. Mead, *J. Org. Chem.*, 2009, **74**, 7529-7532.

127. J. A. Murphy, *J. Org. Chem.*, 2014, **79**, 3731-3746.

128. E. Doni and J. A. Murphy, *Chem. Commun.*, 2014, **50**, 6073-6087.

129. J. A. Murphy, T. A. Khan, S.-z. Zhou, D. W. Thomson and M. Mahesh, *Angew. Chem. Int. Ed.*, 2005, **44**, 1356-1360.

130. J. A. Murphy, S.-z. Zhou, D. W. Thomson, F. Schoenebeck, M. Mahesh, S. R. Park, T. Tuttle and L. E. A. Berlouis, *Angew. Chem. Int. Ed.*, 2007, **46**, 5178-5183.

131. E. Cahard, F. Schoenebeck, J. Garnier, S. P. Y. Cutulic, S. Zhou and J. A. Murphy, *Angew. Chem. Int. Ed.*, 2012, **51**, 3673-3676.

132. N. Uchiyama, E. Shirakawa and T. Hayashi, *Chem. Commun.*, 2013, **49**, 364-366.

133. E. Shirakawa, F. Tamakuni, E. Kusano, N. Uchiyama, W. Konagaya, R. Watabe and T. Hayashi, *Angew. Chem. Int. Ed.*, 2014, **53**, 521-525.

134. E. Doni, B. Mondal, S. O'Sullivan, T. Tuttle and J. A. Murphy, *J. Am. Chem. Soc.*, 2013, **135**, 10934-10937.

135. E. Doni, S. O'Sullivan and J. A. Murphy, *Angew. Chem. Int. Ed.*, 2013, **52**, 2239-2242.

136. Gaussian 09, M. J. Frisch, G. W. Trucks, H. B. Schlegel, G. E. Scuseria, M. A. Robb, J. R. Cheeseman, G. Scalmani, V. Barone, B. Mennucci, G. A. Petersson, H. Nakatsuji, M. Caricato, X. Li, H. P. Hratchian, A. F. Izmaylov, J. Bloino, G. Zheng, J. L. Sonnenberg, M. Hada, M. Ehara, K. Toyota, R. Fukuda, J. Hasegawa, M. Ishida, T. Nakajima, Y. Honda, O. Kitao, H. Nakai, T. Vreven, J. A. Montgomery Jr., J. E. Peralta, F. Ogliaro, M. J. Bearpark, J. Heyd, E. N. Brothers, K. N. Kudin, V. N. Staroverov, R. Kobayashi, J. Normand, K. Raghavachari, A. P. Rendell, J. C. Burant, S. S. Iyengar, J. Tomasi, M. Cossi, N. Rega, N. J. Millam, M. Klene, J. E. Knox, J. B. Cross, V. Bakken, C. Adamo, J. Jaramillo, R. Gomperts, R. E. Stratmann, O. Yazyev, A. J. Austin, R. Cammi, C. Pomelli, J. W. Ochterski, R. L. Martin, K. Morokuma, V. G. Zakrzewski, G. A. Voth, P. Salvador, J. J.

Dannenberg, S. Dapprich, A. D. Daniels, Ö. Farkas, J. B. Foresman, J. V. Ortiz, J. Cioslowski and D. J. Fox, Gaussian, Inc., Wallingford, CT, USA, 2009

137. Y. Zhao and D. G. Truhlar, *J. Chem. Phys.*, 2006, **125**, 194101.

138. W. J. Hehre, R. Ditchfield and J. A. Pople, *J. Chem. Phys.*, 1972, **56**, 2257-2261.

139. P. C. Hariharan and J. A. Pople, *Theor. Chim. Acta*, 1973, **28**, 213-222.

140. J.-P. Blaudeau, M. P. McGrath, L. A. Curtiss and L. Radom, *J. Chem. Phys.*, 1997, **107**, 5016-5021.

141. B. I. Dunlap, *J. Chem. Phys.*, 1983, **78**, 3140-3142.

142. B. I. Dunlap, *J. Mol. Struct. Theochem*, 2000, **529**, 37-40.

143. G. S. Hammond, *J. Am. Chem. Soc.*, 1955, **77**, 334-338.

144. M. Albrecht and H. Stoeckli-Evans, *Chem. Commun.*, 2005, 4705-4707.

145. M. Tullberg, M. Grøtli and K. Luthman, *Tetrahedron*, 2006, **62**, 7484-7491.

146. Nonappa, K. Ahonen, M. Lahtinen and E. Kolehmainen, *Green Chem.*, 2011, **13**, 1203-1209.

147. T. H. Dunning, *J. Chem. Phys.*, 1989, **90**, 1007-1023.

148. V. A. Rassolov, M. A. Ratner, J. A. Pople, P. C. Redfern and L. A. Curtiss, *J. Comput. Chem.*, 2001, **22**, 976-984.

149. K. A. Peterson, D. Figgen, E. Goll, H. Stoll and M. Dolg, *J. Chem. Phys.*, 2003, **119**, 11113-11123.

150. K. A. Peterson, B. C. Shepler, D. Figgen and H. Stoll, *J. Phys. Chem. A*, 2006, **110**, 13877-13883.

151. M. Hirsch, S. Dhara and C. E. Diesendruck, *Org. Lett.*, 2016, **18**, 980-983.

152. S. Zhou, E. Doni, G. M. Anderson, R. G. Kane, S. W. MacDougall, V. M. Ironmonger, T. Tuttle and J. A. Murphy, *J. Am. Chem. Soc.*, 2014, **136**, 17818-17826.

153. P. M. Dewick, John Wiley & Sons, 2006, ch. 4, pp. 123-124.

154. W. Reeve, C. M. Erikson and P. F. Aluotto, *Can. J. Chem.*, 1979, **57**, 2747-2754.

155. J. H. Wotiz, R. D. Kleopfer, P. M. Barelski, C. C. Hinckley and D. F. Koster, *J. Org. Chem.*, 1972, **37**, 1758-1763.

156. R. B. Woodward, N. L. Wendler and F. J. Brutschy, *J. Am. Chem. Soc.*, 1945, **67**, 1425-1429.

157. P. C. Too, G. H. Chan, Y. L. Tnay, H. Hirao and S. Chiba, *Angew. Chem. Int. Ed.*, 2016, **55**, 3719-3723.

158. P. O'Brien and S. Warren, *J. Chem. Soc., Perkin Trans. 1*, 1996, 2117-2127.

159. I. Coldham, P. M. A. Houdayer, R. A. Judkins and D. R. Witty, *Synthesis*, 1998, **1998**, 1463-1466.

160. I. Coldham, R. A. Judkins and D. R. Witty, *Tetrahedron*, 1998, **54**, 14255-14264.

161. V. V. Dunina, O. N. Gorunova, V. A. Stepanova, P. A. Zykov, M. V. Livantsov, Y. K. Grishin, A. V. Churakov and L. G. Kuz'mina, *Tetrahedron: Asymmetry*, 2007, **18**, 2011-2015.

162. M. T. Conconi, G. Marzaro, L. Urbani, I. Zanusso, R. Di Liddo, I. Castagliuolo, P. Brun, F. Tonus, A. Ferrarese, A. Guiotto and A. Chilin, *Eur. J. Med. Chem.*, 2013, **67**, 373-383.

163. S. Gendler, A. L. Zelikoff, J. Kopilov, I. Goldberg and M. Kol, *J. Am. Chem. Soc.*, 2008, **130**, 2144-2145.

164. H. Staats, F. Eggers, O. Haß, F. Fahrenkrug, J. Matthey, U. Lüning and A. Lützen, *Eur. J. Org. Chem.*, 2009, **2009**, 4777-4792.

165. L. M. Greig, A. M. Z. Slawin, M. H. Smith and D. Philp, *Tetrahedron*, 2007, **63**, 2391-2403.